UTS UNIVERSITY OF TECHNOLOGY SYDNEY

3D Microfluidic System to Study of Tumour Microenvironment

by Hamidreza Aboulkhyer Estarabadi

Thesis submitted in fulfilment of the requirements for the degree of

Doctor of Philosophy

under the supervision of Prof. Majid Ebrahimi Warkiani

University of Technology Sydney
Faculty of Engineering and Information Technology

April 2022

CERTIFICATE OF ORIGINAL AUTHORSHIP

I, **Hamidreza Aboulkheyr Estarabadi** declare that this thesis, is submitted in fulfilment of the requirements for the award of Doctor of Philosophy, in the School of Biomedical Engineering at the University of Technology Sydney.

This thesis is wholly my own work unless otherwise reference or acknowledged. In addition, I certify that all information sources and literature used are indicated in the thesis.

This document has not been submitted for qualifications at any other academic institution. This research is supported by the Australian Government Research Training Program.

Signature: Date: 21-09-2022

Production Note:
Signature removed prior to publication.

Impact of COVID-19 on the completion of the thesis

This thesis's research aims, and objectives have been planned to complete within three years of candidature; however, the Covid-19 crisis and pandemics followed by long term lockdowns and restrictions in laboratory experiments significantly affected the few numbers of objectives of this research. Among all chapters, Chapter 8 of this thesis is affected extremely by Covid-19 restrictions ruled by the state government, campus lockdowns, and limitations in a daily laboratory working time. A detailed explanation of these impacts on methodology and results of Chapter 8 has been stated on the starting page of this chapter.

Acknowledgement

I would like to express my sincerest gratitude and appreciation to my supervisor, Prof. Majid Ebrahimi Warkiani, for his invaluable guidance, encouragement, patience, and, most importantly support through my PhD. He is an exceptional role model for both my academic and personal life. I am grateful for giving me the opportunity to be a member of his research team and for all that I have learned from him. My PhD research always benefited from his constructive and invaluable scientific guidance. I would like to thank my co-supervisor Prof. Dyong Jin, for his guidance and constant support through my PhD and for serving on my examination committee. Also, a sincere thank you to Prof. Thomas R Cox from the Garvan Institute of Medical Science for his insightful biological inputs and for sharing his invaluable expertise with me.

I extend my thanks to all past and present members of Warkiani Lab. It was an amazing experience and honour to work with a group of friendly, motivated, and knowledgeable scholars and students during my PhD. I would like to additionally thank to Sydney Vital Translational Cancer Research for awarding me a prestigious supporting grant.

Finally, my deepest gratitude and appreciation goes to my wonderful and lovely wife Monireh for her unconditional and endless encouragement and love. She dedicated her precious time and life to support me during my PhD journey. I am extremely lucky to have her in my life. Thank you, Monireh, for being my best friend and always believing in me. A special thank you to my father, Mohammad-Masoud and my mother, Malihe, for their unconditional love, dedication, and many years of moral support during my life. I am sincerely thankful to my brother and sister in Iran who have made it possible for me to focus on my work by supporting our parents.

Format of Thesis

This thesis is prepared in one introduction and six chapters, including published and under-publication research articles. The chapter 1; “Introduction” provides an overview of the tumour microenvironment (TME) and its cellular and molecular features, emphasizing the importance of modelling TME and current TME models. In Chapter 2, the current application of microfluidic technology in cancer research and therapy is discussed comprehensively and the remain challenges that required to be addressed are highlighted as well. Following these, in Chapter 3, a comprehensive in-silico data analysis has been performed to figure-out the association of cellular components of TME with tumour immunity and activation of invasion and migration. Moreover, in this chapter we highlighted potential of drug repurposing in cancer treatment and targeting TME. The findings and output of this chapter are modeled in our microfluidic system through the next chapters. Chapter 4 – Chapter 8 are the application-specific chapters showcasing the application of microfluidic-based 3D cell culture in particular modelling features of TME and drug discovery. Chapter 4 demonstrates modelling tumour stromal cells and cancer cell interaction and its effect on immune suppression on cancer cells which has not been before. Moreover, in this chapter, the application of an anti-fibrotic drug on reversion of immune sensitivity has been shown for the first time. Following this, in Chapter 5, the immune-modulation role of mesenchymal stem cells in the stimulation of immune escape and drug response is explored using a microfluidic device. To model the biological and molecular aspect of initiation and invasion of cancer cells, Chapter 6 illustrates the application of microfluidic for mimicking cancer and tumour-stromal cells invasion and cancer-stem cells formation using the culture of organotypic tumour spheroids containing stromal cells in the device. Moreover, this chapter highlights the therapeutic potential of an anti-fibrotic agent discovered in Chapter 3 on targeting key cytokines and suppression of invasion. As ECM is the main component of TME, in Chapter 7, we modeled the role of matrix stiffness on cancer cells immunity and invasion. In Chapter 8, the formation of microvasculature and pre-vascular tumour organoids in the microfluidic device has been shown. Finally, in last chapter, “Conclusion and Future Work”, the limitations and challenges of this thesis project and future research direction are discussed.

List of publications

- Azadi, Shohreh, Hamidreza Aboulkheyr Es, Arutha Kulasinghe, Pritam Bordhan, and Majid Ebrahimi Warkiani. "Application of microfluidic technology in cancer research and therapy." In Advances in clinical chemistry, vol. 99, pp. 193-235. Elsevier, 2020.

- Aboulkheyr Es, Hamidreza, Sareh Zhand, Jean Paul Thiery, and Majid Ebrahimi Warkiani. “Pirfenidone reduces immune-suppressive capacity of cancer-associated fibroblasts through targeting CCL17 and TNF-beta.” Integrative Biology 12, no. 7 (2020): 188-197.

- Aboulkheyr Es, Hamidreza, Bahareh Bigdeli, Sareh Zhand, Amir R. Aref, Jean P. Thiery, and Majid E. Warkiani. "Mesenchymal stem cells induce PD-L1 expression through the secretion of CCL5 in breast cancer cells." Journal of Cellular Physiology 236, no. 5 (2021): 3918-3928.

- Es, Hamidreza Aboulkheyr, Thomas R. Cox, Ehsan Sarafraz-Yazdi, Jean Paul Thiery, and Majid Ebrahimi Warkiani. "Pirfenidone Reduces Epithelial–Mesenchymal Transition and Spheroid Formation in Breast Carcinoma through Targeting Cancer-Associated Fibroblasts (CAFs)." Cancers 13, no. 20 (2021): 5118.

- Azadi, Shohreh, Hamidreza Aboulkheyr Es, Sajad Razavi Bazaz, Jean Paul Thiery, Mohsen Asadnia, and Majid Ebrahimi Warkiani. "Upregulation of PD-L1 expression in breast cancer cells through the formation of 3D multicellular cancer aggregates under different chemical and mechanical conditions." Biochimica et Biophysica Acta (BBA)-Molecular Cell Research 1866, no. 12 (2019): 118526.

Table of Contents

Chapter 1 17

Introduction 17

1.1 Tumour microenvironment 19

1.2 Cancer-Associated Fibroblasts (CAFs) 21

1.2.1 CAF in tumour development and metastasis 21

1.2.2 CAF and tumour immune suppression 22

1.2.3 CAF and drug resistance 23

1.3 Tumour Associated Mesenchymal Stem Cells (TA-MSCs) 25

1.4 T-cells in TME 26

1.5 Tumour associated blood vasculature 27

1.6 Extracellular Matrix (ECM) 28

1.7 Importance of modeling TME 29

1.7.1 Conventional Models of TME 29

1.7.2 Organoid culture technology 30

1.7.3 Microfluidic technology for modeling TME 31

1.8 Conclusion 32

Chapter 2 35

Literature Review 35

1.1 Microfluidic device in modelling cancer biology and metastasis 37

1.2 Modelling Tumour growth 42

1.3 Modelling cancer cell-endothelial cell interactions 42

1.4 Modelling the tumour microenvironment (TME) 46

1.4.1 Biochemical cues 47

1.4.2 Biomechanical cues 48

1.4.3 Cellular components of TME 49

1.5 Modelling migration and invasion 51

1.5.1 Initial migration 51

1.5.2 Intravasation 52

1.5.3 Extravasation 52

1.5.4 Modeling colonization of extravasated cancer cells 54

1.6 Microfluidic systems for circulating tumour cells detection, characterization and analysis Circulating tumour cells (CTCs) 56
1.6.1 CTCs enumeration 57
1.6.2 Circulating tumour cell (CTC) clusters 57
1.6.3 Single Cell CTC characterization 58
1.6.4 Immunotherapeutic biomarkers 58
1.6.5 Shift towards high throughput CTC isolation 59
1.7 Microfluidic CTC enrichment technologies 59
1.7.1 Inertial microfluidics 59
1.7.2 Nanovelcro 61
1.7.3 Acoustic Separation 61
1.7.4 Parstotix 62
1.7.5 Vortex 62
1.8 Microfluidic approach in cancer treatment 62
1.9 Microfluidic and modeling anticancer drug response 65
1.10 Microfluidic and personalized cancer treatment 68
1.11 Challenges and limitations 71
Chapter 3 73
In-silico Study of Tumour Microenvironment in Triple-Negative Breast Cancer 73
3.1 Introduction 75
3.2 Materials and Methods 76
3.2.1 Datasets 76
3.2.2. The EMT scores and immune feature analysis 77
3.2.3 Cell, ligand and receptor abundance diagram 77
3.2.4 Statistical analysis 78
3.3. Results 78
3.3.1 Fibroblasts in the TME and its association with EMT and immunity 78
3.3.2 EMT score positively associates with stromal score and negatively with the immune score in different subtypes of breast cancer 82
3.3.3 EMT scores negatively associate with infiltration of immune cells in the TME 83
3.3.4 Association between EMT-TFs and infiltration of immune cells in TME 87
3.3.5 Hot TME versus cold TME 89
3.4 Discussion 91
Chapter 4 95

The role of CAF in Tumour Microenvironment and Tumour Immunity 95
4.1 Introduction 97
4.2 Materials and Methods 98
4.2.1 In-silico data analysis 99
4.2.2 Generation of CAF cells from normal fibroblasts 100
4.2.3 Production of conditioned medium from CAF cells 100
4.2.4 Microfluidic Device Design and cell culture 100
4.2.5 Culturing single cells and multi-cellular aggregate (MCA) in microfluidic device. 101
4.2.6 Immunofluorescent staining 102
4.2.7 Cytokine array 102
4.2.8 Statistical analysis 103
4.3 Results 103
4.3.1 Association between CAF derived cytokines with PD-L1 103
4.3.2 CAFs induce a phenotype switch in cancer cells 105
4.3.3 CAFs induce expression of PD-L1 on PD-L1 low cancer cells 109
4.3.4 Pirfenidone reduces invasion and migration capacity of CAF and cancer cells 109
4.3.5 Pirfenidone reduces expression of PD-L1 on CAF cells by targeting various cytokines 111
4.4 Discussion 113
Chapter 5 117
The Role of Tumour-Associated Mesenchymal-Stem Cells in Regulation of Tumour Immunity 117
5.1 Introduction 119
5.2 Materials and Methods 120
5.2.1 Cell culture 120
5.2.2 Preparation of conditioned medium 121
5.2.3 Microfluidic device design and cell culture 121
5.2.4 Culturing single and multi-cellular aggregate (MCA) in the microfluidic device 122
5.2.5 Immunofluorescent staining 122
5.2.6 Cytokine array 123
5.2.7 Statistical analysis 123
5.3 Results 124
5.3.1 MSC in various stages of breast cancer and its correlation with immune suppression 124

5.3.2 MSC induces breast cancer cell proliferation and invasion behavior 127
5.3.3 MSC induce expression of PD-L1 on low PD-L1 breast cancer cells 129
3.3.4 Cytokine expression 130
5.4 Discussion 134
Chapter 6 138
Targeting Epithelial-Mesenchymal Transition and Tumour Spheroid formation in Breast Carcinoma 138
6.1 Introduction 140
6.2 Materials and Methods 141
6.2.1 In-Silico Data Analysis 141
6.2.2 Cell lines and Media 141
6.2.3 Spheroid Formation 142
6.2.4 Preparation of CAFs Condition Medium 142
6.2.5 Microfluidic Device Design and Cell Culture 143
6.2.6 Cytokine Profiling Assays on Treated samples 144
6.2.7 Immunofluorescence Staining and Imaging Analysis 144
6.2.8 Statistical Analysis 145
6.3 Results 145
6.3.1 The Association of Tumour Stromal Content with the Expression of YAP1 and Metastasis Feature 145
6.3.2 Association of YAP1 with EMT and Stemness Markers 147
6.3.3 CAFs Induce Spheroid Formation 149
6.3.4 Pirfenidone Reduces the Migration of CAFs and Carcinoma Cells 151
6.3.5 Pirfenidone Reduces YAP1 and CD44 Expression in Spheroids by Targeting Key Cytokines 153
6.4 Discussion 157
6.5 Conclusions 160
Chapter 7 161
The role of ECM stiffness in tumour Immunity 161
7.1 Introduction 163
7.2 Materials and methods 164
7.2.1 Cell culture 164
7.2.2 Substrate preparation and characterization 165
7.2.3 Anti-EGFR treatment 166

7.2.4 Evaluation of the PDL-1 expression 167
7.2.5 Immunofluorescence staining of PDL-1 167
7.2.6 PDL-1 ELISA assay 168
7.2.7 Spheroid formation 168
7.2.8 Cell seeding in the microwells 169
7.2.9 Isolation of the cancer spheroids from the microwells 169
7.2.10 Spheroid characterization 170
7.2.11 Cell viability of spheroids 170
7.2.12 Measurement of spheroid number and diameter 170
7.2.13 Immunofluorescence staining of PDL-1 171
7.2.14 Spheroid spreading 171
7.2.15 Statistic 172
7.3 Results 172
7.3.1 PDMS substrates elastic modulus 172
7.3.2 Expression of PDL-1 protein in breast cancer cells 173
7.3.3 Characterization of the breast cancer spheroids 174
7.3.4 Assessment of the PDL1 expression in spread breast cancer spheroids 178
7.4 Discussion 181
Chapter 8 187
Generation of vascularized organoids 187
8.1 Introduction 189
8.2 Methods and Materials 190
8.2.1 Cell culture and organoid formation 190
8.2.2 Culturing microvasculature in device 191
8.2.3 Generation of vascularized organoids 191
8.2.4 Immunofluorescence and Confocal Imaging 192
8.2.5 Statistical analysis 192
8.3 Results 193
8.3.1 Microvasculature in device 193
8.3.2 Generation of vascularized organoids 195
8.4 Discussion 197
Chapter 9 200
Conclusion and future work 200

List of Illustrations and Figures

Figure 1: Schematic of tumour microenvironment. 20

Figure 2: CAFs and their secretome remodel the TME.. 22

Figure 3.1: Overview of cell populations cluster and its signature identified in TME of TNBC. 78

Figure 3.2: Gene-set enrichment analysis and association between EMT, immunity and CAFs activity. 79

Figure 3.3: Pathway activity and the expression of 35 immuno-modulatory cytokines in breast cancer. 81

Figure 3.4: The correlation between immune and stromal score with EMT scores in different subtypes of breast cancer. 83

Figure 3.5: Comparison of TME features across three different EMT groups 84

Figure 3.6: Association between EMT scores and expression of immune-checkpoints, immuno-inhibitors and immuno-stimulators 85

Figure 3.7: Expression of cytokines/chemokines and their receptors in different EMT groups 86

Figure 3.8: Correlation coefficient analysis between classical EMT related genes with infiltration of various immune cells 88

Figure 3.9: Cell, ligand and receptor abundance analysis of tumour cells, T cells, macrophages, and DC cells 91

Figure 4.1: The workflow of study. 99

Figure 4.2: In-silico analysis of PFD target proteins and their alterations across breast carcinoma samples in TCGA 105

Figure 4.3: Transformation of normal fibroblast to CAFs and its characterization. 106

Figure 4.4: Migration of CAFs 107

Figure 4.5: Phenotypic transformation of MCF7 cells cultured with CAF-CM 108

Figure 4.6: Culturing MCF7-derived MCA with CAF-CM. 110

Figure 4.7: Effects of PFD on phenotype transformation and migration of cells. 111

Figure 4.8: Effects of PFD on expression of PD-L1 in CAFs 112

Figure 4.9: Cytokine profiling of CAF-CM 113

Figure 5.1: Schematic workflow of the study 124

Figure 5.2: Expression of MSC related genes and its correlation with PD-L1 126

Figure 5.3: Effects of MSC-CM on proliferation and invasion behavior of cancer cells 127

Figure 5.4: EMT induction effects of MSC-CM on MCF7 cells. 128

Figure 5.5: MSC-CM induces expression of the PD-L1 130

Figure 5.6: Cytokine expression profiling of MSC-CM and MSC-CM+PFD 132

Figure 5.7: The expression profile comparison of identified cytokines between PD-L1-negative and PD-L1 negative samples 133

Figure 6.1: Genomic analysis of the TCGA breast cancer cohort 147

Figure 6.2: In-Silico data analysis between samples expressing high and low levels of *YAP1*. 148

Figure 6.3: CAFs induces spheroid formation with increased diameter and expression of YAP1. 150

Figure 6.4: Assessing the migration and invasion inhibitory effects of PFD on MDA-MB-231 carcinoma cells and CAFs. 152

Figure 6.5: PFD reduces CAFs activity and expression of CD44 and YAP1 through the blockade of key cytokine secretion. 154

Figure 6.6: The association between targeted cytokines with EMT and YAP1 156

Figure 7.1: Regulation of PDL-1 expression by EGFR signaling and substrate stiffening. 174

Figure 7.2: Schematic of the SpheroFilm utilized to generate the spheroids and representative images of the spheroid formation of breast cancer cells. 175

Figure 7.3: Spheroid characterization**.** 176

Figure 7.4: Role of the spheroid formation in the PDL-1 expression of breast cancer cells 178

Figure 7.5: PDL-1 expression of spread spheroids of breast cancer cells as a function of the EGFR activity and the substrate stiffness. 180

Figure 7.6. Comparison of protein concentration of PDL-1 in the chemical and mechanical groups, before and after formation of the spheroids. 181

Figure 8.1. Schematic of workflow for the generation of tumour microenvironment in vascularized device equipped with tumour organoids, cancer-associated fibroblasts, and T-cells. 190

Figure 8.2. Generation of 3D microvasculature in a microfluidic device. 194

Figure 8.3. Generation of vascularized tumour organoids 196

List of Abbreviations

αSMA: Alpha Smooth Muscle Actin

CAF: Cancer-Associated Fibroblasts

ECM: Extra-Cellular Matrix

EGM: Endothelial Growth Medium

EMT: Epithelial-Mesenchymal Transition

FAP: Fibroblasts-Activated Protein

MCA: Multi-Cellular Aggregates

PD-L1: Programmed Death-Ligand 1

PFD: Pirfenidone

TAM: Tumour-Associated Mesenchymal Stem Cells

TCGA: The Cancer Genome Atlas

TIL: Tumour Infiltration Lymphocytes

TME: Tumour Microenvironment

TNBC: Triple-negative Breast Cancer

YAP: Yes-Activated Protein

3D microfluidic system to study of tumour microenvironment

Hamidreza Aboulkheyr Estarabadi
Doctor of Philosophy
School of Biomedical Engineering
University of Technology Sydney
2022

Abstract

The tumour microenvironment (TME) plays a crucial role in cancer initiation, progression, and development. To better understand the cellular and molecular feature of TME, various in-vitro, ex-vivo and in-vivo models of TME have been developed, ranging from 2D cancer cells lines, 3D organoids to genetically engineered animal models. However, these models faced a series of challenges and drawbacks limiting the study of the particular feature of TME in a specific type of cancer. Recently, microfluidic technology introduced a new platform to mimic the TME ecosystem at the micro-scale through an advanced engineered system. This platform enables modelling a wide range of TME properties from ECM to the vasculature and the complex cellular structure by co-culturing 3D tumour cells cost-efficient, real-time, and controllable fashion. However, the major focus of the current microfluidic models of TME is on cancer cells rather than tumor-stromal cells and their effects on tumour immunity and immunotherapy. Moreover, these models unbale to provide a space for down-stream molecular analysis including cytokines analysis or RNA-sequencing. Additionally, the design of majority of these models is complex which might limit broad application of these models.

This thesis focuses on addressing these challenges using a low-cost and easy to use microfluidic device which enable wide range of applications from in-vitro to ex-vivo and drug discovery and immune-oncology. Using developed model in this thesis, the most impactful contributions of this thesis was the discovery of the role of the tumor stromal cells including cancer-associated fibroblasts (CAFs) and tumour-associated mesenchymal stem cells (TAMs) in tumour immunity and that targeting these populations can significantly reduce immune-suppression capacity in TME. We discovered and introduced potential of an anti-fibrotic drug called Pirfenidone for targeting CAFs and secreted cytokines through a comprehensive in-silico data analysis at both bulk and single cell level in breast cancer for the first time. Using our developed microfluidic model of TME, we showed that how pirfenidone reduce CAFs and MSC activity, invasion, immune-suppression, and tumor initiation in breast carcinoma. Moreover, we modeled the effects of matrix stiffness which is regulated by CAFs on tumour immunity and expression of immune checkpoints. Finally, we tried to develop a novel method for generation of vascularized tumor organoids in device which extremely affected by Covid-19 pandemics and lockdowns.

Chapter 1

Introduction

Summary:

This chapter introduces the tumor microenvironment (TME) and its cellular and non-cellular components and explains their role in cancer initiation, progression, and metastasis. Moreover, in this chapter, the importance of the study of TME is discussed. Additionally, the current models of TME and their limitations and how microfluidic technology can resolve these challenges and limitations are highlighted in this chapter.

Cancer is a heterogeneous disease and a leading cause of death worldwide. Over the past decade, our understanding of various cancer's biology and genomic properties has been significantly improved, resulting in the development of novel cancer diagnostic and prognostic markers and the discovery of a new generation of anticancer therapeutics agents, including targeted therapy and immunotherapy. However, clinically, a significant proportion of patients met a poor outcome due to diagnosis of cancer at a late stage, lack of reliable biomarker for early detection, and acquired resistance to standard of care therapies. It has been proved that the tumour and its surrounding area, known as the tumour microenvironment (TME), play a crucial role in tumour evolution, metastasis, and outcome of patients [1]. Additionally, various clinical and pre-clinical studies highlighted that TME could reshape therapeutic response and drug resistance.

To uncover the dark side of TME biology and its dynamic ecosystems, various in-vitro and in-vivo tumour models have been developed, ranging from cancer cell lines to animal models. Considering the hallmarks of cancer [2] and its correlation with TME, the proposed models failed to recapitulate all major features of TME due to numerous limitations. Lack of tumour stromal cells, immune system elements, and vascular network are major drawbacks of conventional in-vitro tumour models [3]. Although, in comparison with in-vitro models, animal models overcome these challenges, however, suppression of the immune system as a critical step of generating tumour xenograft limited its application to study of TME, tumour immune microenvironment (TIME) and its crosstalk with cancer and stromal cells and screening of immunotherapy drugs.

The microfluidic cell culture platform recently opened a new window to model TME in a dynamic and more humanized fashion. The possibility of assembly of all cellular and non-cellular components of TME in a small microfluidic device can overcome the limitations of conventional models and serve as a reliable pre-clinical model for drug discovery and personalized medicine.

1.1 Tumour microenvironment

Cancers develop in a complex and dynamic tissue ecosystem, which they depend on for sustained growth, invasion, and metastasis. The tumour mass consists of a heterogeneous

population of cancer cells and a variety of resident and infiltrating host cells, secreted factors and extracellular matrix proteins, collectively known as the tumour microenvironment. The cellular part of TME is composed of various cell types, including endothelial cells, fibroblasts, mesenchymal stem cells (depending on the types of cancer), immune cells, etc., while the non-cellular part includes extra-cellular components such as cytokines, growth factors, hormones, and extracellular matrix.

Considering the hallmark of cancer [2], growing evidence highlighted the crucial role of TME in tumour development and metastasis, where bidirectional communication between cancer cells and tumour stromal cells can reprogram cancer cells toward achieving an aggressive behaviour, resulting in induction of metastasis [1]. In addition, TME can reshape therapeutic response against wide varieties of anticancer drugs ranging from chemotherapy to immunotherapy agents [4].

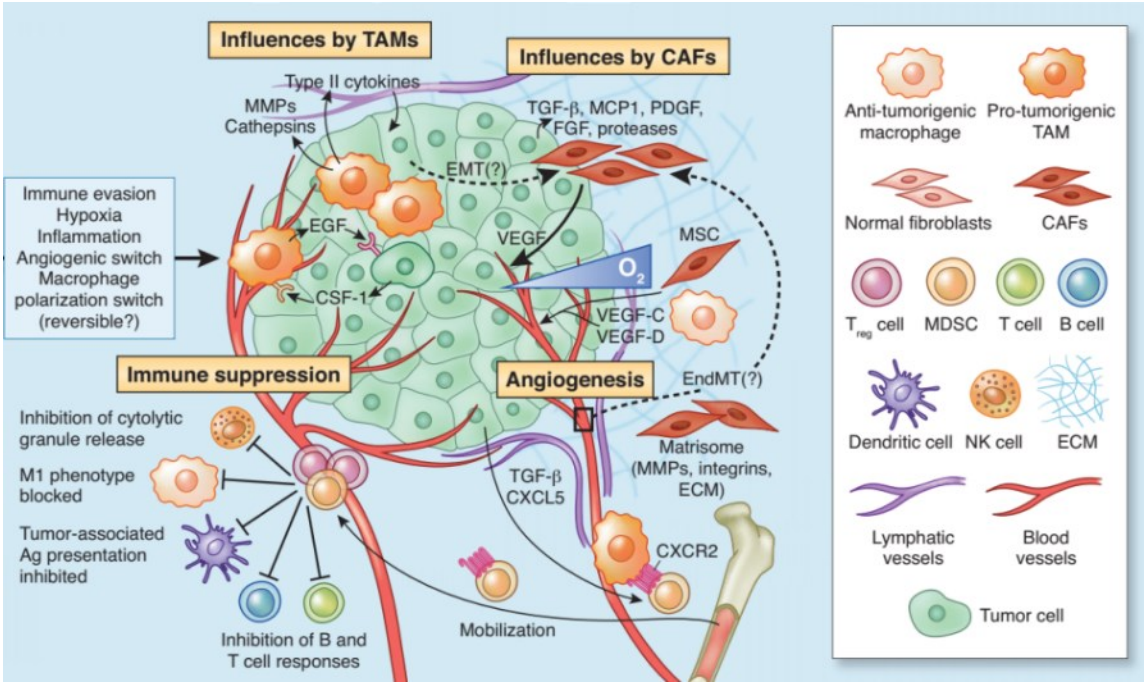

Figure 1: Schematic of tumour microenvironment. The TME is composed of various cell types including cancer cells, immune cells, vascular formation related cells, cancer-associated fibroblasts and in some cases mesenchymal stem cells [1].

1.2 Cancer-Associated Fibroblasts (CAFs)

A dominant component of the tumour microenvironment is fibroblasts, and many studies over the years have suggested a prominent functional role for these types of cells in cancer progression, metastasis, and drug resistance to various treatment regimens [5, 6]. Fibroblasts associated with cancer have been known as cancer-associated fibroblasts (CAFs), tumour-associated fibroblasts, activated fibroblasts or activated myofibroblasts. In the past decade, large number of studies highlighted crucial role CAFs as key components of tumour progression, metastasis, drug resistance, and tumour immune suppression, suggesting that they probably contribute to a wide range of stromal programs of many different tumours [7, 8]. Emerging evidence suggests that CAFs are a heterogeneous population of cells within TME [9]. This heterogeneity might be ascribed to the numerous potential cellular sources of CAFs, which consist of six dominant categories based on the tumour histological type [9, 10].

1.2.1 CAF in tumour development and metastasis

CAFs isolated from various solid tumours exhibited many distinct properties when compared with normal fibroblasts cultured from healthy organs [11]. Using co-culture experiments, CAFs enhance tumourigenesis of cancer cells when compared with normal fibroblasts [12, 13]. CAFs also induce invasion feature on benign and non-invasive cancer cells [14]. The ability of CAFs to influence tumour growth and progression was partly dependent on their ability to induce angiogenesis by various CAF derived stromal cytokines including but not limited to CXCL12 and recruitment of bone marrow-derived endothelial cells [15]. Besides the pro-tumourigenic role of CAF, several secreted molecular regulators of CAFs have been identified that regulate metastasis, drug resistance and immune suppression in TME (Figure 2) [16]. In addition to these, CAFs are essential mediators of secondary tumour growth at the metastatic site. At the primary site, CAFs may enhance metastasis by releasing growth factors and cytokines into the circulation to stimulate, indirectly or directly, the growth and invasive features of cancer cells at a distant site [17-19]. From a biomechanical aspect, CAFs may reshape physical characteristics of the TME by affecting ECM stiffness at primary tumours,

enabling the synthesis of ECM proteins, expression of ECM-remodeling enzymes which consequently enhance cancer cell invasion via epithelial to mesenchymal transition [20-24], and drug resistance through the suppression of drug penetration[25].

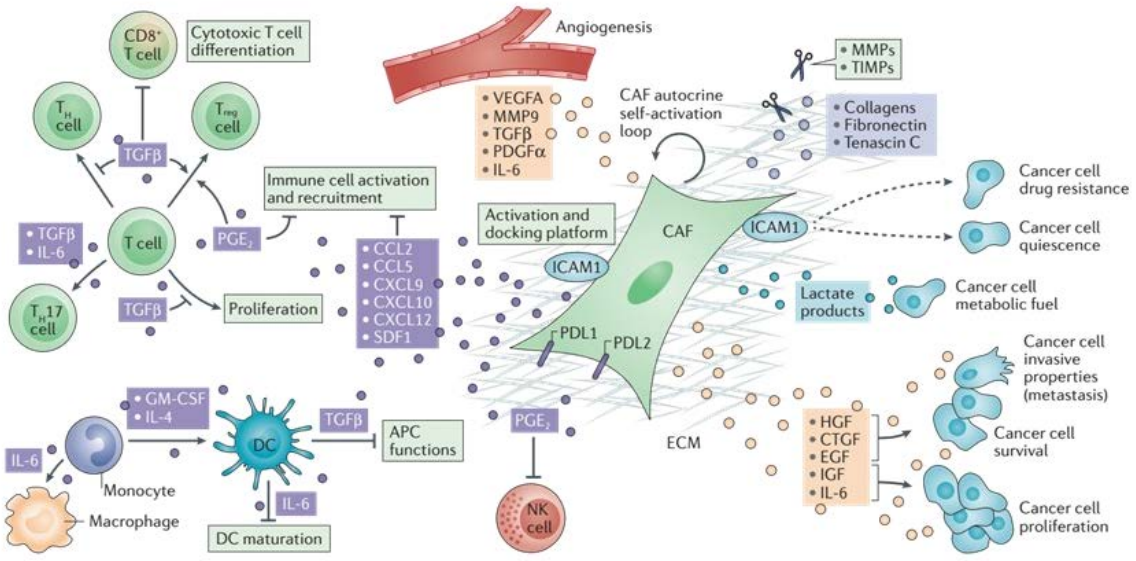

Figure 2: CAFs and their secretome remodel the TME. The extracellular matrix (ECM), together with cellular components of the tumour microenvironment (TME), are actively remodeled and reprogrammed by cancer-associated fibroblasts (CAFs). Secretory functions mediate immune reprogramming (left) and self-sustained activation (middle), and engage cancer cells (right), promoting or restraining their growth, survival or resistance to therapy [16].

1.2.2 CAF and tumour immune suppression

The immunomodulatory functions of CAFs within TME may be direct or indirect. The released secretome from CAFs not only contributes to their sustained activated state during tumour progression but may also dynamically evolve during cancer progression, thus potentially affecting tumour immunity differently at different stages of cancer progression. The CAF secretome has also been implicated indirectly regulating tumour immunity and rewiring tumour immune microenvironment (Figure 2) [16]. Generally, CAFs are considered to promote an immunosuppressive TME in a context depending manner [26, 27]. For

instance, in the hypoxic TME, CAFs interact dynamically with cancer cells, endothelial cells, and immune cells, and this could enhance the complexity of their paracrine signaling responses. Furthermore, most of the in vitro and in-vivo studies suggested CAF immunomodulatory secretomes and immune responses.

Secretion of cytokines, chemokines and pro-angiogenic factors by CAFs in established tumour, including, but not limited to, IL-6, IL-4, IL-8, IL-10, tumour necrosis factor (TNF), TGFβ, C-C motif chemokine ligand 2 (CCL2), CCL5 (also known as RANTES), C-X-C motif chemokine ligand 9 (CXCL9), CXCL10, SDF1, prostaglandin E2 (PGE2), nitric oxide (NO), HGF and human leukocyte antigen G (HLAG) may have direct and/or indirect implications for tumour immunity[28-30]. Based on the in vitro evaluations, CAF production of IL-4, IL-6, and IL-8 may induce immunosuppressive myeloid cell differentiation [31, 32]. Furthermore, CAF-derived CXCL14 affects tumour immunity, mainly through the affecting macrophage recruitment and polarity to the TME [33].

These studies highlight paracrine CAF–immune cell signaling that places their interaction at a central node of control for neoplasia and malignancy [34, 35]. It has also been implied that T cell recruitment involves cytokines that are found in the CAF secretome, such as CXCL9, CXCL10 and SDF1 [36]. Cultured fibroblasts from normal human colons have been reported to express negative co-regulatory immune signals against programmed cell death one ligand 1 (PDL1) and PDL2 impacting on T cell activation [37]. In contrast, in a subset of CAFs positive for a-SMA and FAP derived from tumour specimens with lung and breast cancer, expression of PDL1 and PDL2 may convey an immune-suppressive effect on cytotoxic T cell from an activation state to regulatory state ex vivo [38] where CAF can induce elimination of CD8+ T cells via PDL2 and FASL in an antigen-dependent manner [39].

1.2.3 CAF and drug resistance

A major clinical challenge for cancer therapy is the development of resistance, which re-enables cancer dissemination and metastasis despite therapeutic efforts. Cancer therapy resistance is defined as the progression of a cancer lesion concurrent with an initial response

to therapeutic intervention. Early studies pointed to the role of organ-specific TME for drug resistance, and CAFs have emerged as key players in promoting cancer cell evasion of anticancer therapies [40]. Recently, a stroma-associated gene signature is associated with chemoresistance to 5-fluorouracil, epirubicin, and cyclophosphamide in breast cancer, with a predictive value for response to chemotherapy in the neoadjuvant setting [41], however, numerous studies linked reactive stroma signatures with poor response to chemotherapy indicating CAFs as promoters of resistance to therapy only in an association manner rather than by establishing a causal association.

Continuing efforts to establish such mechanistic connections are ongoing and are naturally of great interest to better harness the therapeutic value of anticancer therapies. Other mechanisms of resistance induced via stroma include the modulation of pathways involving cancer cell–ECM interactions, CAF–ECM adhesion and cytokine- or chemokine-mediated signaling pathways [42, 43]. CAFs may also participate in increased intra-tumoural interstitial fluid pressure, thus indirectly inhibiting penetration and uptake of anticancer drugs[44]. Other studies have suggested that CAF-mediated pro-angiogenic actions and metabolic rewiring of the TME aid cancer cell survival and facilitate escape from therapy-induced cancer control particularly in case of chemotherapy drugs [6, 45, 46]. CAFs may also confer resistance to anticancer drug therapy on cancer cells through soluble factors [43]. In this context, TGFβ, IL-6, and HGF produced by CAFs have emerged as potential drug resistance mediators. TGFβ may induce cell plasticity in cancer cells via epithelial to mesenchymal transition program, enabling their enhanced adhesion to ECM rather than neighboring cells, and CAF-produced IL-6 induces well-studied pro-survival signaling cascades [47]. HGF is also a key modulator of CAF-mediated resistance to various receptor tyrosine kinase inhibitors[48]. CAF-derived HGF was shown to promote resistance in preclinical cancer models treated with BRAF-V600E209 or epidermal growth factor receptor (EGFR) inhibitors [49].

1.3 Tumour Associated Mesenchymal Stem Cells (TA-MSCs)

Multipotent mesenchymal stem cells (MSCs), also known as mesenchymal stromal cells, are a heterogeneous group of progenitor cells that play a vital role in tissue regeneration. The wound healing is the best example of the role of MSCs in tissue regeneration and cellular homeostasis, a complex and dynamic process that involves modulation of tissue inflammation, regulation of cellular proliferation, and differentiation and remodeling of the injured tissue [50, 51]. During this process, inflammatory mediators have been shown to facilitate the recruitment, proliferation, and differentiation of MSCs [52, 53].

Since MSC cells migrated to the wound site, these cells actively integrate into damaged tissues and participate in tissue repair through the alteration in the local inflammatory microenvironment [50, 53], facilitating wound repair activities of intrinsic tissue stem cells via producing immunoregulatory factors, growth factors and chemokines [52]. However, MSCs do not always promote healing, and their properties can change according to the pathophysiological status of the tissue in which they reside [52-54]. A large number of studies have been found that MSCs can migrate to tumour site and evolve into cells like tumour associated MSCs (TA-MSCs) and, depending on TME context differentiate into cancer-associated fibroblasts (CAFs) [55, 56]. These characteristics of MSC cells have recently emerged as attractive targets or tools for anticancer approaches [57, 58].

Growth factors, chemokines, and cytokines produced by TA-MSCs and other stromal cells may also directly confer growth and survival advantages to tumour cells during tumour initiation and progression. For instance, VEGF and neuregulin-1 released from MSCs have been shown to promote tumour growth in xenograft tumour models [59, 60]. In another example, upon intra-tumoural injection of BM-MSC conditioned medium, human colorectal cancer cells exhibited accelerated progression in nude mice.

Moreover, it has also been shown that direct cell-cell interactions between human umbilical cord MSCs and MDA-MB-231 breast cancer cells can significantly induce tumour cell proliferation in mouse models of triple-negative breast cancer [61], although the molecular mechanisms underlying this effect remained to be discovered. Interestingly, in comparison

studies between different sources of MSc (BM-MSCs and AD-MSCs) and TA-MSC, MSCs isolated from patients with ovarian cancer or multiple myeloma were found to have an altered secretome profile of growth factors that specifically promoted tumour growth [62, 63]. Therefore, although much remains to be investigated, the available data suggest an essential role of TA-MSCs in promoting tumour growth. In addition to these, several studies uncovered the role of MSC in developing drug resistance. It has been shown that cellular heterogeneity of the tumour stroma cells, as well as genetic mutations in stromal cells, such as TA-MSCs, associate to potential recurrent tumour growth in patients undergoing chemotherapy and radiotherapy [64].

Furthermore, some recent clinical studies indicated that the proportion of tumour stromal cells in the tumour mass could be key indicator for poor survival prognosis of patients undergoing chemotherapy [64, 65]. Moreover, there is a strong positive correlation between the proportion of tumour stromal cells and tumour growth and invasion [65], and various studies have revealed that MSCs and CAFs can render cancer cells resistant to chemotherapy and radiotherapy both in vitro and in vivo [66, 67].

1.4 T-cells in TME

Evasion and suppression of the host immune system is one of the hallmarks of cancer and a critical step in the malignant progression of incipient tumours [68-70]. This can be achieved through inhibition of various effector immune cells, or via stimulation of immunosuppressive cells. Regulatory T (Treg) cells are another TME cell type that has diverse immune-modulatory functions in cancer cells within TME [71]. At the normal physiological conditions, Treg cells regulate the expansion and activation of T and B cells and play a critical role in maintaining homeostasis of innate cytotoxic lymphocytes and immune balance [72].

Given their complex regulatory roles in response to different environmental stimuli, it is not surprising that Treg cells have diverse effects on tumourigenesis and patient outcome [68]. In some tumour types, including breast cancer and hepatocellular carcinoma, increased infiltration of Treg cells correlates with reduced overall survival [73, 74], while in colorectal cancer, Treg cells are associated with improved survival [75]. In addition to this, Treg cells can suppress tumour-associated antigen presentation, and interfere with cytotoxic T cell

function by inhibiting cytolytic granule release [76]. The mechanisms underlying divergent Treg cell functions in cancer remain elusive. It is not clear that Treg cells exhibit context-dependent functionality, or they encompass multiple subpopulations with distinct functions. Indeed, tumour-associated Treg cell phenotypes are heterogeneous [77], suggesting they likely accumulate by various mechanisms such as peripheral recruitment, the proliferation of cells in the TME, or differentiation of progenitors in response to tumour-secreted factors.

The CD8+ cytotoxic T cells have been shown that play a crucial role in immunosurveillance and immunoediting of various carcinomas [20]. However, recent in-vitro studies have implicated their role in tumour metastasis and local invasion via inducing EMT program in which epithelial cells lost expression of E-cadherin and acquired high expression of the vimentin and ZEB1 [20, 78]. In line with in-vitro results, in-vivo studies shown that CD8+ cytotoxic T cells can induce EMT on breast cancer cells via the generation of breast cancer stem cells [79, 80]. They suggested that IL-6, TNF and TGFβ released by activated effector T cells may facilitate this process.

1.5 Tumour associated blood vasculature

Solid tumours that have grown beyond a few cubic millimeters require to induce tumour angiogenesis and vascular network, to receive nutrients for their high energy demand and growth [81]. In 1971, Judah Folkman published a revolutionary article proposing that all tumours are angiogenesis-dependent [82], initiating a paradigm shift throughout the cancer research community despite initial resistance. Angiogenesis is now accepted as a hallmark of cancer in response to a growing need for oxygen and nutrients from the bloodstream, without which tumours would succumb to dormancy [2]. Tumour vascularization requires co-operation of multiple TME cell types, including vascular endothelial cells (which form tight adhesions to ensure vessel integrity), cancer-associated fibroblasts (for releasing a plethora of pro-angiogenic signals into the TME including FGF, IGF, VEGF and ECM remodeling cytokines), tumour-associated mesenchymal stem cells, pericytes (for vessel converging and vessel maturity), and BM-derived precursor cells [81, 83-85]. Recent studies showed that the morphological and functional abnormality of tumour vasculatures mediated by tumour

stromal cells contribute to the immune suppressive microenvironment (via inducing killing of effector T cells) within solid tumours and drug resistance [83].

Lymph-angiogenesis is another mode of vascularization in tumours, and lymphatic vessels and nodes represent an alternate route for cancer cell dissemination and tumour cell dormancy [86, 87]. It has been shown that M2 macrophages produce VEGF-C and VEGF-D, which correlates with peritumoural inflammation and lymph-angiogenesis in human cervical cancer [86, 87]. Besides macrophages, myeloid cell populations also have critical influences on lymphatic endothelial cells (LECs), by modulating their signal transduction and transdifferentiating into functional LEC-like cells 84. In a study performed on a mouse model of cancer, presence of VEGF-C and heparanase mediated myeloid cell incorporation and trans-differentiation into LECs [88].

1.6 Extracellular Matrix (ECM)

Beyond the contributions of specific cell types of TME to tumourigenesis, the ECM can limit cancer initiation at early stages and drive disease progression towards malignancy at elderly stage [89]. Indeed, the composition of the extracellular TME is a significant predictor of clinical prognosis. In breast cancer, tumours can be stratified into four subclasses based strictly on ECM composition, which is predictive of patient outcome [90]. Tumours with high expression of protease inhibitors such as serpin family members in their ECM are associated with good prognosis, while tumours with high expression of integrins and MMPs correlate with poor prognosis and risk of recurrence [90].

Beside composition of ECM, stiffness of ECM can regulate tumour invasion, metastasis and drug resistance [91-94]. Recent studies showed activation of EMT program on cancer cells cultured in ECM with high stiffness feature which mostly observed in late stages of tumour progression [95]. Additionally, a positive correlation between activation of stemness program via expression of CD133 and CD44 and drug resistance with ECM was observed in metastatic breast cancer treated with Cetuximab [95]. Moreover, ECM stiffness regulated via tumour stromal cells can inhibit penetration of immune cells and chemotherapy agents into TME [96-98].

1.7 Importance of modeling TME

Each tumour is associated with a heterogeneous tumour microenvironment, which can significantly affect the response to therapy and clinical outcomes. However, the use of gene-drug association (see Glossary) treatment strategies may be limited due to a lack of biological understanding of tumour response to drugs [3, 99]. In other words, detecting mutations (e.g., EGFR or PIK3CA mutations) matched with approved, targeted drugs (e.g., EGFR and PIK3CA inhibitors) does not necessarily mean that the molecular alterations in these pathways are sensitive to the selected therapy [3, 100]. In the field of personalized cancer medicine, the link between functional genomics and pathological data to patient outcomes is the main challenge. To tackle this challenge, different tumour models have been proposed, including cancer cell lines, patient-derived xenografts (PDXs), and 3D culture tumour models, such as organoid culture methods.

1.7.1 Conventional Models of TME

The initial results of in vitro tumour modeling were obtained from tumour-derived cell lines due to their high-throughput capacity for pharmaceutical drug screening [101]. However, there is evidence showing the limitations of cancer cell lines, such as the lack of tumour and stromal cells, and interactions between the cells and the extracellular matrix (ECM) [66]. Also, cancer cell lines lack immune–tumour cell interactions in vitro, whereas immune cells can dramatically alter the efficacy of cancer therapies in patients. Thus, available cancer cell lines have primarily failed to model a tumour microenvironment to evaluate new targets and chemotherapy medicines [102]. After the emergence of 3D cultures, partial mimicking of the tumour microenvironment allowed researchers to test the functionality of drugs or evaluation of chemoresistance in the presence of cell-cell and cell–ECM interactions in a 3D architecture [103]. Nonetheless, these methods also face several limitations and have so far failed in applications to personalized tumour modeling.

Conventional 3D tumour models, known as tumour spheroids, can be generated from single-cell types of cancer cell lines (homotypic spheroids) or co-cultured with other cell types

(heterotypic spheroids). These models have a series of challenges that limit their applications as preclinical tumour models. These challenges include variations in 3D culture methods, lack of immune cell interactions in the culture, and inability to fully mimic the tumour microenvironment in terms of cell types and their spatiotemporal architecture [104]. In terms of gene expression profiles, the comparison between original tumours and corresponding cell line-based tumour spheroids has shown significant differences, where common mutations can be observed in cancer cell lines, whereas rare mutations are not preserved. Thus, cell line-based models are unable to imitate the complete genomic background of tumours and, consequently, the drug response of targeted therapy agents [105].

1.7.2 Organoid culture technology

Organoids are 3D cell cultures that preserve numerous key features of the represented organ. The organoids contain multiple and organ-specific cell types with a spatial architecture similar to that of the corresponding organ. These models can recapitulate some key functions of that organ. Organoids may be generated from one or a few cells derived from primary tissue samples, adult stem cells, the directed differentiation of pluripotent stem cells, or tumour specimens [106-108]. Tumour organoids are 3D cultures of cancerous cells that can be derived from tumour tissues for better mimicking the cellular and molecular heterogeneity of a tumour in the body [107-112]. The first organoid culture was reported in murine intestinal cells, further developed for other organs, and eventually translated into human cells [113]. These features of organoids made them useful tools for cancer research and therapy for in vitro and clinical studies [114].

In patients with resected tumours, multiple organoids can be generated from different areas of the tumour to better mimic tumour heterogeneity [115, 116]. Tumour organoids show tremendous potential for modeling specific cancer subtypes that have unique genomic mutations [117]. Taken together, these key findings suggest that this new model has great potential in modeling tumour microenvironment and the response of tumour cells to anti-cancer drugs in an in-vitro setting. Recent pre-clinical and clinical studies highlighted potential application of tumour organoids in prediction of chemotherapy and targeted therapy agents [3, 118].

Despite the advantages of tumour organoids, numerous challenges may hamper the implementation of this approach in modeling a complex tumour microenvironment similar to the original TME. Challenges include the lack of immune system elements, other essential stromal cells such as CAFs and TA-MSCs, and vasculature network in tumour organoid cultures. These can restrict functional testing of immunotherapy drugs or stromal targeted agents on tumour organoids, leading to development of a complementary tool and advanced model of TME.

1.7.3 Microfluidic technology for modeling TME

Microfluidics is the science of manipulating fluids in sub-millimeter channels. This method can control several parameters, such as relative cell and tissue location, fluid flow levels and patterns, mechanical cues, and gradients within a system [119]. The advantages of this technology include (i) smaller sample and material requirements, (ii) enhanced quality of microscopic imaging and quantification of cells, (iii) control over experiments, (iv) low cost of production, (v) the possibility of a targeted design, and (vi) co-culturing various cell types in a dynamic fashion (Figure 3).

These advantages make microfluidic technology a complementary tool for other platforms. A complex tumour microenvironment can be created with the support of this technology and by determining different cell regions [120]. Microfluidic technology can be used to model different aspects of TME, such as the metastatic microenvironment [120], immune–cancer cell interactions [121], modeling vascular network formation, and specific behavior of cancer cells [122-125].

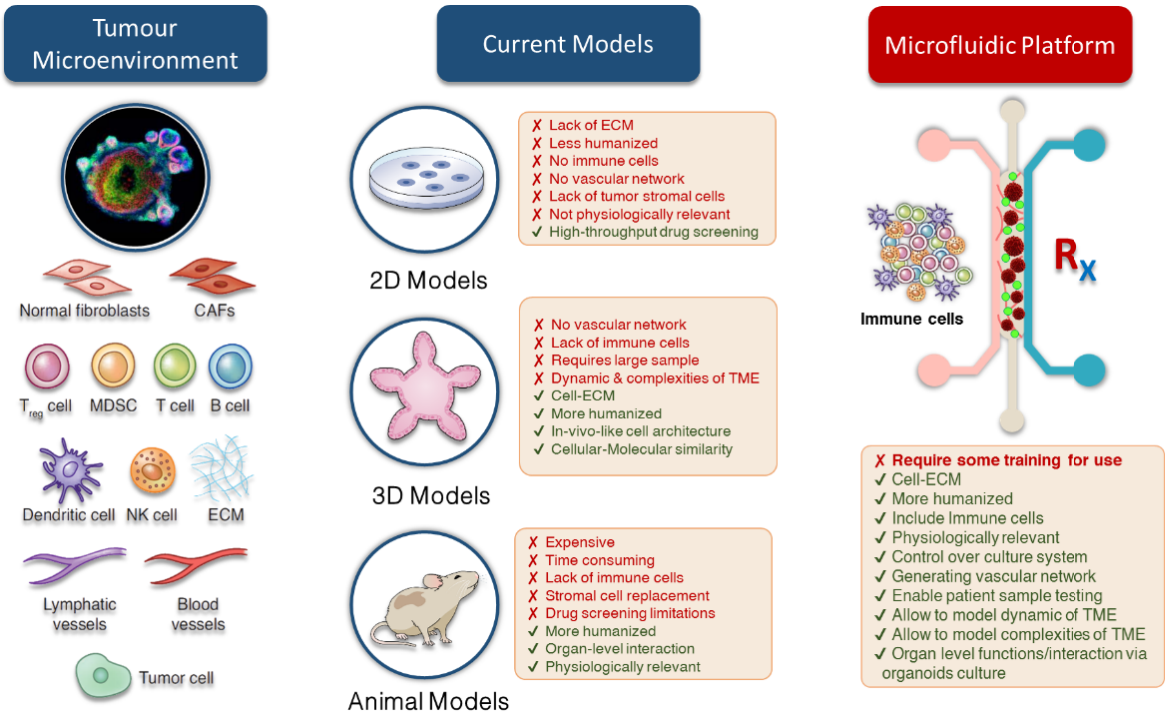

Figure 3: Comparison of microfluidic technology with conventional in-vitro and in-vivo models. The microfluidic system shows number of advantages over other models. Besides these, the possibility of direct culturing patient derived tumour sample into this system allows us not only to preserve TME, but also develop a reliable and more humanized model.

1.8 Conclusion

In this chapter, I explained the importance of the of TME and its components, during my thesis I attempted to address couple of burning questions around TME in cancer particularly breast cancer. Initially in the chapter 2, I look at the landscape of model and works around the TME. As immunotherapy revolutionized the treatment of cancer, In chapter 3, I did comprehensive in-silico data analysis based on the clinical, genomic and transcriptomic data from The Cancer Genome Atlas (TCGA) and other publicly available datasets to figure out the role of stromal cells in tumor immunity of TME in breast cancer and how targeting these

population of the cells accelerate efficacy of immunotherapy in one of the worse sub-type of breast cancer known as triple-negative breast cancer. Additionally, I showed link between tumor stromal cells activity, tumour immunity and epithelial-mesenchymal transition (EMT) in breast cancer. Using gene-drug association analysis and drug repurposing analysis, I identified a potential agent that able to effectively target CAFs and other stromal cells. In Chapter 4, I studied the role of the CAFs in immunotherapy using 3D microfluidic model of cancer cells-CAFs and demonstrated the effect of anti-fibrotic drug on CAFs activity and reduction of immune-suppression for the first time in breast cancer. In chapter 5, I looked at another angle of TME, the role MSC in TME and their role in immunotherapy. Given immune-modulatory role of MSC, I showed that these cells positively regulate immune-suppression through the secretion of various cancer-promoting and immune-suppressive cytokines in which targeting MSC reverse immunity by reduction of proportion of immune checkpoints. Following these studies, in chapter 6, I focused on modeling tumor initiation and the role of CAFs in tumor formation in microfluidic device using organotypic tumor spheroids that include CAFs. Moreover, I showed that targeting CAFs not only reduce tumor spheroid formation but also inhibit initiation of epithelial-mesenchymal transition. Given the role of matrix stiffness regulated by CAFs in tumor formation and metastasis, In Chapter 7, I highlighted that ECM stiffness can induce the expression of immune checkpoints in breast cancer. Finally, in chapter 8, I focused on developing vascularized tumor organoids in device for the purpose of the study of immune infiltration in microfluidic device. However, the completion of this chapter had been extremely affected by Covid-19 pandemic which warrant future works and efforts.

Collectively together, using microfluidic platform, this thesis presents together various critical novelties to address challenges and questions are remained to be resolved in the context of modeling and targeting TME including:

- Comprehensive in-silico data analysis on TME of TNBC at the single-cell level and highlighting role of tumour stromal cells in the stimulation of immune-suppression.
- Discovery of a potential therapeutic agent to target tumour stromal cells in TNBC using drug repurposing and gene-drug association studies.
- Modeling tumour stromal cells and cancer cell interaction using dynamic and static microfluidic devices.
- Exploring how tumor stromal cells rewire TME and cancer cells using paracrine factors.
- Introducing for the first time the potential application of pirfenidone in targeting tumor stromal cells and restoring immune response in TNBC by reducing immune checkpoints expression and increasing immune cells infiltration.
- Highlighting the effects of pirfenidone in reducing invasion, progression and stemness feature of cancer cells through targeting activity of tumour stromal cells.
- Developing 3D micro-vasculature and organotypic vasculature in microfluidic device.

Chapter 2

Literature Review

Summary:

This chapter summarizes the application of various microfluidic platforms in the study of cancer from several aspects and highlights numerous challenges in the study of TME. Part of this chapter has been published as Book Chapter *.

*Azadi, Shohreh, Hamidreza Aboulkheyr Es, Arutha Kulasinghe, Pritam Bordhan, and Majid Ebrahimi Warkiani. "Application of microfluidic technology in cancer research and therapy." In Advances in clinical chemistry, vol. 99, pp. 193-235. Elsevier, 2020.

1.1 Application of microfluidic device in modelling cancer biology and metastasis

Metastasis results from a complex and multi-step process which initiates with the formation of primary tumours followed by proliferation of cancer cells [126]. Upon tumour growth, some cells in the primary tumour undergo processes such as epithelial to mesenchymal transition (EMT) and several genetic alterations which lead to breaching of the basement membrane and entering into the blood or the lymphatic system in the intravasation process. These circulatory tumour cells (CTC) further flow through the human body and experience shear stresses, high velocities, and immune-surveillance. Some cells with higher metastatic potential can survive this condition and extravasate into distant tissues. Ultimately, if they find a suitable environment for colonization, form the secondary tumour/re-seed at the primary site [126-129].

The process of metastasis is driven by different chemical, mechanical, and genetic factors which determine the specific target organ for the formation of secondary tumours. For example, breast tumour cells preferentially invade to the bone tissue, while lung tumour cells prefer to invade to the brain tissue [130-132]. This selective invasion suggests a complex process affected by various components of tumour microenvironment (TME), cellular interactions, mechanical cues, and chemical gradients. All these factors need to be considered to achieve a comprehensive analysis of the metastatic cascade. Despite the recent progress in the field of cancer modelling, current models still lack incorporating the full complexity of the metastatic process.

Initially, cancer modelling was assessed using 2D approaches [133-135]. These methods could not provide the complexity of TME and changed to more complex trans-well-based assays such as Boyden chamber. Usually, in these assays, cancer cells migrate and invade from one side of the chamber through a porous membrane or a thin layer of the biological matrix to the other side of the chamber [136, 137]. The membrane is pre-coated with extracellular matrix (ECM) molecules such as collagen, fibronectin, and laminin. Moreover, this assay can be used to investigate cancer cell-endothelial cell interaction through the

formation of a confluent layer of endothelial cells before introducing cancer cells to the chamber [138]. Although trans-well-based methods extensively have been used to model tumour cell migration, these semi-quantitative methods do not provide the complexity of TME, specifically in terms of mechanical cues.

To overcome the above-mentioned limitations, microfluidics devices have been developed to model cancer metastasis in a more accurate environment [139, 140]. Microfluidic models significantly improved physiologically relevance of the microenvironment and quantitative measurements of the metastasis models. These models enable incorporating multicellular structures, cell-cell interactions, and chemical and mechanical features of TME in a single chip. Moreover, these models provide single cell analysis and real-time monitoring of processes which enable the assessment of specific signaling pathways. Several review papers have described cancer modelling techniques using a microfluidic approach [140-144].

Here, we briefly describe the microfluidics methods used to model the metastatic process. Firstly, we review the various devices which have been successfully utilized for modelling of tumours in 2D and 3D environments. Furthermore, the application of the microfluidic devices in modelling different steps of the metastatic process and influential factors including tumour growth, angiogenesis, TME, migration and invasion are presented.

A complex model of metastasis should incorporate multiple cell types including cancer cells, endothelial cells, immune cells, stromal cells, ECM components (e.g. collagen), biochemical and biophysical cues. Generally, microfluidic device configurations for cancer modelling can be categorized into five groups as shown in figure 1 including 2D devices, lumen chips, 3D devices, Y-shape chips, and trans-well chips [140-142, 144]. Besides this categorization, other specific designs have been introduced by several groups [145, 146]. These configurations vary in terms of controllable parameters, in providing 2D or 3D environment, the possibility of multiple cell type co-culturing and read-out methods.

The first configuration consists of two main parallel microchannels which are connected with several interconnecting microchannels usually with a diameter of 3-10 μm (Figure 1A) [128, 147-150]. This design, which is known as a 2D device, is often used to study the migration of cancer cells in a specific chemical gradient. Cancer cells are cultured in one of the main

channels and start migrating to the other channel by exposing to a chemical gradient. In one study, the device was used to model and generate the oxygen gradient of TME [151]. Moreover, this design can be used for co-culture of cancer cells and other cell types to monitor migration and viability of cancer cells under co-culture condition [149]. Cell deformation through the narrow interconnecting channels also had ben probed through this model [150].

The second design is a lumen chip which provides a model of blood vessel for the cancer cells while surrounded by a suitable ECM (Figure 1B, C) [152-154]. In other applications, this design can be used to tightly pack cancer cells for the formation of multicellular aggregates and cancer spheroids. For example, Tien et al. used a similar device to probe the effect of elevated pressure on the invasion of 3D aggregates of breast cancer cells [154]. They used a polydimethylsiloxane (PDMS) channel filled with collagen to form cancer aggregates.

While the first and second configurations still lack a physiologically relevant microenvironment, the third design successfully overcame these limitations. This design usually consists of three parallel channels, which are connected to each other through some empty space between channels (Figure 1D) [140, 144, 155, 156]. The specific design of the chip is related to the array of blocks, which separate the device into three channels, while keeping cell-cell signaling and cellular movements. Presence of these blocks increases the surface tension in the central channel, which leads to confinement of biological matrix solution (e.g. collagen, Matrigel) in the central channel. The device usually is used for 3D culture of cells in the central channel while 2D culture is also possible through the side channels. Different cell types can be incorporated into the central and side channels to mimic intravasation, extravasation angiogenesis, TME condition, and cell-cell interactions [156-158]. Moreover, adding extra channels to the main design provides the possibility of culturing several cell types in a 3D environment and modelling the metastatic process [159, 160]. The device is versatile and controllable which provides the possibility of introducing flow to the model in a controlled manner.

The fourth design is called a Y-shape chip. This design is an example of co-flow devices consisting of two channels which merge together. Two different types of cells can be

introduced to the microchannels through separate inlets and meet in the interface [161, 162]. One successful example of this device is related to the co-culture of mammary ductal carcinoma cells and fibroblasts [162]. The presented model demonstrated the transition of ductal carcinoma in situ (DCIS) to invasive ductal carcinoma (IDC) in the presence of fibroblasts which is a critical step in breast cancer progression.

The last model, transwell chip, is one of the most complex designs in modelling cancer metastasis and the TME. This multi-layer device consists of microchannels separated by a porous ECM-coated membrane (figure 1E, F) [163-166]. The device is run with two different configurations. In the first configuration, cancer cells and organ-specific epithelial cells are cultured in the upper channel, while other stroma cells and fibroblast are cultured in the lower channel. This configuration can be used to model the initial tumour growth in a more physiologically relevant environment. Choi and co-workers used this method to replicate the microenvironment of breast cancer tissue. They co-cultured breast tumour spheroids with human mammary ductal epithelial cells and mammary fibroblasts in a compartmentalized transwell microfluidic device and explored the potential of the system as a drug screening platform (figure 1E) [164]. The second configuration aims to model cancer invasion. In this configuration, cancer cells and organ-specific epithelial cells are introduced to one channel, while endothelial cells cover the other channel. By introducing chemical cues to the endothelial channel, cancer cells can migrate through the porous membrane and endothelial junctions to enter the second channel [165, 166]. Adding extra hollow side chambers makes the device flexible for stretching and relaxing (figure 1F), which can be used to mimic TME mechanical cues in a lung cancer model. This model successfully utilized for monitoring the responses of lung tumour cells to tyrosine kinase inhibitor (TKI) agents including Erlotinib and Rociletinib [163].

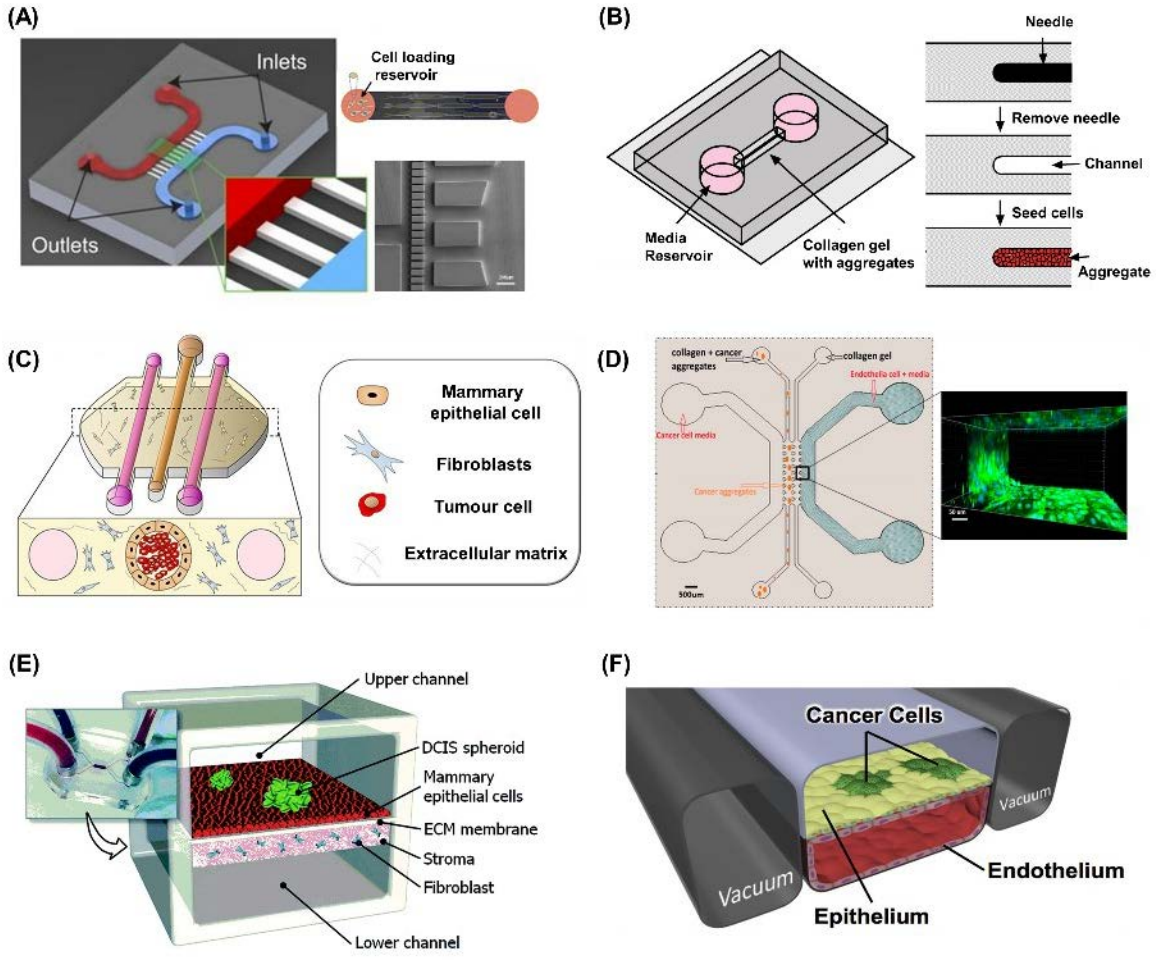

Figure 1. Different configurations of microfluidic devices in cancer modelling. (A) 2D design with two parallel channels and several interconnecting channels for investigating cellular interactions, migration, and cell deformability [128, 149, 150], (B) Lumen chip design for formation of cellular aggregates [154], (C) Lumen chip design for providing a vessel like structure [153], (D) 3D design with three parallel channels for providing a 3D ECM-like structure and cancer cell-endothelial cell-co-culture. The confocal image displays the endothelial monolayer at the interface of channels [140], (E) Transwell design for co-culturing breast tumour spheroids with human mammary ductal epithelial cells and mammary fibroblasts [164], (F) Modified Transwell design by adding extra hollow side chambers for making the device flexible for stretching and relaxing [163].

1.2 Modelling Tumour growth

Tumour growth models have been developed to mainly probe how TME conditions and cell-cell interactions affect the growth of various types of tumours [167-169]. In these models, co-culture or tri-culture of cancer cells with other cell types including normal epithelial cells, fibroblasts, endothelial cells, and immune cells provide a more accurate physiological environment for tumour growth and proliferation. Moreover, tumour growth on chip models can be used for drug screening applications by assessing the effect of various drugs on the tumour growth and survival. In recent work, Hassell et al. used a transwell tri-culture microfluidic model [163]. They cultured lung cancer cells on a layer of epithelial cells in the upper chamber, while endothelial cells covered the lower chamber. The cancer growth and responses to TKI therapy were probed in the presence of mechanical cues mimicking breathing motions (figure 1F) [163]. In another study, an integrated microfluidic-3D device was used to create a physiologic environment for breast cancer cells containing stromal cells, fibroblasts, and different ECM molecules (collagen, fibronectin, laminin). In this study, the morphology and proliferation of breast cancer clusters were monitored which resulted in higher metastatic capacity of cancer clusters compared to single cells. Additionally, they used different composition of ECM and found that fibronectin-rich ECM increases tumour growth [169].

1.3 Modelling cancer cell-endothelial cell interactions

Endothelial cells play an important role in the metastasis cascade through two distinct mechanisms, angiogenesis and vasculogenesis, which implement the formation of the vascular network in the tumour. Angiogenesis is the outgrowth of exciting capillary vessels which is a necessary step to change lesions from hyperplasia to neoplasia [140, 170]. Angiogenesis not only occurs in the first step of the metastasis process and tumour growth but also during transmigration of cancer cells in intravasation and extravasation steps. Vasculogenesis is assembling of singular endothelial cells into functional microvessels [140, 170].

Both angiogenesis and vasculogenesis are induced upon tumour growth to deliver sufficient nutrient and oxygen to cancer cells [170]. Different chemical and mechanical cues from TME involve in the initiation of these two processes. Signalling interactions between cancer cells and endothelial cells play a critical role in successful invasion of cancer cells to the vasculature. It has been shown that cancer cell-endothelial cell interactions change the characteristics of both cell types and facilitate the metastasis process [157, 171, 172]. For example, it has been demonstrated that the permeability of the endothelium layer changed in the presence of cancer cells [157], and endothelial cells exhibited a faster proliferation in co-culture with cancer cells [173]. Moreover, cancer cells can easily migrate upon the formation of endothelial pathways through both angiogenesis and vasculogenesis processes. All these findings suggest that a systematic model of tumour on-chip cannot be achieved without considering cancer cell-endothelial cell interactions. Several papers have reviewed modelling this interaction using microfluidic platforms [172, 174].

Several groups attempted to recreate both angiogenesis and vasculogenesis using engineered microvessels (figure 2A, B) [157, 173, 175]. To present a model of angiogenesis, firstly the formation of a confluent layer of endothelial cells which can be extended to new capillaries has been considered [173]. 3D devices have been extensively used for this approach. In these devices, endothelial cells are cultured in the side channel to cover the gel-fluid interface and form a confluent layer. The channel represents a vessel wall and is used to model intravasation, extravasation, and angiogenesis in three different configurations which are described as follows.

In the first configuration, cancer cells are embedded into the collagen and loaded to the central channel, while endothelial cells are introduced to the side channel to form a confluent layer. Upon the formation of endothelial layer, and the presence of chemical gradients, cancer cells can migrate through EC junctions to inter to the side channel (figure 2C) [171]. Moreover, loading tumour angiogenesis factors will result in the extension of capillary sprouts from the side channel toward cancer cells [173]. This method has been used successfully to model intravasation of cancer cells [143, 157]. Zervantonakis et al. recreated the tumour-vascular interface in three-dimensions and showed that biochemical factors from the interacting cells and cellular interactions with macrophages mediate intravasation of

tumour cells [171]. In other work, Bersini and co-workers used a three-channel device to model intravasation of cancer cells in a bone-mimicking environment. Their tri-culture system consisted an osteo-cell conditioned microenvironment with human osteo-differentiated bone marrow-derived mesenchymal stem cells and cancer cells in the gel region, while endothelial cells were cultured in the side channel [176]. This approach was further used by Jeon and co-workers to monitor organ-specific extravasation of breast cancer cells (figure 2D) [175]. Several other studies used the same approach to investigate cell-cell interactions [177].

In the second configuration, collagen is loaded to the central channel, while endothelial and cancer cells are cultured separately in the side channels. By introducing angiogenesis factors in the cancer cell channel, endothelial cells initiate angiogenesis toward cancer cells (figure 2A) [173]. Usually, fibroblast and stromal cells are used to secrete angiogenesis and vasculogenesis factors. Kim and colleagues introduced a multi-channel device and successfully modelled both angiogenesis and vasculogenesis in the presence of endothelial cells, fibroblasts, and cancer cells (Figure 2F) [173]. In their more recent work, they developed a microfluidic 3D in vitro model to investigate the role of interstitial flow (IF) during vasculogenesis and angiogenesis. They showed that IF significantly facilitated the vasculogenesis regardless of the flow direction, whereas its effect on the angiogenesis depends on the flow direction [160].

In the third configuration, collagen is loaded to the central channel, while endothelial cells are loaded to the side channel. Upon the formation of a confluent layer of endothelial cells, cancer cells enter into the same channel. This method has been used to model extravasation of cancer cells (Figure 2E) [155]. Cancer cells attach to the endothelial cell layer and transmigrate through endothelial cell junctions to enter into the collagen. Jeon et al. developed a microfluidic system to mimic tumour cell extravasation by transmigration of cancer cells across an endothelial monolayer into a hydrogel [155]. They examined the permeability of the endothelial layer in the presence of cancer cells and concluded that cancer cells increase the permeability of endothelial layer and extravasate to the biological matrix generally within 24 hours of cancer cell-endothelial cell co-culture [155]. Several other studies used the same approach to model extravasation of cancer cells in the presence of

different chemokines [178, 179] and tumour secreted factors [180].

Modelling vasculogenesis is a more challenging process. 3D microfluidic devices demonstrated great potential in modelling vasculogenesis. In this approach, multiple dispersed endothelial cells are embedded in an appropriate matrix such as collagen, Matrigel, or combination and loaded to the central channel. By introducing vasculogenesis factors, endothelial cells self-assemble into a network composed of functional perfusable capillaries with different length and diameter (figure 2 B) [173]. This model has been utilized to provide an accurate 3D environment for both endothelial and cancer cells. Cancer cells can be either loaded with collagen before the formation of capillaries to model intravasation, or after the formation of the capillaries to model extravasation.

This vasculogenesis model is powerful in live observation of events in the single cell level. Chen at al., used a 3D device with three separate gel-regions. They introduced human umbilical vein endothelial cells (HUVEC) to the central gel region, while two other gel regions were used for normal human lung fibroblasts (NHLF)-embedded gels. After the formation of the vascular network, cancer cells were introduced to the system to mimic the extravasation process. They investigated the role of tumour integrin β1 (ITGB1) in the extravasation and revealed a critical requirement for ITGB1 in several steps of this process [181]. Furthermore, this model extensively has been used for the organ-specific extravasation of cancer cells [182] and found that the underlying mechanism of extravasation could be related to cell adherence to vessel walls or trapping into the capillaries [159]. Recently a modified 3D device was used to probe the effect of tumour-associated macrophages (TAMs) and interstitial flow in the invasion of cancer cells in a vascularized environment [183]. Nagaraju and co-workers also proposed a novel 3D microfluidic platform comprised of concentric three-layer cell-laden hydrogels to investigate the breast cancer cell invasion and intravasation in a vascularized environment [184].

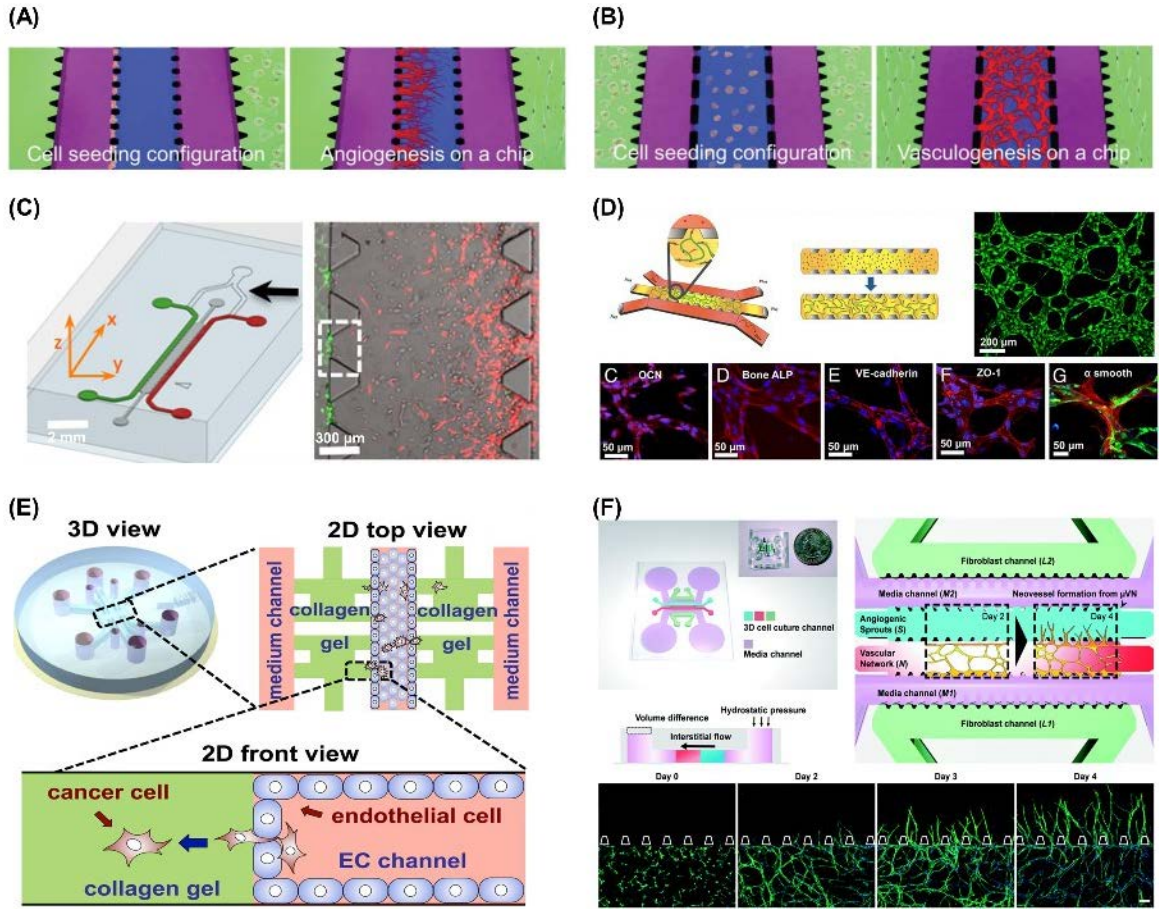

Figure 2. Modelling angiogenesis and vasculogenesis (A) A model of angiogenesis on-chip, endothelial cells are loaded to the side channel [173], (B) A model of vasculogenesis on-chip, endothelial cells are embedded into the biological matrix [173], (C) Forming a confluent monolayer of endothelial cells in the side channel to model intravasation [157], (D) Organ-specific extravasation of breast cancer cells in vascularized bone-mimicking microenvironment [182], (E) Formation of an endothelial monolayer to model extravasation of breast cancer cells [155], (F) Simultaneous modelling of angiogenesis and vasculogenesis on a modified 3D chip [160].

1.4 Modelling the tumour microenvironment (TME)

The tumour mass consists not only of a heterogeneous population of cancer cells but also a variety of resident and infiltrating host cells, secreted factors and extracellular matrix

proteins, collectively known as the tumour microenvironment (TME). TME cues have been demonstrated to play a pivotal role in the different stages of the tumour progression and metastatic cascade. TME cues can be characterized into three parts including biochemical factors, biomechanical factors, and TME cellular components, which are discussed in this section. Investigating the effect of these cues in a microfluidic model of cancer is challenging but essential to understanding the underlying mechanisms involved in metastasis. Current microfluidic platforms have emerged as a powerful tool to model TME parameters in a controlled manner.

1.4.1 Biochemical cues

TME undergo various alterations, which result in a change in pH, oxygen level, and chemokine gradients. Hypoxia is a low oxygen condition which occurs in the TME and affects angiogenesis, cell survival, EMT, and invasion [128]. Several studies used a microfluidic approach to model TME in terms of pH and oxygen level [147, 151, 185, 186]. Chen and colleagues generated oxygen gradients in a microfluidic device using spatially confined chemical reactions. They cultured A549 lung carcinoma cells with an anti-cancer drug (Tirapazamine, TPZ) under various oxygen gradients and demonstrated the hyperoxia-induced cell death and hypoxia-induced cytotoxicity of TPZ [151]. Moreover, Wang and co-workers studied tumour cell–drug interactions in a dynamic hypoxia microenvironment. They used two antitumour drugs (Tirapazamine and Bleomycin) and two tumour cell lines (human lung adenocarcinoma A549 cells and human cervical carcinoma HeLa cells). Their results indicated the dose-dependent antitumour effect of the drugs and hypoxia-induced cytotoxicity of TPZ [147]. In another study, Acosta et al. used a 3D two-layer microfluidic platform to model the migration of cancer cells under hypoxia condition. They probed that cancer cell invasion was a function of oxygen concentration. Cancer cells which maintained under 1% oxygen in the device showed increased migration, suggesting that hypoxia induces a more aggressive phenotype [186].

1.4.2 Biomechanical cues

Effect of TME is not limited to the biochemical cues. Mechanical signals play an important role in inhibiting or promoting cancer invasion through different mechanisms. Mechanical signals affect both the direction that migration of tumour cells occurs and the degree of invasiveness. TME biophysical cues include flow signals and ECM biophysical properties, which are discussed below.

Generally, there are two kinds of flow that can be found in TME including interstitial fluid flow (IFF) and intramural flow [187]. It has been shown that interstitial fluid pressure (IFP) increased by tumour progression leads to the formation of IFF [187]. These changes help cancer cells to migrate easily toward the desirable locations e.g. circulatory system. Effect of IFF in the invasion and migration of cancer cells has been investigated previously by several groups [187-189]. Besides IFF, intramural flow is also important and determines the survival of circulating cancer cells under the applied flow-stress. Moreover, this flow is important in determining the attachment and transmigration of cancer cells during the extravasation process. One study showed that fluid shear stress induces cancer stem cell-like phenotype in breast cancer cells [189]. Polacheck et al. investigated the effects of interstitial flow and fluidic stress on the cell migration and demonstrated that there is a force balance between fluid drag and matrix adhesion tension on the cells which control their migratory behaviour [190]. A microfluidic platform was also developed which allowed for the introduction of both intramural flow and IFF at the same time. This device showed great potential to model tumour cell invasion and transmigration in the presence of both flow types [191].

ECM biomechanical properties which modulate cancer migration and invasion have been studied in terms of ECM porosity, stiffness, and topography. Microfluidic devices have demonstrated great potential for modelling ECM biophysical properties. Collagen and Matrigel are often used to present a 3D biological matrix [192]. The studies revealed that matrix alignments promote directional cell migration. Additionally, by changing the matrix composition (e.g. collagen or Matrigel) and concentration, the effect of both stiffness and porosity of ECM in the invasion of cancer cells has been examined using a microfluidic approach [192]. Carvalho et al. examined both fibrin hydrogel and Matrigel as a biological

matrix in a 3D microfluidic device. They demonstrated that the mechanical properties of ECM affect the extravasation of colorectal cancer cells [193].

1.4.3 Cellular components of TME

Heterotypic interaction of cancer cell with other cell types including stromal cells, endothelial cells, and immune cells play a critical role in the invasion of tumour cells to surrounding matrix and further to the secondary site. Stromal cells as the main cellular component of TME significantly affect the migration and invasion behaviour of cancer cells. Many studies have emphasized the importance of TME in terms of cellular components [128, 139, 194]. Microfluidic models allowed for the integration of multiple cell type with biochemical and biophysical properties of TME in 2D and 3D environment which led to better mimic of in vivo condition.

Several studied probed the role of carcinoma-associated fibroblasts (CAFs) in invasion and migration of cancer cells. A 3D co-culture device has been used to investigate the effect of CAFs on the invasion of salivary gland adenoid cystic carcinoma (ACC) cells. It was observed that CAFs promoted ACC cell invasion in a 3D matrix in a spheroid fashion, and MMP inhibitors successfully decreased this invasion [195]. Hsu and colleagues used a 2D three-chamber device and tri-cultured fibroblast, macrophages, and lung cancer cells. They probed that paracrine signalling from tumour stroma affects the cancer cell invasiveness. In this study, lung cancer cells induced transformation of fibroblasts to myofibroblasts. Moreover, they showed that the combination of macrophage conditioned medium and myofibroblast conditioned medium resulted in a significant increase in lung cancer cells' migration speed [196]. Bischel and co-workers used a three-dimensional lumen structure and demonstrated that mammary fibroblasts induced the invasion of ductal carcinoma in situ (DCIS) of breast cancer cells [197].

In another study, a 3D co-culture device was used to investigate the role of pancreatic stellate cells (PSCs), a major component of the tumour microenvironment in pancreatic cancer, in the migration and drug resistance of pancreatic tumour spheroids. This study showed that the

number of tumour spheroids increased in co-culture conditions. Moreover, the co-culture conditions demonstrated an increase expression of α-SMA and EMT-related markers [198]. A recently published review paper highlighted the vital role of EMT in cancer progression through inducing treatment resistance, decreasing sensitivity to chemotherapeutic agents, inducing the stemness features, upregulating the angiogenesis factors and immune checkpoints across many cancer types [199].

The immune cells are one of the key components of the TME. Investigating cancer cell-immune cell interaction has been accelerated in recent years due to the great potential of the immune cells to be involved in both attenuation and promotion of cancer. Several studied identified different cellular and molecular interactions from the immune side which lead to the development of metastatic cascade [121]. These findings resulted in significant progress in understanding the underlying mechanism of immune cell function and cancer immunotherapy. Zervantonakis et al. used a 3D microfluidic chip to investigate intravasation of cancer cells in the presence of macrophages. They demonstrated that the permeability of endothelial layer changed in the presence of macrophages led to intravasation of cancer cells [200].

More recently, the effect of monocytes on tumour cell extravasation has been investigated in a 3D microfluidic model [201, 202]. One study demonstrated differentiation of monocytes to macrophages upon transmigration through the vasculature in an extravasation model. This study probed that monocytes can directly reduce cancer cell extravasation in a non-contact dependent manner [201].

A series of studies investigated the role of interferon regulatory factor-8 (IRF-8) on the migration of immune cells toward tumour cells. In these studies, a 2D microfluidic device with parallel channels was used to model interaction of spleen cells from immunodeficient mice with murine melanoma cells [203, 204]. A similar device was used to probe the interaction of colorectal cancer cells and dendritic cells which are a subtype of immune cells [205]. In this model, dendritic cells migrated toward cancer cells treated with antitumour compounds. They found that CXCR4/CXCL12 signalling plays a critical role in cancer cell-dendritic cell interaction. Currently, a modified 3D microfluidic chip with two gel region and

two side channels was developed to culture tumour aggregates, macrophages, monocytes, and endothelial cells in the presence of interstitial flow. They found that mesenchymal-like breast cancer cells and interstitial flow, activated the monocytes to tumour associated macrophage phenotype through the stimulation of colony-stimulating factor 1 (CSF-1) [183].

1.5 Modelling migration and invasion

As mentioned before, metastatic cascade is a multistep process which includes several types of cancer cell migration in different stages. Migration of cancer cells in a metastasis cascade can be categorized into three types including initial migration, intravasation, and extravasation. Microfluidics platforms extensively have been utilized to model all kinds of cancer cell migration which are described as follows.

1.5.1 Initial migration

The initial migration of cancer cells occurs in the primary site of the tumour upon a change in TME chemical and mechanical features, lead to a change in cancer cell phenotype. EMT is a complex process, which changes the phenotype of epithelial cells to more motile mesenchymal type. Upon EMT, cancer cells lose their cell-cell connections and initially migrate through the surrounding environment (e.g. basement membrane) toward the circulatory system. Microfluidic approaches have been developed to model this initial migration using 2D or 3D devices. In 3D devices, cancer cells usually are embedded into the collagen and loaded to the central channel. By introducing chemical gradients, cell-cell signalling, and TME biophysical properties into the devices, the initial migration of cancer cells can be modelled. Truong et al. developed a microfluidic chip allowing side-by-side positioning of 3D hydrogel-based matrices to model 3D chemotactic tumour-stroma invasion. Their model demonstrated that cancer cell invasion significantly increased in response to epidermal growth factor (EGF) signalling as well as co-culturing with CAFs (figure 3A) [206]. In another study by Peela and colleagues a similar device was utilized for the anti-cancer effect of suberoylanilide hydroxamic acid (SAHA), a histone deacetylase (HDAC) inhibitor. They co-cultured breast tumour and stromal fibroblasts in a

compartmentalized 3D model which allowed drug transport to the tumour region [207]. This device demonstrated a high potential in modelling intravasation of breast cancer cells by incorporating three regions of tumour, stromal, and vascular cells [208]. More recently, a modified 3D device consisting of two gel channels and two side channels was utilized to model tumour invasion to the surrounding stroma to screen the drug performance. Their results suggested that co-culture of tumour and healthy cells led to increased secretion of IL-6 and consequently increased cell invasiveness [209].

1.5.2 Intravasation

The second type of migration during the metastasis process is related to intravasation of cancer cells. In this step, cancer cells interact with endothelial cells through existing capillaries or newly formed branches to enter the circulatory system. 3D devices have been extensively utilized to recreate this step by incorporating cancer cell-embedded collagen/Matrigel to the central channel, while endothelial cells formed a confluent layer in the side channels. By introducing chemical gradients and signalling pathways, cancer cells move and transmigrate from endothelial layer. As mentioned before, Zervantonakis et al. presented an intravasation model of breast cancer cells in the presence of endothelial cells and macrophages. They showed that secretion of tumour necrosis factor (TFN) by macrophages results in an increase of permeability of the endothelial layer and consequently intravasation rate (figure 2C) [200]. It has been demonstrated that TME mechanical cues including interstitial flow, fluid stresses, and orientation of biological matrix affect the intravasation of cancer cells [210-212].

1.5.3 Extravasation

The third major migration event during the metastatic cascade occurs in the extravasation step where CTCs invade to the secondary site through different proposed mechanisms. While several groups have reported physical trapping of CTCs in capillaries or adhering to the vessel walls as a possible mechanism of extravasation, Au and co-workers presented a

microfluidic devices mimicking human capillary constrictions and demonstrated that CTC clusters can traverse capillary-sized constrictions through reorganizing into single-file chain-like geometries [213]. Generally, two common approaches have been utilized to model extravasation process in 3D microfluidic devices. In the first approach, a monolayer of endothelial cells is formed in the side channel which is in contact with the biological matrix in the central channel. Cancer cells are loaded to the endothelial channel and extravasate to the biological matrix in the presence of suitable signalling [155]. In the second approach, a vascularized network is formed in the central channel, then cancer cells are loaded to this network and circulate in the capillaries. Depending on the size of the vessel, cancer cells can be trapped or adhere to the wall and extravasate through the lumen walls [159]. This model demonstrates a great potential in providing a physiological condition for both cancer and endothelial cells and extensively has been used by several groups.

Chen at al. examined the role of tumour integrin β1 in the extravasation of cancer cells in a modified 3D microfluidic device consisting of three gel channels for endothelial cells and fibroblasts. They probed that although integrin did not mediate adhesion to endothelium but mediated the adhesion to the subendothelial matrix [214]. More recently, Bersini et al. used a similar 3D device to combine microfluidic-transcriptomic approaches and tri-cultured cancer cells, endothelial cells and osteo-cells to assess the extravasation potential of cancer cells. They found that the bone-mimicking microenvironment increased the extravasation of breast, bladder, and ovarian cancer cells (figure 3B) [180]. Organ-specific extravasation of cancer cells has been further investigated by several other groups [179]. In these studies, either local signalling chemokine gradients or specific cellular components were utilized to mimic the specific organ. For example, Riahi and co-workers probed the extravasation of breast cancer cells in the presence of CXCL12-CXCR4 signalling and an endothelial cell monolayer in a 3D microfluidic device [179]. The same device was utilized by Zhang and co-workers to probe extravasation of tumour aggregates under CXCL12-CXCR4 signalling [215]. Jeon and co-workers also developed a 3D vascularized model and examined the extravasation of breast cancer cells to the bone- and muscle-mimicking environment. They showed that A3 adenosine receptor modulates bone-specific extravasation of breast cancer cells [182]. In another study, a 3D microfluidic model was utilized to model extravasation of

breast cancer cells to an osteo-cell conditioned microenvironment. In this study, CXCL5-CXCR2 signalling was proposed for organ-specific extravasation of breast cancer cells (figure 3C) [156].

More complex models have been developed in the recent years. One study developed a 3D microfluidic model of breast cancer to monitor invasion of cancer cells in a model containing tumour aggregates, macrophages, monocytes and endothelial cells in the presence of interstitial flow (figure 3D) [183]. This work demonstrated the differentiation of monocytes to tumour-associated macrophages in the presence of both invasive breast cancer cells and interstitial flow. Moreover, a good model of brain tumour extravasation was proposed by Xu and colleagues. They modelled the complex blood-brain barrier by incorporating endothelial cells, astrocytes, and different types of cancer cells and examined brain metastasis of human lung, breast and melanoma cells and their therapeutic responses to chemotherapy (figure 3E) [216].

Another complex model of cancer metastasis was proposed by Xu et al. [217]. They developed a multi-organ microfluidic chip mimicking the in vivo microenvironment of lung cancer metastasis. Their model included one “upstream” lung cancer model and three “downstream” brain, bone, and liver sections. Bronchial epithelial, lung cancer, microvascular endothelial, mononuclear, and fibroblast cells were used together in the “upstream” to model lung cancer, while astrocytes, osteocytes, and hepatocytes were used to model brain, bone, and liver, respectively. In this model, EMT of lung cancer cells was observed, where cancer cells invaded into all three brain, bone, and liver sections and damaged the cellular components (Figure 3F).

1.5.4 Modeling colonization of extravasated cancer cells

Colonization is the last step in the metastatic process. Cancer cells extravasate through vessel walls to enter to the secondary site. If they find a suitable environment in terms of chemical and mechanical characteristics, they will form the secondary tumour. To the best of our knowledge, few studies have attempted to model this step of metastasis. Current microfluidic

devices which are extensively are used for cancer modelling lack of providing a suitable environment for cellular activity in the long term. Migration and invasion of cancer cells usually occur in 24 to 48 hours, while colonization requires several days. In one model of extravasation, the formation of micrometastases was followed in the chip for up to five days. The extravasated cancer cells proliferated and formed colonies in size of 4 to more than 60 cells [156].

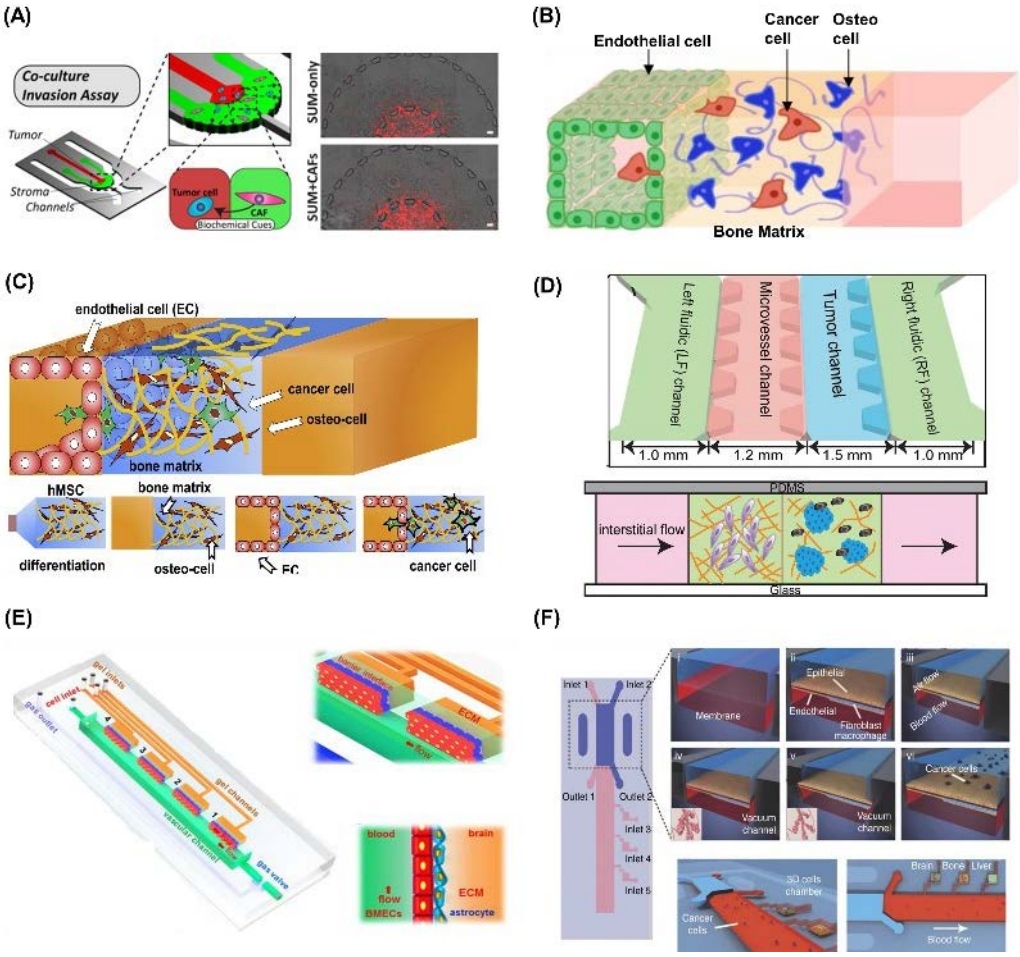

Figure 3. Initial invasion, intravasation, and extravasation of cancer cells on a chip. (A) Modelling the invasion of breast cancer cells by incorporating two regions of tumour and stromal cells. The device was used to model the invasion of SUM-159 cells into the stroma region with or without CAFs [208], (B) A microfluidic approach for tri-culture of cancer cells, endothelial cells and osteo-cells to assess the extravasation potential of breast cancer cells to the bone-mimicking microenvironment [130] (C) A 3D microfluidic model of extravasation of breast cancer cells in a osteo-cell conditioned microenvironment [156] (D)

Incorporating tumour aggregates, macrophages, monocytes and endothelial cells in a multi-channel microfluidic device to models invasion of cancer cells in the presence of interstitial flow [183], (E) A model of brain tumour extravasation with a complex blood-brain barrier [216], (F) A multi-organ microfluidic chip mimicking the in vivo microenvironment of lung cancer metastasis [217].

1.6 Microfluidic systems for the detection, characterization and analysis Circulating tumour cells (CTCs)

Circulating tumour cells were first described by Thomas Ashworth, an Australian physician that observed cells identical to the tumour itself in the blood of a metastatic cancer patient in 1869 [218]. Since these findings, technological advances have resulted in the capture of these rare cancer cells in the blood of solid tumour patients. In 2004, Allard et al., described the capture of CTCs using the CellSearch (Menarini Silicon Biosystems) [219]. This system is currently the only FDA-approved technology for the capture of epithelial tumour cells and has shown prognostic and clinical relevance of epithelial cell adhesion molecule (EpCAM)-positive CTCs in breast, prostate and colorectal cancers. In these tumours, CTC enumeration was found to be prognostic and correlate with disease outcomes [220, 221] . The reliance and preselection of epithelial cell adhesion molecule (EpCAM)-positive CTCs was found to be limiting in capturing the total population of CTCs due to factors such as epithelial-mesenchymal transition[222, 223]. Other competing technologies which used epitope-independent capture were successively developed such as microfluidics, filtration, bead and antibody based CTC capture to name a few. Emerging evidence from these technologies has shown that epitope independent CTC capture may capture a greater proportion of CTCs from circulation, including CTCs that have undergone EMT. However, the verdict is still out as to whether EpCAM-negative CTCs are of clinical significance and more research is warranted in this space to understand the role of CTC subpopulations.

1.6.1 CTCs enumeration

CTC counts and thresholds have been established using the FDA approved CellSearch (Menarini Silicon Biosystems) platform for metastatic breast (mBC), prostate (mPC) and colorectal cancer (mCRC). In these tumour types, ≥5 CTCs/7.5ml were associated with poorer outcomes in mBC and mPC and ≥3 CTCs/7.5ml for mCRC. Whilst studies using the CellSearch instrument have been performed In other tumour types such as lung, head and neck [224] and other solid tumour streams [225, 226], clinical cut-offs have not been established. Larger studies in these other tumour types is warranted for determination of whether a threshold can be developed. However, due to a number of factors, including downregulation/low expression of EpCAM and tumour heterogeneity, EpCAM may not be the most suitable marker for preselecting CTCs in other tumour types.

1.6.2 Circulating tumour cell (CTC) clusters

CTC clusters were first described by Watambe and colleagues in 1954 and since these findings a number of groups have described these tumour cells across a number of cancers [227-230]. Using microfluidic technology Au et al., demonstrated that CTC clusters in fact retain their cluster forming capacity whilst travelling in a single-line format through narrow capillaries [213]. Moreover, Aceto and colleagues demonstrated that CTCs have a 23-50 times higher metastatic capacity in the blood compared to single CTCs and a shorter half-life in the blood. More recently the group has shown that CTC clusters contain neutrophils within the cluster which may demonstrate immune-evasion strategies by neutrophils 'escorting' CTC clusters to distant sites [231]. The presence of CTC clusters is an emerging field and a number of groups have reported on these, including for the first time in aggressive forms of brain cancer (glioblastoma) where clusters have shown to cross the blood brain barrier [231]. It is important to determine the role of these CTC clusters, whether they are indeed clusters which break through the basement membranes and into the lymphovasculature or the clusters form in the blood. In so doing, strategies can be employed to reduce cluster mediated metastasis by targeting the interactions that are holding the clusters together. Early evidence has shown that gamma-catenin (57lakoglobin) is upregulated in CTC clusters. Moreover,

binding sites for stemness and proliferation markers were hypomethylated in CTC clusters [228]. Further research into CTC cluster reporting and composition is needed to understand these multicellular aggregates in more depth and their role in metastasis.

1.6.3 Single Cell CTC characterization

To gain a further understanding of CTCs, molecular analysis has revealed that there is vast heterogeneity in CTCs at single cell resolution. Studies have revealed 3 types of CTCs when whole genome amplification (WGA) and next generation sequencing (NGS) was performed on single CTCs. Type 1 shares genomic copy number changes concordant with the tumour. Type 2 were copy number changes detected in the CTCs but not in the tumour and type 3, where no copy number changes were detected [232, 233]. Recent molecular analysis performed using Hydro-seq CTC capture and massively parallel single-cell RNA-sequencing in breast cancer has revealed that breast cancer drug targets for hormone/targeted therapies could be tracked in individual cells that expressed marker of cancer stem cells and EMT transitioned states [234].

1.6.4 Immunotherapeutic biomarkers

Immunotherapies have been identified as a pillar in cancer therapeutics with an urgent need for predictive biomarkers of response. To this end, early data has revealed that CTCs frequently express these markers and may be used to identify patients likely to benefit from immunotherapy. CTCs expressing PD-L1 have been shown in various solid tumours [235] including breast [236], non-small cell lung cancer [237] and head and neck cancer CTCs [238, 239]. Initial studies have shown that PD-L1 may be up-regulated in response to radiation and that gene expression analysis showed that higher PD-L1 was associated with a poorer overall survival in NSCLC.[237].

1.6.5 Shift towards high throughput CTC isolation

Recent reviews of literature [240] have revealed that as the volume of blood is increased for CTC analysis, the higher the probability and number of CTCs that is captured. This has been enabled through methodologies such as diagnostic leukapheresis (DLA) where larger blood volumes are accessible. The DLA product has been estimated to harvest around 205 times more CTCs compared to a standard 7.5ml blood draw [241]. In vivo methodologies for CTC capture include the Gilupi device. This device contains a wire which remains in the cubital vein for up to 30 min [242]. The narrow wire interacts with blood and EpCAM-positive cells bind to the antibody posts. After removal from the vein, the device is washed with PBS, fixed with acetone and stored for analysis. These cells can then be interrogated for downstream analysis outside the patient's body. This technology, though somewhat invasive, allows for the interrogation of larger volumes of blood compared to the standard 7.5ml typically analysed for CTCs. In a 30 min duration, a few litres of blood can pass by the Gilupi device allowing for a higher interaction blood volume and thereby opportunity to capture CTCs. Initial studies have been carried out in colorectal cancer, lung and prostate cancer [242-244].

1.7 Microfluidic CTC enrichment technologies

1.7.1 Inertial microfluidics

Over the last decade, microfluidic based technologies have come to the fore of CTC enrichment and downstream applications with improvements in isolation, improved sensitivity and high separation efficiencies. Inertial microfluidic devices which utilise the hydrodynamic forces for particle separation have demonstrated utility across a range of tumour types. To this end, 'dean flow fractionation' has been used to isolate CTCs, with the latest iteration using spiral channels with trapezoidal cross sections. The chip uses a single inlet containing the sample and two outlets for waste and the enriched CTC sample (Figure 4). The technology has demonstrated efficient capture of CTCs in metastatic lung [245, 246], breast [245, 246], melanoma [247] and head and neck cancer [248] with head-to-head comparative studies with the CellSearch demonstrating that the spiral technology is able to capture a higher proportion of CTCs[245] . The technology allows for the enrichment of

viable CTCs with a high purity and yield. By using micro-milling and PDMS casting, the chip can be developed at low cost and is suitable for automation. A number of studies have shown that the purity of the final product has yielded lower white blood cell background cells by repeat enrichments [247]. This chip has been commercialized by Clearbridge Biomedics (Singapore) [249].

A further iteration of the microfluidic technology has been demonstrated by Zhou and colleagues recently [250]. Where the microchip was designed to accommodate multiple flows by initially confining cells near channel sidewalls. The sample is introduced through the sample inlet and buffer solution through a buffer inlet, in so doing and in such a configuration that three flow steams are formed in the main channel with clean buffer flow in the middle to collect larger target cells which are captured using size-dependent inertial forced of which rotation induced lift force is predominant. In so doing, cells from the blood are separated into two groups based on cell size. This chip has shown utility in head and neck cancers too [229] .

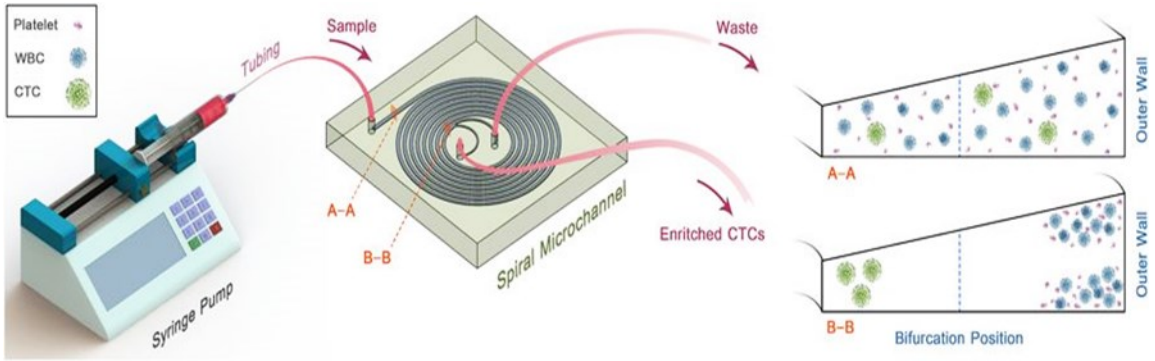

Figure 4. An example of CTC enrichment using inertial microfluidic (Spiral) technology. A combined sample/sheath fluid is pumped through a syringe pump and the cells are separated to either wall of the spiral chip allowing for CTCs (larger than normal blood cells) to be separated into one channel whilst the smaller cells pass into a waste channel. Figure reproduced from Kulasinghe et al. 2017 [248].

1.7.2 Nanovelcro

This technology uses a microfluidic chip which contains anti-EpCAM coated posts for the capture of CTCs. As blood flows through this chip, CTCs expressing EpCAM bind using immuno-affinity to the nanowires like 'velcro.' Four generations of this technology have been developed with the 1st generation composed of silicon nanowire substrate (SiNS) which is overlaid with a microfluidic chaotic mixer for CTC enumeration. The second generation were based on polymer nanostrubstrates which captured CTCs with laser microdissection methodologies. This was developed for single CTC isolation. By combining thermoresponsive polymer brushes onto SiNS, a 3rd generation of this chip was developed which allowed for the capture and release of CTCs at varying the temperatures. The fourth generation chip was developed with boronic acid grafted conducting polyer nanomaterial on a chip surface and utilised to purify CTCs for RNA transcript analysis [251] .

1.7.3 Acoustic Separation

Peng and colleagues used tilted-angle standing surface acoustic sound waves flowing through microchannels to offer a unique approach for separating tumour cells from the blood [252]. The technology allowed for cellular separation based on size, compressibility and other physical properties. The acoustic separation appeared to offer a gentler methodology to sorting cancer cells from the blood. Similar technologies for the enrichment of rare cell types from blood have been developed by Shields et al. [253] where a tri-modular microfluidic chip was developed. The first module uses an acoustic standing wave to align cells, the second magnetically labels cells and the third module captures the cells in microwells with micromagnets to capture individual cells for an on-chip analysis allowing for staining, imaging and quantification.

1.7.4 Parstotix

This microfluidic technology enriches for rare cells from whole blood by passing the cells through a separation cassette under constant pressure to enable separation. The cassettes allow for continuous cell separation using a 'step configuration' which yields to a final critical gap to capture cells. Cells are captured as a function of size and resistance to compression. Larger cells are typically captured in the wider steps at the top of the structure. For collection of the capture cells, the flow is reversed to release the cells from the cassettes steps and is collected externally. This technology has been tested in prostate [254-256] , breast and small cell lung cancer. The Parsortix technology is available through Angle PLC.

1.7.5 Vortex

Under high flow rates, laminar microscale vortices develop in rectangular reservoirs, allowing for larger cancer cell capture while smaller blood cells pass through and are not trapped under the flow. The captured cells can be released by reducing the flow rate to dissipate the vortices [257]. The technology has demonstrated CTC capture across a number of tumour types and more recently used for the detection of PD-L1 (an immunotherapeutic biomarker) in non-small cell lung cancer [258]. This technology is commercially available through the Vortex VTX-1 system which is a fully automated benchtop system for capturing CTCs.

1.8 Microfluidic approach in cancer treatment

Currently, surgery/chemotherapy and radiation are the treatment options of choice in the first line setting. In recent years, with the development of new generations of small molecule inhibitors revolutionized treatment regimens for cancer patients where using targeted therapy agents alone or in combination with chemotherapy and other regimens not only improved treatment efficacy and overall survival in most of the cancer but also reduced the adverse side effects.

Cancer drug development is a complicated process that involves several costly and time-consuming steps [259, 260]. The drug development process includes drug discovery and preliminary in-vitro validation, preclinical testing in animal models, and clinical trials. In the preclinical phase, efficacy and performance of drugs is tested in both in-vitro and in-vivo tumour models toward investigation of cytotoxic activity before initiation of clinical trials in humans. Considering In vivo screening of candidate drugs, several critical issues limited translational application of mouse models including ethical issues, lack of modeling tumour physiology, variation in engraftment rate, lack of modeling specific types of cancer with particular mutations, time and cost inefficiency [3]. In vitro platforms can be used to study a variety of biological and physiological processes. However, conventional in vitro platforms are based on a 2D monolayer of cells and/or simple 3D models, failing to mimic cellular and non-cellular features of the tumour microenvironment including presence of immune cells, vascular network and tumour stromal cells [261-264]. Microfluidics-based culture platforms have recently emerged as powerful tools for modeling complexities of diseases including cancer and its tumour microenvironment [120, 265].

To evaluate the treatment potential and efficacy of a large library of anti-cancer agents, high-throughput screening (HTS) platforms are using in target discovery. Considering the merits of microfluidics cell culture platforms requiring low amount of reagents (cost-effective) and allowing parallel processing (less time-consuming), microfluidic cell culture systems can be employed as a high-throughput drug screening platform [266].

Identification of effective doses of an anticancer agent is an important issue for drug development. Recently, developing concentration gradient generators (CGG) included with culturing cancer cells in both 2D and/or 3D structure by means of microfluidic platform enable us to identify appropriate and effective dosage of single and combination anticancer agents. For instance, Ye et al. developed a microfluidic platform composed of a concentration gradient generator (CGG) connected to cell culture chambers, in which hepatocellular carcinoma cells (HCC) were cultured [267]. Employing a CGG allow us to measure cytotoxic effects of wide range of drugs on the cultured cells using different concentrations of anticancer drugs. In this study, cytotoxic effects of two chemotherapy drugs known as actinomycin and daunorubicin were assessed in the hepatocellular carcinoma cell line HepG2

and hepatocytes using the platform, where selectivity of inducing apoptosis in the carcinoma cells was detected [267].

In line with these studies, Xu et al. combined a CGG in a microfluidic platform to screen drug sensitivity and resistance in the treatment of lung adenocarcinoma [268]. Co-culture of human lung fibroblast cells (HLF1) and human non-small cell lung cancer cells (SPCA-1) were suspended in a basement membrane extract (BME) and added to the cell culture chambers. The side channels delivered cell culture medium included with or without anticancer drugs to the co-culture site. The microfluidic device was used to test the toxicity of several chemotherapy and targeted therapy drugs, including gefitinib (EGFR inhibitor), paclitaxel, gemcitabine, and cisplatin. They assessed treatment efficacy of cisplatin and paclitaxel in a combination manner in the CGG microfluidic platform by measuring their IC50 values.

The obtained results showed that the combination of paclitaxel and cisplatin was more effective (higher rate of apoptosis) than the treatment of cancer cells in a single agent chemotherapy fashion. Additionally, a drug resistance behavior was observed in the co-culture group compared with mono-culture group where majority of cells were sensitive to the chemotherapy, highlighting the role of tumour stromal cells on induction of drug resistance in cancer cells [268]. In a preclinical study, the microfluidic platform was used to test drug sensitivity in a co-culture of eight patient derived lung adenocarcinoma cells and tumour stromal cells. Drug sensitivity studies resulted to identification of a similar cytotoxicity pattern between cell lines and patient derived samples screened against similar drugs. Additionally, this study identified various IC50 values that obtained from different patient samples, indicating the impact of lung cancer stages on treatment efficacy [260].

Combination treatment regimens and it is impact on improving patient survival have been studies for a long time [80–82]. However, the assessment of efficacy of numerous combinations of chemotherapy and targeted therapy drugs in a 2D and/or conventional 3D cell cultures platform is time-consuming and non-correlative compared to the dynamic and cellular heterogeneity of the tumour tissues. The possibility of directly culturing patient derived tumour specimens into microfluidic platform where cellular heterogeneity of the

original tumour is preserved can serve as a reliable platform for combinatorial drug screening. In this regards, recently, Eduati et al., developed a plug-based microfluidics platform for functional screening of numerous drug combinations including chemotherapy and targeted therapy agents on various tumour biopsy derived from pancreatic cancer patients [269]. In this study, using an integrated Braille valve enabled changing the plug composition and testing 56 different condition. Interestingly, they highlighted high efficacy of combination of oxaliplatin and AKT-inhibitor for patient with non-metastatic tumour, while combination of AKT-inhibitor and BRAF-inhibitor (ADZ-6244) effectively targeted and suppressed liver metastasis in pancreatic cancers [269].

1.9 Microfluidic and modeling anticancer drug response

As discussed earlier, many groups have used microfluidic culture devices to analyze how tumour microenvironmental factors including cellular and physical influence tumour cell responses to anticancer therapies. Culturing lung adenocarcinoma cancer cells A549 under various oxygen gradients created within a microfluidic device resulted into various treatment response rate against Tirapazamine. Interestingly, lung cancer cells cultured in hypoxic condition showed increased drug-induced cancer cell killing [270]. This study provides an example of the application of microfluidics systems to modeling chemical gradient of the tumour microenvironment, and how this platform can be used to gain new insights into fundamental processes of tumour development and therapeutic targeting [270].

It is well understood that tumour stromal cells particularly cancer associated fibroblasts (CAFs) play a critical role in the tumour development and drug response in various cancers. Modeling crosstalk between tumour and stromal cells can enhance our understanding of the tumour microenvironments and treatment response regulated by tumour stromal cells. In a simple microfluidic device A549 lung cancer cells cultured in a 3D chambers connected to a chamber seeded with CAFs. The chambers linked to a linear microfabricated concentration gradient generator to mimic paracrine effect of CAFs on treatment response of cancer cells. This study revealed that secretion of HGF by CAFs induce resistance by means of inhibiting

paclitaxel-induced apoptosis in lung cancer cells [271].

In the context of hematopoietic malignancies including leukemia, drug screening analysis of large number of primary chronic myeloid leukemia (CML) cells and normal hematopoietic stem cells (HSCs) in a microfluidic culture platform revealed tumour cell-specific responses to a dual BCR/ABL and Src family tyrosine kinase inhibitor named Dasatinib in which, HSCs exhibit a substantially elevated level of apoptosis rate in comparison with CML cells [272].

In the case of the advanced breast cancer, microfluidic culture technology enabled culturing multicellular tumour spheroids (MCTS) structures with cancer cells, tumour stromal cells, endothelial cells, and immune cells to model the complexity and dynamics of the tumour microarchitecture of breast DCIS towards the evaluation of the efficacy and toxicity of paclitaxel when administered at in vivo-relevant doses [273]. In this model, paclitaxel had insignificant cytotoxic effects on normal epithelial cells, while the growth of the DCIS spheroids was suppressed. Another microfluidic model was used to identify drugs with the potential of reduction in EMT and cancer cell dissemination in a single or combination manner [274]. In this study, human lung adenocarcinoma or bladder carcinoma cell lines were embedded in a collagen scaffold in one channel, while HUVECs were seeded in another channel in order to generate vessel-like structures. The entire culture was then treated with different drugs, MK-2206 (AKT inhibitor), AZD-0530(Src inhibitor), A83-01(TGFβ kinase/activin receptor-like kinase (ALK 5) inhibitor) and CI-1033(EGFR, HER-2 and ErbB-4), known to affect EMT signalling pathways. Interestingly, the drugs significantly reduced expression of EMT related markers in cancer cell monocultures, while these effects were significantly diminished when the cancer cells were co-cultured with HUVECs indicating the role of cytokines and chemokines released from endothelial cells on induction of resistance of cancer cells against anti-cancer drugs [274]. The generation of the perfusable and 3D microvascular networks within microfluidic device toward a reliable organ-on-a-chip model opened the new way to evaluate the cytotoxic therapies such chemotherapy and vascular-targeting agents. This microfluidic device can distinguish between drugs that were not effective in disrupting the vascular networks and drugs that had multiple targets such as VEGFR2 and PDGFR, which led to regression of the vasculature [275].

Another model cultured human colon carcinoma cells spheroids derived from LS174T cell line and then transferred them to microfluidic devices and exposed them continuously to flowing medium included with doxorubicin to mimic chemical gradients in blood vessels in the TME and to measure the diffusion coefficient of the doxorubicin and quantify the accumulation of a therapeutic bacterium, Salmonella enterica [276].

One of the challenges in the treatment of primary brain tumours is delivering drugs and antibodies across the blood-brain barrier (BBB). Recently, Kamm and colleagues developed a two-channel microfluidic device in which HUVECs were grown in an outer channel under flow conditions while rat brain astrocytes or metastatic HER2+ mouse breast cancer cells were cultured in the inner channel under static conditions to model both the normal BBB condition and the blood–tumour barrier [277]. Interestingly, when the monoclonal therapeutic antibody Trastuzumab, a HER2 targeted drug, was perfused through the outer channel, there was a considerable uptake of the antibody into the inner compartment under both BBB and blood–tumour barrier conditions. Importantly, in parallel with these observations, similar results were obtained in an in-vivo study [277]. Furthermore, both the in vivo and the in vitro studies highlighted lack of a clear correlation between the size of the metastases or metastatic cell clusters and antibody uptake across the blood–tumour barrier. This study emphasizes that there is still a great need to develop reliable and suitable preclinical models, including human-relevant BBB models, to aid the development of more effective therapeutic monoclonal antibodies for treatment of the brain tumours.

In recent years, cell-based immunotherapy by using engineered T -cells shed new light in treatment various types of haematological malignancies such as leukaemia. Currently, using animal models are the gold standard for evaluating treatment efficacies. However, time consumption, variation in rate of tumour development in mice and cost inefficiency limited large applications of this model. Microfluidic technology can be used to develop a preclinical in vitro model to evaluate the anti-tumour efficacy of T cell receptor (TCR)-redirected engineered T cells for cancer immunotherapy [278]. For instance, to investigate the migration potential of the engineered T cells into the side of the tumour cells, the human liver carcinoma cells HepG2 were cultured either dispersed or aggregates within a collagen matrix within one channel of a microfluidic device, and engineered T cells were introduced in the

another channel [278]. This microfluidic model was able to detect that lower oxygen levels (2%) led to reduced killing of dispersed cancer cells by engineered T cells compared with higher levels of oxygen (20%). In addition to these, by using this model, they found that, the addition of the inflammatory cytokines interferon-γ (IFNγ) or TNF significantly increase the killing of cancer cell aggregates by the engineered T cells [278].

Growing studies highlighted the role of monocytes in regulation of an immune suppressive tumour immune microenvironment through modulation of PD-1/PD-L1 signalling in the TME, which impede function of cytotoxic T-cells in the TME [279]. The microfluidic device showed the potential to model TME particularly tumour-immune interactions. In this regard, an intrahepatic microfluidic model of hepatitis B virus (HBV)-related hepatocellular carcinoma was developed to investigate the immunosuppressive potential of monocytes towards HBV-specific TCR-engineered T cells and the role of PD-1 and PD-L1 signalling [202]. In this device, the central channel of a three-channel microfluidic device was filled with a hydrogel containing embedded HepG2 cancer cell aggregates transduced with a construct containing the gene of the preS1 portion of the envelope protein from HBV genotype D, and the two side channels were filled with medium containing engineered T cells [202]. This microfluidic model was able to identify a suppressing effect of monocytes via PD-1/PD-L1, whereas this was not the case in the 2D model [202, 278]. Collectively, these two studies demonstrate the potential of using microfluidic tools to predict TCR-engineered T cell efficacy in a preclinical setting.

1.10 Microfluidic and personalized cancer treatment

In conventional approaches to cancer therapy, most patients with particular types of cancer receive similar ‘one-size-fits-all’ treatments. However, it has recently become clear that therapies only work in certain subsets of patients [3]. Currently, individualized cancer treatments are progressively improving due to better characterization of the molecular and pharmacogenomic features of tumours and the patient’s disease. This recent approach, called precision or personalized cancer medicine, can be described as a ‘one dose, one patient’

treatment. In the field of personalized cancer medicine, the link between functional genomics and pathological data to patient outcome is a major challenge. To address this challenge, different personalized tumour models have been proposed, including cancer cell lines, patient-derived xenografts (PDXs), 3D culture tumour models, and microfluidic tumour on chip models. Although, these models represent great potential and application for personalized cancer therapy, numerous challenges and critical issues limited their wide application in this field of oncology [3].

The ability to predict a patient's response to an anti-cancer therapies is a major challenge in clinical oncology. Despite the years of research and development with countless investments, clinical trials in oncology still experience high failure rates, resulting in patients suffering from severe side effects with little benefits. Personalized approaches could lower treatment toxicity, improve patients' quality of life, and ultimately reduce mortality. In order to pursue personalized treatment, advanced technologies and tools are urgently needed. Recently microfluidic technology shows great potential for complementing and, in some instances, replacing the use of animal models in the testing of medicines and in developing personalized treatments for cancer patients in a real-time and routine clinical setting [280].

Compared with the current in-vitro models, ability of direct culturing patient derived tumour cells in microfluidic devices paved new ways to not only preserve spatiotemporal composition of the tumour microenvironment, but also screening of the candidate drugs in a reliable manner [281]. Recently, a few pre-clinical studies employed microfluidic culture system to predict response of tumour cells to a wide range of anticancer drugs mostly targeted therapy and immunotherapies [280-282]. In a pre-clinical effort, Jenkins and colleagues recently represented that ex-vivo culturing of patient-derived organotypic tumour spheroids (PDOTS) in a microfluidic device can model the dynamic response to immune checkpoint blockade (ICB) and may facilitate efforts in precision 69mmune-oncology and the development of effective combination therapies for patient with lung adenocarcinoma [282]. In this pre-clinical study, miniaturization of tumour samples derived human tumours not only preserved spatiotemporal composition of the tumour microenvironment (TME), but also importantly retained autologous lymphoid and myeloid cell populations and respond or resistance to ICB in short-term 3D microfluidic culture. Additionally, profiling of cultured

PDOTS demonstrated that TBK1/IKKε inhibition enhanced response to PD-1 blockade, which effectively predicted tumour response in vivo. Systematic profiling of secreted cytokines in PDOTS captured key features associated with response and resistance to PD-1 blockade [281]. Considering the merits of organoid technology and their application in personalized cancer medicine [3], culturing these self-organized and multicellular 3D tumour models in microfluidic device toward development of reliable organ-on-chip opened new way for accurately prediction of drug response in-vitro. In line with this concept, Shirure et al. demonstrated, long term culture and treatment of patient derived breast cancer organoids in a vascularized microfluidic device. Targeting cultured organoids with paclitaxel and bevacizumab resulted into shrinkage of organoids and disruption of formed microvascular network [283]. These findings indicate feasibility of employing this platform for both drug discovery and personalized medicine.

The role of immune cells in reshaping the tumour microenvironment and consequently therapy response has been proven [68]. Co-culturing autologous immune cells and tumour organoids derived from individual patients in a 3D vascularized microfluidic device to model a complex tumour microenvironment not only overcomes the challenge of screening current immunotherapy drugs and combination regimens, but also can predict the effects of new generation of cell-based immunotherapy agents including CAR-T cells, engineered natural killer cells, and dendritic cells on tumour organoids in the preclinical setting [3, 278] (Figure 5), which remained to be explored.

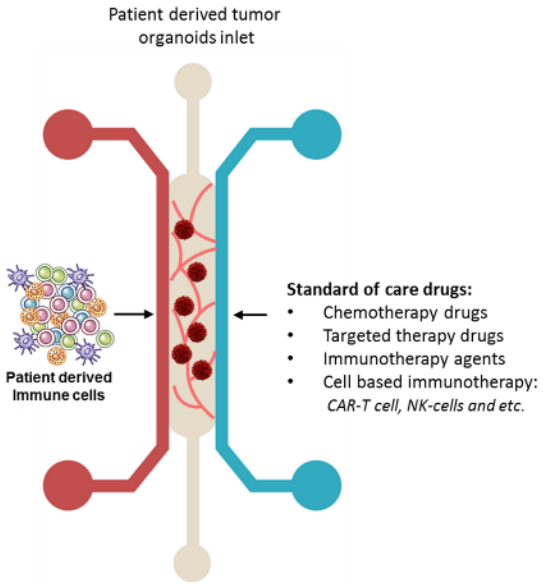

Figure 5. Schematic of co-culturing patient derived tumour organoids, with immune system elements derived from the peripheral blood of patients, in a microfluidic device and screening of current and future anti-cancer therapeutics toward treatment selection [141].

1.11 Challenges and limitations

Taken together, these findings demonstrate that microfluidic technology can be used to screen novel types of anticancer molecular, cellular, and nanotechnology-based therapies, optimize treatment parameters, and investigate effects of combination therapies in an in vivo-like TME. An application where microfluidic device could be particularly helpful in the future is in the development of a personalized tumour model in which the direct culture of patient-derived tumour spheroids into microfluidic device and screening them against either library of the anticancer drugs or agents can aid in the identification of most effective drugs for individual patients. However, in these models the role of tumor stromal cells in regulation of TME and its properties is not studied. Moreover, another aspect of TME including tumor immunity and tumor immune-microenvironment and the role of other components of TME

in treatment response remained to show. Additionally, from a technical point of view, complexity and labor-intensive properties of these device significantly limit broad application of them to model various feature of TME. Thus, developing a low-cost and easy to use device that allow modeling complex features of TME in a simple and reliable fashion is required.

Chapter 3

In-silico Study of Tumour Microenvironment in Triple-Negative Breast Cancer

Summary:

In this chapter, I performed a comprehensive in-silico data analysis on two large cohorts of breast cancer with a focus on TME. In this study, I highlighted the role of tumour stromal cells in regulation of tumor immunity, induction of epithelial-mesenchymal transition, and how drug-repurposing aids in the treatment of breast cancer. The part of the presented results in this chapter has been submitted and is under review in the journal of Cell Report.

3.1 Introduction

Breast carcinoma is the most prevalent cancer in women and remains a significant cause of cancer-associated death, despite attempts to provide effective therapies. Immune checkpoint blockade therapy has demonstrated success in various cancers but remains limited in breast cancer treatment [284, 285]. There is increasing interest in understanding the role of the tumour microenvironment (TME) and intra-tumour heterogeneity in the immune activity and response to immune checkpoint inhibitors [68]. Among cells present in the tumour microenvironment, cancer-associated fibroblasts (CAFs), play a critical role in the complex process of tumour-stroma interaction. In aggressive forms of breast cancers such as triple-negative breast cancer (TNBC), the high abundance of stromal fibroblasts associates with the aggressiveness of adenocarcinoma, disease recurrence, drug resistance, and lack of immune response. The mechanisms by which tumour cells escape immune surveillance are now better understood, but the role of stromal cells on induction of an immunosuppressive environment to evade immune surveillance is not well defined.

Epithelial-mesenchymal transition (EMT) is one mechanism shown to play a critical role in the modulation of tumour progression regulated by TME, [199, 286]. Numerous studies highlighted a link between the initiation of EMT and activity of the tumour stromal cells in TME which consequently might alter immune properties of TME toward an immune-escape ecosystem. Although the role of the TME in inducing EMT has been well established [23, 287], however, the reciprocal process, where carcinoma cells residing in the more-mesenchymal state and regulate the activities of stromal constituents in TME, particularly immune cells, is still poorly understood [20]. Considering resistance to immunotherapy regulated by EMT [288], in studies encompassing a broad spectrum of malignancies, including breast cancer, a positive correlation has been observed between immune-suppression and EMT-related transcription factors (TF) [20, 289-292]. However, the impact of EMT activated through the tumour stromal cells on reprogramming of the tumour immune microenvironment (TIME) toward the development of immune-suppressive TIME is mainly unknown. Therefore, in this study we combined available single-cell data of TME with The Cancer Genome Atlas (TCGA) and several other open-access cancers-immune databases to

analyze tumour immune activity at molecular and cellular levels across the EMT spectrum.

We highlight association between cancer-associated fibroblasts and their cytokines with the activity of EMT and demonstrated the associations of various EMT scores with TME features including infiltration of immune cells, and the expression of immune-checkpoints in TME. We indicated low immune activity known as cold TME [14] characterized by reduced infiltration of lymphocytes, and increased expression of immune checkpoints was identified across samples with high EMT scores. In contrast, hot TME samples were represented by low EMT scores, increased tumour immunogenicity, favored intra-tumoral T-cell infiltration particularly CD8+ T-cells and enhanced immune-checkpoint blockade efficacy. This study suggests the potential of using EMT score as a biomarker for cancer immunotherapy response in breast cancer. It also indicates that targeting pathways leading to EMT-TF expression could be a powerful approach to enhance immune response and overcome immunotherapeutic resistance in clinical applications. Finally, using two drug-protein interaction and gene-drug association database, we scored a list of therapeutic agents that possibly can reverse this process through the targeting either CAFs directly or cytokines that regulate both EMT and immune suppression.

3.2 Materials and Methods

3.2.1 Datasets

In this study, The Cancer Genome Atlas (TCGA) (https://portal.gdc.cancer.gov/) breast cancer clinical data, including gene expression and clinical information, were downloaded from Xena-browser (https://xenabrowser.net/datapages/). The immune and stromal scores data of TCGA breast cancer cohort was retrieved from ESTIMATE portal, MD Anderson Cancer Centre (https://bioinformatics.mdanderson.org/estimate/) [293]. The TCGA data, ESTIMATE scores and correlation analysis were performed under TCGA-BioLink package in R software [294]

3.2.2. The EMT scores and immune feature analysis

The EMT scores were analyzed according to the previous study [295]. The immune features, tumour-infiltration lymphocyte analysis and correlation analysis were performed using CRI-iAtlas portal (https://isb-cgc.shinyapps.io/shiny-iatlas/) [296] and Tracking Tumour Immunophenotype (TIP) portal (http://biocc.hrbmu.edu.cn/TIP/) [297]. The correlation between the expression of EMT-TF and filtration of individual immune cells were analyzed using Tumour Immune Estimation Resource (TIMER) application (http://timer.comp-genomics.org/) [298-300].

3.2.3 Cell, ligand and receptor abundance diagram

The cell, ligand and receptor abundance diagram were generated using Cell-Interaction Diagram module under iAtlas portal [296]. A detail description of the applied algorithm is available in iAtlas portal (https://isb-cgc.shinyapps.io/shiny-iatlas/). Briefly, to yield values for display, the gene expression values for each protein shown were first binned into tertiles (low, medium, high). The binning was performed over all TCGA samples. The 'abundance' was computed as the fraction of samples within the selected subtype that map to the mid and high-value bins. The abundance can thus range from 0 to 1. Identical binning was performed to yield cell abundance within the subtype. Immune cell abundance was estimated with CIBERSORT. The T Cell estimate corresponds to the CD8+ T Cell estimate from CIBERSORT; Macrophage level is given by the sum of M0, M1, M2 macrophages according to CIBERSORT; Dendritic cells are a combination of CIBERSORT resting and activated Dendritic cells. The Tumour Cells estimate are estimated by TCGA tumour purity. The T cell receptor (TCR) value was approximated by the T Cell estimate. MHC Class I values (MHC) were set to the expression of the single HLA gene HLA-A, and MHC Class II (MHC-II) approximated by the expression of HLA-DPA1. In the network diagram, the TCR and peptide-mediated binding interactions are not shown. Inducible T Cell Co-stimulator Ligand (ICOSLG) gene codes for the protein ICOSL.

3.2.4 Statistical analysis

The Mann–Whitney, Fisher's exact and Spearman's correlation coefficient tests were computed by GraphPad Prism version 8.0. A p-value < 0.0001 was considered as highly significant.

3.3. Results

3.3.1 Fibroblasts in the TME and its association with EMT and immunity

We first analyzed the TME content of TNBC through the available sing-cell databases (Figure 1). We found 10 different cell clusters according to their genomic signature. Beside the epithelial cells which include most of the cell population, a large population of the fibroblasts (cluster 3) and macrophages (cluster 4) was also observed (Figure 3.1A, 3.1B).

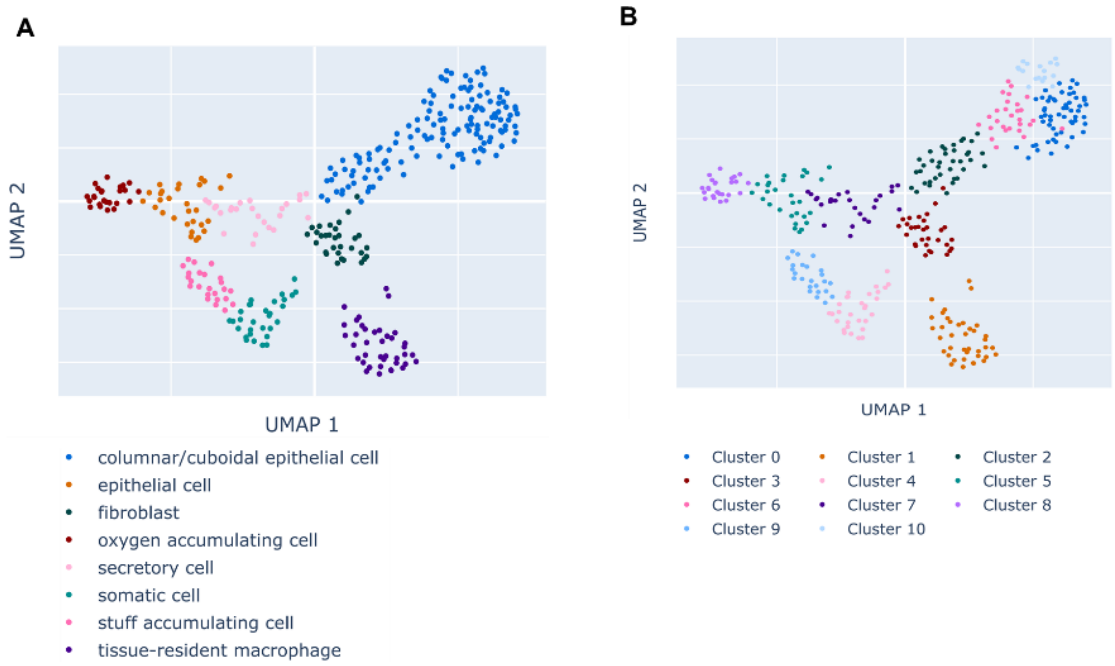

Figure 3.1: Overview of cell populations cluster and its signature identified in TME of TNBC. **(A)** identified subpopulations and clusters **(B)**.

Following this observation, we performed gene-set enrichment analysis and pathway enrichment analysis. Interestingly we found a positive association between pathways involved or regulate metastasis among three population of TME including fibroblasts (cluster 3; score:0.5), secretory cells (Cluster-7; score:0.3), and oxygen-accumulating cells (Cluster-8; score:0.2) (Figure 3.2A). in line with this, the gene-set enrichment analysis showed association of the signature of hallmark of EMT in among fibroblasts (Figure 3.2B).

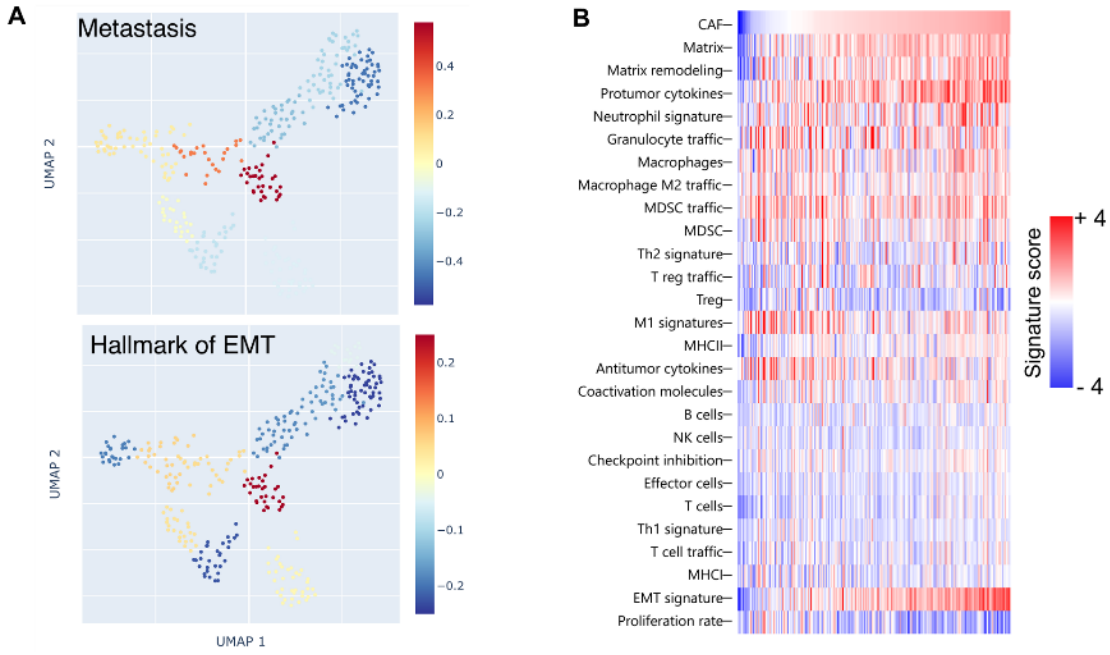

Figure 3.2: Gene-set enrichment analysis and association between EMT, immunity and CAFs activity. **(A)**. GSEA of TNBC sub-populations highlight positive correlarion of fibroblasts with metastasis related pathways and hallmark of EMT. **(B)** immune content analysis of TNBC breast cancer and EMT demonstrat positive association between EMT and CAFs activity with immune-suppression feature of TME, including high infiltration of Treg cells, MDSC, immune checkpoints and M2 macrophages and reduction of cytotoxic T cell activity.

To better characterizing these associations and performing cross validation, we analyzed single-cell data of a large cohort of samples with a fully enriched TME included with immune cells and calculated EMT score (*low score = more epithelial, high score = more mesenchymal*) and CAF activity scores for individual samples and performed unsupervised clustering. We found that increase of CAFs activity positively associates with high score of

EMT (Figure 3.2C). Moreover, infiltration of cytotoxic cells and other tumor suppressor immune cells reduced at the high score of both EMT and CAF activity, while matrix remodeling, expression of pro-tumour cytokines, M2 macrophages infiltration, and MDSC trafficking significantly raised indicting a positive association between immune-suppression, CAFs activity and EMT (Figure 3.2C). Interestingly, the analysis of the 35 immuno-modulation cytokines which are mostly secreted by CAFs demonstrated involvement of majority of these cytokines in activation of EMT in breast cancer (Figure 3.3A). Moreover, these cytokines are highly expressed in TNBC sub-types of breast cancer in comparison with other subtypes, indicating that why patient with a detected TNBC subtypes are mostly resistant to both immunotherapy and targeted therapy (Figure 3.3B) in which targeting these cytokines might reverse tumor immunity to ward an immune promoting TME (Figure 3.3C). All in all, these data clearly illustrated a triple-link between activity of EMT, immune-suppression and CAFs activity.

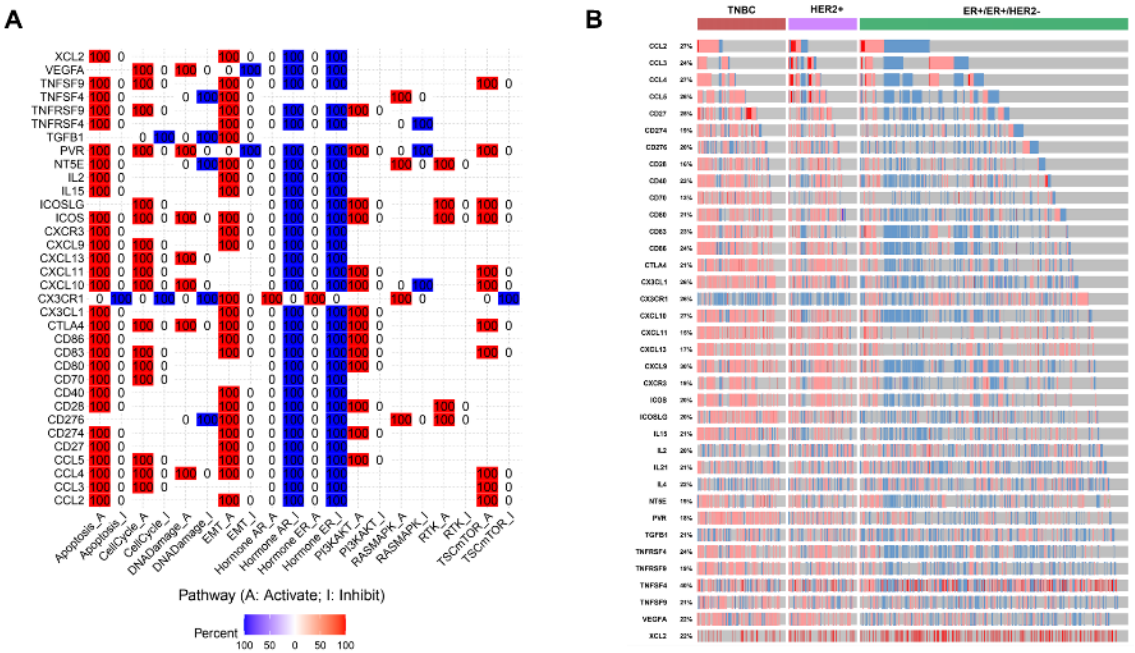

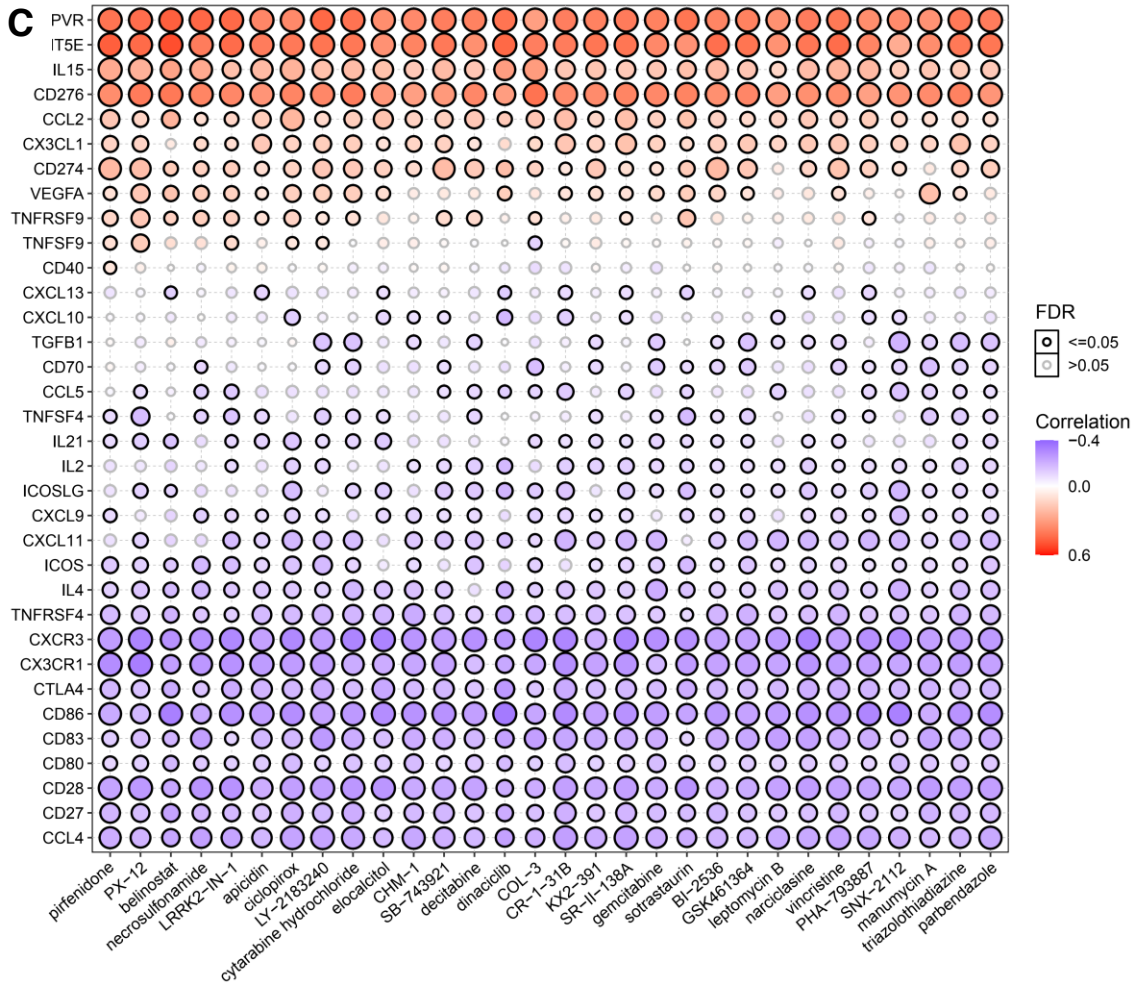

Figure 3.3: Pathway activity and the expression of 35 immuno-modulatory cytokines in breast cancer. **(A)** Pathway activity analysis depict involvment of most of the cytokines in activation of EMT. **(B)** Comparing the expression of cytokines in three main sub-types of breast cancer, showing that high expression of cytokines is enriched in TNBC sub-types. **(C)** Correlation between CTRP drug sensitivity and mRNA expression.

3.3.2 EMT score positively associates with stromal score and negatively with the immune score in different subtypes of breast cancer

It has been shown that EMT is a dynamic transition program. The role of tumour stromal cells in the induction of EMT program in carcinoma cells and, consequently, regulating an immune-suppressive TME have been shown previously [20, 301].

To better understand the association between stromal and immune factors during the EMT program in different subtypes of breast cancer, we first assessed stromal score and immune score across three main subtypes of breast carcinoma namely, ER/PR+, HER2+ and triple-negative breast cancer (TNBC) and then analyzed its correlations with EMT scores (Figure 3.4; Supplementary Table 1; Supplementary Table 2). We found a high level of stromal score among HER2+ samples compared to ER/PR+ and TNBC samples. Interestingly, in contrast to stromal score, a high level of the immune score was found across TNBC samples compared to other subtypes, indicating a negative association between the stromal and immune score in different subtypes of breast cancer. (Figure 3.4A and 3.4B). As numerous studies highlighted the role of carcinoma-stromal cells in EMT induction, we analyzed the association between different EMT scores from epithelial (Score: -1) to mesenchymal (Score: +1), stromal- and immune scores among these three groups of patients. We observed that the stromal score increased in all subtypes when the EMT score increased (Figure 3.4C, 3.4D, and 4E) with a strong positive association in TNBC samples (Figure 1E). In contrast, the immune score negatively associated with increased EMT score in HER2+ and TNBC samples (Figure 3.4F, 3.4G, and 3.4H). These data in line with previous observations, highlight the tri-directional link between induction of EMT, stromal factors and immune suppression in different subtypes of breast cancer.

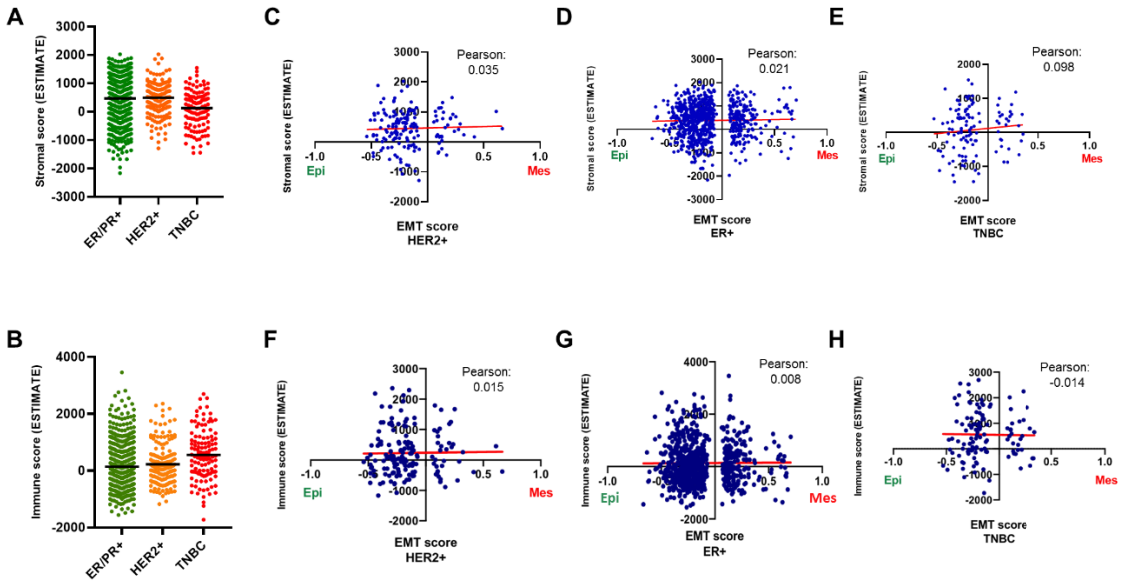

Figure 3.4. **The correlation between immune and stromal score with EMT scores in different subtypes of breast cancer**. **(A and B)** Stromal score and immune score measurement across three subtypes of breast cancer from TCGA cohort. **(C-E)** Correlation coefficient analysis between EMT scores and stromal score in three subtypes of breast cancer, **(C)** HER2+, **(D)** ER/PR+, and **(E)** TNBC from TCGA. **(F-H)**. Correlation coefficient analysis between EMT scores and immune score among **(F)** HER2+, **(G)** ER/PR+, and (H) TNBC samples. The data represented a positive association between increased EMT score and increased stromal score, while negatively associated with the immune scores in different breast cancer subtypes.

3.3.3 EMT scores negatively associate with infiltration of immune cells in the TME

To better understand the correlation between EMT score and immune-suppression, we analyzed intratumoral heterogeneity, leukocyte fraction, stromal fraction, and infiltration of immune cells among three EMT groups namely low-EMT score (L-EMT), intermediate-EMT score (I-EMT), high-EMT score (H-EMT) (Figure 3.5; Supplementary Table 3). We found a significant increase in the level of intratumoral heterogeneity among H-EMT score samples compared to low and intermediate EMT scores samples (Figure 3.5A). Moreover,

the analysis of leukocyte fraction and stromal fraction illustrated a positive trend with the increase EMT scores in which a significant level of these fractions was observed in the H-EMT group with a mesenchymal phenotype (Figure 3.5B and 3.5C).

Following these observations, we next analyzed the association between EMT scores and tumour infiltrating lymphocytes (TILs) using TIL-map cluster portal. Interestingly, we found a reduction in the number of TIL clusters by increasing EMT score from an epithelial to a mesenchymal state (Figure 3.5D). Moreover, the image processing analysis of histopathological images using TIL-map illustrated a low filtration of TILs in TME samples identified as H-EMT score compared to the L-EMT samples (Figure 3.5E).

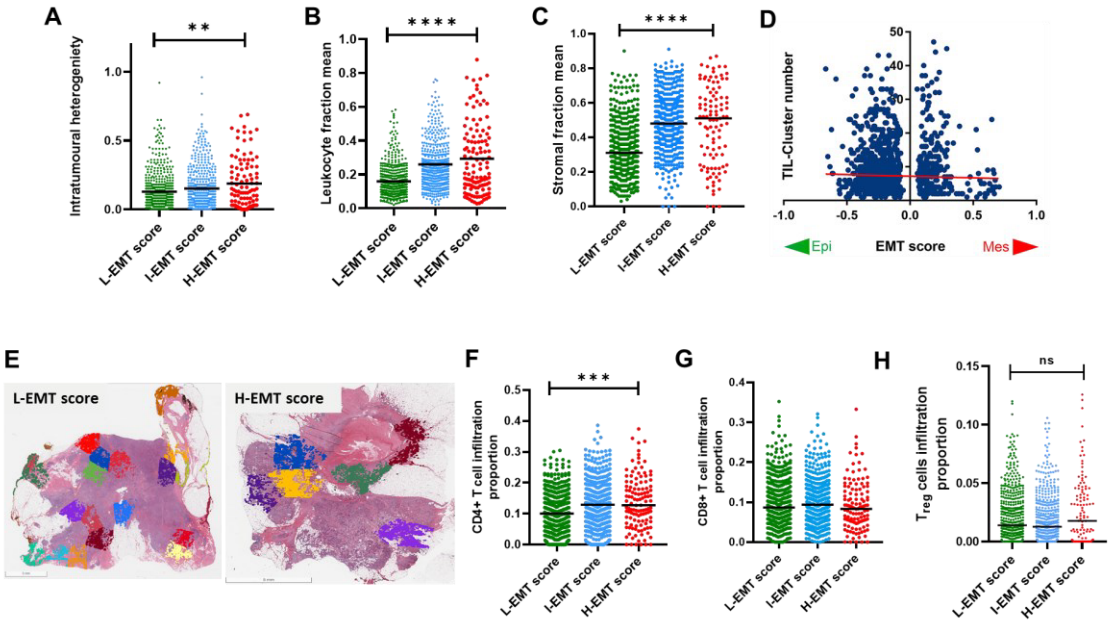

Figure 3.5. Comparison of TME features across three different EMT groups. (A-C) Distribution and level of intra-tumoral heterogeneity **(A)**, leukocyte fraction **(B)**, and stromal fraction **(C)** among three different EMT groups. **(D)** The association between EMT score and tumour infiltration lymphocytes (TIL). The graph illustrates a negative association between increase EMT score and reduction of TIL clusters. **(E)** Representative images of identified TIL clusters in the low-EMT score (left) and high EMT score (right) analyzed using TIL-Map algorithm. **(F-H)** The comparison between infiltration level of CD4+ T-cells **(F)**, CD8+ T-cells **(G)**, and Treg cells **(H)** across three EMT groups. The results depict a significant increase in the CD4+ T-cells and Treg cell infiltration in tumour samples with high EMT score compared to the low EMT groups. (Data are represented as mean ± SEM). ns, not significant; $*p < 0.05$; $**p < 0.01$; $***p < 0.001$; $****p < 0.0001$.

Furthermore, we assessed infiltration of CD4+ T-cells (Figure 3.5F), CD8+ T-cells (Figure 3.5G), and Treg cells (Figure 3.5H) in TME and their association with EMT scores. We found an immune-suppressive state among samples with an H-EMT score compared to L-EMT score, in which a significant increase in infiltration of CD4+ T-cells was observed while the number of cytotoxic T cells (CD8+ T cells) was reduced in H-EMT score (Figure 3.5F and 3.5G). Moreover, although Treg cell infiltration in H-EMT group did reach a statistically significant point, however we found a high proportion of infiltrated Treg cells in H-EMT samples.

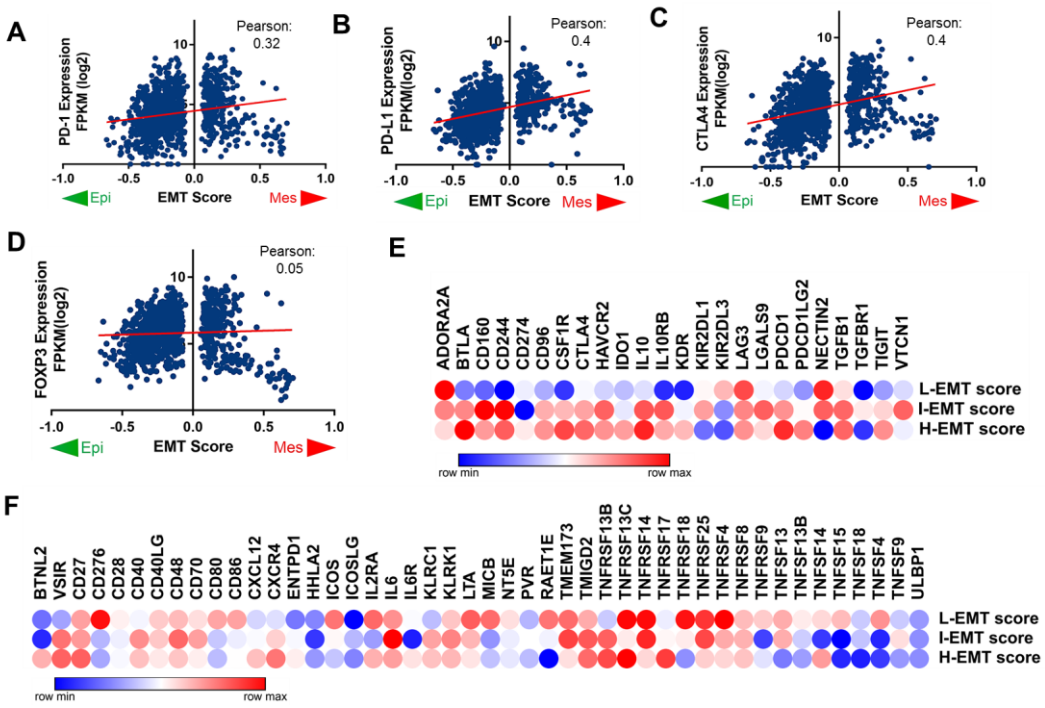

Figure 3.6. Association between EMT scores and expression of immune-checkpoints, immuno-inhibitors and immuno-stimulators. **(A-D)** The correlation coefficient analysis between EMT scores and the expression of PD-1 **(A)**, PD-L1 **(B)**, and CTLA4 **(C)** across 1108 samples from TCGA. The results illustrate a positive association between increase EMT score and high expression of immune checkpoints. **(E and F)** The expression of **(E)** immuno-inhibitor- and **(F)** immuno-stimulators-related genes across three EMT groups. A high expression of immuno-inhibitors genes enriched in H-EMT score samples, while L-EMT score and I-EMT score represent the expression of immuno-stimulators compared to H-EMT score samples.

We next analyzed the expression of immune-checkpoint proteins and their association with various EMT scores recognized as they represent a hallmark of immune-suppressive TIME. As expected, expression of the PD-1(Figure 3.6A), PD-L1 (Figure 3.6B), CTLA4 (Figure 3.6C), and FOXP3 (Figure 3.6D) showed a strong positive association with increased EMT score. In addition to these checkpoint inhibitors, the high expression of other inhibitors including IL10, PD-L2 (PDCD1LG2), and IDO1 enriched in samples with high EMT score. (Figure 3.6E). We also analyzed the expression of a panel of immuno-stimulators (Figure 3.6F), and found that, in contrast to immune-inhibitors, immuno-stimulators genes enriched in both L-EMT and I-EMT score samples rather than in H-EMT score specimens. Among these, CD80, CD276, and LTA represent a high expression level in samples with L-EMT score compared to I-EMT and H-EMT score groups (Figure 3.6F).

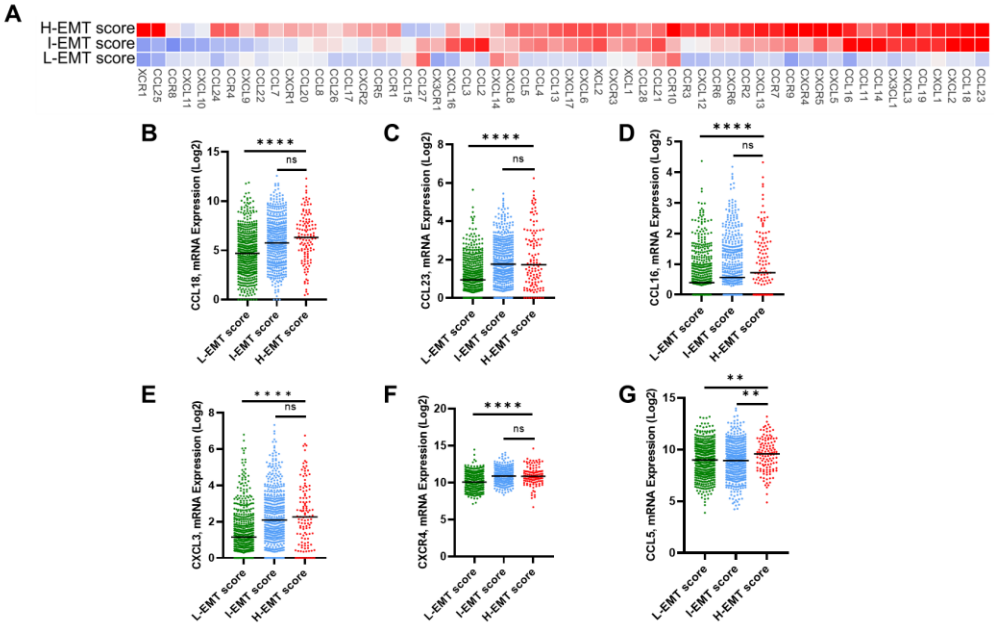

Figure 3.7: Expression of cytokines/chemokines and their receptors in different EMT groups. (A). The heatmap depicts the expression of a panel of 58 cytokines, chemokines and their receptors in three EMT groups. **(B-G)**. The statistical comparison between three EMT groups against most differentially expressed cytokines. The H-EMT score samples significantly expressed CCL18 **(B)**, CCL23 **(C)**, CCL16 **(D)**, CXCL3 **(E)**, CXCR4 **(F)**, and CCL5 **(G)** in comparison with other EMT groups. (Data are represented as mean ± SEM) ns, not significant; ∗p < 0.05; ∗∗p < 0.01; ∗∗∗p < 0.001; ∗∗∗∗p < 0.0001.

The secretion of cytokines and chemokines from tumour stromal cells and cancer cells plays a crucial role in rewiring TME toward developing an immune-suppressive TME. We assessed the expression of 59 different cytokines/chemokines and their receptors across EMT groups. As depicted in Figure 3.7, the expression of various cancer- and immune-suppression promoting cytokines and their ligands enriched in H-EMT group (Figure 3.7A). Among these, CCL18 (Figure 3.7B), CCL23 (Figure 3.7C), CCL16 (Figure 3.7D), CXCL3 (Figure 3.7E), CXCR4 (Figure 3.7F), and CCL5 (Figure 3.7G) were significantly expressed in H-EMT samples in comparison with other EMT groups. Taken together, these data indicate a negative association of EMT score with immune surveillance in breast carcinoma TIME.

3.3.4 Association between EMT-TFs and infiltration of immune cells in TME

An increasing number of *in-vitro* and *in-vivo* studies highlighted the crucial role of classical EMT markers in both expressions of immune-checkpoints and infiltration of immune cells, particularly Treg cells in various cancer types, including breast cancer [68, 302] For expanding our understanding of association between classical EMT markers with the infiltration of other immune cells, we analyzed the correlation coefficient between classical EMT markers and the infiltration level of immune cells (Figure 3.8). We found a strong positive association between the expression of mesenchymal markers including *ZEB1*, *VIM*, and *TWIST1* and infiltration of Treg cells (Figure 3.8A, 3.8B, and 3.8C; *blue panel*) and M2 macrophages (Figure 3.8A, 3.8B, and 3.8C; *green panel*), while the infiltration of NK cells (Figure 3.8A, 3.8B, and 3.8C; *brown panel*), DC cells (Figure 3.8A-C; *yellow panel*) and CD8+ T cells (Figure 3.8A, 3.8B, and 3.8C; *red panel*) negatively associated with the expression of these EMT-TFs. Moreover, although in comparison with mesenchymal-related genes, the expression of *CDH1*(E-cadherin) represents a weak negative association with infiltration of immune cells including CD8+ T cells. However, it seems that expression of this epithelial-related gene positively correlates with infiltration of DC cells (Figure 3.8E; *yellow panel*).

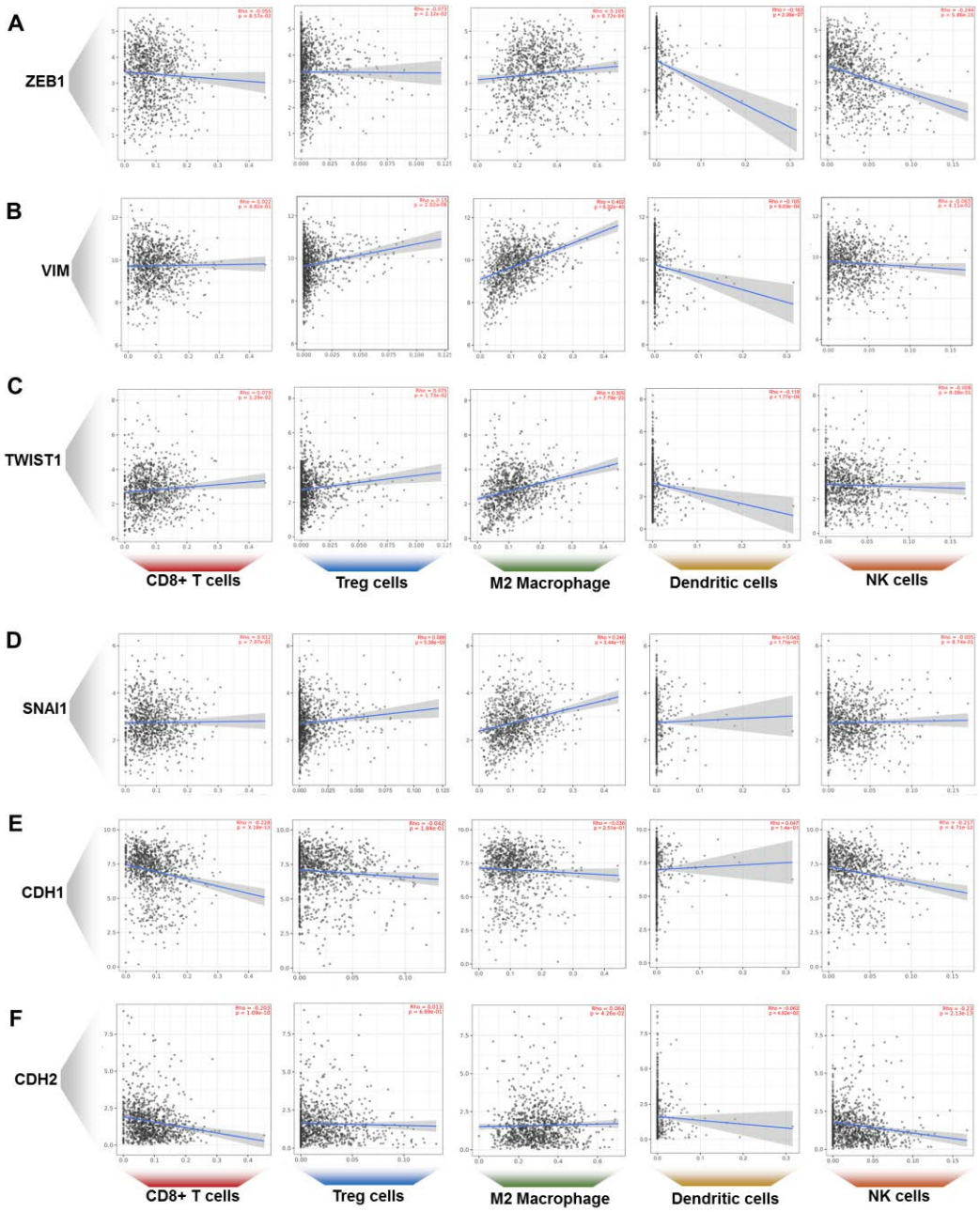

Figure 3.8: Correlation coefficient analysis between classical EMT related genes with infiltration of various immune cells. Associations between CD8+ T cells (*red*), Treg cells (*blue*), M2 macrophages (*green*), DC cells (*yellow*), and NK cells (*brown*) with the classical EMT-related genes, **(A)** ZEB1, **(B)** VIM, **(C)** TWIST1, **(D)** SNAI1, **(E)** CDH1(E-cadherin), and **(F)** CDH2 (N-cadherin). The data illustrate a strong positive association between the expression of mesenchymal-relate genes with a reduced infiltration of various immune cells.

3.3.5 Hot TME versus cold TME

To better demonstrate immune activity and its association with EMT status, we used a cell, ligand and receptor abundance diagram using the CRI-iAtlas portal (Figure 3.9). In this diagram, we included tumour cells, T-cells, macrophages, and dendritic cells and measured ligand-receptor binding abundances ranging from weak (Score: 0) to strong (Score: 1) in three different EMT groups (*Methods section*). As illustrated in Figureure-6, L-EMT score tumours represent a weak binding abundance (0.25-0.5) of major immune checkpoints PD-L1, PD-L2, PD-1, TIM3 and CTLA4 between tumour cells and immune cells resulting in a hot TME (Score: 0.75-1.0) (Figure 3.9A). Besides, intermediary state of binding abundance was illustrated for those samples with an I-EMT score state (Figure 3.9B). In contrast, a strong abundance score in the ligand-receptor binding of immune checkpoints in tumour cells and immune cells was observed in H-EMT score tumour cells indicating a cold TME (Score: 0.25-0.5) (Figure 3.9C). Taken together, these data indicate a negative association between EMT and tumour immunity.

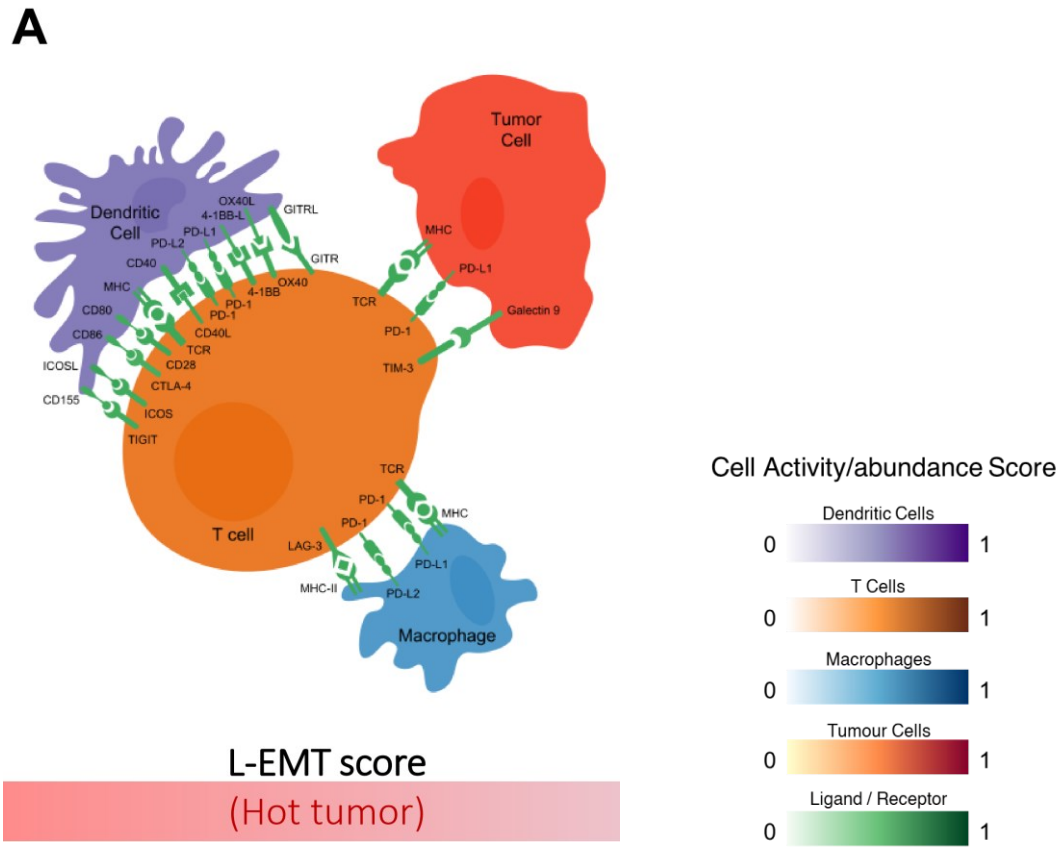

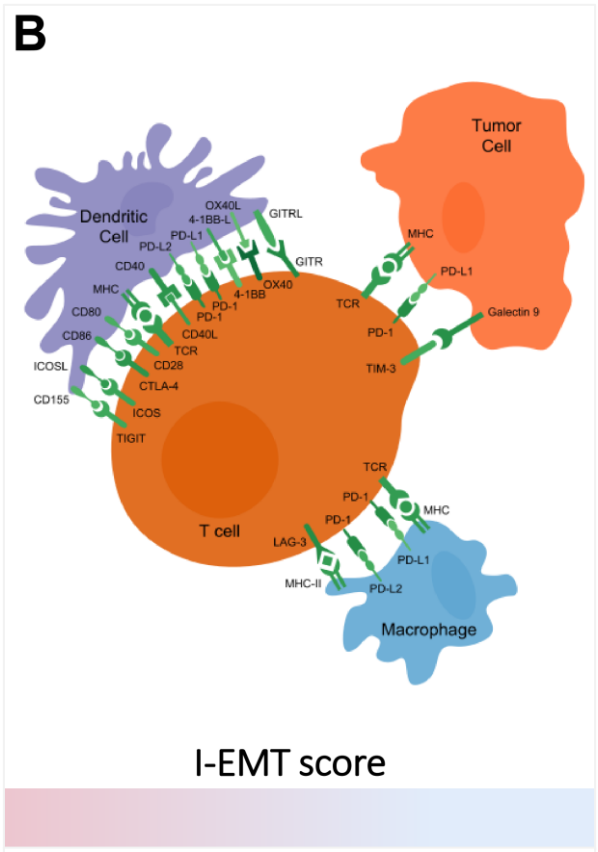
B
Tumor Cell
Dendritic Cell
OX40L
4-1BB-L
GITRL
PD-L1
PD-L2
GITR
CD40
MHC
4-1BB
OX40
PD-1
CD80
CD86
CD40L
TCR
ICOSL
CD28
CTLA-4
CD155
ICOS
TIGIT
MHC
PD-L1
Galectin 9
PD-1
TIM-3
T cell
LAG-3
MHC-II
PD-L2
Macrophage
I-EMT score
C
Tumor Cell
Dendritic Cell
H-EMT score
(Cold tumor)

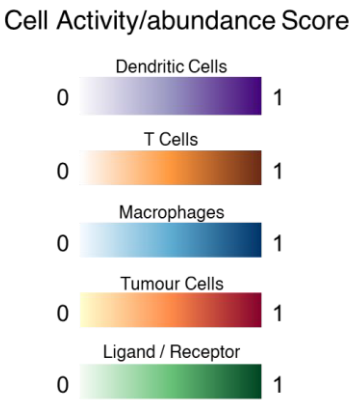
Cell Activity/abundance Score
Dendritic Cells
0
1
T Cells
0
1
Macrophages
0
1
Tumour Cells
0
1
Ligand / Receptor
0
1

Figure 3.9: Cell, ligand and receptor abundance analysis of tumour cells, T cells, macrophages, and DC cells. The diagram illustrates a comparison between immune cell activity of T cells, macrophages and DC cells in three different EMT states. Compared to the L-EMT score **(A)**, and I-EMT score **(B)** in which high immune activity is present (Hot TME), in H-EMT score samples **(C)** an increase in abundance level of immune checkpoints, and reduction in the level of MHC class I and II activity represent a cold TME.

3.4 Discussion

The role of the EMT program in rewiring TME toward tumour progression is well known [199, 303]. Recently, growing evidence highlighted the crucial role of the EMT program in promoting an induction a TIME through the expression of immune-suppressive proteins, including PD-1/PD-L1 and CTLA4 in both tumour and immune cells [68]. However, as EMT is a dynamic process, the immune activity of TME during the transition of carcinoma cells in the EMT program remains to be determined. In this study, we computationally investigate the immune activities of the TME across various EMT scores ranging from epithelial (Score -1) to mesenchymal (Score +1) in different subtypes of breast cancer. Numerous studies highlights tumour stromal cells, particularly cancer-associated fibroblasts (CAF) as regulator of tumour progression and immune-suppression through the induction of EMT in various cancer types, including breast cancer [22, 304]. To further validate these findings, our results revealed a positive association between tumour stromal cells and increase EMT score in three different sub-types of breast cancer particularly in TNBC samples which in turn can reduce tumour immunity in this sub-type through the upregulation of PD-1/PD-L1, CTLA4, FOXP3 [290, 305]. The activation of the EMT program by stromal constituents of the TME has been observed [20]. It has been shown that different immune cells that accumulated in the tumour stroma can crosstalk with carcinoma cells and activate EMT [78]. In recent studies, co-culturing pancreatic ductal epithelial cells with activated CD8+ T-cells and CD4+ T-cells resulted in the loss of epithelial marker E-cadherin expression acquisition of mesenchymal

markers ZEB1 and Vimentin in pancreatic cancer cells [78]. Similarly, an immune-induced EMT was observed in breast cancer, both in-vivo and in-vivo [79, 80].

Although we first observed a reduction in the level of TIL clusters via an increasing EMT score, we found a significant increase of CD4+ T-cells in samples with High EMT score in comparison with low EMT score, although no significant differences between the level of CD8+ T-cells observed between EMT groups.

The role of macrophages in inducing EMT via secretion of a distinct cohort of cytokines and chemokines has been extensively studied. Similar to tumour stromal cells, including CAFs, the TAMs secrete TGFβ, which in turn activate and induce EMT in carcinoma cells, including breast cancer [306, 307]. Moreover, the secretion of TNF by TAMs and its synergistic effects with TGFβ can promote EMT. Recent studies using mouse models highlighted crosstalk between tumour stromal cells, particularly tumour associated mesenchymal stem cells and TAM, in EMT regulation [308]. It has been shown that mesenchymal stem cells resident in TME enhance the formation of TAMs via secretion of GM-CSF. The activated TAMs released CCL18 which induce EMT and metastasis in breast cancer [309].

These studies highlighted the role of immune and stromal cells within TME to modulate and activate EMT. Once EMT is activated, carcinoma cells undergoing EMT or quasi-mesenchymal neoplastic cells able to modulate and rewire TME toward the acquisition of fully immune-suppressive TME through the induction of PD-1/PD-L1, CTLA4 and the secretion of TGF-β which in turn induce existence of T-reg cells in TME [310-312]. Similarly, we observed a high level of TGF-β and T-reg population in samples with high EMT scores compared low EMT score samples. The association between EMT-TFs, expression of the immune checkpoints, and immune cell infiltration has been studied [290, 313]. For instance, the expression of ZEB1 and SNAIL induce the expression of PD-L1 and suppress T cell-mediated attacks on carcinoma cells [291, 314].

The consistent association between EMT-related genes expression and T-cell infiltration has led to speculation regarding how EMT might impact the development of anti-tumour immunity and response to immune checkpoint blockade [289]. Our obtained results strongly highlighted link between the expression of EMT-related genes with immunotherapy

resistance regulated through the expression of various immune-checkpoints including PD-L1 [301].

The density and variety of tumour-infiltrating immune cells are closely related to prognosis and prediction of treatment efficacy, particularly immunotherapy [315]. Thus, understanding the differential composition of immune cells between the primary and metastatic TME may be an essential factor in predicting response to distinct immunotherapy strategies [316, 317]. Moreover, different patients with the same cancer type may represent differences in immune cell composition within the TIME, highlighting that mapping the composition of TIME in terms of infiltration of immune cells and their functional state plays a crucial role in both diagnosis and designing treatment approaches [318]. The TME could be characterized into cold (not T-cell inflamed) or hot (T-cell inflamed), which primarily relates to the levels of pro-inflammatory cytokine production and T cell infiltration [319]. A hot TME is characterized by T-cell infiltration and molecular signatures of immune activation and low expression of immune checkpoints, whereas a cold TME shows striking features of T-cell absence or exclusion. In general, the hot tumours present high mutational load (tumour mutation burden) and higher response rates to immunotherapy targeting PD-1/PD-L1 therapy [320]. Therefore, various studies have focused on converting noninflamed cold tumours into hot ones to achieve better response to immunotherapy [321]. The role of tumour stromal cells and non-immune cells in turning hot into cold TME have been highlighted in which they regulate infiltration of immune cells and expression of immune checkpoint through the various mechanisms, including EMT.

Through the cell, ligand and receptor abundance analysis, we showed that EMT scores positively associate with the switch of TME from hot-to-cold in which the immune activity of T cells reduce via expression of PD-L1 and PD-1 on cancer and T cells respectively. Additionally, attenuation in the cell surface display of major histocompatibility complex (MHC) class I and HLA molecules on cancer cells and macrophages on tumours with high EMT score indicate short presentation of antigen to T-cells and increase the presence of T-reg cells, a signature of cold TME. Hence, by decreasing the expression of MHC class I, tumour cells can evade T cell cytolytic functions [322, 323].

Taken together, our observations highlight low immune activity known as cold TME in tumour cells with high EMT score suggesting that patients with low EMT score of tumour tissue (considered as hot TME) may be eligible for immunotherapy. Additionally, these results emphasize the potential application of EMT scores as biomarker for predicting immunotherapy response in breast cancer particularly TNBC patients after recent approval of immunotherapy for this proportion of patients [324, 325].

Chapter 4

The role of CAF in Tumour Microenvironment and Tumour Immunity

Summary:

In the Chapter 3, I highlighted the role of cancer-associated fibroblasts (CAFs) in TME and regulation of both EMT and tumor immunity in triple-negative breast cancer. We hypothesized that targeting this population of cells in TME might reduce immune-suppression and invasion in cancer cells through the depletion of major cytokines. In this chapter, using 3D microfluidic device, I modeled CAFs-cancer interaction and demonstrated for the first time the effects anti-fibrotic drug called Pirfenidone on reduction of immune-suppressive capacity of CAFs and cancer cells by targeting cytokines. This chapter has been published as research article*.

* Aboulkheyr Es, Hamidreza, Sareh Zhand, Jean Paul Thiery, and Majid Ebrahimi Warkiani. "Pirfenidone reduces immune-suppressive capacity of cancer-associated fibroblasts through targeting CCL17 and TNF-beta." Integrative Biology 12, no. 7 (2020): 188-197.

4.1 Introduction

Breast cancer (BC) is the most prevalent cancer in women and remains a significant cause of cancer-associated death, despite attempts to provide effective therapies. Patients diagnosed with TNBC do not benefit from endocrine or targeted therapies, and conventional chemotherapy is still considered the clinical state of the art for this subtype. Immune checkpoint blockade (ICB) therapy has demonstrated success in various cancers but remains limited in TNBC treatment [1]. Among significant mechanisms responsible for tumour cells chemo/immunoresistance, there is increasing interest in understanding the role of the tumour microenvironment (TME) and its components in response to immune checkpoint inhibition [2–4]. Cancer-associated fibroblasts (CAFs) in the TME play a critical role in the complex process of tumour-stroma interaction. In aggressive breast cancers such as TNBC, the high abundance of CAFs associated with the aggressiveness of adenocarcinoma [5,6], disease recurrence [6–8], drug resistance [9,10], and lack of immune response [5,11]. Although tumour-promoting activities of CAFs is well explored [12], the immunomodulatory role of CAFs, as well as their potential application for therapeutic intervention, especially in the field of cancer immunotherapy, remain to be explored [13]. Thus, given their crucial role of CAFs in tumourigenesis and immunosuppression, in combination with the conventional treatments directed against carcinoma cells themselves, targeting CAFs might be a promising therapeutic approach. The recent approval of pirfenidone (PFD) for the treatment of idiopathic pulmonary fibrosis of lung relies on targeting activated fibroblast and their secretory functions[14].

Some recent studies were prompted to attempt co-targeting of CAFs and breast carcinoma cells with PFD and standard chemotherapy, respectively[15–17]. Although PFD was identified to mainly targets CAFs and their released cytokines however it remains elusive how PFD abrogate CAF induced immune suppression. Herein, we hypothesized whether targeting CAFs with PFD would enhance tumour immunity for immunotherapy by inhibiting various factors such as PD-L1 and related cytokines.

4.2 Materials and Methods

Figure 4.1 illustrates the workflow of this study, initiating from in-silico data analysis of cancer genome alteration and gene-drug association of pirfenidone, followed by microfluidic-based co-culture of CAF cells and breast carcinoma cells in the device and assessing the influence of pirfenidone on expression and secretion of PD-L1 and associated cytokines.

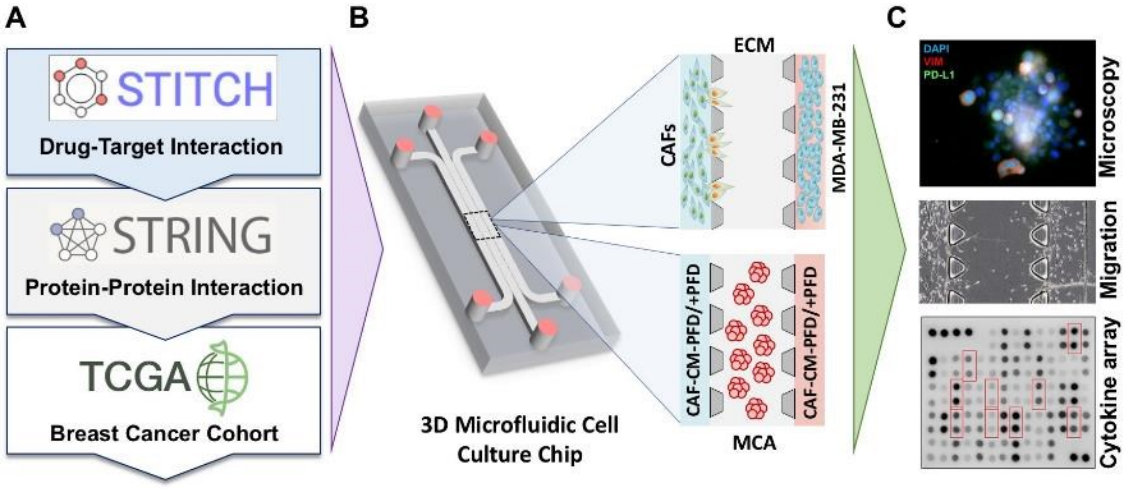

Figure 4.1. The workflow of study. (A). In-silico data analysis of PFD through the drug-protein interaction, protein-protein interaction of PFD and its target proteins followed by genomic alteration analysis of these proteins across 1085 breast carcinoma samples deposited in The Cancer Genome Atlas (BRCA-TCGA). (B). The schematic design of used microfluidic cell culture device in this study for both co-culturing CAFs and breast carcinoma cells and culturing multicellular aggregates (MCA) with CAF-CM included with or without PFD. (C). The downstream analysis performed on cells cultured in microfluidic device including immunofluorescent microscopy, distant migration analysis and cytokine profiling on derived conditioned medium from CAF cells.

4.2.1 In-silico data analysis

The TCGA-breast cancer genomic information and clinical data were downloaded from cBioportal data portal (https://www.cbioportal.org/) and analyzed under Bioconductor tools in R-Software (version 3.8). A detail description of used packages and related scripts to gene expression and mutation analysis are available at: https://bioconductor.org/packages/release/bioc/vignettes/maftools/inst/doc/maftools.html. The protein-protein-interaction and drug-protein interaction analysis were performed by using STRING PPI and SNITCH package under Cytoscape software (version 3.7.0).

4.2.2 Generation of CAF cells from normal fibroblasts

The normal fibroblasts purchased from Lonza (Cat no: CC-2512) and maintained with FGM-2 Fibroblast Growth Medium-2 BulletKit (Cat no: CC-3132) according to manufacture protocol. To produce MDA-MB-231 conditioned medium, we cultured MDA-MB-231 (Cat no: HTB-26. ATCC) cells at 100% confluence with serum-free Dulbecco's Modified Eagle's Media (DMEM) supplemented with 100 U/ml penicillin, and 100 μg/ml streptomycin (Sigma-Aldrich, St. Louis, MO, USA) for 48 hours. Normal fibroblasts were cultured at 80 percent confluence with condition medium derived from MDA-MB-231 for 48 hours.

4.2.3 Production of conditioned medium from CAF cells

We produced conditioned media of CAF (CAF-CM) using serum-free Dulbecco's Modified Eagle's Media (DMEM) to exclude the effects of growth factors present in serum for the following experiments. The confluent (80%) CAF cells were maintained in serum-free DMEM for 48 hours. In experiments designed to analyze the effects of pirfenidone (PFD) on CAFs, 100% confluent CAFs were cultured in serum-free DMEM containing 100 μM PFD for 48 hours (CAF-CM+PFD) [18]. The conditioned media were centrifuged for 10 minutes at 1,000 rpm after collection and stored at 80ºC until use. The resulting conditioned media were used to stimulate breast cancer cells. Proteins secreted into the supernatant were also examined through a cytokine profiling array against 42 targets.

4.2.4 Microfluidic Device Design and cell culture

The microfluidic tissue culture devices used in this study are purchased from AIM Biotech (Singapore). The devices consist of 2 media channels running parallel to and located on either

side of an extended central region containing the extracellular gel matrix like collagen type I named gel channel. Then, 200 µl collagen gel solution (2.5 mg/ml) at pH 7.4 was prepared on ice with 20 µl 10× PBS was mixed with 4 µl NaOH (0.5 N), 129.2 µl collagen type I (Corning), 10 µl freshly trypsinized and dissociated MCF7 targets at 50 × 10^6cells/ml (for 2D studies) or 10 µl cell suspension medium with 50–100 tumour spheroids (for 3D studies), and 22.9 µl dionized water. The collagen gel solution containing the MCF7 aggregates cells was then injected into the dedicated gel region of the device and kept in the cell culture incubator at 37°C and 5% CO_2 for 40 minutes to allow gel polymerization via thermal cross-linking. Devices with gel only (no embedded cells, control) were prepared as described above except adding cell suspension. Immediately after gel polymerization, DMEM or CAF-CM media were subsequently introduced to respective media channels. In case of migration assay, the central channel was filled with collagen gel solution, while the side channels were loaded with 2000 cell /120µl cultured medium.

4.2.5 Culturing single cells and multi-cellular aggregate (MCA) in microfluidic device

In order to obtain cell aggregates with the appropriate size for 3D studies, MCF7 cells were trypsinized and resuspended as individual cells at 100,000 cells/ml in DMEM, and cultured for 3 consecutive days onto a 100 mm ultra-low attachment dish (Corning Inc, NY, USA). Aggregates were collected and filtered in two consecutive filtration steps: (a) 40-µm filtration, in order to exclude cell aggregates smaller than 40 µm, and (b) 100-µm filtration, in order to exclude aggregates larger than 100 µm in diameter, and centrifuged by 250 g for 5 min to separate them from the supernatant. For 2D studies, cells were harvested with Trypsin/EDTA and centrifuged at 200 × g for 5 min. Cells were resuspended in growth

medium and mixed with collagen I solution for a final concentration of 6×10^5 cells per mL total collagen solution. The single cells and aggregates were then mixed with the collagen solution in order to inject to gel channel of AIM Biotech devices.

4.2.6 Immunofluorescent staining

Cell culture media was removed from the devices and samples in the microfluidic devices were first rinsed in cold PBS in this way that add 70 µl of media into one port and then add 50 µl into the opposite connected port of a media channel and then fixed in 4% paraformaldehyde (PFA) (Sigma-Aldrich, St. Louis, MO, USA) for 15 min at room temperature. Then 0.1% Triton-X 100 (Sigma-Aldrich, St. Louis, MO, USA) was added and incubated for 10 min before blocking by BSA 1% (cat no: A5611. Sigma-Aldrich, St. Louis, MO, USA) for 2 h, followed by staining of cells for α-SMA (1:100, cat no: ab197240. Abcam) Vimentin (1:200, cat no: 677804. Biolegend) and PD-L1(1:200, cat no: ab214958. Abcam). The mean fluorescent intensity of obtained images was analyzed using Cell-Sense software (Olympus, Japan). The normal fibroblasts and cancer cells cultured in DMEM were considered as control. To cell morphogenesis analysis, the cell area, circularity and aspect ratio were analyzed using MorphoLibJ in ImageJ software.

4.2.7 Cytokine array

The cytokine profiling of CAF-conditioned media included with and without PFD analyzed against a panel of 42 different inflammatory and cancer-promoting cytokines using the

Human Cytokine Antibody Array (Abcam, ab133997) according to the manufacturer's instructions.

4.2.8 Statistical analysis

All experiments were performed in three independent technical replicates (n=3). The results of quantitative experiments were expressed as mean ± SD. Statistical analysis was performed with Student t-test. *p-Value < 0.05 was considered as a statistically significant and ****p-value < 0.005 was considered as an extremely significant. Microscopic images are representative images from three independent experiments. The mean fluorescent intensity was measured and analyzed using ImageJ software.

4.3 Results

4.3.1 Association between CAF derived cytokines with PD-L1

According to the drug-bank information, PFD is an orally active small molecule that may inhibit collagen synthesis, down-regulate production of multiple cytokines and block fibroblast proliferation and stimulation in response to cytokines. In an in-silico analysis, first, we analyzed the drug-protein interaction of PFD (Figure 4.2A). As depicted in Figure 4.2A, PFD potentially targets IL-10 (Score: 0.836), TGFB1 (Score: 0.859), TIPM1 (Score: 0.824), and FN1 (Score: 0.822) (Figure 4.2A). Interestingly, the tissue-specific protein-protein interaction analysis between proteins targets of PFD and immune suppression protein PD-L1 (CD274) showed a positive correlation between IL10, and IL6 with CD274 (PD-L1), IL8 (CXCL8), and TNF-β (LTA) in breast cancer (Figure 4.2B). Following these observations, we analyzed alteration frequencies of these proteins across 1085 breast carcinoma samples

deposited in TCGA (Figure 4.2C). As shown in Figure 2C, high expression of TNF-β, TGF-β1, IL8, IL6 and IL10 was identified across patients diagnosed with breast invasive ductal carcinoma (IDC) compared to other subtypes such as breast invasive lobular carcinoma and mixed ductal-lobular carcinoma (Figure 4.2C). In line with the PPI interaction results, the Pearson correlation analysis shows a positive correlation between IL6, IL8, IL10, and TNF-β with PD-L1 among samples with IDC sub-types (Supplementary figure-1). It is well established that tumour stromal cells, particularly CAFs, can reprogram cancer cells in TME through the secretion of various cytokines and induce an immune-suppression TME (TIME) [19]. In line with these findings, we analyzed the expression of PD-L1 among samples with low- (LSI) and high-stromal index (HSI) according to their ESTIMATE score [20] (Figure 2D). As we expected, a significant expression of the PD-L1 (Figure 4.2D) was observed among HSI tumour samples compared to LSI group, indicating a positive association between the proportion of tumour stromal cells and expression of PD-L1. Taken together, these data suggest that targeting CAFs and its released cytokines may reduce the immune-suppression capacity of TME through the reduction of PD-L1 expression.

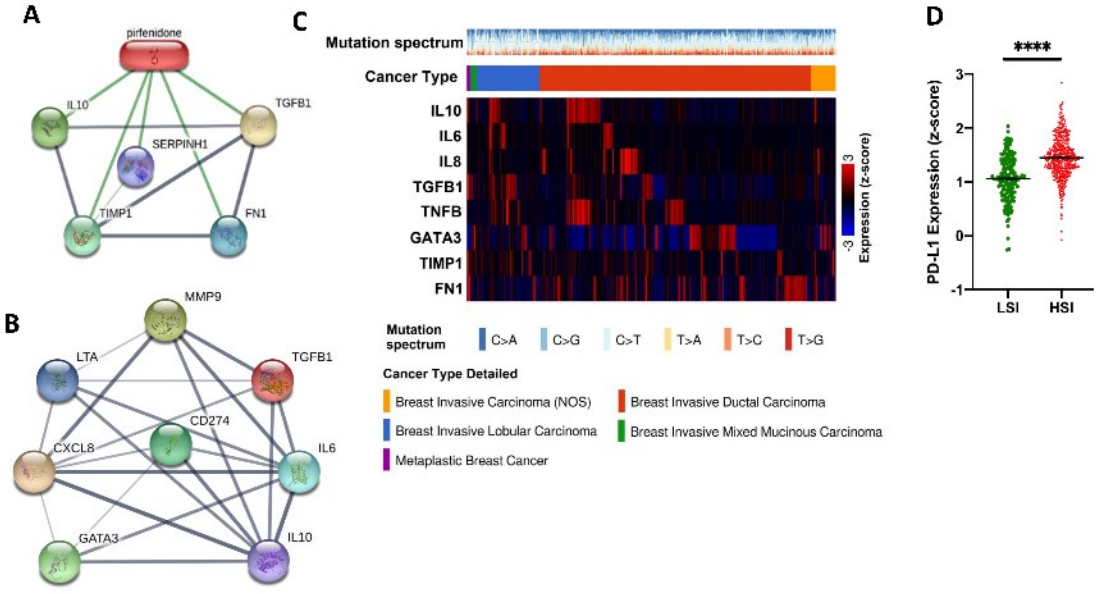

Figure 4.2. **In-silico analysis of PFD target proteins and their alterations across breast carcinoma samples in TCGA**. (A). Drug-protein interaction analysis results showing main targets of PFD. (B). The protein-protein interaction results retrieved from STRING database. The result shows a positive correlation between PFD protein targets with various interleukins including IL6 and IL8 (CXCL8), TNF-β (LTA), and PD-L1 (CD274). (C). The oncoprint results of genomic alteration status of PFD targets proteins and their positive associated proteins across 1085 breast carcinoma samples in TCGA. The data depicts a high expression level of TNF-β, IL8, and IL10 in patient with invasive ductal carcinoma subtypes in comparison with other subtypes. (D). Comparison between expression level of PD-L1 among samples with high and low stromal index ($P < 0.005$).

4.3.2 CAFs induce a phenotype switch in cancer cells

To generate CAF cells, we cultured normal human lung fibroblasts with condition medium derived from MDA-MB-231 for 72 hours (Figure 4.3A), followed by characterization of induced cells in terms of expression of the CAF marker alpha-smooth muscle actin (α-SMA) and also the expression of PD-L1. As an expression of α-SMA is one of the hallmarks of CAF cells, we observed significant expression of α-SMA in cultured fibroblasts with MDA-MB-

231 condition medium compared to the cells cultured with DMEM (Figure 4.3B, 4.3C). Various studies have shown the expression of PD-L1 on CAF cells [5]. In line with these results, we assessed the expression of PD-L1 on generated CAFs at the protein level. As depicted in Figure 4.3D, our generated CAFs significantly expressed PD-L1 compared to the normal fibroblasts.

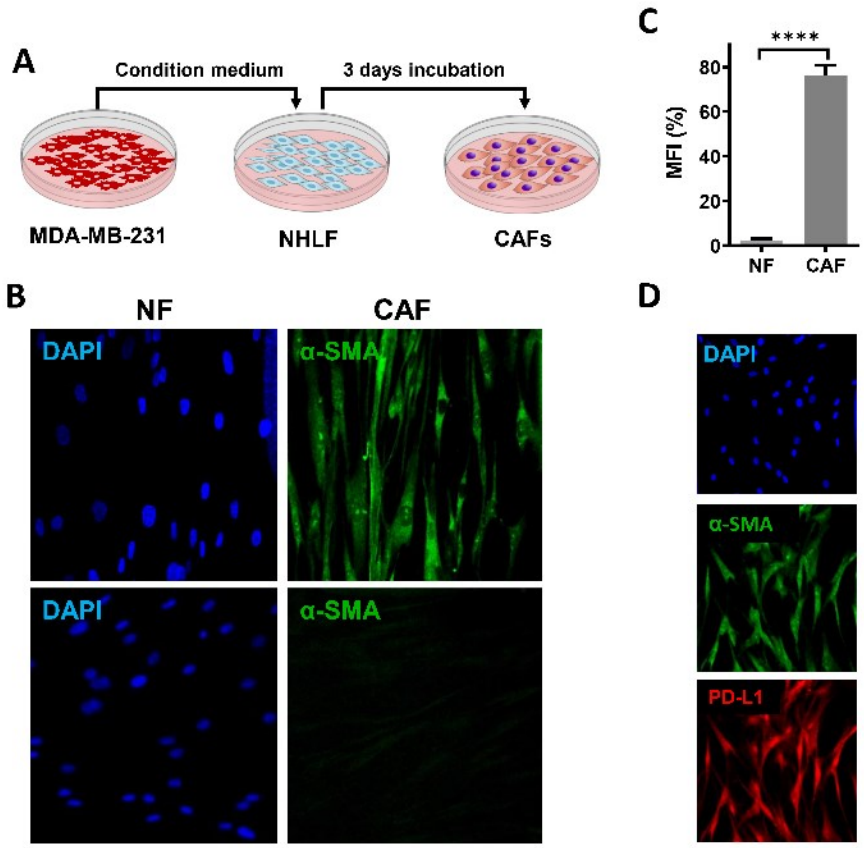

Figure 4.3. Transformation of normal fibroblast to CAFs and its characterization. (A). Schematic of method used to generate CAF from normal fibroblasts (NF). (B, C). Confocal immunofluorescence image of α-SMA expression (green) in generated CAFs compared to the NF. The nucleus is stained with DAPI (blue) (scale bar: 20μm. $P < 0.005$). (D). Expression of PD-L1 in CAFs (scale bar: 50μm).

Numerous in-vitro and in-vivo studies highlighted migration and recruitment of CAF cells to the TME [21]. To model this characteristic feature of CAFs, we performed a co-cultured assay in a three channels 3D microfluidic cell culture device (Figure 4.4A), where the central channel was filled with collagen type-I, while CAF cells and cancer cells were cultured in one of two side channels (Figure 4.4A). Compared to the normal fibroblasts, the CAFs not only invaded the central channel containing collagen type-1 and migrated toward the cancer cell containing channel (Figure 4.4B), but also significantly expressed both α-SMA (Figure 4.4C) and PD-L1 (Figure 4.4D), indicating a trans-differentiation of normal fibroblasts into CAF.

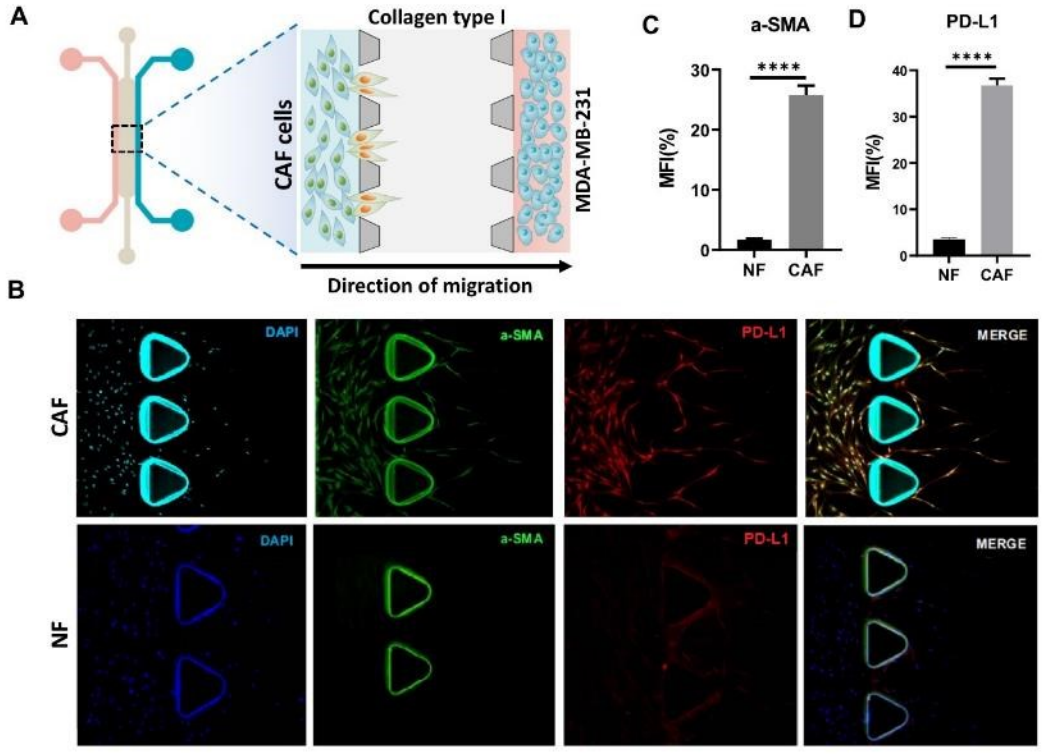

Figure 4.4. Migration of CAFs. (A). the schematic design of experiments in a microfluidic device by culturing CAFs in one of side channels while the MDA-MB-231 cells are cultured in opposite channel. The central channel is filled by collagen type-I as a standard ECM. (B). immunofluorescence image of migrating CAFs toward opposite

channel where invasive breast cancer cells are seeded. The CAFs highly expressed both α-SMA (green) and PD-L1 (red) in comparison with NF. (Scale bar: 100µm). (C, D). Quantitative analysis of mean fluorescent intensity (MFI) of α-SMA and PD-L1 expression in CAFs and NF. (n=3) ($P < 0.005$).

The phenotypic transformation from an epithelial- to mesenchymal-like, is a significant step in invasion and metastasis of carcinoma cells, which can be induced through the tumour stromal cells, particularly CAF cells. To assess the effects of cytokines derived from CAFs on the phenotypic switch of carcinoma cells, we cultured MCF7 cells known as an epithelial-like breast carcinoma with CAF-CM for 72 hours, followed by a shape descriptor analysis. As depicted in Figure 5, in line with a microscopic observation (Figure 4.5A), increase in aspect ratio and reduction of circularity level indicated phenotypic switch of carcinoma cells from epithelial to a mesenchymal-like phenotype acquiring invasive phenotype induced by CAF-CM (Figure 4.5B, C. *$P < 0.001$*). These results are in line with previous observations showing that CAF cells directly or indirectly able to reprogram cancer cells toward induction of an aggressive TME.

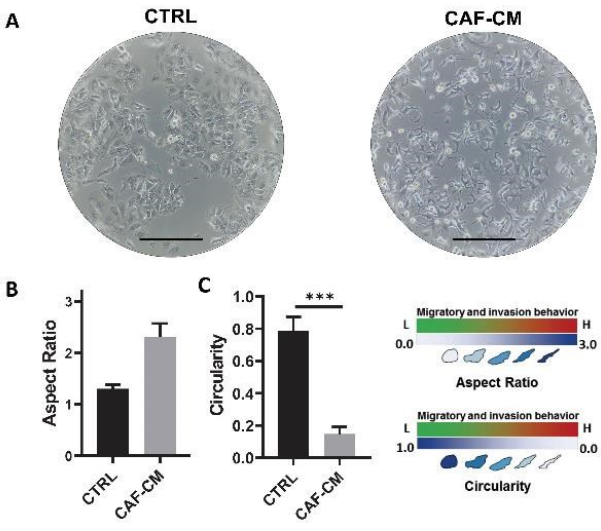

Figure 4.5. Phenotypic transformation of MCF7 cells cultured with CAF-CM. (A). Microscopic image of MCF7 cells cultured with CAF-CM (right) and conventional culture medium (left), showing a phenotype switch in group of cells cultured in CAF-CM toward an invasive behavior compared to the control group (B, C). The quantitative results of morphometric analysis of aspect ratio (B) and circularity level (C) in transformed cells. (n=3).

4.3.3 CAFs induce expression of PD-L1 on PD-L1 low cancer cells

To determine whether CAFs cells able to induce expression of PD-L1 on breast cancer cells, we generated tumour aggregate from MCF7 cells; a PD-L1 negative breast cancer cell [22] and cultured with CAF condition medium (CAF-CM) in a microfluidic device for 72 hours (Figure 4.6A). The generated aggregates mixed with collagen type I as standard ECM and were loaded in the central channel of the device followed by filling the side channels with standard cell culture medium (control) or CAF-CM (Figure 4.6A). Interestingly, CAF-CM significantly increased expression of both PD-L1 and VIM at the protein level in MCF7 aggregates (Figure 6B-D). Notably, we observed low expression of PD-L1 and VIM in the control group. We previously reported [22] effects of ECM and tumour cell aggregation on the expression of PD-L1 and VIM; here, we show that CAF-CM also induced the expression of these genes. These data suggest that cytokines released from CAF cells play an immune suppression role through the induction of PD-L1 expression.

4.3.4 Pirfenidone reduces invasion and migration capacity of CAF and cancer cells

To assess the inhibitory effects of PFD on invasion and migration capacity of both breast cancer cells and CAFs, first, we cultured CAF cells at the highest confluence in a serum-free medium with PFD (100μM) for 48 hours (CAF-CM/+PFD), followed by culturing MCF7 cells with this generated condition medium. MCF7 cells cultured with CAF-CM+PFD showed a significant increase in circularity level and a slight reduction in aspect ratio and cell area (Figure 4.7A-D) as compared to untreated conditioned medium (Figure 4.7A

middle), indicating that treating CAFs with PFD may inhibit invasive properties of cancer cells induced by CAFs. To show migratory inhibition effects of PFD, we performed co-culture assay of CAFs and invasive breast cancer cell line MDA-MB-231 in the presence (+PFD) or absence (-PFD) of PFD (100µM) in a 3D cell culture microfluidic device for 72 hours (Figure 4.7E). Figure 7E shows a snapshot image of migration of cells through the collagen type-1 toward the opposite channel in three different time-points. We found that PFD reduced migration of the cells in a time-dependent manner, where after 48 hours, a significant reduction in migration distance of both cells was observed. The maximum inhibition recorded after 72 hours of treating cells with PFD. (Figure 4.7E, 4.7F).

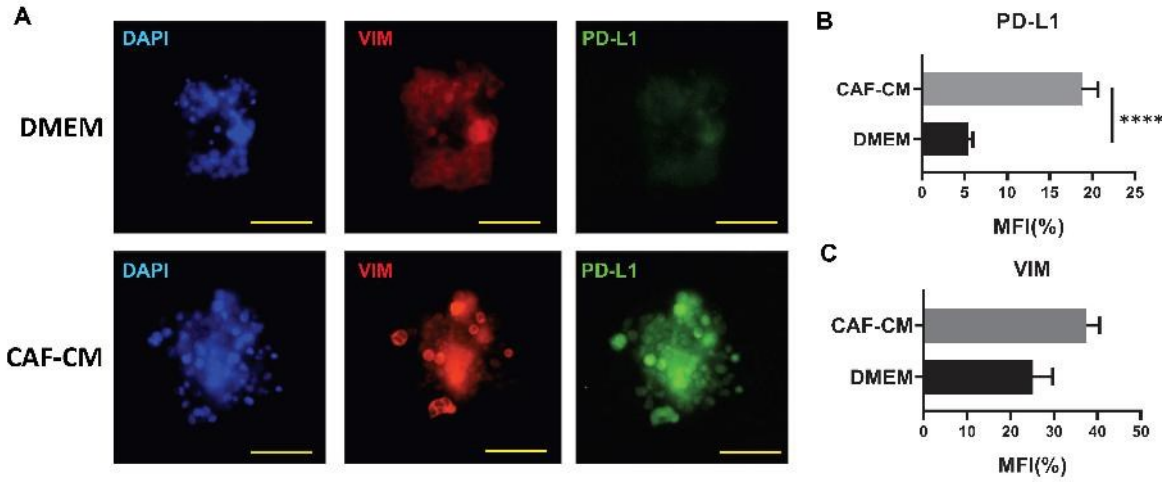

Figure 4.6. Culturing MCF7-derived MCA with CAF-CM. (A). Immunofluorescent image of MCA cultured with either CAF-CM or conventional culture medium (DMEM) and expression of VIM (red), PD-L1 (green), and nucleus (blue) in these group of cells. (Scale bar: 100µm) (B, C). Quantitative analysis of mean fluorescent intensity (MFI) of PD-L1 (B) and VIM (C) in MCAs. CAF-CM significantly induced expression of PD-L1. (n=3) ($P < 0.005$).

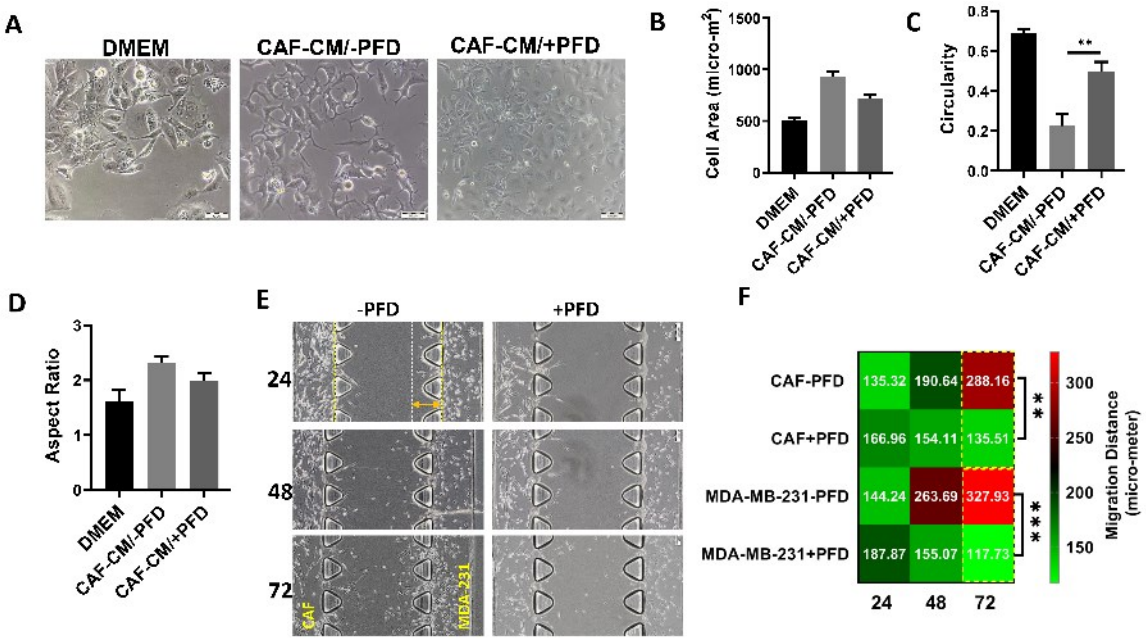

Figure 4.7. Effects of PFD on phenotype transformation and migration of cells. (A). representative image of cells cultured with CAF-CM included with and without PFD for 72 hours. (B-D). Quantitative analysis of morphometric parameters; cell area (B), circularity level (C), and aspect ratio (D) of cells cultured in conventional DMEM and CAF-CM including with or without PFD. (E). A snapshot of co-culture microfluidic device contained CAF cells and breast carcinoma cells cultured with serum free medium included with or without PFD. The central channel is filled with collagen type-I as ECM. (scale bar: 200µm). (F). Quantitative analysis of migration distance (µm) of both CAF cells and breast carcinoma cells cultured in microfluidic device.

4.3.5 Pirfenidone reduces expression of PD-L1 on CAF cells by targeting various cytokines

We next assessed the expression level of PD-L1 protein on CAF cells treated with PFD. Interestingly, we observed that in comparison with non-treatment samples, PFD treatment not only reduced the level of s-SMA in CAFs but also significantly decreased level of PD-L1 at protein level (Figure 4.8A, 4.8B).

To better understand the PFD effects, we assess the expression and secretion of various cytokines in both treated- and non-PFD treated groups (Figure 4.9). We found that PFD significantly dropped the secretion of TNF-beta and CCL17 in CAF cells in comparison with the non-treated group (CAF-CM-PFD) (Figure 4.9A, B, E). Besides, levels of other cytokines, including OSM, CSF, IL6, IL8, and CXCl1 were reduced following treatment with PFD. Additionally, the PPI network analysis showed a positive association between PFD targeted cytokines and PD-L1, particularly IL6, CCL17, and CXCL1 (Fig 4.9I). Taken together, these data suggest that PFD can reduce both invasion and immune suppression capacity of cancer cells in TME by targeting various cytokines in CAF cells.

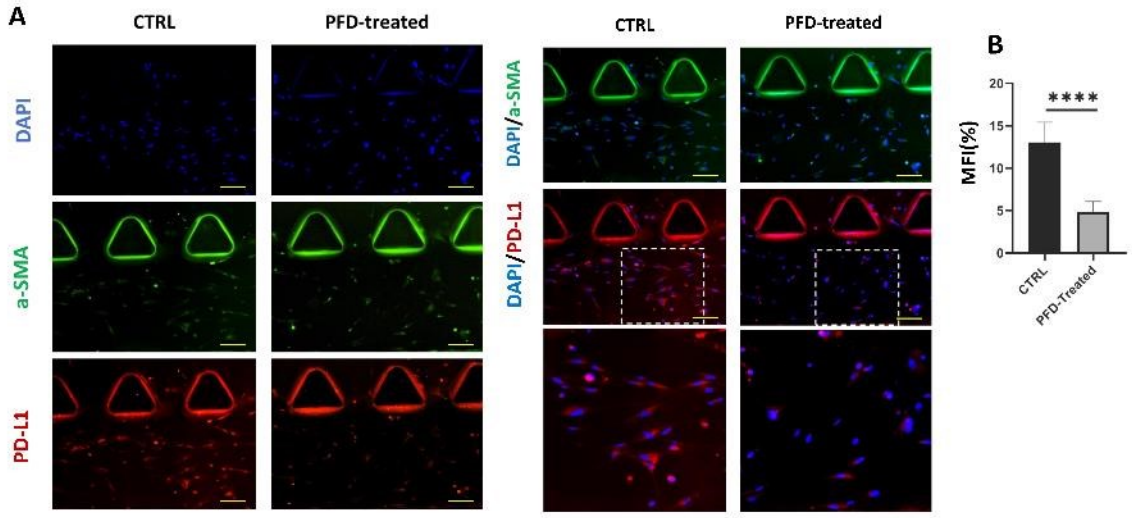

Figure 4.8. **Effects of PFD on expression of PD-L1 in CAFs**. (A). Immunofluorescent image of CAFs cultured and treated with or without PFD in microfluidic device and stained with α-SMA (green), PD-L1 (red), and nucleus (blue) (scale bar: 200μm). (B). quantification of mean fluorescent intensity (MFI) of PD-L1 expression in both un-treated and treated CAFs with PFD. (n=3) ($P < 0.005$).

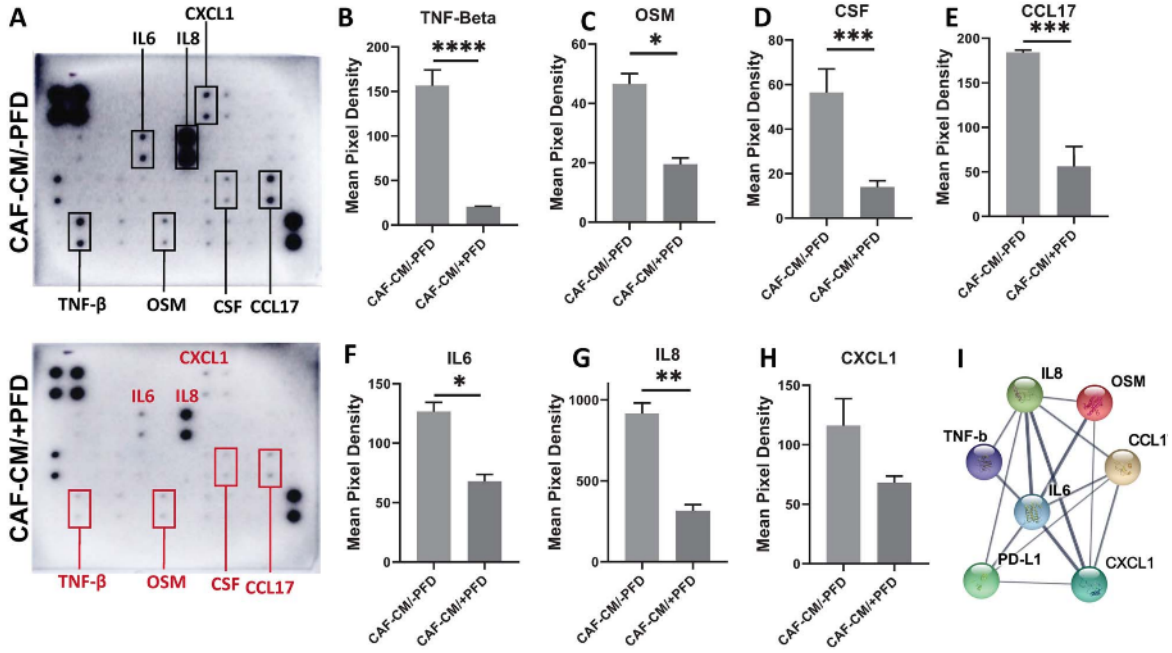

Figure 4.9. Cytokine profiling of CAF-CM. (A). The picture of cytokine array results performed for CAF-CM before and after treatment with PFD. The top left and bottom right dots are negative and positive control of array respectively. (B-H). The mean pixel density analysis results of differentially released cytokines TNF-β (B) ($P < 0.005$), OSM (C), CSF (D), CCL17 (E), IL6 (F), IL8 (G), and CXCL1 (H) from CAF treated with (CAF-CM/+PFD) and without (CAF-CM/-PFD) PFD (n=3). (I). Protein-protein interaction network and correlation analysis between differentially released cytokines and PD-L1.

4.4 Discussion

Within the tumour stromal milieu, CAFs are the most prominent cell type and are known to be critical contributors to tumour progression, metastasis and drug resistance against a broad spectrum of therapies including immunotherapy [2]. CAF directed therapy designed to either eliminate them or potentially reprogram them back to their normal resting phenotype is showing some promise. For example, a recent study on pancreatic adenocarcinoma has demonstrated that targeting vitamin-D receptor (VDR) by calcipotriol in stromal cells can

reprogram pancreatic cell-derived CAFs, resulting in higher intra-tumoural penetration of gemcitabine, tumour shrinkage and improved patient survival[23].

Although numerous studies highlighted various therapeutic agents to target CAFs in different cancers[15,16,24,25]; its effects on the reduction of immune suppression potential of CAFs in breast carcinoma remained to show [26]. Herein, for the first time, we show that targeting CAFs with PFD can retard immunosuppressive capacity of CAFs and consequently its PD-L1 expression stimulation on breast carcinoma cells through production blockage of various cytokines including CCL17, CXCL1, TNF-β, IL6, and IL8 in CAFs. Additionally, through the using microfluidic co-culture platform [27–29], we demonstrated that treatment of CAF cells with PFD not only reduce expression of a-SMA in CAF cells but also decrease migration potential of CAFs and breast carcinoma cells in a time-dependent manner.

A large number of studies highlighted the critical role of these factors in the interaction of the tumour-stromal cell toward the induction of an immune-suppressive TME [5]. Studies on genome and proteome analysis of CAFs showed that CAFs exhibit particular immunomodulatory secretome including but not limited to these factors to reshape TME toward tumour progression and potentially regulate the innate immune suppression in several ways [30–34]. The CCL17 was reported as a key element in the re-education of monocytes and generation of tumour-associated macrophages that expressed IDO and PD-L1 [35]. Additionally, it has been shown that production and secretion of CCL17 within TME through the CAFs trigger recruitment of Myeloid-derived suppressor cells (MDSCs) and T_{reg} cells to TME promoting an immunosuppressive TME in various cancers[36–39]. Furthermore, Omland and colleagues [40] reported that CXCL12 and CCL17 secreted from resident CAFs

within Cutaneous basal cell carcinoma TME increase tumour progression and immunosuppression.

The immune-modulation role of inflammatory cytokines has been evident extensively. A large amount of in-vitro and in-vivo studies documented that secretion of IL-6 and IL-8 by CAFs positively regulate expression of PD-1/PD-L1 axis in TME, in which targeting these interleukins may reverse immune resistance[34,41–43]. In this regard, Tsukamoto and colleagues [41] found that combinatorial targeting of IL6 and PD-L1 not only improves infiltration of IFNγ-producing CD4+ T cells in tumour tissues but also enhance expression of T-cells attracting related chemokines in TME. Consistence with these results, we show that CAF-CM significantly increased immunosuppression capacity of breast carcinoma cells through the expression of PD-L1, in which cytokine profiling and PPI network analysis depicted a positive association between secretion of IL6, IL8, CCL17, and CXCL1 with PD-L1. In addition to these data and line with previous studies [44], we also show that CAFs able to stimulate phenotype switch in carcinoma cells from a non-invasive to an invasive phenotype in which increased expression of vimentin in non-invasive carcinoma cells by CAFs can trigger EMT program and invasiveness. Additionally, we demonstrated that treatment CAFs cells with PFD decreased migration potential of both CAFs and breast carcinoma cells modelled in a microfluidic device. Similar observations were reported previously for migratory inhibition effect of PFD on both cancer cells and CAFs in pancreatic cancer [18] and breast cancer [45]. For instance, Ren and colleagues demonstrated that CAF-CM significantly induces expression of HOTAIR and consequently promote EMT program in invasive breast cancer in which targeting CAFs with PFD blocks TGF-β1/HOTAIR axis and decrease migration potential of MDA-MB-231 cells [45].

Taken together, at an in-vitro stage, these data suggest that targeting CAFs with PFD may reduce both metastasis and immune-suppressive capacity of CAFs in TME. Additionally, the potential application of PFD to deplete secretion of the various cancer-promoting cytokines and chemokines expressed in different sub-types of BC (Figure 2C) (Figure 9) suggesting the potential of applying PFD in combination with current treatment regimens particularly immunotherapy. Further studies focused on complex models of TME, including genetically engineered mouse model (GEMM) included with immune systems elements are required to approve the potential application of PFD on improving immunotherapy and chemotherapy efficacy.

Chapter 5

The Role of Tumour-Associated Mesenchymal-Stem Cells in Regulation of Tumour Immunity

Summary:

Following study CAFs in previous chapter, in this chapter, I studied another angle of tumour microenvironment; tumour-associated mesenchymal stem cells (TAMSCs). This chapter demonstrates that mesenchymal-stem cells as a potent immune-modulator regulate immune-suppression in breast cancer and induce the expression of immune-checkpoints mainly PD-L1. Moreover, this chapter highlights targeting these cells using Pirfenidone reduce the expression of immune-suppressive and cancer-promoting cytokines. The results of this chapter have been published*.

* Aboulkheyr Es, Hamidreza, Bahareh Bigdeli, Sareh Zhand, Amir R. Aref, Jean P. Thiery, and Majid E. Warkiani. "Mesenchymal stem cells induce PD-L1 expression through the secretion of CCL5 in breast cancer cells." Journal of Cellular Physiology 236, no. 5 (2021): 3918-3928.

5.1 Introduction

Although in recent years, immunotherapy has become a breakthrough in cancer therapy and clinical trials with antibodies to PD-1/PD-L1 checkpoint inhibitors have shown unprecedented responses in numerous solid tumours; however, few tumour types have shown weak response to this class of immunotherapy including breast cancer, bladder cancer, pancreatic cancer, and colon cancer [284, 326].

The tumour microenvironment (TME), especially its cellular components, are now known to interfere with the response to immune checkpoint inhibitors [1, 68]. Mesenchymal stem cells (MSCs) with multiple differentiation potentials and immune-modulating functions are one of the essential cell components of the TME [54]. It has been shown that MSCs colonising tumours and developing into tumour associated MSCs (TA-MSCs) and cancer-associated fibroblasts (CAFs) [55, 56] have recently emerged as therapeutic targets [57, 58]. Besides, in response to paracrine signals from growing tumours in the TME, TA-MSCs continuously rewire the TME, facilitating tumour growth, metastasis, and modifying the response to various anticancer treatments including immunotherapy [67, 327].

The bidirectional interactions between MSCs and cancer cells can result in the production of various growth factors, chemokines, and cytokines, facilitating cell migration, survival, proliferation, and organisation of cancer cells [54]. Moreover, MSCs have been extensively reported to possess immunosuppressive properties via the modulation of immune cells within both the innate and adaptive systems. Recently, numerous studies highlighted the immunosuppressive potential of MSCs in TME employing induction of PD-1 and PD-L1 expression on T-cells and tumour cells, respectively [328-332]. In the context of breast cancer, besides the activation of PD-1 on T cells, the expression of PD-L1 on tumour cells

facilitates immune resistance to immunotherapy.

The role of CAFs cells in acquired resistance of cancer cells to a wide range of anticancer therapeutics including immunotherapy has been demonstrated in previous studies in breast cancers [9]; however, whether MSCs with immunomodulatory properties able to generate an immunosuppressive TME through induction of PD-L1 expression on breast cancer cells remained to be shown. This study aimed to investigate whether MSC regulates the PD-L1 expression in breast cancer cells and explore the specific molecular mechanism. Our results evidenced the expression of PD-L1 on PD-L1 low expressing breast cancer cells by MSC cells.

5.2 Materials and Methods

5.2.1 Cell culture

Human adipose derived mesenchymal stem cells (AD-MSCs, Regeneus. Australia) were maintained in α-modified minimum essential medium (α-MEM) (Thermo Fisher Scientific, USA) supplemented with 10% (v/v) fetal bovine serum (FBS) (Thermo Fisher Scientific, USA) and 1% pen/strep in a humidified atmosphere of 5% CO_2 at 37°C. Human breast adenocarcinoma MCF7 cells were cultured in Dulbecco's modified Eagle's medium (DMEM) (Thermo Fisher Scientific, USA) supplemented with 10% (v/v) FBS and 100 U penicillin/ml and 100µg streptomycin/ml in the same mentioned condition. The culture medium was changed two to three times per week, and subculture was performed by digestion with 0.25% trypsin/0.02 % EDTA when the cells were nearly confluent. AD-MSCs cells from passages 2–5 was used for the experiments.

5.2.2 Preparation of conditioned medium

AD-MSCs were cultured at a density of 10,000 cells/cm^2 in α-MEM medium supplemented with 10% FBS until they reached 90% confluence. Then, the cells were washed three times with PBS and the culture media were replaced with serum-free DMEM and were incubated for an additional 48 h. The concentrated supernatant was collected by centrifuging (Eppendorf, Hauppauge, NY, USA) at 1200 RPM for 5 min at room temperature, filtered through 0.45μm filters, and designated as MSC-conditioned medium (MSC-CM). The MSC-CM was then stored at -70˚C until use.

5.2.3 Microfluidic device design and cell culture

The microfluidic tissue culture devices used in this study are purchased from AIM Biotech Company (Singapore). The devices consist of 2 media channels running parallel to and located on either side of an extended central region containing the extracellular gel matrix like collagen type-I named gel channel. Then, 200 µl collagen gel solution (2.5mg/ml) at pH 7.4 was prepared on ice with 20µl 10× PBS was mixed with 4µl NaOH (0.5N), 129.2µl collagen type-I (Corning, Cat# 354236.), 10µl freshly trypsinised and dissociated MCF7 targets at 50×10^6 cells/ml (for 2D studies) or 10µl cell suspension medium with 50–100 tumour spheroids (for 3D studies), and 22.9µl cell culture water. The collagen gel solution containing single MCF7 cells or cell clusters designated multicellular aggregates was then injected into the dedicated gel region of the device and kept in the cell culture incubator at 37°C and 5% CO_2 for 40 minutes to allow gel polymerisation via thermal cross-linking. Devices with gel only (no embedded cells, control) were prepared similarly by adding

collagen gel solution containing 20µl 10×PBS, 4µl NaOH(0.5N), 129.2µl collagen type-I, and 42.8µl of deionised water. Immediately after gel polymerisation, the two side channels filled with 120µl of DMEM and MSC-CM.

5.2.4 Culturing single and multi-cellular aggregate (MCA) in the microfluidic device

In order to obtain multi-cellular aggregates with the appropriate size for 3D studies, MCF7 cells were trypsinised and resuspended as individual cells at 100,000 cells/ml in DMEM and cultured for 3 consecutive days onto a 100mm ultra-low attachment dish (Corning). Aggregates were collected and filtered in two consecutive filtration steps: (a) 40µm filtration, in order to exclude all the cell aggregates smaller than 40µm, and (b) 100µm filtration, in order to exclude all aggregates larger than 100µm in diameter, and centrifuged by 250×g for 5 min to separate them from the supernatant. For 2D studies, cells were harvested with Trypsin/EDTA and centrifuged at 200×g for 5 min. Cells were resuspended in growth medium and mixed with collagen type-I solution for a final concentration of 6×10^5 cells/ml total collagen solution. The single cells and aggregates were then mixed with the collagen solution in order to inject to gel channel of AIM Biotech devices [281, 333].

5.2.5 Immunofluorescent staining

Cell culture media was removed from the devices, and samples in the microfluidic devices were washed with PBS followed by fixation of samples with 4% paraformaldehyde (PFA) (Sigma-Aldrich, Cat# 158127) for 15 min at room temperature. Next, 0.1% Triton-X(Sigma-

Aldrich, Cat# X100) was added and incubated for 10 min before blocking by BSA 1% for 2h. Finally, the samples were stained with E-cadherin (1:200, Biolegend, Cat# 324104), Vimentin (1:200, Biolegend, Cat# 677804), N-Cadherin (1:200, Biolegend, Cat# 350816), and PD-L1 (1:200, Abcam, Cat# ab214958). The mean fluorescent intensity of obtained images was analyzed using Cell-Sense software (Olympus, Japan). To cell morphology analysis, the MCF7 cells stained with calcein-AM (Sigma-Aldrich, Cat# 17783) according to the provided protocol. The cell area, circularity and aspect ratio were analyzed by ImageJ software.

5.2.6 Cytokine array

The MSC-conditioned media was analyzed using the Human Cytokine Antibody Array (Abcam, Cat# ab133997) according to the manufacturer's instructions. Briefly, The MSC-conditioned medium was collected by centrifugation and then hybridized to the array membrane overnight at 4^{o}C. A 1 X biotin-conjugated anti-cytokines second antibody was used after washing membrane, and cytokines were detected by pipetting HRP-conjugated streptavidin on membrane. The captured signals were quantifies using ImageJ software.

5.2.7 Statistical analysis

The results of quantitative experiments were analyzed as mean ± SD. The statistical analysis was performed with the Student t-test. *p-value< 0.05 was considered as a statistically significant and ****p-value< 0.005 was considered as an extremely significant. Microscopic images are representative images from three independent experiments. The mean fluorescent intensity was analyzed using ImageJ software.

5.3 Results

5.3.1 MSC in various stages of breast cancer and its correlation with immune suppression

Figure 5.1 illustrates the workflow of this study, initiating with in-silico data analysis of MSC related markers across a large cohort of breast cancer patients, followed by co-culturing an epithelial-like/low expressing PD-L1 breast cancer cell line with MSC-CM in a microfluidic device and assessment of released cytokine through the cytokine profiling. To investigate the association between the presence of the MSC cells in TME and stimulation of immune suppression, we analyzed gene expression of three MSC markers Endoglin (CD105), NT5E (CD73), and THY1 (CD90) among 1826 breast cancer patients registered in METABRIC cohorts (Figure 5.2).

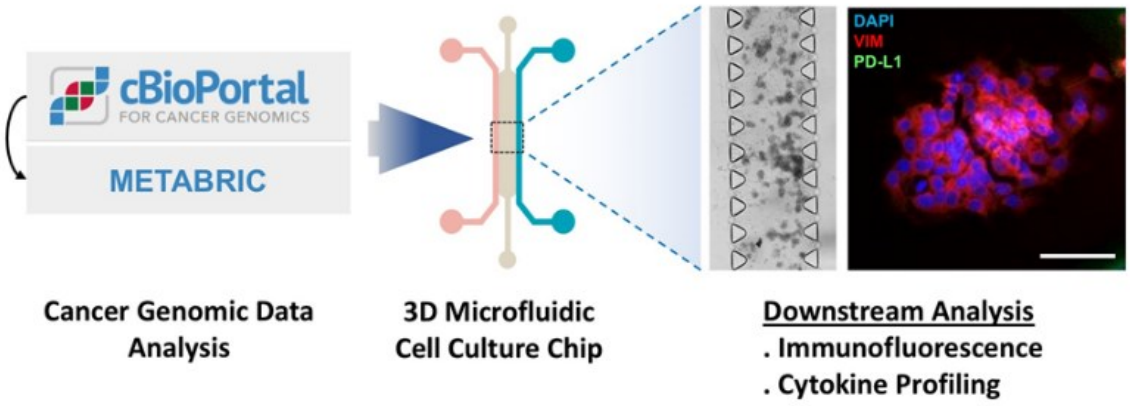

Figure 5.1. Schematic workflow of the study. It was initiated by an in-silico analysis of MSC related gene expression across 1826 breast cancer patients from METABRIC cohorts. The gene expression and clinical information of patients were downloaded from cBioportal. The genomic analysis was performed using different Bio-conductor packages under R software. Next, the MCF7 cells as single cells and multi-cellular aggregate (MCA) were cultured with MSC-CM in a 3D culture microfluidic device followed by microscopic data analysis. Finally, cell migration, invasion, immunosuppression capacity, and secreted cytokines of the cancer cells and MSC cells are assessed by means of microscopy analysis

and cytokine profiling.

According to the PAM50 subtype classification method provided in this cohort, we clustered patients in five groups namely Basal (n=209), Claudin-low (n=218), Luminal-A (n=700), Luminal-B (n=475), and HER2 (n=224) (Figure 5.2A). We observed a high expression of NT5E, ENG, THY1 among patients diagnosed as invasive ductal carcinoma (IDC) type, and in claudin-low subtypes (Figure 5.2A, 5.2B). Moreover, in the claudin-low subtype, tumour samples with the negative status of ER/PR and HER2 showed the highest expression of ENG and NT5E compared to other groups of tumours with at least one positive status in ER/PR or HER2 (Figure 5.2B), while the expression of THY1 mostly observed in ER+/HER2- low-proliferative tumour cells (Supplementary Figure 1).

We next analyzed the expression of the PD-L1. As depicted in Figure 2C and in line with previous studies [9, 284, 334], tumours with triple-negative status showed a significantly high level of PD-L1 expression in comparison with other subtypes (Figure 5.2C). The Pearson correlation coefficient and protein-protein interaction analysis between MSC related genes and PD-L1 resulted in the identification of a positive association between THY1, ENG and NT5E with PD-L1 (CD274) (Figure 5.2D. Supplementary Figure 2). Together, these data suggest a positive association between MSC related genes and induction of an immune suppression TME through the regulation of PD-L1 expression on cancer cells.

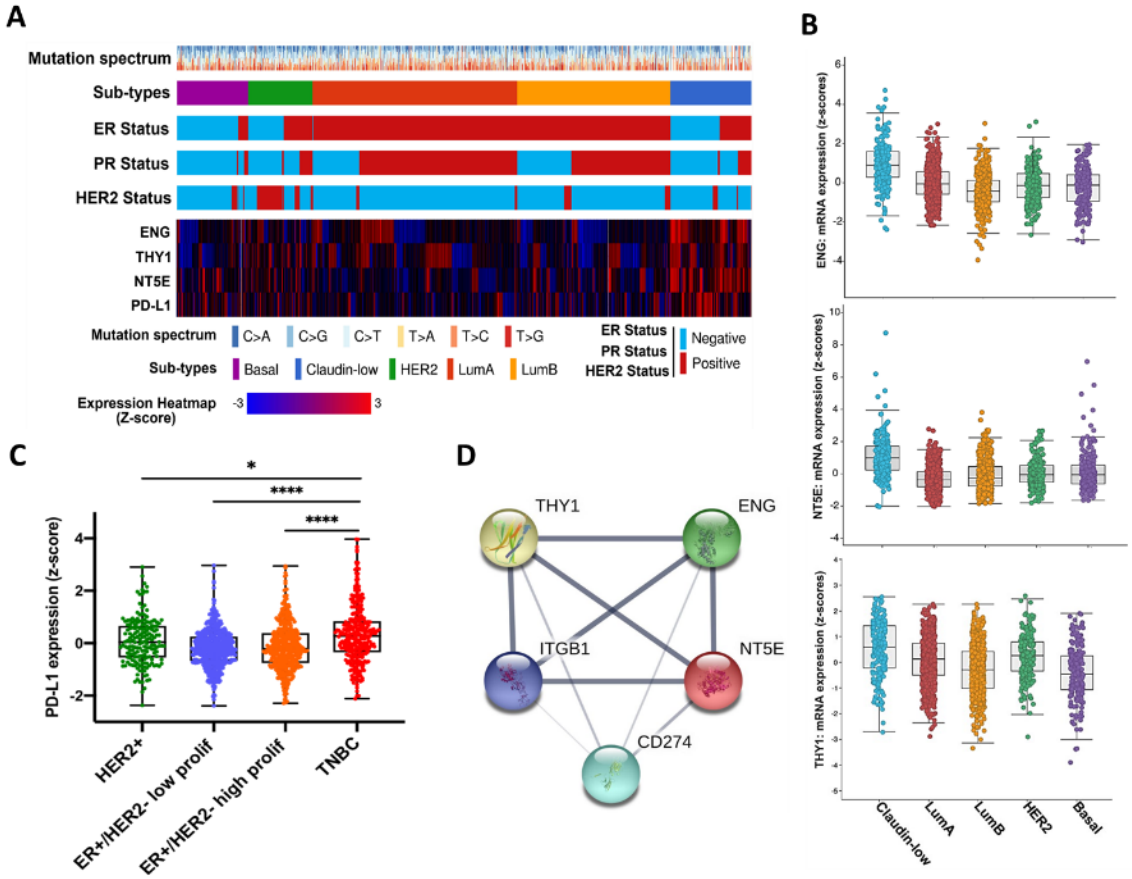

Figure 5.2. Expression of MSC related genes and its correlation with PD-L1. (A) onco-print and showing frequency of MSC-related genes ENG, THY1, and NT5E and PD-L1 across different types and subtypes of breast cancer from METABRIC cohort. (B) Detailed expression frequency of MSC-related genes in five different types of breast cancer. The high expression of the ENG, NT5E, and THY1 was identifies in Claudin-low types. (C) Expression of PD-L1 in different sub-types of breast cancer. Patients with triple-negative status showed a significant highest expression level of PD-L1 compared to the other sub-types. (* $p<0.05$, **** $p<0.005$) (D) protein-protein interaction analysis between MSC-related genes and PD-L1.

5.3.2 MSC induces breast cancer cell proliferation and invasion behavior

To assess the influence of the MSC cells on the behavior of breast cancer cells, we cultured a differentiated ER+ and low PD-L1 carcinoma cell line known as MCF7 with MSC derived condition media (*Method section*) to assess its potential for inducing PD-L1 in the presence of MSC-CM. A significant increase in cell population observed when MCF7 cells cultured in MSC-CM for 72 hours in comparison to the control group (Figure 5.3A, 5.3B).

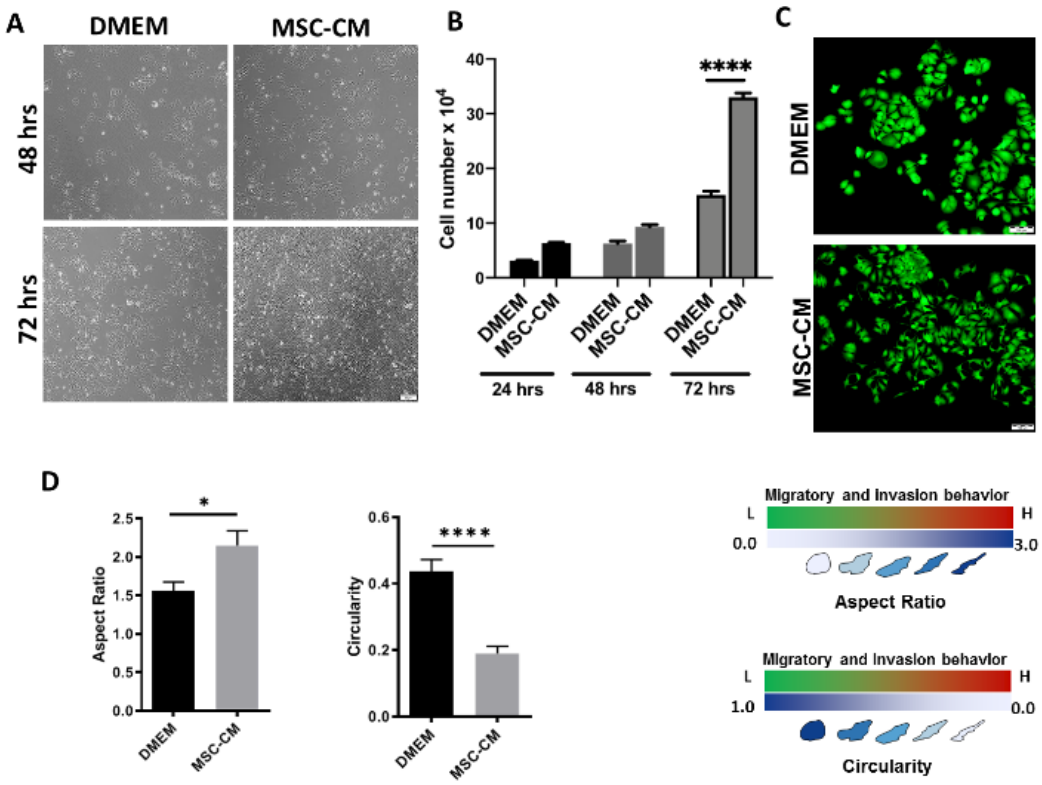

Figure 5.3. Effects of MSC-CM on proliferation and invasion behavior of cancer cells. (A, B) Influence of MSC-CM on proliferation rate of MCF7 cells after 72 hours ($P < 0.005$). (C, D) Morphology switch of MCF7 cells cultured with MSC-CM. Besides microscopy observation (C), the assessment of circularity, aspect ratio, and cell area showed a phenotype changes on MCF7 cells from an epithelial-like to mesenchymal-like toward an invasion behavior (D) ($P<0.005$).

As morphology is closely linked to cell migratory behavior [335], we analyzed the morphology of cancer cells by assessing the circularity and aspect ratio of MCF7 cells that cultured with MSC-CM. Interestingly, in constant with microscopic observations (Figure 5.3C), we found a significant increase in aspect ratio, and a reduction in circularity level those group of cells cultured with MSC-CM, indicating morphology changes toward the acquisition of aggressive behavior (Figure 5.3D). To investigate the influence of MSC cells on the stimulation of invasive behavior in cancer cells, we cultured MCF7 cells as single cells in a microfluidic device with or without MSC-CM and assessed the expression of EMT related markers (Figure 5.4A). Immuno-labeling showed a significantly elevated expression of mesenchymal markers N-cad and Vim, while the level of epithelial marker E-Cad reduced after 72 hours culture of cells with MSC-CM (Figure 5.4A, 5.4B). In constant with previous observations, these data indicate EMT-promoting effects of MSC-CM.

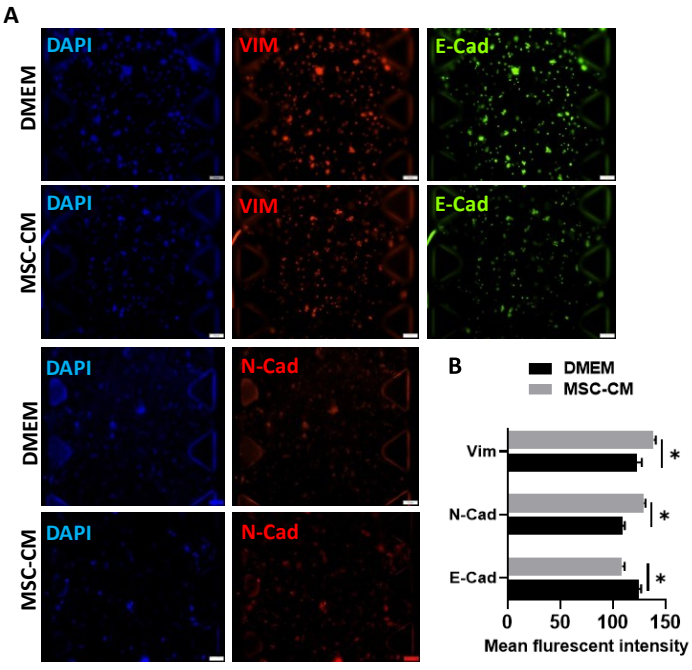

Figure 5.4. EMT induction effects of MSC-CM on MCF7 cells. (A) The immunofluorescent images of expression of EMT-related marker vimentin (Red) and reduction of E-cadherin (Green) at protein level (Scale bar:100μm). (B). Quantification results of mean fluorescent intensity measurement of Vim, N-Cad, and E-Cad ($p<0.05$).

5.3.3 MSC induce expression of PD-L1 on low PD-L1 breast cancer cells

Numerous studies highlighted an immunosuppressive role of TME during disease progression in which the infiltration of immune cells and the function of cytotoxic T-cells are limited by tumour cells and tumour stromal cells through the expression of PD-L1. We next asked whether MSC as an immune modulator has the potential to induce an immune-suppression through the expression of PD-L1 at the early stage of the disease. In this regard, we cultured MCA derived from MCF7 cells (an epithelial and low PD-L1 expressing cell line) with or without MSC-CM. Figure 5.5A exhibits the immunofluorescent analysis of PD-L1 and Vim expression in MCAs cultured in MSC-CM for 72 hours, demonstrating a significantly elevated level of Vim (Figure 5.5B). Interestingly, an increase in expression of PD-L1 was observed in MSC-CM treated group compared to the control group, although a low expression of PD-L1 was observed in this group (Figure 5.5C). We previously showed that the formation of MCA could stimulate the expression of numerous stemness related genes, including CD44 [144].

The protein-protein interaction analysis of stemness marker CD44 and EMT related markers Vim, E-cad, N-cad, and ZEB1 with PD-L1 (CD274), showed a positive association between ZEB1, E-Cad, and CD44 with PD-L1, where expression of ZEB1 and CD44 may induce the level of PD-L1 (Figure 5.5D). Together, these data suggest that MSC-CM able to stimulate expression of PD-L1 through the regulation of EMT and stemness related genes in a positive manner.

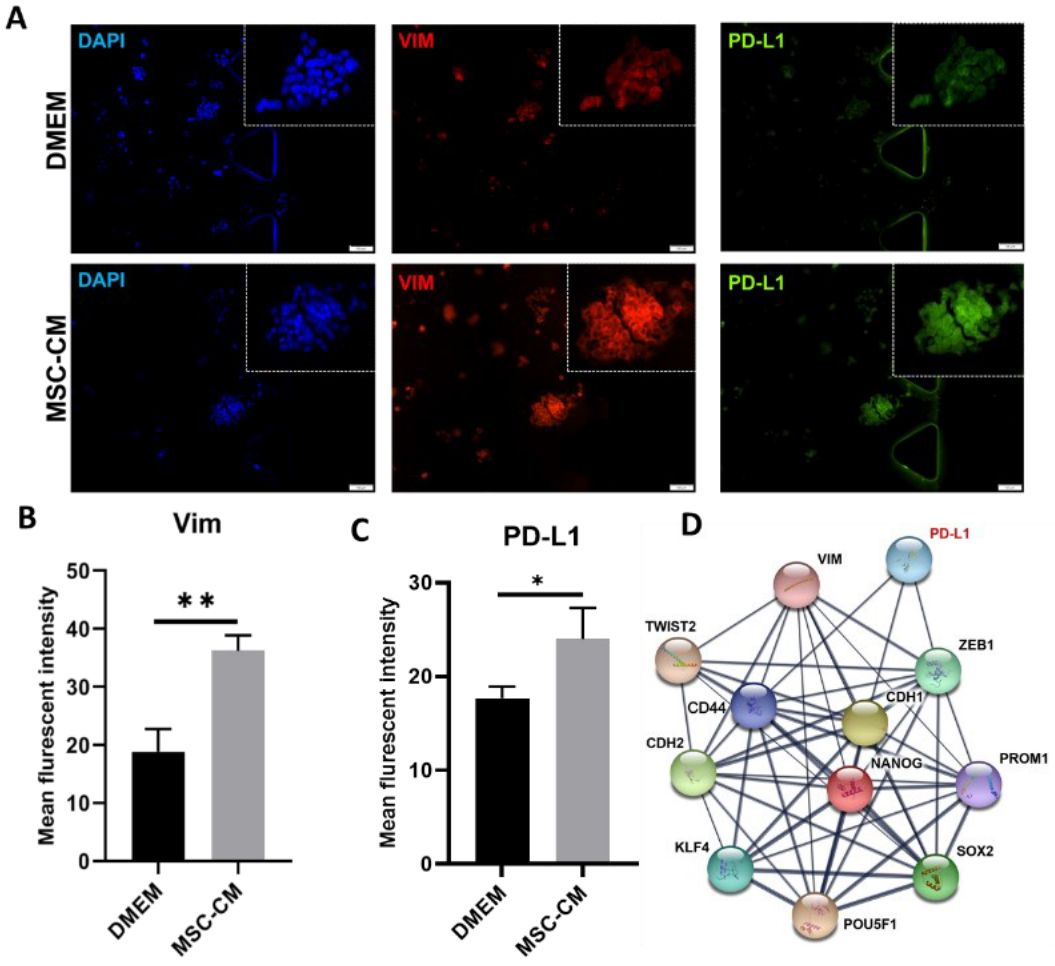

Figure 5.5. MSC-CM induces expression of the PD-L1. (A-C) The microscopy images (A) and quantitative analysis of expression of both Vim (B) and PD-L1(C) in MCF7-MCA cultured with MSC-CM and stained in microfluidic device (Scale bar: 100µm. $p<0.05$). (D) Protein-protein interaction analysis of EMT- and stemness-related markers with PD-L1, showing positive association between CD44, ZEB1, and CDH1 with PD-L1.

3.3.4 Cytokine expression

Our co-culture experiments showed that MSC-CM stimulates the expression of PD-L1 on breast cancer cells. To better characterize a potential inducer, we analyzed the MSC-CM using a cytokine array. Among 42 screened cytokines, a high level of several inflammatory

cytokines, including CCL2, CCL5, CXCL5, IL-6, IL-8, and GRO-a was identified from MSC-CM (Figure 5.6A). The correlation analysis between identified cytokines and PD-L1 showed a positive association between IL6, CCL2, CCL5, and CXCL5 with PD-L1(CD274) (Figure 5.6B. Supplementary Figure 3).

We next sought to determine how targeting these cytokines may reduce the expression of PD-L1. In this regard, we treated MSC cells with Pirfenidone (PFD)(100μM), a well-known cytokine inhibitor for 48 hours and generated condition medium from these cells (MSC-CM+PFD) followed by assessing expression of PD-L1 on MCA cells cultured with this conditioned medium. Interestingly, we found that the expression of PD-L1 significantly decreased after replacing MSC-CM with MSC-CM+PFD on MCA cells (Figure 5.6C, 5.6D). To better identify suppressed cytokines, we screened released cytokines form MSC cells treated with PFD. Remarkably, we found a significant reduction in expression and release of CCL5 in the MSC-CM+PFD group in comparison with non-treated samples (MSC-CM) (Figure 5.6E, 5.6F). Moreover, the production of CCL2, angiogenin (ANG), IL-6, and CXCL5 was also reduced in treated MSC cells with PFD (Figure 5.6G). To show prevalence and correlation of targeted cytokines by PFD with immune suppression at clinical setting, we analyzed a large cohort of breast cancer and classified samples into two groups of PD-L1 positive and negative. Interestingly, we found significant high expression of ANG, CCL2, CXCL5, IL6, and IL8 in samples with a PD-L1 positive status in comparison with PD-L1 negative samples (Figure 5.7A-G). These data indicate that reducing or depletion of these immune-suppressive cytokines through targeting tumour stromal cells might restore immunotherapy sensitivity in breast carcinoma.

Collectively, these data suggest the immune-suppression regulatory role of MSC cells within TME through the stimulation of PD-L1 on cancer cells by releasing various inflammatory-related cytokines, particularly CCL5.

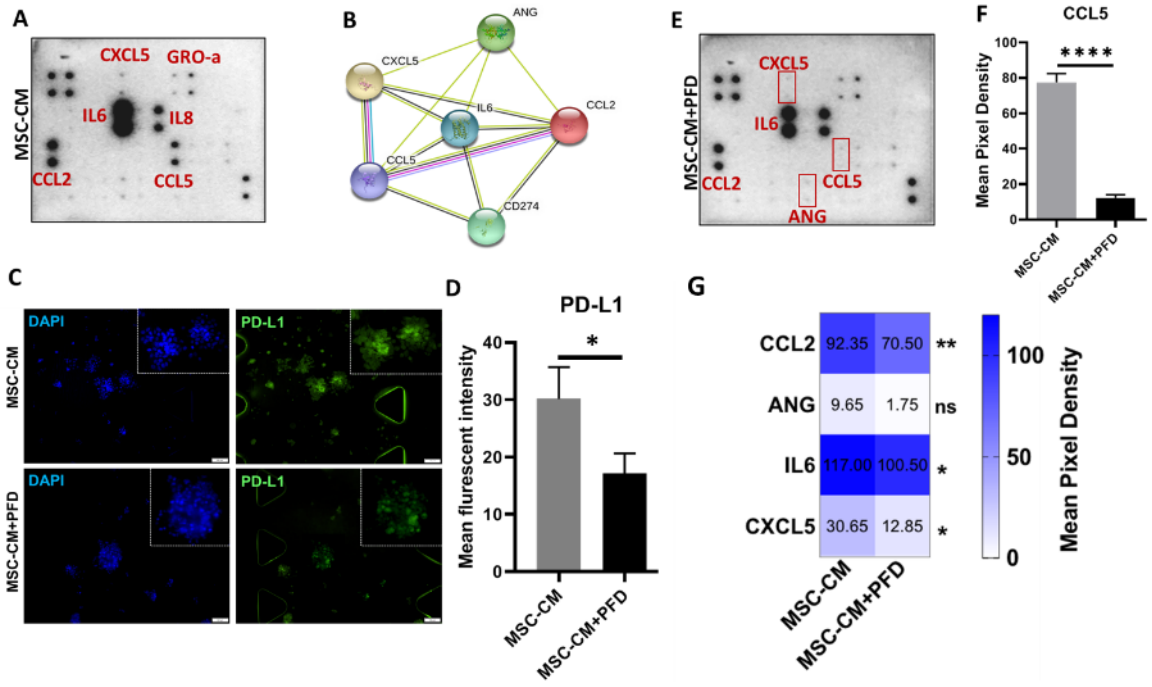

Figure 5.6. Cytokine expression profiling of MSC-CM and MSC-CM+PFD. (A) Cytokine profile of MSC-CM. The highly expressed cytokines labeled in red. (B). Correlation network analysis of expressed cytokines with PD-L1. (C). Immuno-fluorescence image of PD-L1 expression in cancer cells cultured with MSC-CM+PFD in comparison with MSC-CM. (Scale bar: 100µm) (D). Quantitative and statistical analysis of expression of PD-L1 based on the mean-fluorescent intensity ($p<0.05$). (E). Cytokine profiling of the CM derived from MSC cells treated with PFD for 48 hours. The suppressed or decreased cytokines highlighted in red. (F, G). Significant reduction in expression of CCL5 (F) and other cytokines (G) after treatment of MSC cells with PFD ($p < 0.005$).

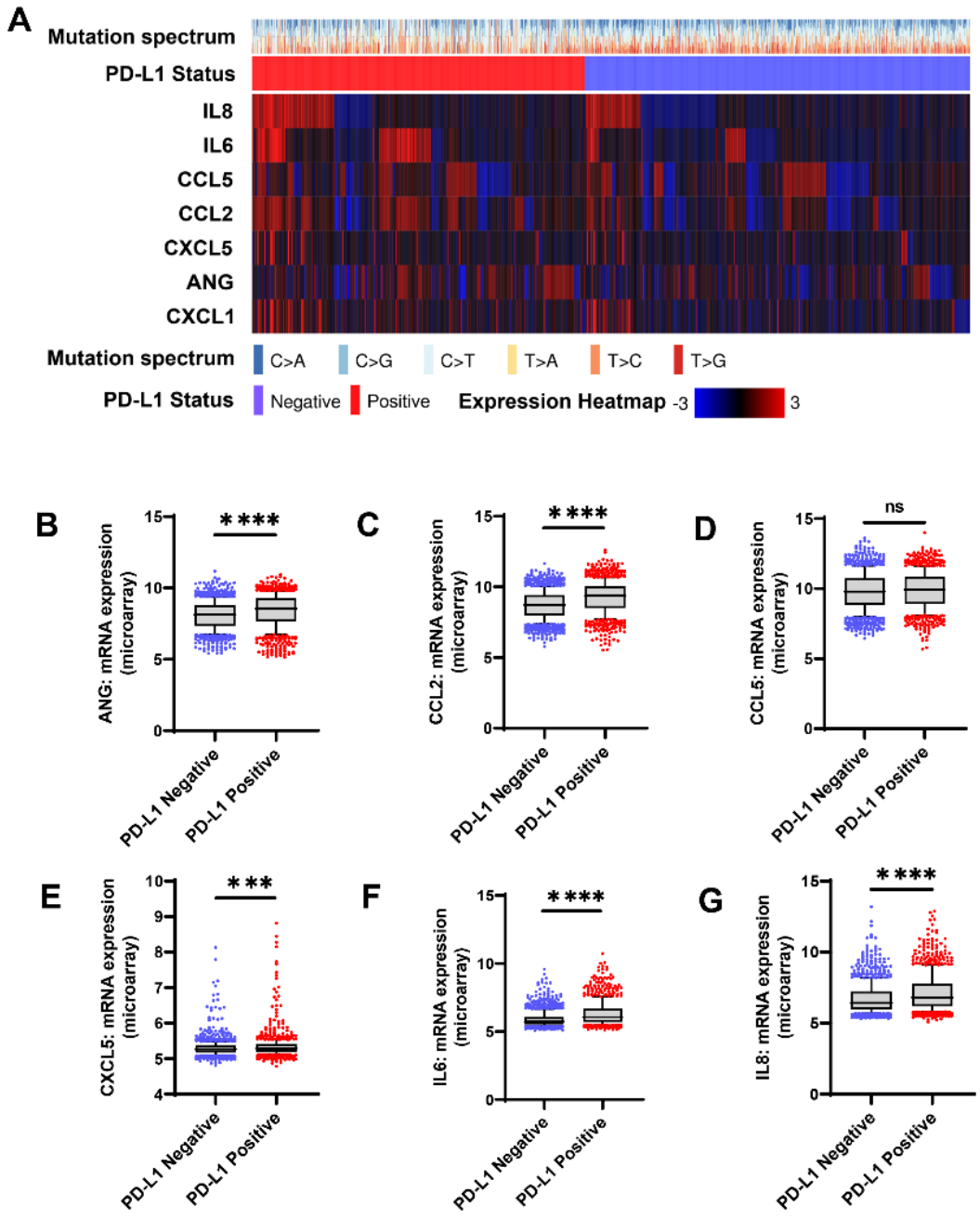

Figure 5.7. The expression profile comparison of identified cytokines between PD-L1-negative and PD-L1 negative samples. (A) The oncoprint plot illustrate expression profile of identified cytokines across 1904 breast cancer samples grouped into PD-L1-positive (n=873) and PD-L1-negative (n=1031). (B-G) The statistical analysis of expression of ANG (B), CCL2 (C), CCL5 (D), CXCL5 (E), IL6 (F), and IL8 (G) between PD-L1-negative and -positive samples. ($p < 0.0001$).

5.4 Discussion

It is well established that the expression of PD-L1 plays an essential role in cancer cell-mediated immune response to immunotherapy. The expression of PD-L1 has been found in 5–40% tumour cells [238, 336], helping tumour cells to escape from immune killer cells [296]. Herein, we showed that MSC cells as an immune modulator able to stimulate the expression of PD-L1 in cancer cells with the low expression profile of PD-L1. The cellular expression of PD-L1 could be affected by cellular components of TME, particularly tumour stromal cells [2, 9, 68]. The influence of tumour stromal cells in the regulation of hallmarks of cancer has been highlighted in various studies [1, 2, 59, 337]. Among tumour stromal cells, MSCs, known as TA-MSCs, have shown direct and indirect effects on each step of tumour progression, metastasis and drug resistance in various solid tumours[16, 54, 61, 67, 327].

In the context of immune suppression capacity of tumour stromal cells, a large number of studies pointed out to the critical role of CAFs in the induction of an immune-tumour microenvironment through the regulation of the immune checkpoints particularly PD-L1 in both themselves and cancer cells in-vitro and in-vivo [9, 39, 338]. Considering the immune-suppression function of MSCs within TME, studies demonstrated that MSCs express not only PD-L1 and PD-L2 but also mediate expression of these proteins on immune compartments of TME including T cells [330], macrophages [338], dendritic cells [339] and cancer cells [329, 332]. However, the role of MSCs as an immune modulator in the expression of PD-L1 in breast cancer cells remained to be explored [54].

For better understanding effects of MSCs in the expression of PD-L1 in breast cancer cells, through the analysis of three MSCs-related markers ENG, THY1, and NT5E across 1826 breast cancer samples from METABRIC cohort, we highlighted a positive association between expression of MSC-related markers and expression of PD-L1 in different sub-types of breast cancer. A similar gene signature have been used to identification of TA-MSC cells across high-grade glioma samples from TCGA [340] and in patient's tumour specimens [341], in which a negative correlation between expression of MSC signature and patient survival was reported.

The expression pattern of immune-checkpoint proteins particularly PD-L1 and its association with EMT program and stemness feature of breast cancer have been discovered through both in-silico and in-vivo studies, in which tumour stromal cells including CAFs play a pivotal role to rewiring TME toward the acquisition of an immune-suppressive TME [342, 343]. In line with these findings, through correlation and protein-protein interaction analysis between MSC related genes and PD-L1, we observed a positive association between NT5E, ENG and THY1 with PD-L1, suggesting that besides CAFs, MSCs may play a critical role in the regulation of PD-L1 in TME of breast cancer [331]. In support of these data, in a pre-clinical study on primary and metastatic prostate cancer, Krueger at al. identified MSC cells in prostate cancer TME using an opal multiplex immunofluorescence assay based on NT5E, THY1, and ENG [332]. Interestingly, they found that infiltrating MSC cells suppress T-cell proliferation and upregulate expression of PD-L1 and PD-L2 on their cell surface, indicating that depletion of MSC cells from TME not only induce immunologic recognition but also can eliminate prostate cancer cells by cytotoxic T-cells.

The phenotypic transformation, such as epithelial to mesenchymal transition, is identified as a critical factor in both stimulations of metastasis behavior and induction of immune suppression within TME. It has been shown that tumour stromal cells can regulate phenotype switch in cancer cells toward the acquisition of invasive phenotype by releasing various cytokines and chemokines in TME [344]. Many studies documented the effects of CAF cells on morphology changes of various types of cancer cells [22, 345-347]. Comparable results observed when we cultured an epithelial-like, non-invasive breast cancer cells with MSC-CM. Our results also indicated that MSC-CM is able to stimulate phenotypic switch in cells toward the acquisition of invasive behavior and immune-suppressive capacity [344], through the induction of EMT-related genes specially vimentin. [295]. These data indicate that released cytokines and chemokines in the conditioned medium of MSCs may mediate the expression of PD-L1 in PD-L1-low expressing cancer cells. Our cytokine profiling analysis against 42 different cytokines highlighted the presence of an elevated level of various cancer-promoting and immuno-modulator related cytokines in MSC-CM, including CCL5, CCL2, IL6, IL8, and CXCL5. In line with these observations, in a syngeneic model of colon adenocarcinoma, O'Malley et al. highlighted stromal cell-mediated immune suppression and tumour-promoting effects of mesenchymal stem cells through the expression and secretion of numerous cytokines [329].

In a study on xenograft and orthotopic mouse models of pancreatic ductal adenocarcinoma (PDAC), it have been shown that cancer Forkhead box protein 3 (C-FOXP3) augment immune evasion of PDAC by recruiting Treg cells into PDAC through the upregulation of CCL5 in which in turn, C-FOXP3 directly bound to the promoter region of PD-L1 in

pancreatic cancer cells [348]. They concluded that combined blockade of PD-L1 and CCL-5 axis may provide an effective therapy for patients with high level of C-FOXP3. A similar observation was reported in colorectal cancer patient suggesting that CCL5 may provide a potential therapeutic target for the combined PD-1-immunotherapy of CRC [349].

Collectively, these data suggest that targeting these cytokines particularly CCL5 may impede invasiveness and immune-suppressive characteristics of cancer cells. In this regard, the recent approval of pirfenidone (PFD) for the treatment of idiopathic pulmonary fibrosis relies on targeting various cytokines. As a proof-of-concept, we showed that treatment of MSCs with cytokine inhibitor PFD significantly reduce expression and secretion of various cytokines especially CCL5 and CCL2 and consequently decrease in the level of PD-L1 in breast cancer cells. Although, understanding the underlying mechanism behind the effects of PFD in reversion of tumour immunity and increase sensitivity of tumour cells to immunotherapy remained to be investigated; however, we showed that targeting tumour stromal cells using PFD indirectly reduce expression of PD-L1 through the targeting key immune-related cytokines and may use as alternative approach for in cancer immunotherapy in a combination manner. Collectively, these results support a crucial role of tumour stromal cells in mediating and regulation of an immune suppression microenvironment through the secretion of various cytokines and rewiring TME.

Chapter 6

Targeting Epithelial-Mesenchymal Transition and Tumour Spheroid formation in Breast Carcinoma

Summary:

Following previous chapter highlighting the potential of targeting CAFs and TAMs in reduction of immune-suppressive capacity of TME and cancer cells, in this chapter, I studied the targeting tumor initiation or spheroid formation and also invasion by reducing stem-ness capacity of cancer cells and also EMT regulated by CAFs in triple-negative breast cancer. This chapter show the potential of pirfenidone discovered in chapter 3 on inhibition of these features on TME. The results of this chapter has been published*.

* Es, Hamidreza Aboulkheyr, Thomas R. Cox, Ehsan Sarafraz-Yazdi, Jean Paul Thiery, and Majid Ebrahimi Warkiani. "Pirfenidone Reduces Epithelial–Mesenchymal Transition and Spheroid Formation in Breast Carcinoma through Targeting Cancer-Associated Fibroblasts (CAFs)." Cancers 13, no. 20 (2021): 5118.

6.1 Introduction

The cellular components of the tumour microenvironment (TME) in promoting invasiveness and stemness features of carcinoma cells are well characterized [350, 351]. Among them, cancer-associated fibroblast (CAFs), a major component of TME, play a key role in the regulation of tumour progression, metastasis and acquisition of stemness in carcinoma cells through the induction of various processes, including epithelial-to-mesenchymal transition (EMT) [16, 352]. CAFs modulate various key factors within the TME and rewire the TME toward an aggressive ecosystem. This is achieved by the secretion of various cancer-promoting chemokines and cytokines, which activate tumour growth, and trigger cancer invasion, and immune escape [22, 23, 353]. Besides, CAFs remodel the extracellular matrix leading to an increased stiffness which modify the phenotype in carcinoma cells [287, 354]. Various studies highlighted the role of CAFs-induced Yes-activated protein(YAP1), a major regulator of cell plasticity, stemness, drug resistance, and metastasis in carcinoma cells [287, 355]. Given the crucial role of CAFs within the TME, targeting these cells might be a promising therapeutic approach to reduce invasiveness and stemness of carcinoma cells regulated by YAP1 [356]. The recent approval of pirfenidone (PFD) for the treatment of idiopathic pulmonary fibrosis relies on targeting activated fibroblast, and their secretory functions. Numerous recent studies demonstrated the therapeutic potential of PFD as a combination treatment modality with chemotherapy, targeted therapy and immunotherapy in various cancers through the depletion of cytokines [357-360]. Herein, we hypothesized that targeting CAFs with PFD should reduce EMT and stemness by blocking the secretion of cytokines and the expression of YAP1 in breast carcinoma cells.

6.2 Materials and Methods

6.2.1 In-Silico Data Analysis

The TCGA-breast cancer genomic information and clinical data were downloaded from the cBioportal data portal (https://www.cbioportal.org/) [361] and analyzed under Bioconductor tools in R-Software (version 3.8). A detailed description of used packages and related scripts to gene expression and mutation analysis is available at https://bioconductor.org/packages/release/bioc/vignettes/maftools/inst/doc/maftools.html. The stromal index was calculated based on the ESTIMATE scoring method [293]. The EMT score in this study was calculated according to our previous study [295]. Protein-protein-interaction analysis was performed with STRING [362, 363].

6.2.2 Cell lines and Media

Human breast adenocarcinoma cells MCF7 (ATCC, Cat# HTB-22, USA) and MDA-MB-231 (ATCC, Cat# HTB-26, USA) were cultured in Dulbecco's modified Eagle's medium (DMEM) (Thermo Fisher Scientific, USA) supplemented with 10% (v/v) FBS and 100 U penicillin/ml and 100µg streptomycin/ml. The breast cancer-derived CAFs (Garvan Institute of Medical Science, Australia) were cultured in DMEM supplemented with 1% (V/V) Insulin-Transferrin-Selenium (ITS) (Thermo Fisher Scientific, USA), 2% FBS (Thermo Fisher Scientific, USA) and 1% penicillin/streptomycin (Sigma-Aldrich) in 37ºC.

6.2.3 Spheroid Formation

To obtain human tumour spheroids with stemness feature, the MCF7 cells were trypsinised and suspended as individual cells at 100,000 cells/ml in Mammo-Cult Human Medium Kit (STEMCELL Technology, Cat# 05620) included with Hydrocortisone (STEMCELL Technology, Cat# 07925) and Heparin solution (STEMCELL Technology, Cat# 07980) and cultured for 14 consecutive days onto a 100mm ultra-low attachment dish (Corning). To use the appropriate size of spheroids in the microfluidic device, the generated spheroids were collected and filtered in two consecutive filtration steps: (a) 40µm filtration, in order to exclude all the spheroids smaller than 40µm, and (b) 100µm filtration, in order to exclude all aggregates larger than 100µm in diameter and centrifuged by 250×*g* for 5 min to separate them from the supernatant. Spheroids were suspended in a serum-free medium and mixed with collagen Type-I solution on ice for loading in microfluidic devices [364].

6.2.4 Preparation of CAFs Condition Medium

CAFs were cultured at a density of 10,000 cells/cm2 in DMEM medium supplemented with 1% (V/V) ITS and 1% (V/V) penicillin/streptomycin until they reached 90% confluence. Then, cells were washed with PBS, and the culture media were replaced with serum and ITS-free DMEM followed by incubation for an additional 48 hrs. The concentrated supernatant was collected by centrifuging (Eppendorf, Hauppauge, NY, USA) at 1200 RPM for 5 min at room temperature, filtered through 0.45µm filters, and designated as CAFs-conditioned medium (CAF-CM). The conditioned medium was then stored at -80˚C until use.

6.2.5 Microfluidic Device Design and Cell Culture

The microfluidic tissue culture devices used in this study are purchased from AIM Biotech Company (Singapore). The devices consist of 2 media channels running parallel to and located on either side of an extended central region containing the 3D extracellular matrix. 200µl collagen gel solution (2.5mg/ml) at pH 7.4 was prepared on ice. Typically, 20µl 10X PBS was mixed with 4µl NaOH (0.5N), 129.2µl collagen Type-I (Corning, Cat# 354236.), 10µl of cell suspension medium with 1000-2000 tumour spheroids, and 22.9µl cell culture grade deionized water. The collagen gel solution containing tumour spheroids was then injected into the dedicated gel region of the device and kept in the cell culture incubator at 37°C and 5% CO2 for 40 minutes to allow gel polymerization via thermal cross-linking. After polymerization, the two side channels filled with 120µl stemness medium or CAF-conditioned medium (CM), with or without PFD, by adding 70µl in one port and another 50µl into the opposite connected port of a media channel. This approach prevents shear stress on gel channel following loading medium.

For migration and co-culture study, devices with gel only (no embedded cells) were prepared similarly by adding a collagen gel solution containing 20µl 10×PBS, 4µl NaOH(0.5N), 129.2µl collagen Type-I, and 42.8µl of deionized water. Immediately after gel polymerization, the two side channels were filled with MDA-MB-231 (one side channel) and CAFs (opposite side channel) at the concentration of 10,000 cells for each cell line. Finally, 120µl of the serum-free cell culture medium with or without PFD was added to the both side channels to feed the cells. In both experiments, the devices were kept in the incubator with the standard condition for four days.

6.2.6 Cytokine Profiling Assays on Treated samples

The culture medium of devices treated with PFD was analyzed using the Human Cytokine Antibody Array (Abcam, Cat# ab133997) according to the manufacturer's instructions. Briefly, the culture medium was collected from microfluidic devices, concentrated by centrifugation, and then hybridized to the array membrane overnight at 4°C. After washing the membrane, a 1X biotin-conjugated anti-cytokine secondary antibody was used, and cytokines were detected by adding HRP-conjugated streptavidin on the membrane. The captured signals were quantified using ImageJ software.

6.2.7 Immunofluorescence Staining and Imaging Analysis

Cell culture media was removed from the devices, and samples in the microfluidic devices were first rinsed in 1X PBS by adding 70µl of PBS into one port and another 50µl into the opposite connected port of a media channel. Then the cells were fixed with 4% paraformaldehyde (PFA) (Sigma-Aldrich, St. Louis, MO, USA) for 15 min at room temperature. Next, 0.1% Triton-X 100 (Sigma-Aldrich, St. Louis, MO, USA) was added, and the device was incubated for 10 min before blocking by BSA 1% (Sigma-Aldrich cat no: A5611) for two hours, followed by staining of cells for α-SMA (1:100, Abcam, Cat# ab197240.), Vimentin (1:200, Biolegend Cat# 677804.), YAP1(1:200, Abcam, Cat# ab205270), CD44 (1:200, Abcam, Cat# ab194988) and CDH1 (1:200, Biolegend Cat# 324104). The images' mean fluorescent intensity (MFI) was analysed using Cell-Sense software (Olympus, Japan).

6.2.8 Statistical Analysis

The results of quantitative experiments were analyzed as mean ± SEM. The statistical analysis was performed with the Student t-test. *p-value< 0.05 was considered as a statistically significant and ****p-value< 0.0001 was considered as an extremely significant. Microscopic images are representative images from three independent experiments.

6.3 Results

6.3.1 The Association of Tumour Stromal Content with the Expression of YAP1 and Metastasis Feature

To the understanding association of YAP1 with classical stemness and EMT markers, we comprehensively analyzed the gene and protein expression levels of YAP1 across 1084 breast cancers from the TCGA cohorts. To show the association between the expression of *YAP1* and stromal content of TME, especially CAFs, we divided samples into two groups of the high-stromal index (HSI) and low-stromal index (LSI) according to the ESTIMATE score of samples (Figure 6.1). We observed a significantly high expression of *YAP1* in samples with HSI scores compared to the LSI group (Figure 6.1A, B, C) at both transcriptome and protein levels. To study the association between *YAP1* with EMT related features, we annotated HSI and LSI samples based on their EMT scores, namely high-EMT score (H-EMT) and low-EMT score (L-EMT) and measured expression of YAP1 across these groups at protein level (Figure 6.1C, D). Interestingly, we found that most of the samples with the HSI score include

an H-EMT score sample compared to the LSI group.

Moreover, HSI samples represented the high expression of YAP1 at the protein level (Figure 6.1C). To better understand the association between YAP1 and EMT, we analyzed the correlation coefficient between *YAP1* and classical EMT genes *VIM* and *CDH1* plus stemness marker *CD44* and immune checkpoint protein *PD-L1*. We found a positive association between *YAP1* and *VIM*, *CD44*, and *PD-L1*, while *YAP1* negatively correlated with *CDH1* (Figure 6.1D).

Following these findings, we analyzed metastatic stages of individual samples across HSI and LSI groups and the prevalence of YAP1 expression. As depicted in Figure 6.1E, in comparison with the LSI group, most of the samples with the high expression of YAP1 at the protein level and a MX or M1 metastatic stage were enriched in the HIS group, indicating a positive correlation between stromal content, expression of YAP1 and high metastatic stage (Figure 6.1E). Taken together, these data highlight the positive association of high tumour stromal content of TME with the expression of YAP1 and induction of EMT and metastasis.

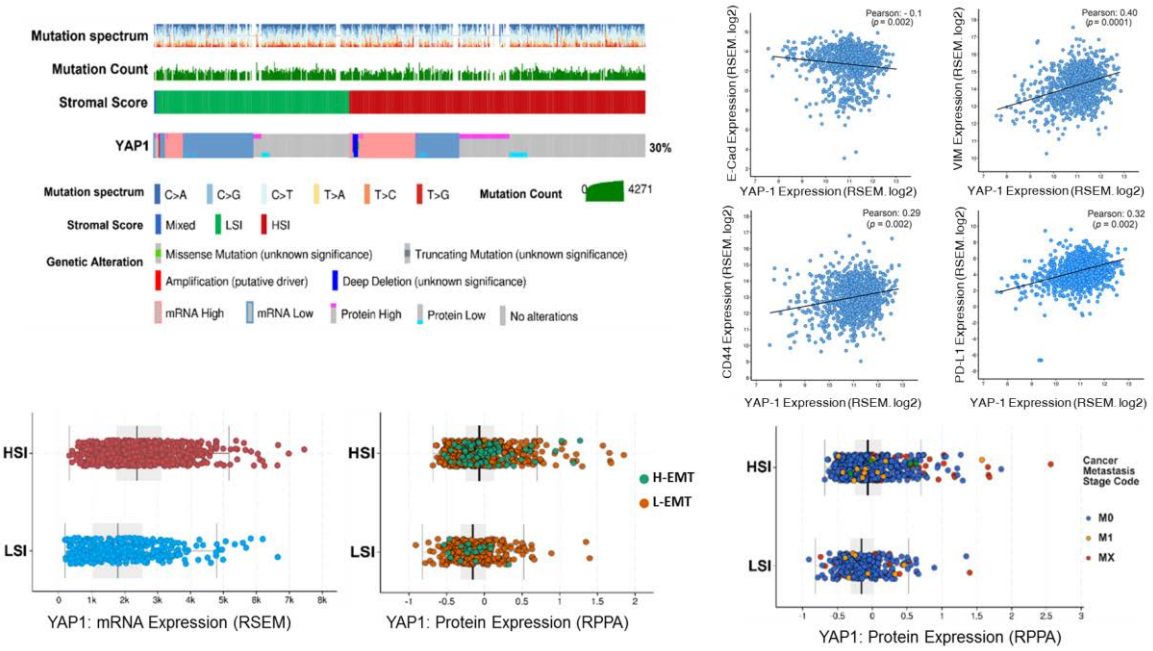

Figure 6.1. Genomic analysis of the TCGA breast cancer cohort. **(A)** The oncoprint plot illustrates the expression of YAP1 in two groups of samples annotated based on the stromal score signature. **(B)** Comparing the expression of *YAP1* between samples with high-stromal index (HSI) and low-stromal index (LSI) indicating that samples with HSI expressed a high level of *YAP1*. **(C)** A High EMT status is enriched in samples with the HSI status and high level of YAP1 at the protein level. **(D)** Correlation coefficient analysis between the expression of *YAP1* and classical EMT markers *VIM*, *CDH1*, stemness marker CD44 and immunosuppressive marker *PD-L1*. The results show a negative association between *YAP1* and *CDH1* and a positive correlation with *CD44*, *VIM*, and *PD-L1*. **(E)** Association between the protein expression of YAP1 and metastatic stages in samples with HSI and LSI score, showing enrichment of an adverse stage of metastasis in samples with high YAP1 expression and HSI score.

6.3.2 Association of YAP1 with EMT and Stemness Markers

To better demonstrate of association between YAP1 and EMT, we classified samples into two groups of YAP1-high and YAP1-low based on its gene expression level. The oncoprint analysis illustrated enrichment high expression of EMT and stemness related genes in

samples with high expression of YAP1 (Figure 6.2A). in line with this observation, the gene-set enrichment analysis (GSEA) of YAP1-low and –high samples resulted in the enrichment of hallmark of EMT in YAP1-high samples in comparison with YAP1-low (Figure 6.2B) in which the expression of classical EMT markers *VIM* and *ZEB1* were significantly higher across YAP1-higher samples (Figure 6.2C, 6.2D). In contrast, CDH1 expression was enriched in the YAP1-low group (Figure 6.2E). Additionally, samples with the high expression of YAP1 represented a significant expression of stemness marker CD44 compared to the YAP1 low expressing samples (Figure 6.2F).

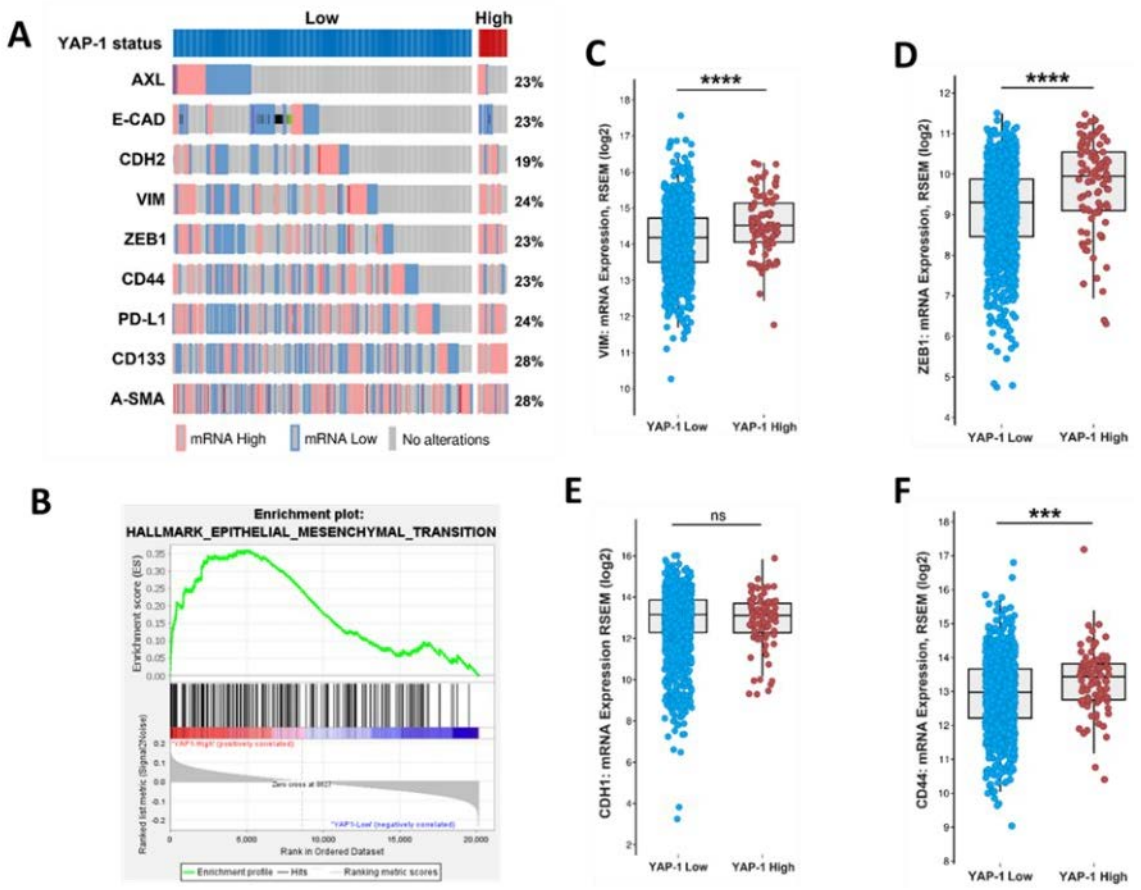

Figure 6.2. In-Silico data analysis between samples expressing high and low levels of *YAP1*. (A) The oncoprint plot depicts the high expression of EMT- and stemness-related genes in samples with YAP1-high status at the transcriptome level. **(B)** The gene-set

enrichment analysis (GSEA) shows the enrichment of hallmarks of EMT in samples with a high level of *YAP1*. **(C-F)** The comparison between high and low *YAP1* groups in terms of *VIM* expression **(C)**, *ZEB1* **(D)**, *CDH1* **(E)**, and *CD44* **(F)**. *** P<0.0002, **** P<0.0001 using student T-test.

6.3.3 CAFs Induce Spheroid Formation

To understand whether CAFs can induce and stimulate spheroid formation, we generated a concentrated condition medium from CAFs (CAF-CM) and co-cultured MCF7 cells in well-plate and microfluidic devices in 50:50 (V/V) ratio of CAF-CM and stemness induction medium for seven days. We found that the number and the diameter of generated spheroids were significantly increased when the cells were co-cultured with CAF-CM (Figure 6.3A-C), while integrated density properties of spheroids were reduced after seven days in comparison with the monoculture group (Figure 6.3D). The assessment of the epithelial marker E-cadherin showed that CAF-CM significantly reduced expression of this gene, suggesting that CAF-CM may induce migration of cells in spheroids (Figure 6.3E, 6.3H). Moreover, we found a significant expression on YAP1 (figure 6.3F, 6.3H) and CD44 in spheroids co-cultured with CAF-CM compared to the monoculture samples (Figure 6.3G, 6.3H). These data indicate an invasion and stemness induction role of CAF cells through the secretion of cytokines.

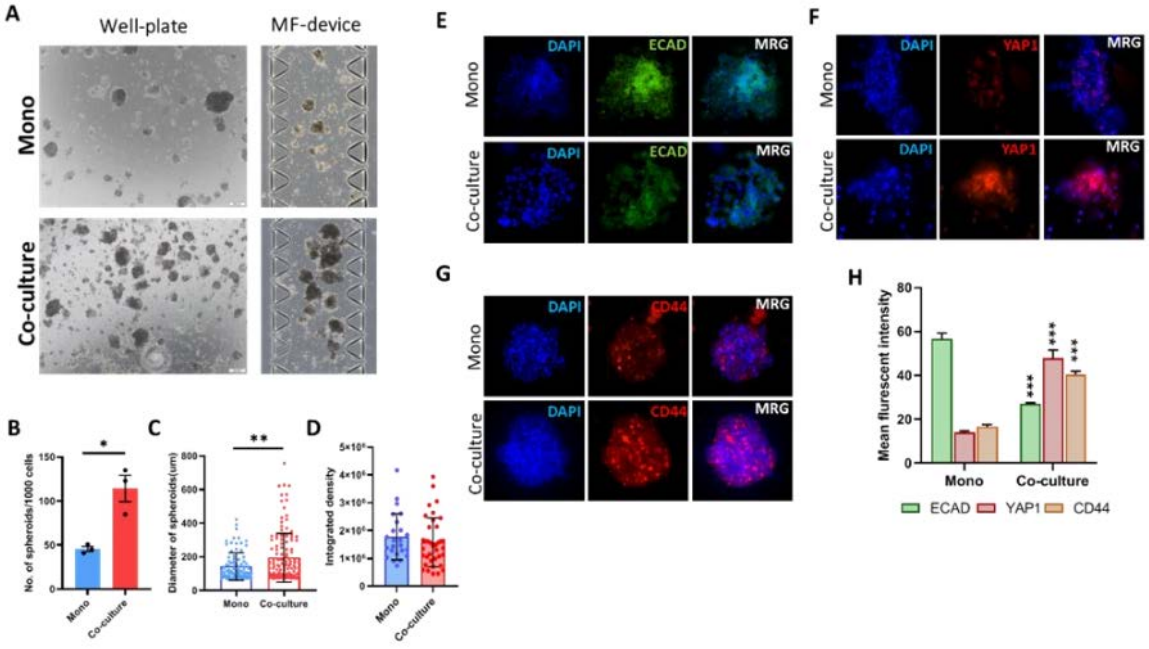

Figure 6.3. CAFs induces spheroid formation with increased diameter and expression of YAP1. **(A)** Bright-filed snapshot image of the formation of spheroids in well-plate (left) and microfluidic device (right) co-culture with or without CAF-CM. The micrographs show an increase in the number and size of generated spheroids on both platforms in the presence of CAF-CM. **(B)** The CAF-CM significantly increased the formation of spheroids per 1000 cells in comparison with monoculture. **(C)** In comparison with monoculture, co-culturing cancer cells with CAF-CM significantly increased the size of generated spheroids. **(D)** The integrated density in spheroids co-cultured with CAF-CM was lower than in monoculture, indicating the stimulation of cell invasion from spheroids in the ECM channel. **(E-G)** The immunofluorescence staining of the EMT marker ECAD **(E)** and stemness marker CD44 **(F)** indicates that CAF-CM stimulates EMT and stemness. Co-culturing with CAF-CM increased the expression of YAP1 in generated spheroids (Scale bar: 100µm). **(H)** The quantitative analysis of mean-fluorescence intensity in ECAD, YAP1, and CD44 resulted in a significant reduction in expression of ECAD and an increase in CD44 and YAP1 in the co-culture group to the monoculture. *P<0.05, **P<0.002, ***p<0.0002 using student T-test.

6.3.4 Pirfenidone Reduces the Migration of CAFs and Carcinoma Cells

The role of tumour stromal cells, particularly CAFs, in the induction of migration in carcinoma cells has been shown previously [365]. To study the potential of PFD in reducing invasive properties of carcinoma cells, we first co-cultured MCF7 carcinoma cells known as low-vimentin expressors with CAF-CM for 48 hours and then treated cells with a low concentration of PFD (40μM) for 72 hours (Figure 6.4A). In comparison with the control group, we observed a significant reduction in vimentin expression in spheroids treated with PFD (Figure 6.4A). Following these results, we assessed the effects of PFD on the migration of carcinoma cells and CAFs. To this aim we co-cultured CAFs and MDA-MB-231 as representative of aggressive breast cancer in the 3D microfluidic device and treated cells with 40μM of PFD for 72 hours, followed by measuring cell migration distance in control and PFD-treated cells (Figure 6.4B). Figure 4C presents a snapshot of the 3D device including migration of CAFs and MDA-MB-231 through the ECM channel in three different time points. In PFD treated samples, we loaded serum-free culture medium containing (40μM) PFD following seeding cells in the device. Interestingly, we found that the presence of PFD in the culture medium significantly reduced the migration of MDA-MB-231 cells (Figure 6.4E) after 48 and 72 hours. In the case of CAFs, although migration inhibitory of PFD did not reach statistical significance, we observed a reduction in migration of CAFs through the ECM after 72 hours compared to the control group. These data highlight the potential of PFD to reduce the invasion and migration capacity of carcinoma cells and CAFs.

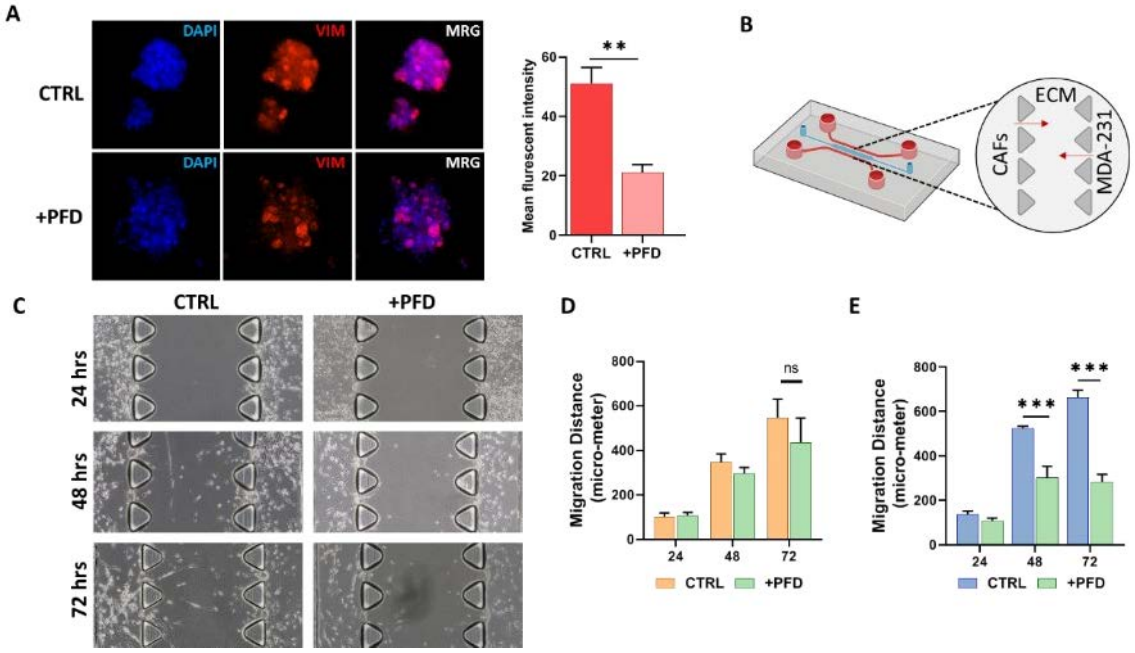

Figure 6.4. Assessing the migration and invasion inhibitory effects of PFD on MDA-MB-231 carcinoma cells and CAFs. **(A)** Tumour spheroids derived from MDA-MB-231 shows a significant reduction in the expression of EMT marker VIM (scale bar: 100µm). **(B)** The schematic image of invasion and migration assay performed in the 3D microfluidic device in which MDA-MB-231 and CAFs are injected in side channels. The migration of cells was monitored for three days after seeding. **(C)** A representative bright-field image of migration of CAFs and MDA-MB-231 in the presence and absence of PFD highlight that PFD significantly suppressed the migration of both cells during 72 hours. (scale bar: 200µm) **(D, E)** The quantitative analysis of migration distance for CAFs **(D)** and MDA-MB-231 cells **(E)** indicated that although PFD did not significantly suppress the migration of CAFs after 72 hours, however, in comparison with the control group, a reduction was observed. In the case of MDA-MB-231 cells, PFD significantly suppressed the invasion and migration of these cells after 48 and 72 hours. ** P< 0.002 using Student T-test, ***P<0.0002 Using ANOVA.

6.3.5 Pirfenidone Reduces YAP1 and CD44 Expression in Spheroids by Targeting Key Cytokines

The cytokine production inhibitory role of PFD has been shown in various studies [360, 364]. Targeting cancer progression-promoting cytokines using PFD may reduce stemness and immune suppression promoted by CAFs. To study the effect of PFD on the expression of stemness marker CD44 and of YAP1, we first cultured MCF7 cells with CAF-CM for 72 hours and then generated spheroids that include both MCF7 and CAFs in a ratio of 2:1 and cultured them into the 3D device. The generated spheroids were treated with stemness medium containing 40μM PFD for 72 hours before performing imaging and cytokine profiling. Interestingly, we found that PFD not only significantly reduced the expression of YAP1 (Figure 6.5A) and CD44 (Figure 6.5C) but also the level of α-SMA was decreased after treatment, indicating a reduction in CAFs activity in spheroids (Figure 6.5A, B). To better understand the inhibitory effects of PFD, we collected culture medium from 3D microfluidic devices from both groups after 72 hours and performed a cytokine profiling array against 42 cancer-promoting cytokines (Figure 6.5C). A significant reduction was observed in the secretion of various cytokines after treatment with PFD, including IL8, CCL17, TNF-β, and CCL2 (Figure 6.5D).

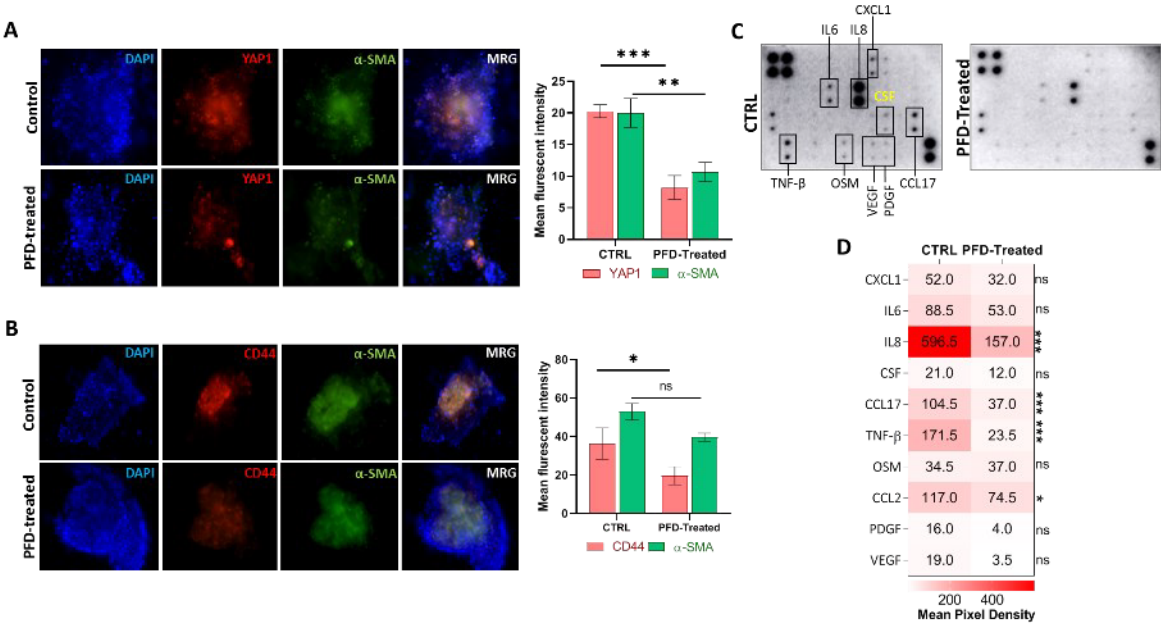

Figure 6.5. PFD reduces CAFs activity and expression of CD44 and YAP1 through the blockade of key cytokine secretion. **(A)** The immunofluorescence staining shows a significant decrease in protein expression of YAP1 and α-SMA following treatment with PFD (scale bar: 100µm). **(B)** Besides α-SMA, PFD also reduced the expression of CD44 in spheroids that include CAFs (scale bar: 100µm). **(C)** The picture of cytokine profiling performed on culture medium retrieved from PFD-treated and non-treated spheroids in devices. The array shows the depletion of numerous cytokines in treated samples. **(D)** The quantitative analysis of the mean-pixel density analysis of cytokine membranes using ImageJ software, shows a significant depletion of IL6, IL8, CCL17, TNF-β. *P<0.05, **P<0.002, ***P<0.0002, using Student T-test **(A, B)** and ANOVA**(D)**.

Moreover, we observed a slight decrease in the level of CXCL1, IL6, CSF, OSM, PDGF, and VEGF in treated samples as compared to the control group (Figure 6.5D). The protein-protein interaction analysis between classical EMT genes, stemness, and PFD targeted cytokines revealed associations between YAP1 and CD44 with VIM, CDH1, and AXL and IL8 (Figure 6.6A, B). To better understand the association between identified cytokines with EMT and YAP1, we analyzed expression of these cytokines in samples with high and low expression

of YAP1 from TCGA breast cancer cohort. As illustrated in Figure 6.6C, a significant expression of IL8 and CCL2 was enriched in samples with high YAP1 level. Besides, high expression of CCL17 and TNF-β was also observed in this group of samples in comparison with YAP1-low samples, although these expression differences did not rich statistical significance (Figure 6.6C).

Following these findings, we analyzed EMT scores across 1084 samples from TCGA and classified samples into EMT-high and -low scores and assessed the expression of identified cytokines. Interestingly, we found the significant enrichment of targeted cytokines in samples with a high EMT score compared to the low-EMT score samples, indicating a positive association between expression of targeted cytokines and EMT in breast cancer (Figure 6.6D). These results indicate that PFD might reduce the stemness and invasion capacity of the carcinoma cells through targeting cytokine production in CAF that regulate EMT, which in turn can stimulate YAP1-associated stemness.

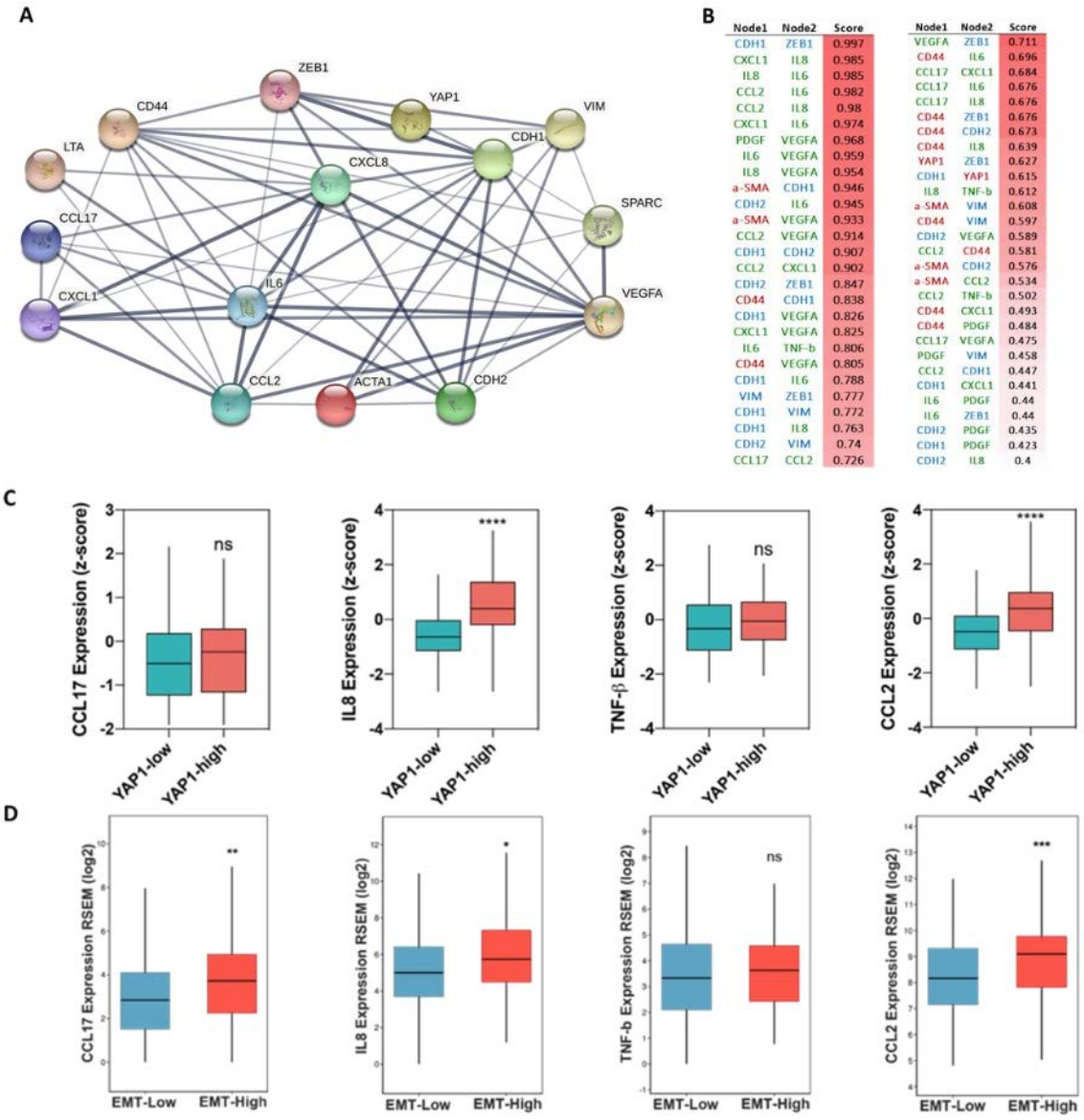

Figure 6.6. The association between targeted cytokines with EMT and YAP1. **(A)** The graphical image of the network between related genes, showing an association between EMT, stemness and YAP1. **(B)** Scoring results between nodes in the PPI network. **(C)** Comparison between the expression of four identified cytokines in samples with high- and low expression of YAP1 in breast cancer indicating enrichment of these cytokines in YAP1-high samples. **(D)** Key cytokines are enriched in samples with high EMT score. *P<0.05, **P<0.002, ***P<0.0002, using Student T-test.

6.4 Discussion

The role of tumour stromal cells, particularly cancer-associated fibroblasts (CAFs), in promoting carcinoma progression is well understood [16, 354]. Numerous studies highlighted that CAFs could induce stemness features in carcinoma cells through the secretion of various cytokines and remodeling ECM toward developing a high stiffness of ECM which in turn stimulates phenotypic changes including EMT and induces the expression of related stemness genes [354, 366-369]. Targeting CAFs to either suppress their activity or reprogram them into an inactive state showed some promising effects [9]. Inhibiting carcinoma progression-promoting cytokines released from CAFs may be an efficacious therapeutic strategy for cancer treatment [370-372].

Recently, various clinical and preclinical studies demonstrated the potential application of PFD as a combination therapy with chemotherapy and radiotherapy in various types of cancers, including lung and pancreatic carcinoma [358, 372]. However, few studies showed PFD application in suppressing invasive properties, particularly EMT, and reduction of carcinoma-stemness through the targeting of key cytokines and genes that regulate ECM synthesis and remodeling [373-375]. As a proof-of-concept study, we hypothesized that PFD could reduce CAF-induced EMT and consequently EMT-regulated stemness in breast carcinoma cells by depletion of key cytokines.

Using a comprehensive in-silico data analysis on the breast cancer cohort from TCGA, we showed the enrichment of high-level YAP1 expression in samples with the highest stromal score. Moreover, we illustrated that samples with high stromal scores exhibit a high score of EMT and invasive properties. A positive association between high level of YAP1 and

EMT-related markers and stemness genes at both transcriptomic and protein levels was observed [376, 377]. In line with these findings, several studies demonstrated that YAP1 is a mediator of EMT and stemness in numerous types of carcinomas, including breast cancer [377-380].

Tumour stromal cells, particularly CAFs, are among the main modulator of EMT and stemness [381] through the induction of YAP1 and secretion of various cytokines. The strategy based on targeting these proteins directly or indirectly by targeting CAFs might be a promising approach to the treatment of advanced carcinoma [371, 374]. In this study, using a 3D microfluidic model of invasion and migration, we demonstrated that CAFs promote spheroid formation and the migration capacity of carcinoma cells [360], possibly through the secretion of cancer-promoting cytokines that play a haptotactic or chemotactic role for carcinoma cells [382]. Following treatment with PFD, we found that PFD significantly reduced the migration of an invasive type of breast cancer cells and CAFs and significantly decreased the expression of EMT marker vimentin, stemness marker CD44, and YAP1 in breast cancer spheroids co-cultured with CAFs at the protein level [376]. Similar observations were reported previously for the migratory inhibition effect of PFD on both carcinoma cells and CAFs in pancreatic cancer [358] and breast cancer [383].

Recent single-cell analysis studies revealed that a sub-population of CAFs called inflammatory CAFs express IL6 and TNF-α/β [384]. The co-culture of colon tumour organoids with this population of CAFs resulted in the upregulation of vimentin and ZEB1 in tumour cells [384]. Moreover, CAF-derived cytokines significantly induce the expression of HOTAIR, which in return promotes the EMT program in metastatic breast cancers [383].

This study also showed that targeting CAFs with PFD blocks the TGF-β1/HOTAIR axis and decreases the migration potential of MDA-MB-231 cells. In addition to these findings, we found that the level of α-SMA decreased after treatment with PFD, indicating that PFD can reduce CAFs activity [9]. In line with these observations, numerous in-vitro studies highlighted the inactivity of CAFs after treatment with PFD [360, 364]. Using cytokine profiling, we demonstrated that PFD significantly depleted the secretion of cancer- and invasion-promoting cytokines, particularly IL8, CCL17 and TNF-β. Many studies highlighted the critical role of these factors in the interaction of the carcinoma–stromal cell and ECM deposition toward the induction of an invasive TME and activation of EMT and stemness [22, 23, 385, 386].

It has been shown that the secretion of IL8 by CAFs known as EMT and stemness modulator [387] and tumour-associated mesenchymal stem cells (TA-MSCs) not only induced the migration of carcinoma cells but also up-regulate immune-suppression in carcinoma cells through the expression of PD-L1. The treatment of TAMs with PFD reduced expression of PD-L1 and migration of carcinoma cells in in-vitro models [364]. CCL17 was reported as a key cytokine in the generation of tumour-associated macrophages [388], which stimulates EMT and stemness [306, 307]. Moreover, it has been shown that the production and secretion of CCL17 within the TME through the CAFs trigger the recruitment of myeloid-derived suppressor cells (MDSCs) to the TME, promoting invasion in various cancers [389-391]. For instance, recently, Omland and colleagues reported that CCL17 secreted from resident CAFs within cutaneous basal cell carcinoma TME increases tumour progression and amplifies immune suppression [392].

Taken together, in line with numerous studies, the results reported in this study highlight the importance of suppressing CAF-derived cytokines that can induce both EMT and stemness. This study also emphasizes the need to further explore the cross-talks between carcinoma cells and other cells of the TME to better control tumour progression.

6.5 Conclusions

Targeting CAFs has a great potential to treat highly aggressive types of cancers, including breast carcinoma. The recent approval of PFD for the treatment of lung fibrosis relies on targeting activated fibroblasts and their secretory functions. In this study, using a microfluidic culture platform, we demonstrated the inhibitory function of PFD on invasion, EMT and stemness properties of invasive breast cancer cells through the depletion of cytokines. However, further in-vivo investigation is needed to delineate the potential of PFD as a treatment modality in combination with current therapeutic agents in the treatment of metastatic cancers.

Chapter 7

The role of ECM stiffness in tumour Immunity

Summary:
This chapter model the effects of matrix stiffness of the TME which is regulated by CAFs in the induction of the expression of immune checkpoint PD-L1 a major immune-suppressive proteins in triple-negative breast cancer. This chapter has been published*.

* Azadi, Shohreh, Hamidreza Aboulkheyr Es, Sajad Razavi Bazaz, Jean Paul Thiery, Mohsen Asadnia, and Majid Ebrahimi Warkiani. "Upregulation of PD-L1 expression in breast cancer cells through the formation of 3D multicellular cancer aggregates under different chemical and mechanical conditions." Biochimica et Biophysica Acta (BBA)-Molecular Cell Research 1866, no. 12 (2019): 118526.

7.1 Introduction

It is broadly understood that the tumor microenvironment (TME) and its interplay with cancer cells play a crucial role in tumor initiation, progression, metastasis, and drug response [1,2]. A large number of studies highlighted the importance of non-cellular features of TME including extracellular matrix (ECM) and its stiffness in the induction of metastasis and drug resistance in various solid tumors [3–6]. The physical and chemical characteristics of TME can control the behavior and function of cancer cells [1,7,8]. Mechanical characteristics of TME changes during cancer progression expose tumor cells to different mechanical signals [9]. Variation of TME stiffness induced by cellular and non-cellular components is recognized as a pro-tumorigenic factor. Activation of various oncogenic signaling pathways through the cellular and physical properties of TME has been reported previously, resulting in enhancing hypoxia, invasiveness, stemness and immune-escaping capability of cancer cells [13,14].

During the past decade, immunotherapy has witnessed a revolution in cancer therapy with the development of immune checkpoint inhibitors, monoclonal antibodies against cytotoxic T lymphocyte antigen 4 (CTLA-4) and programmed cell death protein-1 (PD-1) or their ligands, including PD-1 ligand 1 (PD-L1). Emerging evidence highlighted roles of TME and ECM remodeling in regulating the cancer- immunity cycle [15–17]. However, the contribution of the ECM re- modeling in shaping the immune microenvironment of the tumor is only beginning to be studied. Mechanical features of TME are increasingly recognized as crucial factors in immune cell trafficking, activation and immunological synapse formation [18]. The density of ECM and basement membrane composition are regulated by stromal matrix components and plays a crucial role in immune cell migration, spatial distribution,

and activation of immune-escaping features of cancer cells [15,17,19]. Additionally, numerous growth factors secreted by tumor-supportive cells in TME can enhance the immune-suppression capability of TME and immune-escaping potential of cancer cells. Recently several studies highlighted immune-modulatory effects and positive association of activation of epidermal growth factor receptor (EGFR) signaling with PD-L1 expression in TME [20,21]. However, the association between matrix stiffness and EGFR on the expression of PD- L1 has not been elucidated. Cellular aggregates display a variety of features which could better mimic the tumor microenvironment [22,23]. An increasing number of studies demonstrated that the formation of tumor spheroids and cell aggregates could modulate numerous signaling pathways including stemness-related pathways [24–26]. Despite these studies, it is not yet been established whether the formation of cell aggregates can regulate the PD-L1 expression. This study was designed to determine whether the chemical and mechanical features of TME regulate the multicellular cancer aggregate (MCA) formation ability and PD-L1 expression in human breast cancer cells. Our findings postulated regulation of PD-L1 expression by EGFR signaling pathway, substrate stiffness, and MCA formation.

7.2 Materials and methods

7.2.1 Cell culture

Cells of the human breast cancer cell lines MCF7 (non-invasive) and MDA-MB-231 (highly-invasive) were acquired from University of Technology Sydney (UTS), faculty of science. The cells were maintained in RPMI culture medium (ThermoFisher Scientific, USA)

containing 10% fetal bovine serum (FBS) (ThermoFisher Scientific, USA) and supplemented with 1% L-glutamate (Thermo Fisher Scientific, USA) in an atmosphere of 5% CO2 and 95% air at 37 ºC. Two breast cancer cells were cultured in five different study groups, two as chemical groups and three as mechanical groups that referred as non-treated, Cetuximab (Merk, Germany) treated, stiff, semi soft and soft substrates, respectively.

7.2.2 Substrate preparation and characterization

To examine effect of the substrate stiffness on programmed dead ligand-1 (PDL-1) expression and spheroid formation ability of cancer cells, Poly dimethylsiloxane (PDMS) substrates with different stiffness were utilized. These substrates were prepared by mixing silicone elastomer with the curing agent (Sylgard 184, Dow Corning, USA). Varying the ratio of elastomer to curing agent allowed us to achieved PDMS substrates with different elastic modulus with negligible changes in other chemical and physical properties [393, 394]. Here we fabricated PDMS substrates by mixing silicone elastomer with the curing agent at ratio of 10:1 and 50:1 and 75:1, to obtain stiff, semi soft and soft substrates, respectively. Then, the mixture was degassed to expel bubbles and cured for 24 hours at 70°C. To provide appropriate cell adherence, synthesized substrates were treated via air plasma by a low-frequency plasma generator (230 V, Harrick Plasma, USA) at 30 W for 3 minutes, sterilized by UV for 30 minutes which followed by coating with a thin layer of fibronectin (10µg/ml, Sigma-Aldrich, USA). Finally, the substrates were rinsed with PBS to remove the excess protein and were immediately employed for cell seeding.

The substrates elasticity was measured by atomic force microscopy (AFM) indentation technique using a Nanowizard II atomic force microscope (JPK Instruments, Germany). The indentation was performed with V-shaped silicon nitride cantilever with a spring constant of 0.046 N/m (HYDRA6V-200NG, APPNANO, USA), at approach velocity of 3 μm/s and maximum indentation depth of 0.5 μm. For each substrate, five random points were chosen and 20 force-distance curves were collected for each point. Briefly, in this technique a flexible cantilever with a sharp tip indents the surface. During the indentation, substrate-cantilever interaction leads to a vertical deflection of the cantilever that is converted to the force and is recorded against indentation. The resulting force-indentation curve is used to obtain Young's modulus according to the modified Hertz model for a quadrilateral pyramid tip (equation 1) [395].

$$F(\delta) = \frac{1.49 E_{sub} tan\alpha}{2(1-\vartheta_{sub}^2)} \delta^2 \quad (1)$$

Where, F is the force, δ is the indentation depth, and α is the half angle of the pyramid tip, which was set to 17.5°. The Poisson's ratio of the substrates (ν_{sub}) was assumed to be 0.5 considering incompressible material property for PDMS.

7.2.3 Anti-EGFR treatment

To assess the potential correlation between PDL-1 protein expression with EGFR signaling and spheroid formation ability, EGFR pathway was targeted by Cetuximab (Merk, Germany), an anti-EGFR antibody. Cetuximab blocks EGFR with binding to the extracellular domain of EGFR and preventing receptor dimerization [396]. For immunostaining and ELISA, breast cancer cells were exposed to a culture medium supplemented with 10μg/ml Cetuximab for

48 hours. For spheroid formation experiments, breast cancer cells were treated with the mentioned concentration of Cetuximab during the spheroid formation process. The chosen concentration was below the reported peak plasma concentration of this drug [397].

7.2.4 Evaluation of the PDL-1 expression

The PDL-1 expression of the breast cancer cell lines was analyzed among different chemical and mechanical groups by immunofluorescences staining and ELISA.

7.2.5 Immunofluorescence staining of PDL-1

For PDL-1 immunostaining experiments, PDMS was spin coated onto the glass slides at 2000 rpm for 30 seconds. Two breast cancer cells were cultured among five study groups. After 24 hours, the cells were fixed and permeabilized for 10 min with chilled 100% Methanol (SigmaAldrich, USA). This was followed by three times washing with phosphate buffer saline (PBS) solution (ThermoFisher Scientific, USA) and blocking with 1% bovine serum albumin (BSA) (ThermoFisher Scientific, USA) in PBS for 60 min. Then, the cells were incubated with a rabbit monoclonal anti-PDL-1 antibody (dilution 1:100, ab209960, Abcam, USA) in PBS containing 1% BSA for overnight at 4ºC. Finally, the samples were washed and further incubated with 4,6-diamino-2-phenylindole (DAPI) (dilution 1:1000, D9542; SigmaAldrich, USA) for 5 min at room temperature. An inverted Fluorescence Microscope (OLYMPUS IX71, USA) was utilized to capture the immunofluorescence images.

7.2.6 PDL-1 ELISA assay

PDL-1 concentration was assessed among chemical and mechanical treated groups of two cell lines using quantitative enzyme-linked immunosorbent assay (ELISA) kit (ab214565, Abcam, USA). ELISA assay was performed according to the manufacturer's instruction. First cells were seeded at the concentration of 10^5 cells/ml on three PDMS substrates. The same number of cells were cultured in non-treated and Cetuximab treated groups. After 48 hours, the samples were extracted from the adherent cells and prepared according to the manufacturer's protocol. Briefly, the samples were added to the appropriate wells and incubated with the capture and detecor antibodies for 1hour at room temperature, then washed with the washing buffer that followed by incubation with 3,3',5,5'-Tetramethylbenzidine (TMB) development solution and the stop solution. Finally, optical density (OD) was recorded at 450 nm, immediately after adding the stop solution. Eight standard samples with the pre-determined PDL-1 concentration were used to obtain a standard curve (data not shown). The standard curve was created by plotting the absorbance value for each standard concentration against the target protein concentration. This curve was fitted and employed to determine the concentration of PDL-1 protein in the samples. For each sample two independent measurements were performed, and all the measurements were conducted in duplicate for statistical analysis.

7.2.7 Spheroid formation

Tumor spheroids were formed using microwell technique. The 3D SpheroFilm™ microwell was obtained from Incyto Co. (Korea) with the inner diameter of 300 μm, and the well depth of 300 μm. Each device consisted of 361 silicone elastomer microwells. To prepare the

microwells for cell culturing, their surface was UV sterilized and pretreated with 100% ethanol (SigmaAldrich, USA) which repeatedly pipetted to remove the air bubbles from the wells. Then the wells were washed three times with PBS by repeatedly pipetting and incubated with cell culture medium overnight [398].

7.2.8 Cell seeding in the microwells

For each cell line, five SpheroFilm devices were used, two devices for non-treated and Cetuximab treated cells and three devices for stiff, semi soft and soft groups. First, breast cancer cells were cultured on the three mentioned PDMS substrates for 24 hours before introducing into the micorwells. After removing the medium from the SpheroFilm devices, total number of 1.4×10^6 breast cancer cells were distributed over the microwell surfaces of each group at the concentration of 2×10^5 cells/ml. After 15 minutes of cell seeding, the suspending cells were removed by aspiration, and fresh growth media was added. The medium was changed every day until the end of the spheroid formation assay. For Cetuximab treated group, the cells were exposed to medium containing Cetuximab at the concentration of 10 μg/ml.

7.2.9 Isolation of the cancer spheroids from the microwells

After 2 days of culturing in the microwells, breast cancer tumor spheroids were dislodged by pipetting of growth medium onto the microwells, repeatedly. To isolate spheroids with the size of above 100 μm, they were pipetted gently and added to the top surface of the cell

strainer with pore size of 100 μm. The strainer was flipped and the growth medium added to the bottom surface of the strainer to collect the spheroids. Then, the isolated spheroids were transferred to the appropriate wells or slides for further assessments.

7.2.10 Spheroid characterization

To evaluate spheroid formation ability of breast cancer cells with different expression of PDL-1, the spheroids were characterized by performing live and dead assay, counting number and diameter of formed spheroids, assessment of PDL1 expression and spheroid spreading.

7.2.11 Cell viability of spheroids

Cancer spheroids were labeled directly in 48-well plates using Cellstain double staining kit (Sigma Aldrich, USA) according to the manufacturer's protocol. The viable cells were labeled with Calcein-AM which stained the cytoplasm in green. Nuclei of the dead cells were labeled with propidium iodide in red. The spheroids incubated in the assay solution (5 mL of PBS containing 10 μL of calcein-AM and 5 μL of propidium iodide) in each well for 15 minutes at 37˚C. An inverted Fluorescence Microscope (OLYMPUS IX71, USA) was utilized to capture live/dead fluorescence images.

7.2.12 Measurement of spheroid number and diameter

Spheroids formed with the breast cancer cells among different groups, were imaged using an Olympus IX71 inverted microscope. To count the total number of the formed spheroids, the spheroids suspension reached to the final volume of 4 ml, then 400 μl of the final spheroid suspension was added to the 48-well plate. The number of spheroids in 400 μl was counted

and multiplied by 10 to estimate the total number of the spheroids in 4ml. The average diameter of spheroids was also calculated by measuring the diameter of at least 40 spheroids in each group. ImageJ (NIH, Bethesda, MD) was employed for number and diameter measurements [399]. Most of the spheroids presented a spherical shape. For those had ellipsoid shape, the longest dimension was measured as diameter.

7.2.13 Immunofluorescence staining of PDL-1

To assess PDL-1 expression of the formed spheroids, isolated spheroids were stained with anti-PDL-1 antibody. First, the spheroids were fixed with chilled 100% methanol for 10 min at -20 ºC, then centrifuged at speed of 1200 rpm for 5 min to remove methanol. The samples were washed with PBS followed by blocking with 1% BSA for 1 hour at room temperature. Then the spheroids were stained with a rabbit monoclonal PDL1 antibody by overnight incubation at 4ºC. Later, the samples were washed three times with PBS to remove the unbound antibody. Finally, the nuclei were stained with DAPI for 5 minutes and the images captured using inverted fluorescent microscope (OLYMPUS IX71, USA).

7.2.14 Spheroid spreading

Isolated spheroids were transferred to the 24-well plate and allowed to spread. The spheroids were monitored under a microscope to observe whether they attached to the surface. After spheroid attachment, culture media was removed, and the fresh media added for the further spheroid cultivation and analysis. PDL-1 expression of breast cancer cells in the spread spheroids was analyzed using immunofluorescence staining of PDL-1 followed with PDL-1 ELISA assay as described before in this paper.

To measure PDL-1 concentration of the spread spheroids, first, they were dissociated using trypsin (SigmaAldrich, USA) and the number of cells counted among five study groups of MCF7 and MDA-MB-231 spread spheroids. Then, the cells of each group were transferred to a new well at the concentration of 10^5 cells/ml and incubated for another 24 hours. ELISA assay was performed according to the manufacturer's instruction, as mentioned before in this paper.

7.2.15 Statistic

The results of the quantitative experiments were expressed as mean±SD. Statistical analysis was performed with Student t-test. *p-value<0.05 was considered as a statistically significant and **p-value<0.005 was considered as an extremely significant. Microscopic images are representative images from three independent experiments. Data shown for spheroid diameter are the averages from at least 40 spheroids. PDL-1 ELISA assay was conducted in three separate replicates.

7.3 Results

7.3.1 PDMS substrates elastic modulus

Three PDMS substrates with the different elastic modulus was achieved by controlling the ratio of polymer to crosslinking agent. The elastic modulus of PDMS substrates with the ratio of 10:1, 50:1 and 75:1, were measured as 1.51 MPa, 12.38 kPa, and 3.60 kPa, respectively. These values cover the physiologically relevant elastic modulus of tumor microenvironment

that are used to examine how substrate rigidity affects biological behavior of cancer cells. As mentioned, these substrates are referred to as stiff, semi soft and soft, in this paper.

7.3.2 Expression of PDL-1 protein in breast cancer cells

First, we determined the expression of PDL-1 protein in two breast cancer cell lines among five groups of non-treated, CTX-treated, stiff, semi-soft and soft. Figure 7.1 exhibits immunofluorescent images of PDL-1 and nucleus of breast cancer cells which demonstrates that the degree of PDL1 expression varies considerably among study groups of breast cancer cell lines. Consistent with the findings in the previous literature [400], the considerable expression of PDL-1 protein was observed in MDA-MB-231 cells (figure 1B) whereas, there was little expression of PDL-1 protein in MCF7 cells (Figure 7.1A). Application of anti-EGFR antibody for 24 hours significantly reduced PDL-1 protein level in MDA-MB-231 cells which revealed that PDL1 expression is positively related with the EGFR activity. In addition, the effect of substrate stiffness on PDL-1 expression was examined. PDL-1 expression of MDA-MB-231 cells was affected not only by chemical treatment but also by substrate stiffness. The cells on the stiff substrate expressed the most PDL1 among three PDMS substrates with different rigidity

To confirm the results of PDL-1 staining, ELISA was employed to measure PDL-1 concentration. In agreement with the above reported results of immunostaining, PDL-1 concentration of MCF7 cells was measured below 30 pg/ml for all the study groups (figure 7.6A). The PDL-1 protein concentration of the invasive breast cancer cells was significantly reduced by EGFR targeting ($^{*}p < 0.005$). Similarly, PDL1 concentration of MDA-MB-231

cells grown on the soft substrate was significantly lower than those grown on the stiff substrate ($^{*}p<0.005$) (figure 7.6A). Above mentioned results suggest that PDL-1 expression can be mediated by the chemical and mechanical factors.

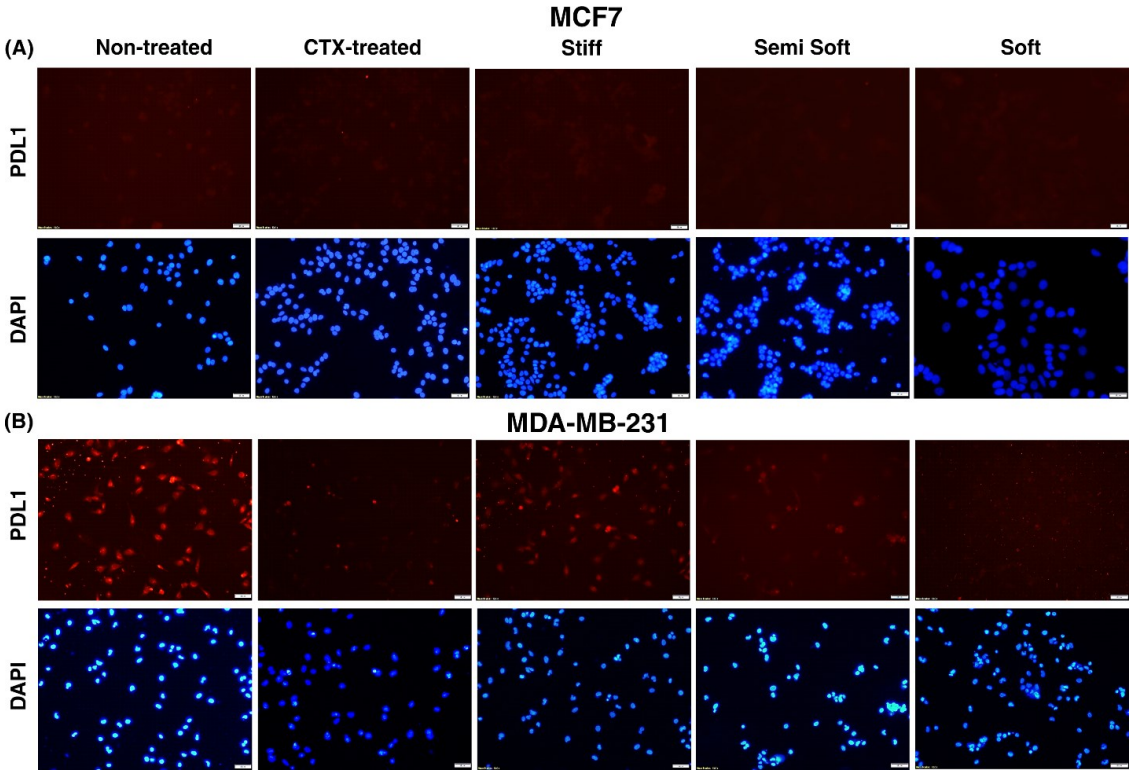

Figure 7.1. Regulation of PDL-1 expression by EGFR signaling and substrate stiffening. Representative immunofluorescent images of **(A)** MCF7 and **(B)** MDA-MB-231 cells cultured on non-treated, EGFR treated, stiff, semi soft and soft groups for 24 hours, stained for PDL-1 (red) and nuclei (blue). Images were obtained using a fluorescent microscopy. Scale bar denotes 50 μm.

7.3.3 Characterization of the breast cancer spheroids

In this paper, spheroid formation was performed by employing the microwells technique. we screened the spheroid formation ability of two breast cancer cells in five study groups. For all groups, single cells were seeded into the microwells and most of the tumor spheroids

reached above 100 µm after 2 days. The SpheroFilm device and spheroid formation steps of two breast cancer cells are schematically illustrated in figure 7.2A. Initially, cells were settled in the bottom of the microwells. After one day, the cells started to attach together and form cell aggregates. Later, on day 2, they formed denser 3D structures (figure 7.2B). Initially, we examined cell viability in the cancer spheroids and confirmed that both cell lines displayed more than 95% viability by Calcein AM staining (figure 7.3A, B) in all groups of study. Due to the small size of spheroids (less than 300 µm), necrotic core was not observed in any of the spheroids.

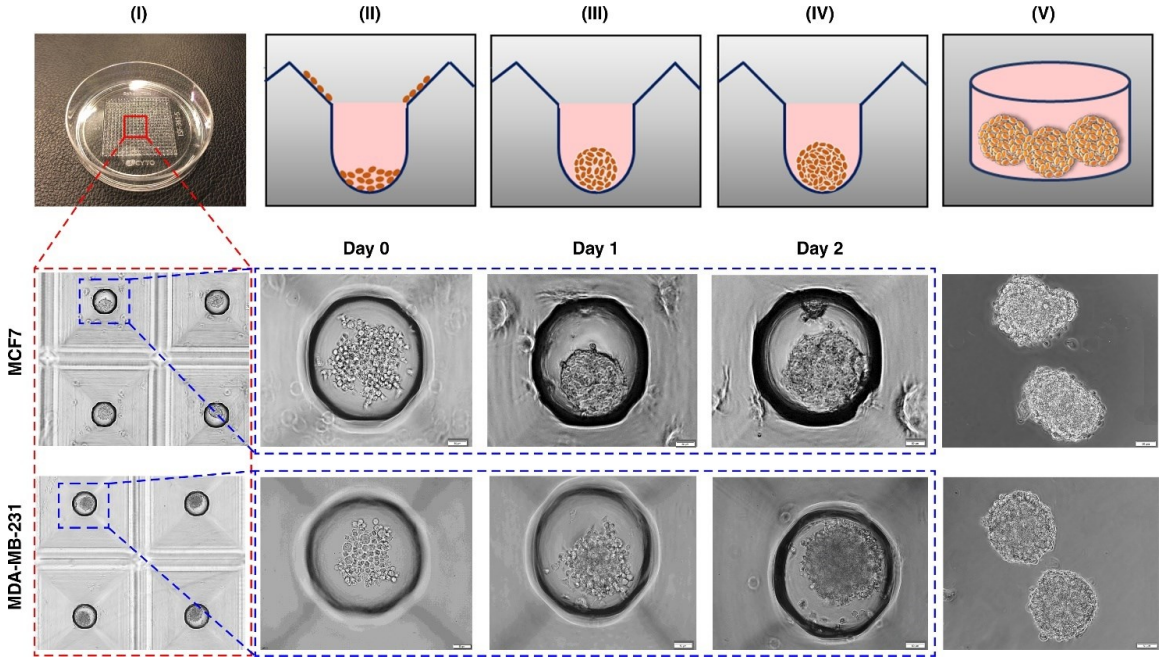

Figure 7.2. Schematic of the SpheroFilm utilized to generate the spheroids and representative images of the spheroid formation of breast cancer cells. Scale bar is 100 µm. (I) Side view of the SpheroFilm contains 361 microwells with the diameter of 300 µm and the depth of 300 µm (II) Breast cancer cells were seeded into the microwells (day 0) among five study groups of non-treated, CTX-treated, stiff, semi soft and soft (III) The cancer cells grouped together to formed cell aggregates after 1 day (IV) Later, cellular aggregates formed tumor spheroids after 2 days (V) Tumor spheroids were isolated from SpheroFilm and strained with the 100µm filter.

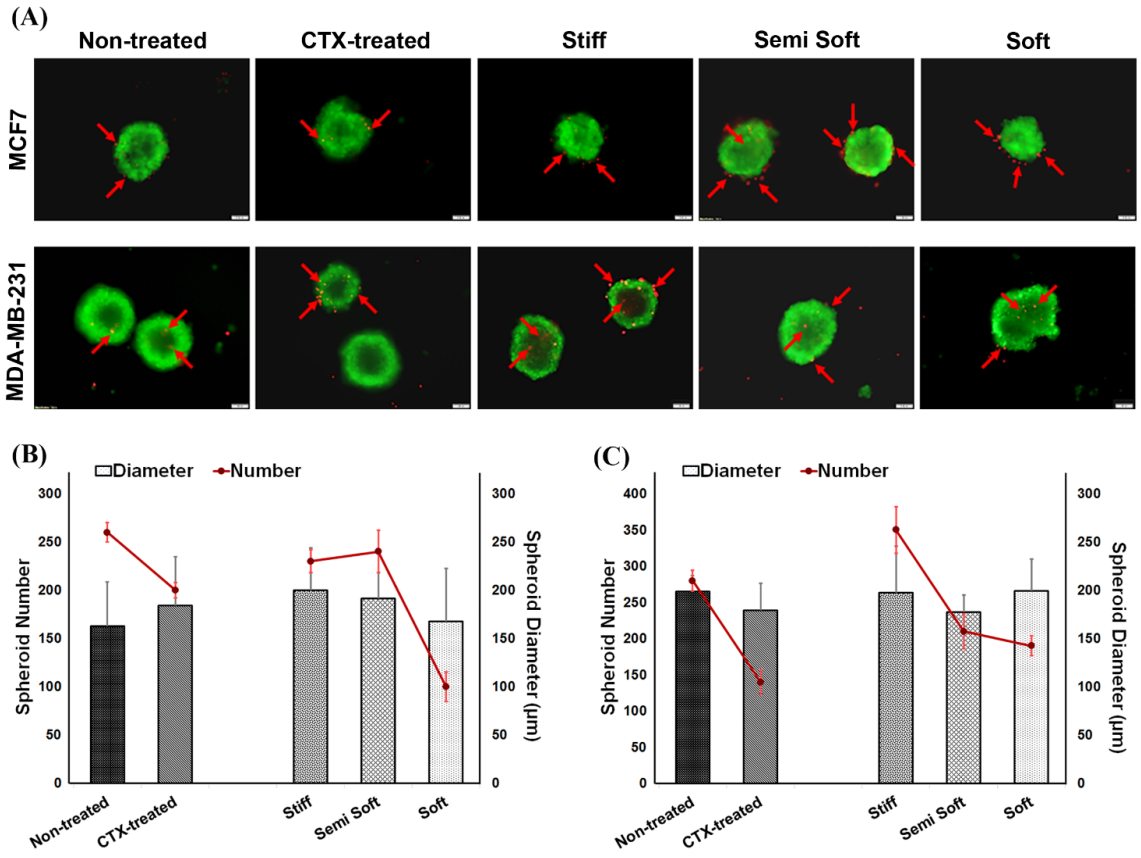

Figure 7.3. Spheroid characterization. (A) live and dead assay exhibits high viability of 3D spheroids of MCF7 and MDA-MB-231 cells among five chemical and mechanical treated groups. The live cells were stained with Calcein AM (Green) and the dead cells were stained with PI (Red), as described in materials and methods. Arrows show some of the dead cells. The images were obtained by fluorescent microscopy with scale bar of 100 µm. **(B and C)** The number and diameter of the formed spheroids of **(B)** MCF7 and **(C)** MDA-MB-231 cells. The number of spheroids has been represented as the mean±SD of three independent experiments. The mean diameter of spheroids has been represented as the mean±SD of at least 40 spheroids in each group.

Next, we examined whether EGFR targeting, and substrate stiffening involved in the spheroid formation. Total number of the formed spheroids and their average diameter have been shown in figure 7.4 (B and C). we observed the considerable difference in the number and diameter across the formed spheroids. Although both breast cancer cells successfully formed tumor

spheroids, MDA-MB-231 cells exhibited more spheroid formation ability by generating more number of spheroids which were bigger in the size. Our results revealed that Cetuximab treatment resulted in the alteration of spheroid formation ability of MDA-MB-231 cells. These cells decreased the spheroid formation ability in terms of number and diameter which suggest that spheroid formation of cancer cells strongly depends on the EGFR activity ($^{*}p<0.005$). In contrast, EGFR targeting did not affect spheroid formation of MCF7 cells. Furthermore, the spheroid formation ability of both cancer cells was altered with the substrate stiffening. MCF7 and MDA-MB-231 cells cultured on the stiff substrates revealed more ability for spheroid formation compared with the soft substrates ($^{*}p<0.05$). Although both cell lines respond to the substrate stiffness, non-invasive MCF7 cells showed more sensitivity than invasive MDA-MB-231 cells. The total number of 230±12 and 350±32 spheroids in the stiff groups of MCF7 and MDA-MB-231 cells decreased to 100±15 and 190±14 spheroids in the soft groups, respectively. These changes were accompanied with the decrease in the average diameter of MCF7 spheroids from 200±43 μm to 167±54 μm by substrate softening ($^{*}p<0.05$).

Next, we examined whether PDL-1 is involved in the spheroid formation induced by EGFR blocking and the substrate stiffening. Figure 7.4 indicates representative immunofluorescent images of tumor spheroids which reveals that spheroid formation interestingly increased PDL1 expression of breast cancer cells in the EGFR-dependent and stiffness-dependence manner. Breast cancer spheroids characterized with the lower expression of PDL-1 in the soft group compared with the stiff group as well as the Cetuximab-treated group compared with the non-treated group. These results suggest upregulation of PDL-1 through spheroid formation which mediated by the chemical and mechanical factors.

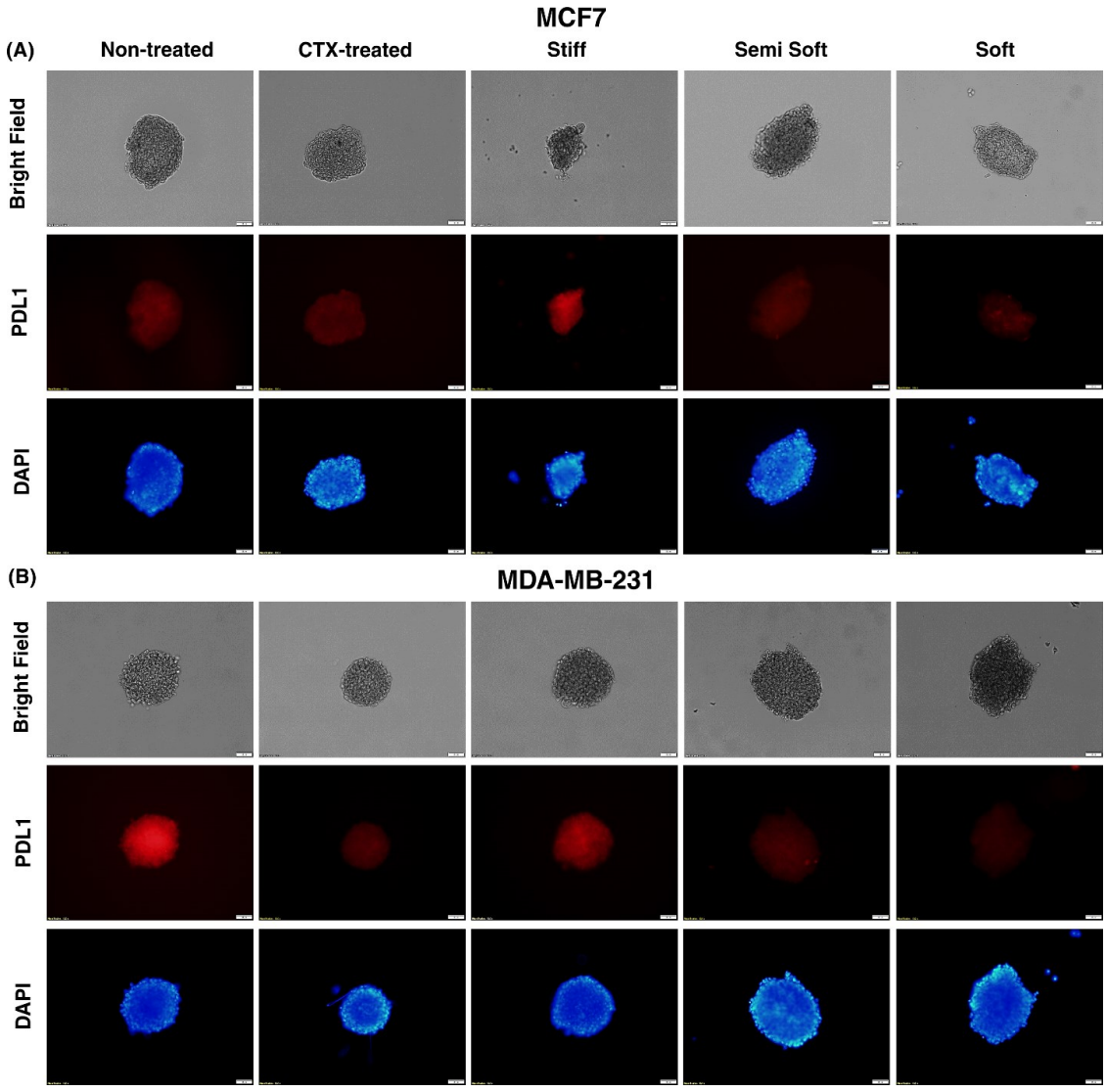

Figure 7.4. Role of the spheroid formation in the PDL-1 expression of breast cancer cells. Representative bright field and immunofluorescence images of **(A)** MCF7 and **(B)** MDA-MB-231 spheroids in five study groups of non-treated, CTX-treated, stiff, semi soft and soft, stained for PDL-1 (red) and nuclei (blue). Images were obtained using a fluorescent microscope and scale bar denotes 50 µm.

7.3.4 Assessment of the PDL1 expression in spread breast cancer spheroids

Next, we examined whether spheroid formation affects PDL-1 expression. Since tumor spheroids are the 3D structures of hundreds of cells, their PDL1 immunostaining would not

be adequate to confirm the induction of PDL1 expression by spheroid formation. Therefore, we examined PDL-1 expression of the tumor spheroids after spreading for 24 hours to ensure about the formation of cancer cell monolayer. Figure 7.5 illustrates spreading of the tumor spheroids and formation of the monolayer which consisted of those cancer cells that successfully involved in the tumor spheroid formation. MCF7 cells showed an increased PDL-1 expression not only in the tumor spheroids but also in the spread spheroids which demonstrates induction of the PDL1 expression by spheroid formation. Remarkably, MCF7 cells revealed substrate dependent PDL1 expression in the spread spheroids. As found before, the spread spheroids of MDA-MB-231 cells showed that the expression of PDL1 is closely related with the EGFR activity.

To further confirm the results, PDL-1 staining of the spread spheroids was accompanied with measuring of PDL-1 concentration using ELISA (figure 7.6B). Among five study groups of MCF7, we found the highest PDL-1 level in the non-treated group. In agreement with the data assessed by the immunofluorescent microscopy, MCF7 cells appeared as a PDL-1 positive after spheroid formation. Furthermore, the PDL-1 concentration of spread spheroids of MCF7 reached to 214±28 pg/ml, 153±19 pg/ml and 151±24 pg/ml in stiff, semi soft and soft groups, respectively. In contrast, MDA-MB-231 cells did not exhibit a significant change in the PDL-1 concentration after spheroid formation. In agreement with the previous results, spread spheroids of MDA-MB-231 cells exhibited noticeable PDL-1 expression which mediated by EGFR blockade and substrate stiffness, so that Cetuximab treatment caused a decrease PDL-1 expression in these cells.

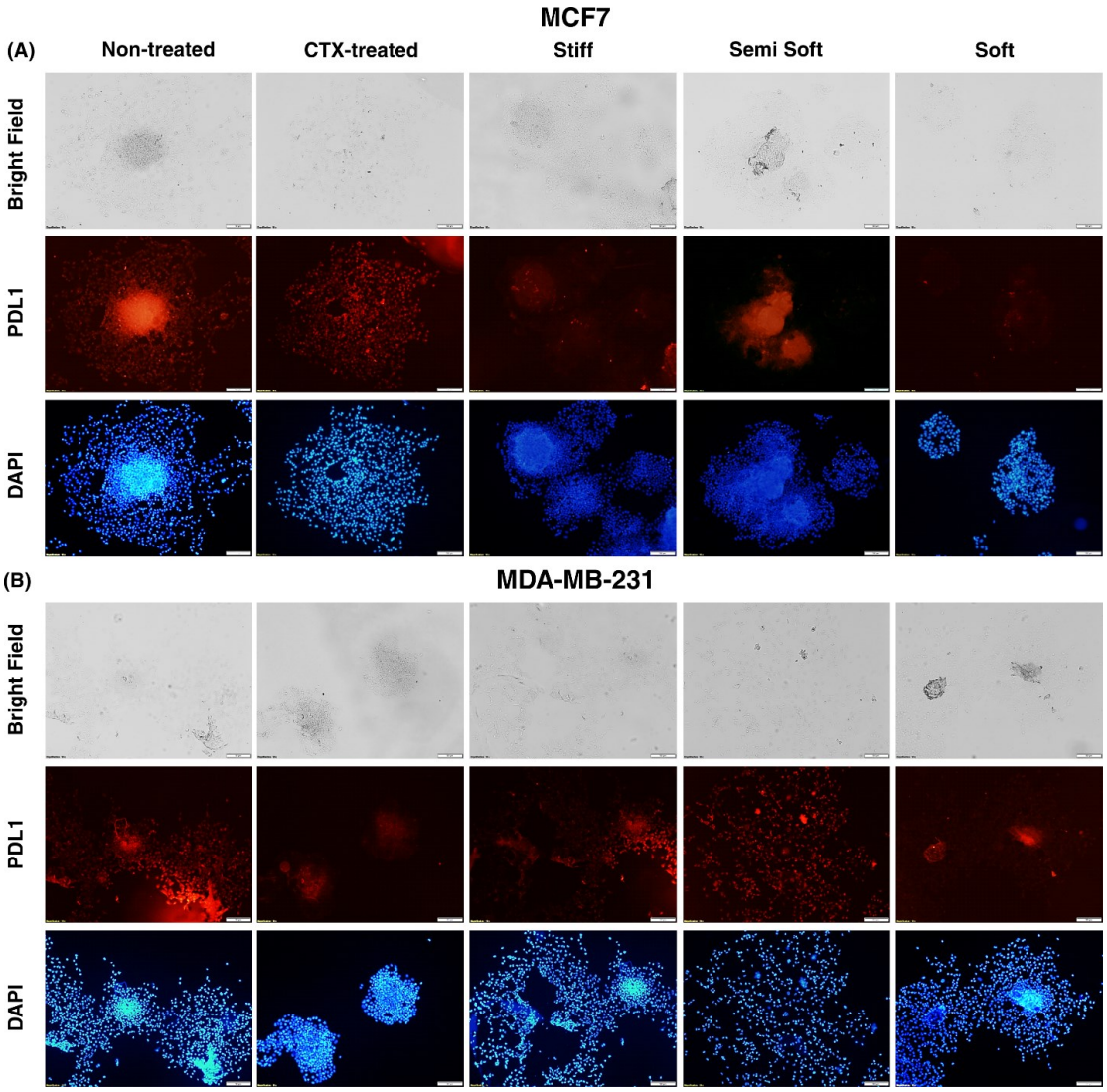

Figure 7.5. PDL-1 expression of spread spheroids of breast cancer cells as a function of the EGFR activity and the substrate stiffness. Representative bright field and immunofluorescence images of (A) MCF7 and (B) MDA-MB-231 spheroids in five study groups which stained for PDL-1 (red) and nuclei (blue). Images were obtained using a fluorescent microscope. Scale bar represents 100 µm.

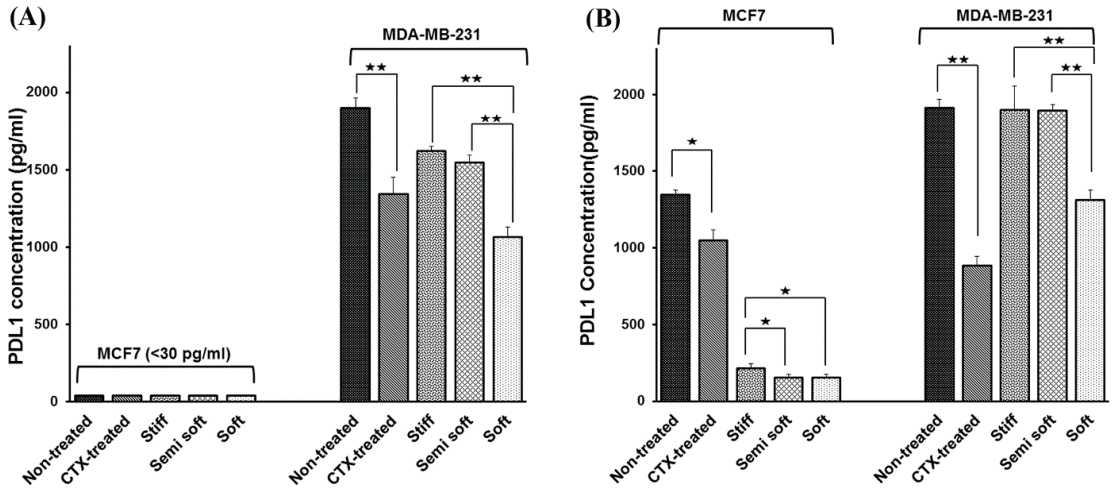

Figure 7.6. Comparison of protein concentration of PDL-1 in the chemical and mechanical groups, before and after formation of the spheroids. PDL-1 concentration of two breast cancer cell lines, MCF7 and MDA-MB-231 cells was measured by ELISA among five study groups of non-treated, Cetuximab treated, stiff, semi soft and soft substrates (A) before and (B) after spheroid formation. The values are mean ± SD of two independent experiment with duplicate measurements for each. * significantly different between the groups ($p< 0.05$) and ** ($p< 0.005$).

7.4 Discussion

It is well established that the expression of PD-L1 plays a significant role in cancer cell-mediated immune response. The cellular expression of PD-L1 could be affected with different chemical and mechanical factors of tumor microenvironment. Hence, identifying the PD-L1 signaling pathway and effective molecular and cellular events is crucial for the successful prediction of response to the PD-L1 targeted therapy. In this paper, the effect of EGFR signaling and substrate stiffness, two important tumor microenvironmental factors, on the PD-L1 expression of breast cancer cells was investigated. Further, we evaluated how the

spheroid formation of breast cancer cells could be related to the PD-L1 expression level. It has been demonstrated that different cancer cell types express a different level of PD-L1 that could be associated with their invasiveness potential [401]. Kim et al. indicated that metastatic lung cancer tumor tissues express more level of PD-L1 compared to the primary tumor [402]. The similar result was observed for breast cancer cells [400, 401]. In this study, we also confirmed the high PD-L1 expression of invasive MDA-MB-231 cells, while non-invasive MCF7 cells did not display a considerable level of PD-L1 ($p<0.05$). Moreover, PD-L1 level of MDA-MB-231 cells indicated a significant sensitivity to both EGFR treatment and substrate stiffening. There are several studies which evaluated the effect of substrate stiffness on the cellular behavior of cancer cells [403, 404]. They reached the conclusion that cancer cells respond to the substrate rigidity by changing the protein expression, proliferation, migration and differentiation ability. Most recently, Myazawa et al. probed the effect of substrate stiffness on the PD-L1 expression of lung cancer cells [405]. They demonstrated that substrate stiffening enhanced the PD-L1 level via actin-dependent mechanisms. Here, we investigated such a relationship by culturing breast cancer cells on stiff, semi-soft and soft PDMS substrates and demonstrated the relation between substrate mechanics and PD-L1 expression.

The association between EGFR and PD-L1 plays an important role in cancer targeted therapy and is gaining much more interest in recent years. The studies clarified a positive correlation between EGFR activity and PD-L1 expression [406, 407]. MDA-MB-231 cells have been reported for a high level of EGFR which recognize them as a suitable target for anti-EGFR treatment [408, 409]. EGFR is involved in the modulation of PD-L1 expression through AKT and STAT3 downstream signaling pathways [410, 411]. Regarding the correlation of these

two important signaling pathways, much more attention has been paid to the combined targeting of EGFR and PD-L1 in recent years [407, 412]. Our results indicated that EGFR-positive MDA-MB-231 cells, expressed a high level of PD-L1, while EGFR-negative MCF7 cells did not show a significant level of PD-L1 which is in good agreement with previously published papers [400, 401]. Moreover, Cetuximab treatment of MDA-MB-231 cells was accompanied with a noticeable reduction of PD-L1 which further confirmed the relationship between PD-L1 expression and EGFR signaling pathway.

There are various factors that could be influential in the PD-L1 expression which among them stemness factors are not adequately addressed [413, 414]. In this study, by analyzing data of invasive breast cancers from The Cancer Genome Atlas (TCGA) and protein-protein interaction, we illustrated a possible correlation between PD-L1, EGFR and stemness-related genes (Supplementary Fig 1). In line with these results, Malta et al. reported positive association between Immune microenvironment content, PD-L1 levels and stemness features in breast cancer (01). Additionally, high expression of PD-L1 in $CD44^{high}$ breast cancer cells and its role in maintaining stemness factors OCT-4A, Nanog and BMI1 have been reported.

It has been demonstrated that both approaches, substrate stiffness and EGFR activity, which were used to change the PD-L1 expression could alter stemness factors [415, 416]. Abhold et al. reported a reduction of mesenchymal markers by EGFR targeting [416] while You at el. probed an enhancement of stemness markers by substrate stiffening [415]. Regarding these studies, it can be concluded that both EGFR signaling and substrate stiffening could modulate the PD-L1 expression through the mediation of stemness markers. Stemness

markers could be affected by different mechanisms among them the spheroid formation of cancer cells plays an important role [417].

Therefore, cancer spheroids were formed to investigate how spheroid formation could alter the PD-L1 expression of breast cancer cells. The results indicated the successful formation of breast cancer spheroids in both cell lines among five study groups. However, noticeable differences were observed in the spheroid formation ability of breast cancer cells in terms of spheroid diameter and number. The effect of substrate stiffness on the various cellular behaviors has been investigated, while there is not any report addressing the effect of substrate stiffening on the spheroid formation. As far as we know, for the first time, we indicated that cancer cells derived from the stiff substrate had more ability to form tumor spheroids. Furthermore, the spheroid formation was influenced not only with the substrate stiffness but also with the EGFR activity. Cetuximab-treated MCF7 and MDA-MB-231 cells indicated a decrease of 23% and 50% in the number of formed spheroids compared to non-treated cells, respectively. The average diameter of formed spheroids also decreased from the stiff to the soft substrate. Moreover, analyzing the number and diameter of formed MDA-MB-231 spheroids revealed that the spheroid formation ability of breast cancer cells positively correlated with the PD-L1 expression level.

The assessment of PD-L1 level by immunostaining as well as ELISA indicated that firstly, cancer spheroids derived from the stiff substrate showed the higher level of PD-L1 among three PDMS substrates, secondly, EGFR targeting decreased the PD-L1 level not only in the cancer cell monolayer but also in the formed spheroids, and thirdly, the spheroid formation considerably enhanced the PD-L1 expression level of MCF7 cells. This result demonstrated

the association between the spheroid formation and PD-L1 expression. Chen et al. reported that spheroid formation led to overexpression of stemness-related genes [417]. Furthermore, as discussed before, stemness markers also correlate to the PD-L1 expression. Hence, there is a triple interaction between stemness markers with the PD-L1 expression and spheroid formation. Taken together, our results suggest that the formation of spheroids could modulate PD-L1 expression of MCF7 cells through the mediation of stemness markers.

Molecular targeted therapy (e.g., EGFR and Her2 inhibitors) and immunotherapy (e.g., PD1/PDL1 inhibitors) are two of the most important approaches in the cancer treatment. Unlike molecular targeted therapy, the prediction of response to immunotherapy has more challenges. Although, the PDL-1 expression is widely used as a predictive biomarker to immunotherapy, to date, many immunotherapy treatments have demonstrated a low efficacy in the most of patients [418]. Our results indicate that even for PD-L1-negative cancer cells such as MCF7, the PD-L1 expression could alter by different cellular and molecular mechanisms, and in such a situation different treatment approach should be considered. Therefore, successful predication of response to immunotherapy, specifically PDL-1 targeting, requires much more experiments in the 2D and 3D microenvironment, under various chemical and mechanical conditions. Moreover, the correlation between EGFR and PD-L1 supports the approach of combination therapy as a more effective strategy to modulate cancer cell- immune cell interactions.

In summary, we revealed that PD-L1, as an important biomarker of immunotherapy, is modulates by both substrate stiffness and EGFR activity. Further, we demonstrated that the PD-L1 expression level associates with the formation of cancer spheroids. So, even for those

cancer cells with a low level of PD-L1, the possible changes in the cancer cell- immune cell interaction should be considered. Overall, to achieve a successful predication of response to immunotherapy, different influential chemical and mechanical factors should be examined. The evidence from this study has gone some way toward enhancing our understanding of factors which modulate the PD-L1 expression. Our findings suggest a triple interaction between the spheroid formation, PD-L1 expression, and stemness markers which are involved in the cancer progression. Despite this, we believe our work is a starting point and further experiments are required to determine exactly how spheroid formation affects PD-L1 expression.

Chapter 8

Generation of vascularized Tumour Organoids

Statement on COVID-19 impact on the completion of this chapter

This chapter provide a new and novel protocol to generation of vascularized tumor organoids in microfluidic device. The spread of Covid-19 and initiation of series of intensive restrictions and lockdowns on state extremely affected the completion of this chapter of thesis. Methodologically, the generation of vasculature and maintaining organoids require a daily basis laboratory work. This issue was affected by monthly lockdowns. Moreover, purchasing required materials particularly cell culture reagents for organoid formation and vasculogenesis faced with a log-term delay due to national and international border closure. Additionally, limitations in daily laboratory working hour (2 hours) and campus lockdowns for using core facilities significantly hindered performing experiments and data gatherings for this chapter. However, regardless of these limitations, we successfully generated microvasculature and pre-vascular organoids partially using an adapted method. We also highlighted remaining steps to completion of this work in post-pandemic context and its implication in future of cancer research.

8.1 Introduction

Various tumour organoids have been developed to the model tumour microenvironment (TME) [419-421]. However, lack of vasculature, tumour stromal cells and importantly, immune cells in these models limited the application of tumour organoids in the study of tumour-immune microenvironment and interaction of cancer cell-stromal cells and immune cells in a dynamic and real-time fashion [422]. Recently, few studies highlighted the potential of co-culturing immune cells and tumour-derived organoids in the study of tumour-reactive T cells and immune therapy response in colon and lung adenocarcinoma [423-426]. Due to the nature of organoid formation from tumour tissues, the majority of immune cells and tumour stromal cells are eliminated during the process of organoid generation. More importantly, the lack of microvasculature in these model systems significantly challenges the study of immune cells infiltration and screen of therapeutics agent target vasculature in TME [427]. Thus, developing a reliable model of TME which include all molecular and cellular properties of TME remain to be developed. To overcome these limitations, microfluidic technology offers a potential platform to generate and incorporation all cellular components of TME in a low-cost, physiology relevant and reliable fashion. This platform enables the study of cell-cell communication analysis of TME in a real-time and single cells manner. Additionally, the generation of perfusable microvasculature in a device coupled with organoids offers a potentiate platform for studying immune cells infiltration in physiologically relevant. In this chapter, we aimed to develop an advanced model of TME by cooperating tumour organoids, tumour stromal cells, and immune cells in a 3D vascularized microfluidic device.

8.2 Methods and Materials

Figure 6.1 illustrate the workflow of developing an advanced model of TME.

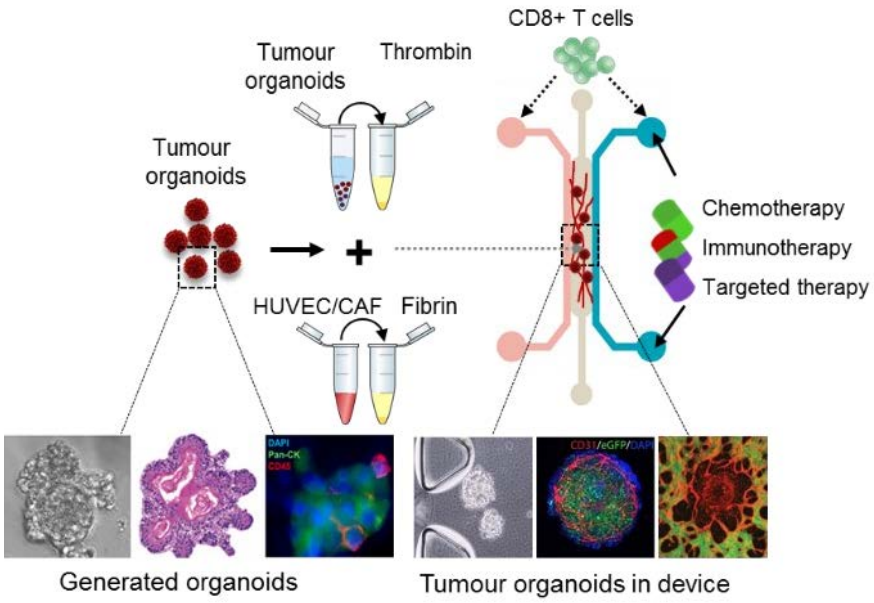

Figure 8.1. Schematic of workflow for the generation of tumour microenvironment in vascularized device equipped with tumour spheroids/organoids, cancer-associated fibroblasts, and T-cells. The generated tumour organoids will be mixed with the defined concentration of thrombin and then add to the mixtured of endothelial cells and CAFs. The final mixure will be loaded in the central channel of device and feed with the a mixture of organoid medium and vascular medium for 15 days.

8.2.1 Cell culture and organoids formation

To generate cell-line derived breast cancer organoids, the MCF7 cells were cultured using MammoCult medium for 10 days in an ultra-low attached flask. The generated mamo-sphere were harvested using 250 × *g* centrifugation for 2 minutes. The plate of cells containing spheroids were transferred to the collagen-gel solution with a concentration of 2.5 mg/ml on ice. A 100µl drop of this suspension was placed in the centre of a well in a 24-well suspension culture plate and allowed to polymerize for 30 min at 37 °C. Finally, 700µl of breast cancer

organoid culture medium (DMEM/F12 supplemented with R-Spondin-1, Neuregulin-1, FGF7, FGF10, EGF, Noggin, A83-01, Y27632, B27, N-Acetylcysteine, Nicotinamide, Glutamax, HEPES, and penicillin/streptomycin) [428] was then placed over the droplet and incubated for 2-4 weeks.

8.2.2 Culturing microvasculature in device

Human umbilical vein endothelial cells, HUVECs (Lonza, Cat. no. CC-2519) were cultured in vascular medium (EGM2-MV BulletKit) (Lonza, Cat. no. CC-3202). NHLF human Lung Fibroblasts (Lonza, Cat. no. CC-2512) were cultured in fibroblast growth supportive medium (Lonza, Cat. no. CC-3132). The culture medium was replaced every 2 days, and all experiments were performed before reaching 15 passages.

Microvascular networks (MVN) were created by detaching HUVEC and NHLF cells from cell culture flasks and resuspending them in a cold vascular medium with 2 U/ml thrombin from bovine plasma (Millipore Sigma, #T7326). The two cell types were combined with cell densities of 12×10^6/ml HUVECs and 2×10^6/ml hLFB. Cell suspensions were mixed 1:1 volume ratio with 6 mg/ml fibrinogen (Millipore Sigma, #341573) and gently injected into microfluidic devices. After allowing several minutes of fibrin polymerization (15–30 min) in a 37◦C incubator, warm vascular medium (EGM2-MV) was added to both side channels and refreshed each day of culture. MVN self-assembled over several days, refreshing media daily.

8.2.3 Generation of vascularized tumour spheroids

To generate the pre-vascular organoids, MVN were co-cultured with tumour organoids. To maintain the same conditions used in each individual protocol, cell densities of 24×10^6/ml

HUVECs and 4×10^6/ml hLFB were mixed 1:1 volume ratio with 6 mg/ml fibrinogen. This cell-gel suspension was mixed 1:1 with collagen-mamo-sphere mixture previously generated by resuspending organoids in 125 mL of collagen hydrogel, resulting in the same final cell density as MVNs or organoids alone. After loading this solution in the central channel of the device, the flanking channels filled with 1:1 ratio of organoid medium and EGM2-MV and devices were incubated for at least 10 days.

8.2.4 Immunofluorescence and Confocal Imaging

Mature microvascular networks and pre-vascular organoids were rinsed with warm PBS followed by 2% paraformaldehyde to the media channels and left at room temperature. After 15 min of fixation, devices were rinsed twice with PBS, and blocking solution (Blocking-Aid, thermo-fisher) was added. Devices were incubated for 1 hour at room temperature (RT), washed with PBS, and stained with primary antibodies: CD31 (Abcam, ab215912), KRT-8/18 (Abcam, ab206091), VE-Cadherin (Abcam, ab225442), and incubated at RT for another 1 hour. Prior to imaging, the primary antibodies were removed from the device and replaced with DAPI for nucleus staining.

8.2.5 Statistical analysis

The microvasculature features and the expression of VE-Cadherin were analysed using Fiji software. The statistical analysis was performed using Graph-Pad Prism (version 9.1).

8.3 Results

8.3.1 Microvasculature in device

To generate 3D microvasculature in the device, we assessed various conditions in terms of the ratio of endothelial and fibroblast cells and thrombin/fibrinogen gel concentration to identify appropriate cell density and ECM composition. Clear differences were observed in the morphology of vascular networks for different conditions (Figure 8.2A, B). Since each condition gave rise to different settings, we assess various features to identify the appropriate setting. A high inter-connected form of endothelial cells was found in setting-03, in which the ratio of HUVEC/Fibroblasts was 5:1. The differences in the size of the microvasculature network were quantified by measuring the present area that HUVECs occupied in the device. This value varied from 59.1 ± 3.6 for setting-01, 51.6 ± 9.8 for setting-02, and 84.3 ± 5.4 for setting03. We further compared networks by quantifying them through different metrics, including the number and the length of branches. While setting-01 had 105 ± 15, setting-03 showed a nearly 2.0-fold increase (182.6 ± 5.8) in the number of branches (Figure 8.2B). The length of all branches was also measured, resulting in a high average branch length of 147 ± 3.2 μm for devices cultured by setting-03 in comparison with other settings. Finally, we measured the expression of the VE-Cadherin in networks by quantifying mean-fluorescent intensity. As we expected, the setting-03 microfluidic devices showed a nearly 5.0-fold increase in the expression of this protein (Figure 8.2B). Overall, these results demonstrated setting-03 as an appropriate condition for generating a mature microvasculature in the device.

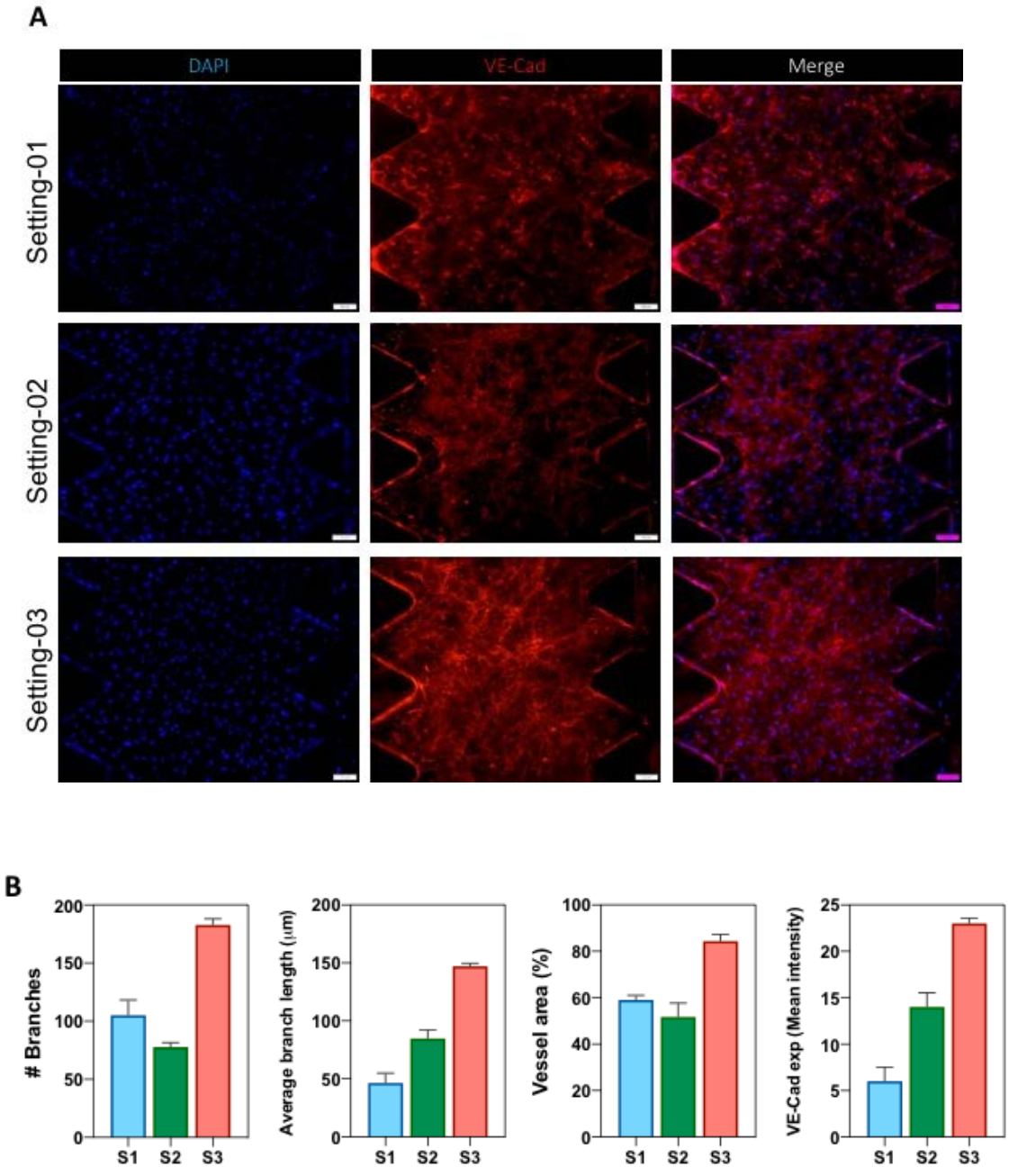

Figure 8.2. Generation of 3D microvasculature in a microfluidic device. **(A)** Comparing various settings on the formation of vasculature in the device (Methods and Materials). The representative images show the expression of VE-cadherin in the formed microvasculatures. **(B)** the assessment of various features of microvasculature between different settings. The analyzed features suggest setting-03 as appropirate condition for generating microvasculature in the device based on the number of branches, vessel area, and VE-cadherin expression.

8.3.2 Generation of vascularized organoids

The lack of micro-vasculature in organoids has been highlighted as one of the main drawbacks of this promising 3D model, which limit the application of tumour organoids to model vasculature properties of TME and screening of the anti-angiogenic compounds. Currently, to generate vascularized tumour organoids, two main approaches have been suggested [427], although the successfulness of this approach remains to be shown. Culturing pre-vascularized tumour organoids in a vascular bed or co-culturing formed, and mature tumour organoids directly by endothelial cells are known as inside-out and outside-in approaches, respectively. To better model vasculature properties of TME, the inside-out approach allows better mimicking of both vasculogenesis and angiogenesis besides fueling the core of the tumour organoids through the formation of a pre-vascular area in the tumour organoids. To use this approach, we tried to generate pre-vascular organoids that are included with endothelial cells. In this regard, we added and cultured a defined ratio of HUVEC cells to tumour cells mixture at the seeding step of organoid formation for at least 15 days before the maturation step of tumour organoid formation (Figure 8.3 A, B). During the first 15 days of the tumour organoid formation, we found high expression of CD31, a specific marker for endothelial cells at the core of the tumour organoids stained with cytokeratin-18 as a maturation marker (Figure 8.3A). Following expanding culture time and using maturation medium included with vasculature medium (50:50 v/v) under a semi-hypoxic condition, we found a vasculature like structure in a small part of the organoids (Figure 8.3B). The analysis of CD31showed the low expression of this protein at the proximal region of the organoids while they were expressed at the distal site of the organoids.

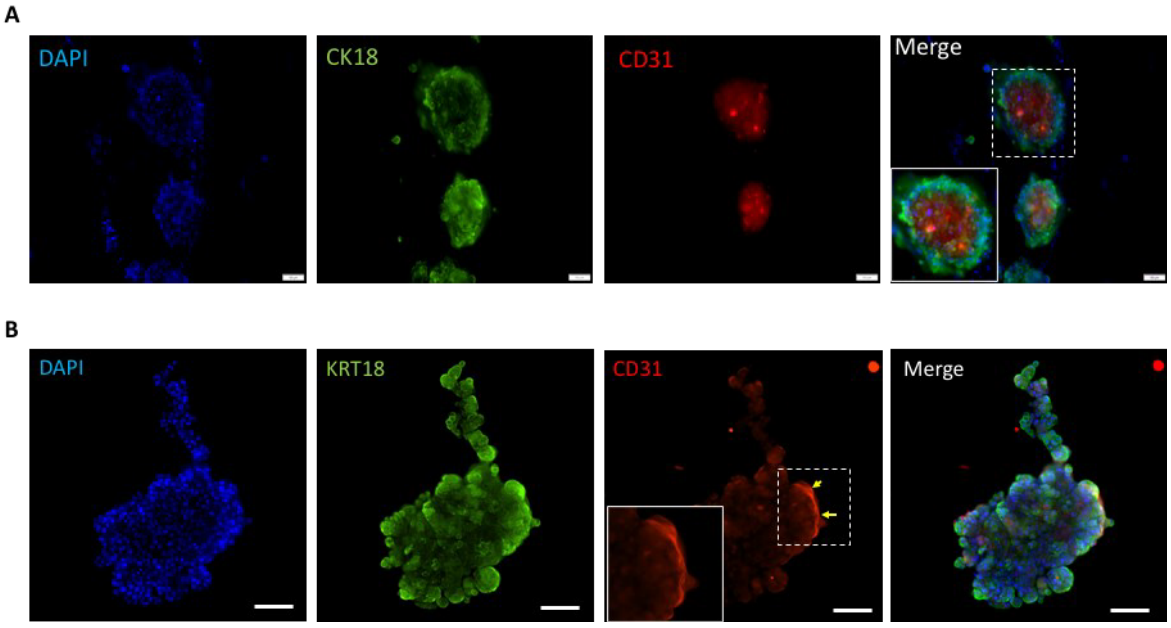

Figure 8.3. Generation of vascularized tumour organoids. (A) the immuno-fluorescent image shows the co-culture of cancer cells and endothelial cells after 15 days. The endothelial cells were localized at the proximal region (core) of tumour organoids stained with CD31(Red). (B) The representative image of a generated tumour organoid showing microvasculature after 28 days of culture in a semi-hypoxic condition using organoid maturation and EGM2 medium. The endothelial cells and tumour organoids were stained with CD31 (Red) and maturation marker KRT18 (Green), respectively. The immuno-fluorescent image shows the formation of microvasculature in a small distal part of the organoids (yellow arrows).

Taken together, these results highlighted the applicability of micro-vasculature formation in the distal part and surface of the tumour organoids using our developed protocol. However, long-term maintenance of co-culture of tumour organoids and microvasculature in culture should be optimized, which requires further effort.

8.4 Discussion

This chapter aimed to generate a complex TME represented in Figure 6.1 using generated microvasculature and tumour organoids in a microfluidic device. In the first step, we developed a fully vascularized microfluidic device. As few research articles used a three-channel device for vascular formation [429-434] and the presence of variations in used protocols, we measured different settings in terms of passage numbers and the ratio of endothelial/fibroblast cells ECM composition. The efficacy of formed vasculature was measured against four features: number of branches, vessel area, average branch length, and expression of the endothelial marker. These features have been introduced as a marker of a mature vasculature in the device [435, 436]. Using these features, we found setting-3 of vasculature formation as an appropriate condition for generating a vascular bed for tumour organoids.

The application of tumour organoids for modelling diseases, including cancer, have been highlighted previously [3, 108, 112]. Recently, the use of tumour organoids to recapitulate a single feature of cancer and tumour microenvironment (TME) and, more recently, tumour immune microenvironment (TIME) has been introduced [114, 117, 424]. The genomic similarity between tumour-derived organoids and parental tumours introduced this model system for the study of cancer genomics and more recently personalized treatment of cancer [3]. However, this model is unable to model the main cellular feature of TME and TIME in terms of tumour stromal cells, vasculature and presence of immune cells and their interaction in a physiologically relevant fashion. Although few studies demonstrated organoid-like structures equipped with vasculature [429]; however, the lack of flow and perfusion in these

models unable the mimicry of TME vasculature in a reliable manner. In recent years, various efforts have been performed to develop a vascularized organoid using bio-engineering approaches [120, 283, 427, 437]. It has been shown that stem-cell-derived organoids without pre-developed microvasculature can be vascularized after transplantation in mice [427, 438]. These data suggest that culturing organoids in an engineered vascular bed might result in vascularized organoids in-vitro. However, few studies demonstrated a fully vascularized and perfusable vasculature in organoids using this approach [439, 440]. Taken together, this evidence suggests that organoid pre-vascularization, even without perfusion, is an essential part towards a truly perfusable organoid platform in-vitro, especially in the case of tumour-derived organoids. In this regard, two main approaches have been suggested: co-culturing organoids and endothelial cells and co-differentiation of mesodermal progenitor cells in the case of stem cell-derived organoids [427].

Co-culturing organotypic tumour spheroids with endothelial cells is an intuitive way to develop pre-vascular organoids. We mixed tumour cells with a defined ratio of endothelial cells and tumour stromal cells and cultured them for 28 days under two different organoid culture mediums. Measuring the localization of endothelial cells after 15 days showed accumulation of these cells at the center of organoids, while when we induced a hypoxic-like condition, not only HUVEC cells moved to the distal sites of tumour organoids, but also few microvasculature-like structures had been formed. Similar to this approach, Takebe et, al developed vascularized liver organoids by seeding iPSC derived hepatic endoderm, human umbilical vein endothelial cells (HUVECs) and human bone marrow mesenchymal stem cells (MSCs) as stromal cells on Matrigel [441]. Recently, a modified version of this approach has been implemented to the generation of functional microvasculature networks within normal

brain organoids [442, 443].

In the case of tumour-organoid vasculature, few numbers of studies demonstrated the formation of microvasculature network around cancer cell line derived spheroids and/or aggregate rather than organoids [429]. In these studies, the pre-generated spheroids co-cultured with endothelial cells in two different channels and allow endothelial cells to migrate toward spheroids sites and generate a vascular network [124, 439, 440]. In another approach, tumour aggregates can be mixed with endothelial cells and loaded into the central channel of a microfluidic device which finally results in vascular-like spheroids [435]. However, the obtained results from these studies showed a lack of a vascular-network coated organoid or spheroids [427]. Recently, Wörsdörfer et al., using a breast cancer cell line (MDA-MB-435) and co-culturing them with a defined ratio of mesodermal progenitor cells, developed a fully coated vasculature spheroid [444]. In this study, they highlighted the impact of a hypoxic condition in the stimulation of vascular formation around spheroids which have been observed in our results. Additionally, they observed the localization of CD31 positive cells at the distal regions of spheroids.

Taken together, besides the obtained results from this study and lesson learnt from developmental normal vascularized organoids, it seems that a feasible strategy to incorporate functional vasculature within organoids, particularly tumour organoids is to simply enable this natural process to occur by developing pre-vascular organoids followed by embedding organoids in an engineered vascular bed in vitro; however, the successfulness of this methodology requires a careful plan in terms of timing of co-culture, number of endothelial cells and composition of culture medium.

Chapter 9

Conclusion and future work

In this research project, we aimed to develop an advanced model of TME using a 3D vascularized microfluidic device equipped with tumour organoids, tumour stromal cells and immune cells. Considering the single feature of TME, we successfully developed a protocol for long terms culture of tumour spheroids and organoids in a microfluidic device and modelled biology and cellular feature of tumour stromal cells and vasculature in the device. Moreover, to show the functionality of these models, we studied and demonstrated for the first time the suppressive effects of an anti-fibrotic drug known as Pirfenidone on two major tumour stromal cells activities and tumour immunity in terms of expression of immune check-point protein PD-L1 and regulated cytokines through the various research articles. Additionally, using our device, we successfully showed the migration of PD-L1 positive cancer-associated fibroblasts (CAFs) and suggested that targeting these cells using PFD can reduce immune-escape capacity. As metastasis is linked to the phenotype transformation of cancer cells to a mesenchymal state, we modelled this feature of TME using organotypic spheroids and CAFs. We demonstrated that targeting CAFs can significantly reduce the EMT capacity of cancer cells and the stemness feature of cancer cells. Finally, we generated a mature microvasculature network followed by pre-vasculature organoids in our device. We used various settings and modified previously developed pre-vascular organoid protocols for stem-cell-derived organoids to generate vascular tumour organoids. However, current situations and restrictions due to the Covid-19 pandemic significantly affected the completion of this phase of the project. Thus, these limitations warrant the feature studies to focus on culturing pre-vascular organoids in a microvasculature bed and load immune cells to model a complex and reliable TME in a microfluidic device. This model can be used to study cell-cell communication of TME and the role of the vasculature in tumour development. Also, the

role of tumour stromal cells and their immune-suppressive capacity can be studied in this complex system. Moreover, the advantages of microfluidic technology enable the incorporation of recent state-of-art technologies, including single-cell analysis in a device in a real-time, cost-effective, and reliable fashion. Thus, the completion of this phase of the study in the near future can result in the development of a new generation of in-vitro model of TME suitable for the study of TME and drug discovery at the single-cell level. Moreover, our model enables the culture of patient-derived organoids and immune cells, highlighting the application of this platform for personalized cancer treatment, including immunotherapy which requires feature works to validate this platform. At the end, the completion of this thesis was faced with various ***Outstanding questions, challenges and recommendations*** which can be considered as opportunities for future research in this field:

- As tumor stromal cells are a heterogeneous population, what sub-population of CAFs is main target of PFD?
- How combination of PFD with current immune-checkpoint blockades can improve immunotherapy response in TNBC?
- The optimum culture condition for developing vascularized organoids remains an unanswered question in which using single culture medium for supporting both tumour organoids and vasculature is a major obstacle.
- Developing a complex microfluidic device that includes all immune cells, vasculature and tumor organoids in a spatially like original tumor remained to be introduced.
- Developing microfluidic culture platforms with the capacity of single-cell analysis can revolutionize the application of microfluidic in study of TME and drug discovery.

References

1. Quail, D.F. and J.A. Joyce, *Microenvironmental regulation of tumor progression and metastasis.* Nat Med, 2013. **19**(11): p. 1423-37.
2. Hanahan, D. and R.A. Weinberg, *Hallmarks of cancer: the next generation.* Cell, 2011. **144**(5): p. 646-74.
3. Aboulkheyr Es, H., L. Montazeri, A.R. Aref, M. Vosough, and H. Baharvand, *Personalized Cancer Medicine: An Organoid Approach.* Trends Biotechnol, 2018. **36**(4): p. 358-371.
4. Sun, Y., *Tumor microenvironment and cancer therapy resistance.* Cancer Lett, 2016. **380**(1): p. 205-15.
5. Kalluri, R. and M. Zeisberg, *Fibroblasts in cancer.* Nat Rev Cancer, 2006. **6**(5): p. 392-401.
6. Ohlund, D., E. Elyada, and D. Tuveson, *Fibroblast heterogeneity in the cancer wound.* J Exp Med, 2014. **211**(8): p. 1503-23.
7. Ostman, A. and M. Augsten, *Cancer-associated fibroblasts and tumor growth--bystanders turning into key players.* Curr Opin Genet Dev, 2009. **19**(1): p. 67-73.
8. Marsh, T., K. Pietras, and S.S. McAllister, *Fibroblasts as architects of cancer pathogenesis.* Biochim Biophys Acta, 2013. **1832**(7): p. 1070-8.
9. Costa, A., Y. Kieffer, A. Scholer-Dahirel, F. Pelon, B. Bourachot, M. Cardon, P. Sirven, I. Magagna, L. Fuhrmann, C. Bernard, et al., *Fibroblast Heterogeneity and Immunosuppressive Environment in Human Breast Cancer.* Cancer Cell, 2018. **33**(3): p. 463-479 e10.
10. Elyada, E., M. Bolisetty, P. Laise, W.F. Flynn, E.T. Courtois, R.A. Burkhart, J.A. Teinor, P. Belleau, G. Biffi, M.S. Lucito, et al., *Cross-Species Single-Cell Analysis of Pancreatic Ductal Adenocarcinoma Reveals Antigen-Presenting Cancer-Associated Fibroblasts.* Cancer Discov, 2019. **9**(8): p. 1102-1123.
11. Tarin, D. and C.B. Croft, *Ultrastructural features of wound healing in mouse skin.* J Anat, 1969. **105**(Pt 1): p. 189-90.
12. Olumi, A.F., G.D. Grossfeld, S.W. Hayward, P.R. Carroll, T.D. Tlsty, and G.R. Cunha, *Carcinoma-associated fibroblasts direct tumor progression of initiated human prostatic epithelium.* Cancer Res, 1999. **59**(19): p. 5002-11.
13. Orimo, A., P.B. Gupta, D.C. Sgroi, F. Arenzana-Seisdedos, T. Delaunay, R. Naeem, V.J. Carey, A.L. Richardson, and R.A. Weinberg, *Stromal fibroblasts present in invasive human breast carcinomas promote tumor growth and angiogenesis through elevated SDF-1/CXCL12 secretion.* Cell, 2005. **121**(3): p. 335-48.
14. Dimanche-Boitrel, M.T., L. Vakaet, Jr., P. Pujuguet, B. Chauffert, M.S. Martin, A. Hammann, F. Van Roy, M. Mareel, and F. Martin, *In vivo and in vitro invasiveness of a rat colon-cancer cell line maintaining E-cadherin expression: an enhancing role of tumor-associated myofibroblasts.* Int J Cancer, 1994. **56**(4): p. 512-21.

15. Ahirwar, Dinesh K., Mohd W. Nasser, Madhu M. Ouseph, Mohamad Elbaz, Maria C. Cuitiño, Raleigh D. Kladney, Sanjay Varikuti et al. *Fibroblast-derived CXCL12 promotes breast cancer metastasis by facilitating tumor cell intravasation*. Oncogene, 2018. **37**(32): p. 4428-4442.
16. Kalluri, R., *The biology and function of fibroblasts in cancer.* Nat Rev Cancer, 2016. **16**(9): p. 582-98.
17. Bruzzese, F., C. Hagglof, A. Leone, E. Sjoberg, M.S. Roca, S. Kiflemariam, T. Sjoblom, P. Hammarsten, L. Egevad, A. Bergh, et al., *Local and systemic protumorigenic effects of cancer-associated fibroblast-derived GDF15.* Cancer Res, 2014. **74**(13): p. 3408-17.
18. Elkabets, M., A.M. Gifford, C. Scheel, B. Nilsson, F. Reinhardt, M.A. Bray, A.E. Carpenter, K. Jirstrom, K. Magnusson, B.L. Ebert, et al., *Human tumors instigate granulin-expressing hematopoietic cells that promote malignancy by activating stromal fibroblasts in mice.* J Clin Invest, 2011. **121**(2): p. 784-99.
19. Scherz-Shouval, R., S. Santagata, M.L. Mendillo, L.M. Sholl, I. Ben-Aharon, A.H. Beck, D. Dias-Santagata, M. Koeva, S.M. Stemmer, L. Whitesell, et al., *The reprogramming of tumor stroma by HSF1 is a potent enabler of malignancy.* Cell, 2014. **158**(3): p. 564-78.
20. Dongre, A. and R.A. Weinberg, *New insights into the mechanisms of epithelial-mesenchymal transition and implications for cancer.* Nat Rev Mol Cell Biol, 2019. **20**(2): p. 69-84.
21. Zhao, L., G. Ji, X. Le, Z. Luo, C. Wang, M. Feng, L. Xu, Y. Zhang, W.B. Lau, B. Lau, et al., *An integrated analysis identifies STAT4 as a key regulator of ovarian cancer metastasis.* Oncogene, 2017. **36**(24): p. 3384-3396.
22. Yu, Y., C.H. Xiao, L.D. Tan, Q.S. Wang, X.Q. Li, and Y.M. Feng, *Cancer-associated fibroblasts induce epithelial-mesenchymal transition of breast cancer cells through paracrine TGF-beta signalling.* Br J Cancer, 2014. **110**(3): p. 724-32.
23. Shintani, Y., A. Fujiwara, T. Kimura, T. Kawamura, S. Funaki, M. Minami, and M. Okumura, *IL-6 Secreted from Cancer-Associated Fibroblasts Mediates Chemoresistance in NSCLC by Increasing Epithelial-Mesenchymal Transition Signaling.* J Thorac Oncol, 2016. **11**(9): p. 1482-92.
24. Pistore, C., E. Giannoni, T. Colangelo, F. Rizzo, E. Magnani, L. Muccillo, G. Giurato, M. Mancini, S. Rizzo, M. Riccardi, et al., *DNA methylation variations are required for epithelial-to-mesenchymal transition induced by cancer-associated fibroblasts in prostate cancer cells.* Oncogene, 2017. **36**(40): p. 5551-5566.
25. Gaggioli, C., S. Hooper, C. Hidalgo-Carcedo, R. Grosse, J.F. Marshall, K. Harrington, and E. Sahai, *Fibroblast-led collective invasion of carcinoma cells with differing roles for RhoGTPases in leading and following cells.* Nat Cell Biol, 2007. **9**(12): p. 1392-400.
26. Harper, J. and R.C. Sainson, *Regulation of the anti-tumour immune response by cancer-associated fibroblasts.* Semin Cancer Biol, 2014. **25**: p. 69-77.
27. Raffaghello, L. and F. Dazzi, *Classification and biology of tumour associated stromal cells.* Immunol Lett, 2015. **168**(2): p. 175-82.
28. Patel, R., A. Filer, F. Barone, and C.D. Buckley, *Stroma: fertile soil for inflammation.* Best Pract Res Clin Rheumatol, 2014. **28**(4): p. 565-76.

29. Poggi, A., A. Musso, I. Dapino, and M.R. Zocchi, *Mechanisms of tumor escape from immune system: role of mesenchymal stromal cells.* Immunol Lett, 2014. **159**(1-2): p. 55-72.
30. Soleymaninejadian, E., K. Pramanik, and E. Samadian, *Immunomodulatory properties of mesenchymal stem cells: cytokines and factors.* Am J Reprod Immunol, 2012. **67**(1): p. 1-8.
31. Paunescu, V., F.M. Bojin, C.A. Tatu, O.I. Gavriliuc, A. Rosca, A.T. Gruia, G. Tanasie, C. Bunu, D. Crisnic, M. Gherghiceanu, et al., *Tumour-associated fibroblasts and mesenchymal stem cells: more similarities than differences.* J Cell Mol Med, 2011. **15**(3): p. 635-46.
32. Kim, J.H., S.H. Oh, E.J. Kim, S.J. Park, S.P. Hong, J.H. Cheon, T.I. Kim, and W.H. Kim, *The role of myofibroblasts in upregulation of S100A8 and S100A9 and the differentiation of myeloid cells in the colorectal cancer microenvironment.* Biochem Biophys Res Commun, 2012. **423**(1): p. 60-6.
33. Augsten, M., E. Sjoberg, O. Frings, S.U. Vorrink, J. Frijhoff, E. Olsson, A. Borg, and A. Ostman, *Cancer-associated fibroblasts expressing CXCL14 rely upon NOS1-derived nitric oxide signaling for their tumor-supporting properties.* Cancer Res, 2014. **74**(11): p. 2999-3010.
34. Van Linthout, S., K. Miteva, and C. Tschope, *Crosstalk between fibroblasts and inflammatory cells.* Cardiovasc Res, 2014. **102**(2): p. 258-69.
35. Mishra, P., D. Banerjee, and A. Ben-Baruch, *Chemokines at the crossroads of tumor-fibroblast interactions that promote malignancy.* J Leukoc Biol, 2011. **89**(1): p. 31-9.
36. Barnas, J.L., M.R. Simpson-Abelson, S.J. Yokota, R.J. Kelleher, and R.B. Bankert, *T cells and stromal fibroblasts in human tumor microenvironments represent potential therapeutic targets.* Cancer Microenviron, 2010. **3**(1): p. 29-47.
37. Pinchuk, I.V., J.I. Saada, E.J. Beswick, G. Boya, S.M. Qiu, R.C. Mifflin, G.S. Raju, V.E. Reyes, and D.W. Powell, *PD-1 ligand expression by human colonic myofibroblasts/fibroblasts regulates CD4+ T-cell activity.* Gastroenterology, 2008. **135**(4): p. 1228-1237, 1237 e1-2.
38. Nazareth, M.R., L. Broderick, M.R. Simpson-Abelson, R.J. Kelleher, Jr., S.J. Yokota, and R.B. Bankert, *Characterization of human lung tumor-associated fibroblasts and their ability to modulate the activation of tumor-associated T cells.* J Immunol, 2007. **178**(9): p. 5552-62.
39. Lakins, M.A., E. Ghorani, H. Munir, C.P. Martins, and J.D. Shields, *Cancer-associated fibroblasts induce antigen-specific deletion of CD8 (+) T Cells to protect tumour cells.* Nat Commun, 2018. **9**(1): p. 948.
40. Fidler, I.J., C. Wilmanns, A. Staroselsky, R. Radinsky, Z. Dong, and D. Fan, *Modulation of tumor cell response to chemotherapy by the organ environment.* Cancer Metastasis Rev, 1994. **13**(2): p. 209-22.
41. Farmer, P., H. Bonnefoi, P. Anderle, D. Cameron, P. Wirapati, V. Becette, S. Andre, M. Piccart, M. Campone, E. Brain, et al., *A stroma-related gene signature predicts resistance to neoadjuvant chemotherapy in breast cancer.* Nat Med, 2009. **15**(1): p. 68-74.
42. Paraiso, K.H. and K.S. Smalley, *Fibroblast-mediated drug resistance in cancer.* Biochem Pharmacol, 2013. **85**(8): p. 1033-41.

43. Meads, M.B., R.A. Gatenby, and W.S. Dalton, *Environment-mediated drug resistance: a major contributor to minimal residual disease.* Nat Rev Cancer, 2009. **9**(9): p. 665-74.
44. Heldin, C.H., K. Rubin, K. Pietras, and A. Ostman, *High interstitial fluid pressure - an obstacle in cancer therapy.* Nat Rev Cancer, 2004. **4**(10): p. 806-13.
45. Correia, A.L. and M.J. Bissell, *The tumor microenvironment is a dominant force in multidrug resistance.* Drug Resist Updat, 2012. **15**(1-2): p. 39-49.
46. Dittmer, J. and B. Leyh, *The impact of tumor stroma on drug response in breast cancer.* Semin Cancer Biol, 2015. **31**: p. 3-15.
47. Kumari, N., B.S. Dwarakanath, A. Das, and A.N. Bhatt, *Role of interleukin-6 in cancer progression and therapeutic resistance.* Tumour Biol, 2016. **37**(9): p. 11553-11572.
48. Wilson, T.R., J. Fridlyand, Y. Yan, E. Penuel, L. Burton, E. Chan, J. Peng, E. Lin, Y. Wang, J. Sosman, et al., *Widespread potential for growth-factor-driven resistance to anticancer kinase inhibitors.* Nature, 2012. **487**(7408): p. 505-9.
49. Wang, W., Q. Li, T. Yamada, K. Matsumoto, I. Matsumoto, M. Oda, G. Watanabe, Y. Kayano, Y. Nishioka, S. Sone, et al., *Crosstalk to stromal fibroblasts induces resistance of lung cancer to epidermal growth factor receptor tyrosine kinase inhibitors.* Clin Cancer Res, 2009. **15**(21): p. 6630-8.
50. Caplan, A.I. and D. Correa, *The MSC: an injury drugstore.* Cell Stem Cell, 2011. **9**(1): p. 11-5.
51. Uccelli, A., L. Moretta, and V. Pistoia, *Mesenchymal stem cells in health and disease.* Nat Rev Immunol, 2008. **8**(9): p. 726-36.
52. Wang, Y., X. Chen, W. Cao, and Y. Shi, *Plasticity of mesenchymal stem cells in immunomodulation: pathological and therapeutic implications.* Nat Immunol, 2014. **15**(11): p. 1009-16.
53. Shi, Y., J. Su, A.I. Roberts, P. Shou, A.B. Rabson, and G. Ren, *How mesenchymal stem cells interact with tissue immune responses.* Trends Immunol, 2012. **33**(3): p. 136-43.
54. Shi, Y., L. Du, L. Lin, and Y. Wang, *Tumour-associated mesenchymal stem/stromal cells: emerging therapeutic targets.* Nat Rev Drug Discov, 2017. **16**(1): p. 35-52.
55. Ren, G., X. Zhao, Y. Wang, X. Zhang, X. Chen, C. Xu, Z.R. Yuan, A.I. Roberts, L. Zhang, B. Zheng, et al., *CCR2-dependent recruitment of macrophages by tumor-educated mesenchymal stromal cells promotes tumor development and is mimicked by TNFalpha.* Cell Stem Cell, 2012. **11**(6): p. 812-24.
56. Quante, M., S.P. Tu, H. Tomita, T. Gonda, S.S. Wang, S. Takashi, G.H. Baik, W. Shibata, B. Diprete, K.S. Betz, et al., *Bone marrow-derived myofibroblasts contribute to the mesenchymal stem cell niche and promote tumor growth.* Cancer Cell, 2011. **19**(2): p. 257-72.
57. Hu, Y.L., Y.H. Fu, Y. Tabata, and J.Q. Gao, *Mesenchymal stem cells: a promising targeted-delivery vehicle in cancer gene therapy.* J Control Release, 2010. **147**(2): p. 154-62.
58. Shah, K., *Mesenchymal stem cells engineered for cancer therapy.* Adv Drug Deliv Rev, 2012. **64**(8): p. 739-48.
59. De Boeck, A., P. Pauwels, K. Hensen, J.L. Rummens, W. Westbroek, A. Hendrix, D.

Maynard, H. Denys, K. Lambein, G. Braems, et al., *Bone marrow-derived mesenchymal stem cells promote colorectal cancer progression through paracrine neuregulin 1/HER3 signalling.* Gut, 2013. **62**(4): p. 550-60.
60. Beckermann, B.M., G. Kallifatidis, A. Groth, D. Frommhold, A. Apel, J. Mattern, A.V. Salnikov, G. Moldenhauer, W. Wagner, A. Diehlmann, et al., *VEGF expression by mesenchymal stem cells contributes to angiogenesis in pancreatic carcinoma.* Br J Cancer, 2008. **99**(4): p. 622-31.
61. Mandel, K., Y. Yang, A. Schambach, S. Glage, A. Otte, and R. Hass, *Mesenchymal stem cells directly interact with breast cancer cells and promote tumor cell growth in vitro and in vivo.* Stem Cells Dev, 2013. **22**(23): p. 3114-27.
62. Roccaro, A.M., A. Sacco, P. Maiso, A.K. Azab, Y.T. Tai, M. Reagan, F. Azab, L.M. Flores, F. Campigotto, E. Weller, et al., *BM mesenchymal stromal cell-derived exosomes facilitate multiple myeloma progression.* J Clin Invest, 2013. **123**(4): p. 1542-55.
63. McLean, K., Y. Gong, Y. Choi, N. Deng, K. Yang, S. Bai, L. Cabrera, E. Keller, L. McCauley, K.R. Cho, et al., *Human ovarian carcinoma-associated mesenchymal stem cells regulate cancer stem cells and tumorigenesis via altered BMP production.* J Clin Invest, 2011. **121**(8): p. 3206-19.
64. Bissell, M.J. and M.A. Labarge, *Context, tissue plasticity, and cancer: are tumor stem cells also regulated by the microenvironment?* Cancer Cell, 2005. **7**(1): p. 17-23.
65. Huijbers, A., R.A. Tollenaar, G.W. v Pelt, E.C. Zeestraten, S. Dutton, C.C. McConkey, E. Domingo, V.T. Smit, R. Midgley, B.F. Warren, et al., *The proportion of tumor-stroma as a strong prognosticator for stage II and III colon cancer patients: validation in the VICTOR trial.* Ann Oncol, 2013. **24**(1): p. 179-85.
66. McMillin, D.W., J.M. Negri, and C.S. Mitsiades, *The role of tumour-stromal interactions in modifying drug response: challenges and opportunities.* Nat Rev Drug Discov, 2013. **12**(3): p. 217-28.
67. Cukierman, E. and D.E. Bassi, *The mesenchymal tumor microenvironment: a drug-resistant niche.* Cell Adh Migr, 2012. **6**(3): p. 285-96.
68. Binnewies, M., E.W. Roberts, K. Kersten, V. Chan, D.F. Fearon, M. Merad, L.M. Coussens, D.I. Gabrilovich, S. Ostrand-Rosenberg, C.C. Hedrick, et al., *Understanding the tumor immune microenvironment (TIME) for effective therapy.* Nat Med, 2018. **24**(5): p. 541-550.
69. Lindau, D., P. Gielen, M. Kroesen, P. Wesseling, and G.J. Adema, *The immunosuppressive tumour network: myeloid-derived suppressor cells, regulatory T cells and natural killer T cells.* Immunology, 2013. **138**(2): p. 105-15.
70. Motz, G.T. and G. Coukos, *Deciphering and reversing tumor immune suppression.* Immunity, 2013. **39**(1): p. 61-73.
71. Whiteside, T.L., P. Schuler, and B. Schilling, *Induced and natural regulatory T cells in human cancer.* Expert Opin Biol Ther, 2012. **12**(10): p. 1383-97.
72. Gasteiger, G., S. Hemmers, P.D. Bos, J.C. Sun, and A.Y. Rudensky, *IL-2-dependent adaptive control of NK cell homeostasis.* J Exp Med, 2013. **210**(6): p. 1179-87.
73. Wagner, J., M.A. Rapsomaniki, S. Chevrier, T. Anzeneder, C. Langwieder, A. Dykgers, M. Rees, A. Ramaswamy, S. Muenst, S.D. Soysal, et al., *A Single-Cell Atlas of the Tumor and Immune Ecosystem of Human Breast Cancer.* Cell, 2019. **177**(5): p.

1330-1345 e18.
74. Bates, G.J., S.B. Fox, C. Han, R.D. Leek, J.F. Garcia, A.L. Harris, and A.H. Banham, *Quantification of regulatory T cells enables the identification of high-risk breast cancer patients and those at risk of late relapse.* J Clin Oncol, 2006. **24**(34): p. 5373-80.
75. Frey, D.M., R.A. Droeser, C.T. Viehl, I. Zlobec, A. Lugli, U. Zingg, D. Oertli, C. Kettelhack, L. Terracciano, and L. Tornillo, *High frequency of tumor-infiltrating FOXP3(+) regulatory T cells predicts improved survival in mismatch repair-proficient colorectal cancer patients.* Int J Cancer, 2010. **126**(11): p. 2635-43.
76. von Boehmer, H. and C. Daniel, *Therapeutic opportunities for manipulating T(Reg) cells in autoimmunity and cancer.* Nat Rev Drug Discov, 2013. **12**(1): p. 51-63.
77. Blatner, N.R., M.F. Mulcahy, K.L. Dennis, D. Scholtens, D.J. Bentrem, J.D. Phillips, S. Ham, B.P. Sandall, M.W. Khan, D.M. Mahvi, et al., *Expression of RORgammat marks a pathogenic regulatory T cell subset in human colon cancer.* Sci Transl Med, 2012. **4**(164): p. 164ra159.
78. Goebel, L., E. Grage-Griebenow, A. Gorys, O. Helm, G. Genrich, L. Lenk, D. Wesch, H. Ungefroren, S. Freitag-Wolf, B. Sipos, et al., *CD4(+) T cells potently induce epithelial-mesenchymal-transition in premalignant and malignant pancreatic ductal epithelial cells-novel implications of CD4(+) T cells in pancreatic cancer development.* Oncoimmunology, 2015. **4**(4): p. e1000083.
79. Santisteban, M., J.M. Reiman, M.K. Asiedu, M.D. Behrens, A. Nassar, K.R. Kalli, P. Haluska, J.N. Ingle, L.C. Hartmann, M.H. Manjili, et al., *Immune-induced epithelial to mesenchymal transition in vivo generates breast cancer stem cells.* Cancer Res, 2009. **69**(7): p. 2887-95.
80. Kmieciak, M., K.L. Knutson, C.I. Dumur, and M.H. Manjili, *HER-2/neu antigen loss and relapse of mammary carcinoma are actively induced by T cell-mediated anti-tumor immune responses.* Eur J Immunol, 2007. **37**(3): p. 675-85.
81. Schaaf, M.B., A.D. Garg, and P. Agostinis, *Defining the role of the tumor vasculature in antitumor immunity and immunotherapy.* Cell Death Dis, 2018. **9**(2): p. 115.
82. Folkman, J., *Tumor angiogenesis: therapeutic implications.* N Engl J Med, 1971. **285**(21): p. 1182-6.
83. Liu, Z., Y. Wang, Y. Huang, B.Y.S. Kim, H. Shan, D. Wu, and W. Jiang, *Tumor Vasculatures: A New Target for Cancer Immunotherapy.* Trends Pharmacol Sci, 2019. **40**(9): p. 613-623.
84. Du, R., K.V. Lu, C. Petritsch, P. Liu, R. Ganss, E. Passegue, H. Song, S. Vandenberg, R.S. Johnson, Z. Werb, et al., *HIF1alpha induces the recruitment of bone marrow-derived vascular modulatory cells to regulate tumor angiogenesis and invasion.* Cancer Cell, 2008. **13**(3): p. 206-20.
85. Semenza, G.L., *Cancer-stromal cell interactions mediated by hypoxia-inducible factors promote angiogenesis, lymphangiogenesis, and metastasis.* Oncogene, 2013. **32**(35): p. 4057-63.
86. Schoppmann, S.F., P. Birner, J. Stockl, R. Kalt, R. Ullrich, C. Caucig, E. Kriehuber, K. Nagy, K. Alitalo, and D. Kerjaschki, *Tumor-associated macrophages express lymphatic endothelial growth factors and are related to peritumoral lymphangiogenesis.* Am J Pathol, 2002. **161**(3): p. 947-56.

87. Alitalo, A. and M. Detmar, *Interaction of tumor cells and lymphatic vessels in cancer progression.* Oncogene, 2012. **31**(42): p. 4499-508.
88. Hunter, K.E., C. Palermo, J.C. Kester, K. Simpson, J.P. Li, L.H. Tang, D.S. Klimstra, I. Vlodavsky, and J.A. Joyce, *Heparanase promotes lymphangiogenesis and tumor invasion in pancreatic neuroendocrine tumors.* Oncogene, 2014. **33**(14): p. 1799-808.
89. Eble, J.A. and S. Niland, *The extracellular matrix in tumor progression and metastasis.* Clin Exp Metastasis, 2019. **36**(3): p. 171-198.
90. Bergamaschi, A., E. Tagliabue, T. Sorlie, B. Naume, T. Triulzi, R. Orlandi, H.G. Russnes, J.M. Nesland, R. Tammi, P. Auvinen, et al., *Extracellular matrix signature identifies breast cancer subgroups with different clinical outcome.* J Pathol, 2008. **214**(3): p. 357-67.
91. Rice, A.J., E. Cortes, D. Lachowski, B.C.H. Cheung, S.A. Karim, J.P. Morton, and A. Del Rio Hernandez, *Matrix stiffness induces epithelial-mesenchymal transition and promotes chemoresistance in pancreatic cancer cells.* Oncogenesis, 2017. **6**(7): p. e352.
92. Broders-Bondon, F., T.H. Nguyen Ho-Bouldoires, M.E. Fernandez-Sanchez, and E. Farge, *Mechanotransduction in tumor progression: The dark side of the force.* J Cell Biol, 2018. **217**(5): p. 1571-1587.
93. Singh, A., I. Brito, and J. Lammerding, *Beyond Tissue Stiffness and Bioadhesivity: Advanced Biomaterials to Model Tumor Microenvironments and Drug Resistance.* Trends Cancer, 2018. **4**(4): p. 281-291.
94. Northey, J.J., L. Przybyla, and V.M. Weaver, *Tissue Force Programs Cell Fate and Tumor Aggression.* Cancer Discov, 2017. **7**(11): p. 1224-1237.
95. Azadi, S., H. Aboulkheyr Es, S. Razavi Bazaz, J.P. Thiery, M. Asadnia, and M. Ebrahimi Warkiani, *Upregulation of PD-L1 expression in breast cancer cells through the formation of 3D multicellular cancer aggregates under different chemical and mechanical conditions.* Biochim Biophys Acta Mol Cell Res, 2019. **1866**(12): p. 118526.
96. Stylianopoulos, T., L.L. Munn, and R.K. Jain, *Reengineering the Physical Microenvironment of Tumors to Improve Drug Delivery and Efficacy: From Mathematical Modeling to Bench to Bedside.* Trends Cancer, 2018. **4**(4): p. 292-319.
97. Choi, I.K., R. Strauss, M. Richter, C.O. Yun, and A. Lieber, *Strategies to increase drug penetration in solid tumors.* Front Oncol, 2013. **3**: p. 193.
98. Najafi, M., B. Farhood, and K. Mortezaee, *Extracellular matrix (ECM) stiffness and degradation as cancer drivers.* J Cell Biochem, 2019. **120**(3): p. 2782-2790.
99. Friedman, A.A., A. Letai, D.E. Fisher, and K.T. Flaherty, *Precision medicine for cancer with next-generation functional diagnostics.* Nat Rev Cancer, 2015. **15**(12): p. 747-56.
100. Voest, E.E. and R. Bernards, *DNA-Guided Precision Medicine for Cancer: A Case of Irrational Exuberance?* Cancer Discov, 2016. **6**(2): p. 130-2.
101. Goodspeed, A., L.M. Heiser, J.W. Gray, and J.C. Costello, *Tumor-Derived Cell Lines as Molecular Models of Cancer Pharmacogenomics.* Mol Cancer Res, 2016. **14**(1): p. 3-13.
102. Wilding, J.L. and W.F. Bodmer, *Cancer cell lines for drug discovery and development.* Cancer Res, 2014. **74**(9): p. 2377-84.

103. Weiswald, L.B., D. Bellet, and V. Dangles-Marie, *Spherical cancer models in tumor biology.* Neoplasia, 2015. **17**(1): p. 1-15.
104. Bartlett, R., W. Everett, S. Lim, N. G, M. Loizidou, G. Jell, A. Tan, and A.M. Seifalian, *Personalized in vitro cancer modeling - fantasy or reality?* Transl Oncol, 2014. **7**(6): p. 657-64.
105. Stein, W.D., T. Litman, T. Fojo, and S.E. Bates, *A Serial Analysis of Gene Expression (SAGE) database analysis of chemosensitivity: comparing solid tumors with cell lines and comparing solid tumors from different tissue origins.* Cancer Res, 2004. **64**(8): p. 2805-16.
106. Weeber, F., M. van de Wetering, M. Hoogstraat, K.K. Dijkstra, O. Krijgsman, T. Kuilman, C.G. Gadellaa-van Hooijdonk, D.L. van der Velden, D.S. Peeper, E.P. Cuppen, et al., *Preserved genetic diversity in organoids cultured from biopsies of human colorectal cancer metastases.* Proc Natl Acad Sci U S A, 2015. **112**(43): p. 13308-11.
107. Gao, D., I. Vela, A. Sboner, P.J. Iaquinta, W.R. Karthaus, A. Gopalan, C. Dowling, J.N. Wanjala, E.A. Undvall, V.K. Arora, et al., *Organoid cultures derived from patients with advanced prostate cancer.* Cell, 2014. **159**(1): p. 176-187.
108. Lancaster, M.A. and J.A. Knoblich, *Organogenesis in a dish: modeling development and disease using organoid technologies.* Science, 2014. **345**(6194): p. 1247125.
109. Pauli, C., B.D. Hopkins, D. Prandi, R. Shaw, T. Fedrizzi, A. Sboner, V. Sailer, M. Augello, L. Puca, R. Rosati, et al., *Personalized In Vitro and In Vivo Cancer Models to Guide Precision Medicine.* Cancer Discov, 2017. **7**(5): p. 462-477.
110. van de Wetering, M., H.E. Francies, J.M. Francis, G. Bounova, F. Iorio, A. Pronk, W. van Houdt, J. van Gorp, A. Taylor-Weiner, L. Kester, et al., *Prospective derivation of a living organoid biobank of colorectal cancer patients.* Cell, 2015. **161**(4): p. 933-45.
111. Verissimo, C.S., R.M. Overmeer, B. Ponsioen, J. Drost, S. Mertens, I. Verlaan-Klink, B.V. Gerwen, M. van der Ven, M.V. Wetering, D.A. Egan, et al., *Targeting mutant RAS in patient-derived colorectal cancer organoids by combinatorial drug screening.* Elife, 2016. **5**.
112. Weeber, F., S.N. Ooft, K.K. Dijkstra, and E.E. Voest, *Tumor Organoids as a Pre-clinical Cancer Model for Drug Discovery.* Cell Chem Biol, 2017. **24**(9): p. 1092-1100.
113. Huch, M. and B.K. Koo, *Modeling mouse and human development using organoid cultures.* Development, 2015. **142**(18): p. 3113-25.
114. Sachs, N. and H. Clevers, *Organoid cultures for the analysis of cancer phenotypes.* Curr Opin Genet Dev, 2014. **24**: p. 68-73.
115. Yachida, S., S. Jones, I. Bozic, T. Antal, R. Leary, B. Fu, M. Kamiyama, R.H. Hruban, J.R. Eshleman, M.A. Nowak, et al., *Distant metastasis occurs late during the genetic evolution of pancreatic cancer.* Nature, 2010. **467**(7319): p. 1114-7.
116. Baker, L.A., H. Tiriac, H. Clevers, and D.A. Tuveson, *Modeling pancreatic cancer with organoids.* Trends Cancer, 2016. **2**(4): p. 176-190.
117. Drost, J., R. van Boxtel, F. Blokzijl, T. Mizutani, N. Sasaki, V. Sasselli, J. de Ligt, S. Behjati, J.E. Grolleman, T. van Wezel, et al., *Use of CRISPR-modified human stem cell organoids to study the origin of mutational signatures in cancer.* Science, 2017.

358(6360): p. 234-238.
118. Ooft, S.N., F. Weeber, K.K. Dijkstra, C.M. McLean, S. Kaing, E. van Werkhoven, L. Schipper, L. Hoes, D.J. Vis, J. van de Haar, et al., *Patient-derived organoids can predict response to chemotherapy in metastatic colorectal cancer patients.* Sci Transl Med, 2019. **11**(513).
119. Bhatia, S.N. and D.E. Ingber, *Microfluidic organs-on-chips.* Nat Biotechnol, 2014. **32**(8): p. 760-72.
120. Sontheimer-Phelps, A., B.A. Hassell, and D.E. Ingber, *Modelling cancer in microfluidic human organs-on-chips.* Nat Rev Cancer, 2019. **19**(2): p. 65-81.
121. Boussommier-Calleja, A., R. Li, M.B. Chen, S.C. Wong, and R.D. Kamm, *Microfluidics: A new tool for modeling cancer-immune interactions.* Trends in cancer, 2016. **2**(1): p. 6-19.
122. Morgan, J.P., P.F. Delnero, Y. Zheng, S.S. Verbridge, J. Chen, M. Craven, N.W. Choi, A. Diaz-Santana, P. Kermani, B. Hempstead, et al., *Formation of microvascular networks in vitro.* Nat Protoc, 2013. **8**(9): p. 1820-36.
123. Osaki, T., V. Sivathanu, and R.D. Kamm, *Engineered 3D vascular and neuronal networks in a microfluidic platform.* Sci Rep, 2018. **8**(1): p. 5168.
124. Nashimoto, Y., Y. Teraoka, R. Banan Sadeghian, A. Nakamasu, Y. Arima, S. Hanada, H. Kotera, K. Nishiyama, T. Miura, and R. Yokokawa, *Perfusable Vascular Network with a Tissue Model in a Microfluidic Device.* J Vis Exp, 2018(134).
125. Chen, M.B., J.A. Whisler, J. Frose, C. Yu, Y. Shin, and R.D. Kamm, *On-chip human microvasculature assay for visualization and quantification of tumor cell extravasation dynamics.* Nat Protoc, 2017. **12**(5): p. 865-880.
126. Sahai, E., *Illuminating the metastatic process.* Nat Rev Cancer, 2007. **7**(10): p. 737.
127. Chaffer, C.L. and R.A. Weinberg, *A perspective on cancer cell metastasis.* Science, 2011. **331**(6024): p. 1559-1564.
128. Sleeboom, J.J., H.E. Amirabadi, P. Nair, C.M. Sahlgren, J.M.J.D.m. Den Toonder, and mechanisms, *Metastasis in context: modeling the tumor microenvironment with cancer-on-a-chip approaches.* 2018. **11**(3): p. dmm033100.
129. Kulasinghe, A., C. Perry, L. Jovanovic, C. Nelson, and C. Punyadeera, *Circulating tumour cells in metastatic head and neck cancers.* Int J Cancer, 2015. **136**(11): p. 2515-23.
130. Bersini, S., A. Miermont, A. Pavesi, R.D. Kamm, J.P. Thiery, M. Moretti, and G.J.O. Adriani, *A combined microfluidic-transcriptomic approach to characterize the extravasation potential of cancer cells.* 2018. **9**(90): p. 36110.
131. Fischer, K.R., A. Durrans, S. Lee, J. Sheng, F. Li, S.T. Wong, H. Choi, T. El Rayes, S. Ryu, and J. Troeger, *Epithelial-to-mesenchymal transition is not required for lung metastasis but contributes to chemoresistance.* Nature, 2015. **527**(7579): p. 472.
132. Shemanko, C., Y. Cong, and A. Forsyth, *What is breast in the bone?* Int J Mol Sci, 2016. **17**(10): p. 1764.
133. Li, L., Y. He, M. Zhao, and J. Jiang, *Collective cell migration: Implications for wound healing and cancer invasion.* Burns Trauma, 2013. **1**(1): p. 21.
134. Friedl, P. and D. Gilmour, *Collective cell migration in morphogenesis, regeneration and cancer.* Nat Rev Mol Cell Biol, 2009. **10**(7): p. 445.
135. Schäfer, M. and S. Werner, *Cancer as an overhealing wound: an old hypothesis*

revisited. Nat Rev Mol Cell Biol, 2008. **9**(8): p. 628.
136. Kramer, N., A. Walzl, C. Unger, M. Rosner, G. Krupitza, M. Hengstschläger, and H.J. Dolznig, *In vitro cell migration and invasion assays.* Mutat Res, 2013. **752**(1): p. 10-24.
137. Kim, Y., K.C. Williams, C.T. Gavin, E. Jardine, A.F. Chambers, and H.S. Leong, *Quantification of cancer cell extravasation in vivo.* Nat Protoc, 2016. **11**(5): p. 937.
138. Reymond, N., B.B. d'Agua, and A.J. Ridley, *Crossing the endothelial barrier during metastasis.* Nat Rev Cancer, 2013. **13**(12): p. 858.
139. Xu, H., X. Liu, and W. Le, *Recent advances in microfluidic models for cancer metastasis research.* Trends in Analytical Chemistry, 2018. **105**: p. 1-6.
140. Sontheimer-Phelps, A., B.A. Hassell, and D.E. Ingber, *Modelling cancer in microfluidic human organs-on-chips.* Nat Rev Cancer, 2019. **19**(2): p. 1.
141. Sleeboom, J.J., H.E. Amirabadi, P. Nair, C.M. Sahlgren, and J.M. Den Toonder, *Metastasis in context: modeling the tumor microenvironment with cancer-on-a-chip approaches.* Dis Model Mech, 2018. **11**(3): p. dmm033100.
142. Huang, Y.L., J.E. Segall, and M. Wu, *Microfluidic modeling of the biophysical microenvironment in tumor cell invasion.* Lab Chip, 2017. **17**(19): p. 3221-3233.
143. Bersini, S., J.S. Jeon, M. Moretti, and R. Kamm, *In vitro models of the metastatic cascade: from local invasion to extravasation.* Drug Discov Today, 2014. **19**(6): p. 735-742.
144. Ma, Y.-H.V., K. Middleton, L. You, and Y. Sun, *A review of microfluidic approaches for investigating cancer extravasation during metastasis.* Microsystems & Nanoengineering, 2018. **4**: p. 17104.
145. Ma, Y., J.-Z. Pan, S.-P. Zhao, Q. Lou, Y. Zhu, and Q. Fang, *Microdroplet chain array for cell migration assays.* Lab Chip, 2016. **16**(24): p. 4658-4665.
146. Shin, M.K., S.K. Kim, and H. Jung, *Integration of intra-and extravasation in one cell-based microfluidic chip for the study of cancer metastasis.* Lab Chip, 2011. **11**(22): p. 3880-3887.
147. Wang, L., W. Liu, Y. Wang, J.-c. Wang, Q. Tu, R. Liu, and J. Wang, *Construction of oxygen and chemical concentration gradients in a single microfluidic device for studying tumor cell–drug interactions in a dynamic hypoxia microenvironment.* Lab Chip, 2013. **13**(4): p. 695-705.
148. Wang, Z., Z. Liu, L. Li, and Q. Liang, *Investigation into the hypoxia-dependent cytotoxicity of anticancer drugs under oxygen gradient in a microfluidic device.* Microfluidics and Nanofluidics, 2015. **19**(6): p. 1271-1279.
149. Mak, M., C.A. Reinhart-King, and D. Erickson, *Elucidating mechanical transition effects of invading cancer cells with a subnucleus-scaled microfluidic serial dimensional modulation device.* Lab Chip, 2013. **13**(3): p. 340-348.
150. Chaw, K., M. Manimaran, E. Tay, and S. Swaminathan, *Multi-step microfluidic device for studying cancer metastasis.* Lab Chip, 2007. **7**(8): p. 1041-1047.
151. Chen, Y.-A., A.D. King, H.-C. Shih, C.-C. Peng, C.-Y. Wu, W.-H. Liao, and Y.-C. Tung, *Generation of oxygen gradients in microfluidic devices for cell culture using spatially confined chemical reactions.* Lab Chip, 2011. **11**(21): p. 3626-3633.
152. Piotrowski-Daspit, A.S., J. Tien, and C.M. Nelson, *Interstitial fluid pressure regulates collective invasion in engineered human breast tumors via Snail, vimentin, and E-*

cadherin. Integr Biol (Camb), 2016. **8**(3): p. 319-331.
153. Ayuso, J.M., A. Gillette, K. Lugo-Cintrón, S. Acevedo-Acevedo, I. Gomez, M. Morgan, T. Heaster, K.B. Wisinski, S.P. Palecek, and M. Skala, *Organotypic microfluidic breast cancer model reveals starvation-induced spatial-temporal metabolic adaptations.* EBioMedicine, 2018. **37**: p. 144-157.
154. Tien, J., J.G. Truslow, and C.M. Nelson, *Modulation of invasive phenotype by interstitial pressure-driven convection in aggregates of human breast cancer cells.* PLoS One, 2012. **7**(9): p. e45191.
155. Jeon, J.S., I.K. Zervantonakis, S. Chung, R.D. Kamm, and J.L. Charest, *In vitro model of tumor cell extravasation.* PLoS One, 2013. **8**(2): p. e56910.
156. Bersini, S., J.S. Jeon, G. Dubini, C. Arrigoni, S. Chung, J.L. Charest, M. Moretti, and R.D.J.B. Kamm, *A microfluidic 3D in vitro model for specificity of breast cancer metastasis to bone.* 2014. **35**(8): p. 2454-2461.
157. Zervantonakis, I.K., S.K. Hughes-Alford, J.L. Charest, J.S. Condeelis, F.B. Gertler, and R.D.J.P.o.t.N.A.o.S. Kamm, *Three-dimensional microfluidic model for tumor cell intravasation and endothelial barrier function.* 2012. **109**(34): p. 13515-13520.
158. Boussommier-Calleja, A., Y. Atiyas, K. Haase, M. Headley, C. Lewis, and R. Kamm, *The effects of monocytes on tumor cell extravasation in a 3D vascularized microfluidic model.* Biomaterials, 2019. **198**: p. 180-193.
159. Chen, M.B., J.A. Whisler, J.S. Jeon, and R.D. Kamm, *Mechanisms of tumor cell extravasation in an in vitro microvascular network platform.* Integr Biol (Camb), 2013. **5**(10): p. 1262-1271.
160. Kim, S., M. Chung, J. Ahn, S. Lee, and N.L. Jeon, *Interstitial flow regulates the angiogenic response and phenotype of endothelial cells in a 3D culture model.* Lab Chip, 2016. **16**(21): p. 4189-4199.
161. Walsh, C.L., B.M. Babin, R.W. Kasinskas, J.A. Foster, M.J. McGarry, and N.S. Forbes, *A multipurpose microfluidic device designed to mimic microenvironment gradients and develop targeted cancer therapeutics.* Lab Chip, 2009. **9**(4): p. 545-554.
162. Sung, K.E., N. Yang, C. Pehlke, P.J. Keely, K.W. Eliceiri, A. Friedl, and D.J. Beebe, *Transition to invasion in breast cancer: a microfluidic in vitro model enables examination of spatial and temporal effects.* Integr Biol (Camb), 2010. **3**(4): p. 439-450.
163. Hassell, B.A., G. Goyal, E. Lee, A. Sontheimer-Phelps, O. Levy, C.S. Chen, and D.E. Ingber, *Human organ chip models recapitulate orthotopic lung cancer growth, therapeutic responses, and tumor dormancy in vitro.* Cell Rep, 2017. **21**(2): p. 508-516.
164. Choi, Y., E. Hyun, J. Seo, C. Blundell, H.C. Kim, E. Lee, S.H. Lee, A. Moon, W.K. Moon, and D. Huh, *A microengineered pathophysiological model of early-stage breast cancer.* Lab Chip, 2015. **15**(16): p. 3350-3357.
165. Musah, S., A. Mammoto, T.C. Ferrante, S.S. Jeanty, M. Hirano-Kobayashi, T. Mammoto, K. Roberts, S. Chung, R. Novak, and M. Ingram, *Mature induced-pluripotent-stem-cell-derived human podocytes reconstitute kidney glomerular-capillary-wall function on a chip.* Nat Biomed Eng, 2017. **1**(5): p. 0069.
166. Pisano, M., V. Triacca, K. Barbee, and M. Swartz, *An in vitro model of the tumor–*

lymphatic microenvironment with simultaneous transendothelial and luminal flows reveals mechanisms of flow enhanced invasion. Integrative biology, 2015. **7**(5): p. 525-533.
167. Lang, J.D., S.M. Berry, G.L. Powers, D.J. Beebe, and E.T. Alarid, *Hormonally responsive breast cancer cells in a microfluidic co-culture model as a sensor of microenvironmental activity.* Integrative Biology, 2013. **5**(5): p. 807-816.
168. Regier, M.C., L.J. Maccoux, E.M. Weinberger, K.J. Regehr, S.M. Berry, D.J. Beebe, and E.T. Alarid, *Transitions from mono-to co-to tri-culture uniquely affect gene expression in breast cancer, stromal, and immune compartments.* Biomed Microdevices, 2016. **18**(4): p. 70.
169. Montanez-Sauri, S.I., K.E. Sung, E. Berthier, and D.J. Beebe, *Enabling screening in 3D microenvironments: probing matrix and stromal effects on the morphology and proliferation of T47D breast carcinoma cells.* Integr Biol (Camb), 2013. **5**(3): p. 631-640.
170. Hendrix, M.J., E.A. Seftor, A.R. Hess, and R.E. Seftor, *Angiogenesis: Vasculogenic mimicry and tumour-cell plasticity: lessons from melanoma.* Nat Rev Cancer, 2003. **3**(6): p. 411.
171. Zervantonakis, I.K., S.K. Hughes-Alford, J.L. Charest, J.S. Condeelis, F.B. Gertler, and R.D. Kamm, *Three-dimensional microfluidic model for tumor cell intravasation and endothelial barrier function.* Proc Natl Acad Sci U S A, 2012. **109**(34): p. 13515-13520.
172. Wang, X., Q. Sun, and J. Pei, *Microfluidic-based 3D engineered microvascular networks and their applications in vascularized microtumor models.* Micromachines, 2018. **9**(10): p. 493.
173. Kim, S., H. Lee, M. Chung, and N.L. Jeon, *Engineering of functional, perfusable 3D microvascular networks on a chip.* Lab Chip, 2013. **13**(8): p. 1489-1500.
174. Chen, L.-J. and H. Kaji, *Modeling angiogenesis with micro-and nanotechnology.* Lab Chip, 2017. **17**(24): p. 4186-4219.
175. Jeon, J.S., S. Bersini, M. Gilardi, G. Dubini, J.L. Charest, M. Moretti, and R.D.J.P.o.t.N.A.o.S. Kamm, *Human 3D vascularized organotypic microfluidic assays to study breast cancer cell extravasation.* 2015. **112**(1): p. 214-219.
176. Bersini, S., J.S. Jeon, G. Dubini, C. Arrigoni, S. Chung, J.L. Charest, M. Moretti, and R.D. Kamm, *A microfluidic 3D in vitro model for specificity of breast cancer metastasis to bone.* Biomaterials, 2014. **35**(8): p. 2454-2461.
177. Blaha, L., C. Zhang, M. Cabodi, and J. Wong, *A microfluidic platform for modeling metastatic cancer cell matrix invasion.* Biofabrication, 2017. **9**(4): p. 045001.
178. Zhang, Q., T. Liu, and J. Qin, *A microfluidic-based device for study of transendothelial invasion of tumor aggregates in realtime.* Lab Chip, 2012. **12**(16): p. 2837-2842.
179. Riahi, R., Y. Yang, H. Kim, L. Jiang, P.K. Wong, and Y. Zohar, *A microfluidic model for organ-specific extravasation of circulating tumor cells.* Biomicrofluidics, 2014. **8**(2): p. 024103.
180. Bersini, S., A. Miermont, A. Pavesi, R.D. Kamm, J.P. Thiery, M. Moretti, and G. Adriani, *A combined microfluidic-transcriptomic approach to characterize the extravasation potential of cancer cells.* Oncotarget, 2018. **9**(90): p. 36110.

181. Chen, M.B., J.M. Lamar, R. Li, R.O. Hynes, and R.D. Kamm, *Elucidation of the roles of tumor integrin β1 in the extravasation stage of the metastasis cascade.* Cancer research, 2016. **76**(9): p. 2513-2524.
182. Jeon, J.S., S. Bersini, M. Gilardi, G. Dubini, J.L. Charest, M. Moretti, and R.D. Kamm, *Human 3D vascularized organotypic microfluidic assays to study breast cancer cell extravasation.* Proc Natl Acad Sci U S A, 2015. **112**(1): p. 214-219.
183. Song, C., D. Gao, T. Yuan, Y. Chen, L. Liu, X. Chen, and Y. Jiang, *Microfluidic three-dimensional biomimetic tumor model for studying breast cancer cell migration and invasion in the presence of interstitial flow.* Chinese Chemical Letters, 2019. **30**(5): p. 1038-1042.
184. Nagaraju, S., D. Truong, G. Mouneimne, and M. Nikkhah, *Microfluidic Tumor–Vascular Model to Study Breast Cancer Cell Invasion and Intravasation.* 2018. **7**(9): p. 1701257.
185. Zhang, Y., J. Wen, L. Zhou, and L. Qin, *Utilizing a high-throughput microfluidic platform to study hypoxia-driven mesenchymal-mode cell migration.* Integrative biology : quantitative biosciences from nano to macro, 2015. **7**(6): p. 672-680.
186. Acosta, M.A., X. Jiang, P.-K. Huang, K.B. Cutler, C.S. Grant, G.M. Walker, and M.P. Gamcsik, *A microfluidic device to study cancer metastasis under chronic and intermittent hypoxia.* Biomicrofluidics, 2014. **8**(5): p. 054117-054117.
187. Huang, Y.L., J.E. Segall, and M. Wu, *Microfluidic modeling of the biophysical microenvironment in tumor cell invasion.* Lab on a chip, 2017. **17**(19): p. 3221-3233.
188. Polacheck, W.J., J.L. Charest, and R.D. Kamm, *Interstitial flow influences direction of tumor cell migration through competing mechanisms.* Proceedings of the National Academy of Sciences of the United States of America, 2011. **108**(27): p. 11115-11120.
189. Triantafillu, U.L., S. Park, N.L. Klaassen, A.D. Raddatz, and Y. Kim, *Fluid shear stress induces cancer stem cell-like phenotype in MCF7 breast cancer cell line without inducing epithelial to mesenchymal transition.* Int J Oncol, 2017. **50**(3): p. 993-1001.
190. Polacheck, W.J., A.E. German, A. Mammoto, D.E. Ingber, and R.D. Kamm, *Mechanotransduction of fluid stresses governs 3D cell migration.* Proceedings of the National Academy of Sciences, 2014. **111**(7): p. 2447.
191. Tung, C.-k., O. Krupa, E. Apaydin, J.-J. Liou, A. Diaz-Santana, B.J. Kim, and M. Wu, *A contact line pinning based microfluidic platform for modelling physiological flows.* Lab on a chip, 2013. **13**(19): p. 3876-3885.
192. Anguiano, M., C. Castilla, M. Maška, C. Ederra, R. Peláez, X. Morales, G. Muñoz-Arrieta, M. Mujika, M. Kozubek, A. Muñoz-Barrutia, et al., *Characterization of three-dimensional cancer cell migration in mixed collagen-Matrigel scaffolds using microfluidics and image analysis.* PloS one, 2017. **12**(2): p. e0171417-e0171417.
193. Carvalho, M.R., F.R. Maia, S. Vieira, R.L. Reis, and J.M. Oliveira, *Tuning Enzymatically Crosslinked Silk Fibroin Hydrogel Properties for the Development of a Colorectal Cancer Extravasation 3D Model on a Chip.* Glob Chall, 2018. **2**(5-6): p. 1700100.
194. Chung, S., R. Sudo, V. Vickerman, I.K. Zervantonakis, and R.D. Kamm, *Microfluidic Platforms for Studies of Angiogenesis, Cell Migration, and Cell–Cell Interactions.*

Annals of Biomedical Engineering, 2010. **38**(3): p. 1164-1177.
195. Liu, T., B. Lin, and J. Qin, *Carcinoma-associated fibroblasts promoted tumor spheroid invasion on a microfluidic 3D co-culture device.* Lab on a Chip, 2010. **10**(13): p. 1671-1677.
196. Hsu, T.-H., Y.-L. Kao, W.-L. Lin, J.-L. Xiao, P.-L. Kuo, C.-W. Wu, W.-Y. Liao, and C.-H. Lee, *The migration speed of cancer cells influenced by macrophages and myofibroblasts co-cultured in a microfluidic chip.* Integrative Biology, 2011. **4**(2): p. 177-182.
197. Bischel, L.L., D.J. Beebe, and K.E. Sung, *Microfluidic model of ductal carcinoma in situ with 3D, organotypic structure.* BMC cancer, 2015. **15**: p. 12-12.
198. Lee, J.-H., S.-K. Kim, I.A. Khawar, S.-Y. Jeong, S. Chung, and H.-J. Kuh, *Microfluidic co-culture of pancreatic tumor spheroids with stellate cells as a novel 3D model for investigation of stroma-mediated cell motility and drug resistance.* Journal of experimental & clinical cancer research : CR, 2018. **37**(1): p. 4-4.
199. Williams, E.D., D. Gao, A. Redfern, and E.W. Thompson, *Controversies around epithelial-mesenchymal plasticity in cancer metastasis.* Nat Rev Cancer, 2019.
200. Zervantonakis, I.K., S.K. Hughes-Alford, J.L. Charest, J.S. Condeelis, F.B. Gertler, and R.D. Kamm, *Three-dimensional microfluidic model for tumor cell intravasation and endothelial barrier function.* Proceedings of the National Academy of Sciences of the United States of America, 2012. **109**(34): p. 13515-13520.
201. Boussommier-Calleja, A., Y. Atiyas, K. Haase, M. Headley, C. Lewis, and R.D. Kamm, *The effects of monocytes on tumor cell extravasation in a 3D vascularized microfluidic model.* Biomaterials, 2019. **198**: p. 180-193.
202. Lee, S.W.L., G. Adriani, E. Ceccarello, A. Pavesi, A.T. Tan, A. Bertoletti, R.D. Kamm, and S.C. Wong, *Characterizing the Role of Monocytes in T Cell Cancer Immunotherapy Using a 3D Microfluidic Model.* Front Immunol, 2018. **9**(416): p. 416.
203. Agliari, E., E. Biselli, A. De Ninno, G. Schiavoni, L. Gabriele, A. Gerardino, F. Mattei, A. Barra, and L. Businaro, *Cancer-driven dynamics of immune cells in a microfluidic environment.* Scientific Reports, 2014. **4**: p. 6639.
204. Mattei, F., G. Schiavoni, A. De Ninno, V. Lucarini, P. Sestili, A. Sistigu, A. Fragale, M. Sanchez, M. Spada, A. Gerardino, et al., *A multidisciplinary study using in vivo tumor models and microfluidic cell-on-chip approach to explore the cross-talk between cancer and immune cells.* J Immunotoxicol, 2014. **11**(4): p. 337-46.
205. Parlato, S., A. De Ninno, R. Molfetta, E. Toschi, D. Salerno, A. Mencattini, G. Romagnoli, A. Fragale, L. Roccazzello, M. Buoncervello, et al., *3D Microfluidic model for evaluating immunotherapy efficacy by tracking dendritic cell behaviour toward tumor cells.* Sci Rep, 2017. **7**(1): p. 1093.
206. Truong, D., J. Puleo, A. Llave, G. Mouneimne, R.D. Kamm, and M. Nikkhah, *Breast Cancer Cell Invasion into a Three Dimensional Tumor-Stroma Microenvironment.* Scientific Reports, 2016. **6**: p. 34094.
207. Peela, N., E.S. Barrientos, D. Truong, G. Mouneimne, and M. Nikkhah, *Effect of suberoylanilide hydroxamic acid (SAHA) on breast cancer cells within a tumor-stroma microfluidic model.* Integr Biol (Camb), 2017. **9**(12): p. 988-999.
208. Nagaraju, S., D. Truong, G. Mouneimne, and M. Nikkhah, *Microfluidic Tumor-*

Vascular Model to Study Breast Cancer Cell Invasion and Intravasation. Adv Healthc Mater, 2018. **7**(9): p. e1701257.
209. Du, Z., S. Mi, X. Yi, Y. Xu, and W. Sun, *Microfluidic system for modelling 3D tumour invasion into surrounding stroma and drug screening.* Biofabrication, 2018. **10**(3): p. 034102.
210. Polacheck, W.J., J.L. Charest, and R.D. Kamm, *Interstitial flow influences direction of tumor cell migration through competing mechanisms.* Proc Natl Acad Sci U S A, 2011. **108**(27): p. 11115-20.
211. Polacheck, W.J., A.E. German, A. Mammoto, D.E. Ingber, and R.D. Kamm, *Mechanotransduction of fluid stresses governs 3D cell migration.* Proc Natl Acad Sci U S A, 2014. **111**(7): p. 2447-2452.
212. Han, W., S. Chen, W. Yuan, Q. Fan, J. Tian, X. Wang, L. Chen, X. Zhang, W. Wei, R. Liu, et al., *Oriented collagen fibers direct tumor cell intravasation.* Proc Natl Acad Sci U S A, 2016. **113**(40): p. 11208-11213.
213. Au, S.H., B.D. Storey, J.C. Moore, Q. Tang, Y.L. Chen, S. Javaid, A.F. Sarioglu, R. Sullivan, M.W. Madden, R. O'Keefe, et al., *Clusters of circulating tumor cells traverse capillary-sized vessels.* Proc Natl Acad Sci U S A, 2016. **113**(18): p. 4947-52.
214. Chen, M.B., J.M. Lamar, R. Li, R.O. Hynes, and R.D. Kamm, *Elucidation of the Roles of Tumor Integrin beta1 in the Extravasation Stage of the Metastasis Cascade.* Cancer Res, 2016. **76**(9): p. 2513-24.
215. Zhang, Q., T. Liu, and J. Qin, *A microfluidic-based device for study of transendothelial invasion of tumor aggregates in realtime.* Lab Chip, 2012. **12**(16): p. 2837-42.
216. Xu, H., Z. Li, Y. Yu, S. Sizdahkhani, W.S. Ho, F. Yin, L. Wang, G. Zhu, M. Zhang, L. Jiang, et al., *A dynamic in vivo-like organotypic blood-brain barrier model to probe metastatic brain tumors.* Scientific Reports, 2016. **6**: p. 36670.
217. Xu, Z., E. Li, Z. Guo, R. Yu, H. Hao, Y. Xu, Z. Sun, X. Li, J. Lyu, and Q. Wang, *Design and Construction of a Multi-Organ Microfluidic Chip Mimicking the in vivo Microenvironment of Lung Cancer Metastasis.* ACS Appl Mater Interfaces, 2016. **8**(39): p. 25840-25847.
218. Ashworth, T., *A case of cancer in which cells similar to those in the tumours were seen in the blood after death.* Aust Med J., 1869. **14**: p. 146.
219. Cristofanilli, M., G.T. Budd, M.J. Ellis, A. Stopeck, J. Matera, M.C. Miller, J.M. Reuben, G.V. Doyle, W.J. Allard, L.W. Terstappen, et al., *Circulating tumor cells, disease progression, and survival in metastatic breast cancer.* N Engl J Med, 2004. **351**(8): p. 781-91.
220. Peeters, D.J., P.J. van Dam, G.G. Van den Eynden, A. Rutten, H. Wuyts, L. Pouillon, M. Peeters, P. Pauwels, S.J. Van Laere, P.A. van Dam, et al., *Detection and prognostic significance of circulating tumour cells in patients with metastatic breast cancer according to immunohistochemical subtypes.* Br J Cancer, 2014. **110**(2): p. 375-83.
221. Tay, R.Y., F. Fernandez-Gutierrez, V. Foy, K. Burns, J. Pierce, K. Morris, L. Priest, J. Tugwood, L. Ashcroft, C.R. Lindsay, et al., *Prognostic value of circulating tumour cells in limited-stage small-cell lung cancer: analysis of the concurrent once-daily versus twice-daily radiotherapy (CONVERT) randomised controlled trial.* Ann

Oncol, 2019. **30**(7): p. 1114-1120.
222. Yu, M., A. Bardia, B.S. Wittner, S.L. Stott, M.E. Smas, D.T. Ting, S.J. Isakoff, J.C. Ciciliano, M.N. Wells, A.M. Shah, et al., *Circulating breast tumor cells exhibit dynamic changes in epithelial and mesenchymal composition.* Science, 2013. **339**(6119): p. 580-4.
223. Satelli, A., I. Batth, Z. Brownlee, A. Mitra, S. Zhou, H. Noh, C.R. Rojas, H. Li, Q.H. Meng, and S. Li, *EMT circulating tumor cells detected by cell-surface vimentin are associated with prostate cancer progression.* Oncotarget, 2017. **8**(30): p. 49329-49337.
224. Kulasinghe, A., L. Kenny, C. Perry, J.P. Thiery, L. Jovanovic, I. Vela, C. Nelson, and C. Punyadeera, *Impact of label-free technologies in head and neck cancer circulating tumour cells.* Oncotarget, 2016. **7**(44): p. 71223-71234.
225. Kraan, J., S. Sleijfer, M.H. Strijbos, M. Ignatiadis, D. Peeters, J.Y. Pierga, F. Farace, S. Riethdorf, T. Fehm, L. Zorzino, et al., *External quality assurance of circulating tumor cell enumeration using the CellSearch((R)) system: a feasibility study.* Cytometry B Clin Cytom, 2011. **80**(2): p. 112-8.
226. Massard, C., M. Oulhen, S. Le Moulec, N. Auger, S. Foulon, A. Abou-Lovergne, F. Billiot, A. Valent, V. Marty, Y. Loriot, et al., *Phenotypic and genetic heterogeneity of tumor tissue and circulating tumor cells in patients with metastatic castration-resistant prostate cancer: A report from the PETRUS prospective study.* Oncotarget, 2016. **7**(34): p. 55069-55082.
227. Watanabe, S., *The metastasizability of tumor cells.* Cancer, 1954. **7**(2): p. 215-23.
228. Gkountela, S., F. Castro-Giner, B.M. Szczerba, M. Vetter, J. Landin, R. Scherrer, I. Krol, M.C. Scheidmann, C. Beisel, C.U. Stirnimann, et al., *Circulating Tumor Cell Clustering Shapes DNA Methylation to Enable Metastasis Seeding.* Cell, 2019. **176**(1-2): p. 98-112 e14.
229. Kulasinghe, A., J. Zhou, L. Kenny, I. Papautsky, and C. Punyadeera, *Capture of Circulating Tumour Cell Clusters Using Straight Microfluidic Chips.* Cancers (Basel), 2019. **11**(1).
230. Aceto, N., A. Bardia, D.T. Miyamoto, M.C. Donaldson, B.S. Wittner, J.A. Spencer, M. Yu, A. Pely, A. Engstrom, H. Zhu, et al., *Circulating tumor cell clusters are oligoclonal precursors of breast cancer metastasis.* Cell, 2014. **158**(5): p. 1110-1122.
231. Szczerba, B.M., F. Castro-Giner, M. Vetter, I. Krol, S. Gkountela, J. Landin, M.C. Scheidmann, C. Donato, R. Scherrer, J. Singer, et al., *Neutrophils escort circulating tumour cells to enable cell cycle progression.* Nature, 2019. **566**(7745): p. 553-557.
232. Zhu, Z., S. Qiu, K. Shao, and Y. Hou, *Progress and challenges of sequencing and analyzing circulating tumor cells.* Cell Biol Toxicol, 2018. **34**(5): p. 405-415.
233. Park, S.M., D.J. Wong, C.C. Ooi, D.M. Kurtz, O. Vermesh, A. Aalipour, S. Suh, K.L. Pian, J.J. Chabon, S.H. Lee, et al., *Molecular profiling of single circulating tumor cells from lung cancer patients.* Proc Natl Acad Sci U S A, 2016. **113**(52): p. E8379-E8386.
234. Cheng, Y.H., Y.C. Chen, E. Lin, R. Brien, S. Jung, Y.T. Chen, W. Lee, Z. Hao, S. Sahoo, H. Min Kang, et al., *Hydro-Seq enables contamination-free high-throughput single-cell RNA-sequencing for circulating tumor cells.* Nat Commun, 2019. **10**(1): p. 2163.

235. Yue, C., Y. Jiang, P. Li, Y. Wang, J. Xue, N. Li, D. Li, R. Wang, Y. Dang, Z. Hu, et al., *Dynamic change of PD-L1 expression on circulating tumor cells in advanced solid tumor patients undergoing PD-1 blockade therapy.* Oncoimmunology, 2018. **7**(7): p. e1438111.
236. Mazel, M., W. Jacot, K. Pantel, K. Bartkowiak, D. Topart, L. Cayrefourcq, D. Rossille, T. Maudelonde, T. Fest, and C. Alix-Panabieres, *Frequent expression of PD-L1 on circulating breast cancer cells.* Mol Oncol, 2015. **9**(9): p. 1773-82.
237. Wang, Y., T.H. Kim, S. Fouladdel, Z. Zhang, P. Soni, A. Qin, L. Zhao, E. Azizi, T.S. Lawrence, N. Ramnath, et al., *PD-L1 Expression in Circulating Tumor Cells Increases during Radio(chemo)therapy and Indicates Poor Prognosis in Non-small Cell Lung Cancer.* Sci Rep, 2019. **9**(1): p. 566.
238. Kulasinghe, A., C. Perry, L. Kenny, M.E. Warkiani, C. Nelson, and C. Punyadeera, *PD-L1 expressing circulating tumour cells in head and neck cancers.* BMC Cancer, 2017. **17**(1): p. 333.
239. Strati, A., G. Koutsodontis, G. Papaxoinis, I. Angelidis, M. Zavridou, P. Economopoulou, I. Kotsantis, M. Avgeris, M. Mazel, C. Perisanidis, et al., *Prognostic significance of PD-L1 expression on circulating tumor cells in patients with head and neck squamous cell carcinoma.* Ann Oncol, 2017. **28**(8): p. 1923-1933.
240. Stoecklein, N.H., J.C. Fischer, D. Niederacher, and L.W. Terstappen, *Challenges for CTC-based liquid biopsies: low CTC frequency and diagnostic leukapheresis as a potential solution.* Expert Rev Mol Diagn, 2016. **16**(2): p. 147-64.
241. Fehm, T.N., F. Meier-Stiegen, C. Driemel, B. Jager, F. Reinhardt, J. Naskou, A. Franken, H. Neubauer, R.P.L. Neves, G. van Dalum, et al., *Diagnostic leukapheresis for CTC analysis in breast cancer patients: CTC frequency, clinical experiences and recommendations for standardized reporting.* Cytometry A, 2018. **93**(12): p. 1213-1219.
242. Dizdar, L., G. Fluegen, G. van Dalum, E. Honisch, R.P. Neves, D. Niederacher, H. Neubauer, T. Fehm, A. Rehders, A. Krieg, et al., *Detection of circulating tumor cells in colorectal cancer patients using the GILUPI CellCollector: results from a prospective, single-center study.* Mol Oncol, 2019. **13**(7): p. 1548-1558.
243. Theil, G., K. Fischer, E. Weber, R. Medek, R. Hoda, K. Lucke, and P. Fornara, *The Use of a New CellCollector to Isolate Circulating Tumor Cells from the Blood of Patients with Different Stages of Prostate Cancer and Clinical Outcomes - A Proof-of-Concept Study.* PLoS One, 2016. **11**(8): p. e0158354.
244. Saucedo-Zeni, N., S. Mewes, R. Niestroj, L. Gasiorowski, D. Murawa, P. Nowaczyk, T. Tomasi, E. Weber, G. Dworacki, N.G. Morgenthaler, et al., *A novel method for the in vivo isolation of circulating tumor cells from peripheral blood of cancer patients using a functionalized and structured medical wire.* Int J Oncol, 2012. **41**(4): p. 1241-50.
245. Khoo, B.L., M.E. Warkiani, D.S. Tan, A.A. Bhagat, D. Irwin, D.P. Lau, A.S. Lim, K.H. Lim, S.S. Krisna, W.T. Lim, et al., *Clinical validation of an ultra high-throughput spiral microfluidics for the detection and enrichment of viable circulating tumor cells.* PLoS One, 2014. **9**(7): p. e99409.
246. Warkiani, M.E., B.L. Khoo, L. Wu, A.K. Tay, A.A. Bhagat, J. Han, and C.T. Lim, *Ultra-fast, label-free isolation of circulating tumor cells from blood using spiral*

microfluidics. Nat Protoc, 2016. **11**(1): p. 134-48.
247. Aya-Bonilla, C.A., G. Marsavela, J.B. Freeman, C. Lomma, M.H. Frank, M.A. Khattak, T.M. Meniawy, M. Millward, M.E. Warkiani, E.S. Gray, et al., *Isolation and detection of circulating tumour cells from metastatic melanoma patients using a slanted spiral microfluidic device.* Oncotarget, 2017. **8**(40): p. 67355-67368.
248. Kulasinghe, A., T.H. Tran, T. Blick, K. O'Byrne, E.W. Thompson, M.E. Warkiani, C. Nelson, L. Kenny, and C. Punyadeera, *Enrichment of circulating head and neck tumour cells using spiral microfluidic technology.* Sci Rep, 2017. **7**: p. 42517.
249. Kulasinghe, A., J. Kapeleris, R. Kimberley, S.R. Mattarollo, E.W. Thompson, J.P. Thiery, L. Kenny, K. O'Byrne, and C. Punyadeera, *The prognostic significance of circulating tumor cells in head and neck and non-small-cell lung cancer.* Cancer Med, 2018. **7**(12): p. 5910-5919.
250. Zhou, J., A. Kulasinghe, A. Bogseth, K. O'Byrne, C. Punyadeera, and I. Papautsky, *Isolation of circulating tumor cells in non-small-cell-lung-cancer patients using a multi-flow microfluidic channel.* Microsyst Nanoeng, 2019. **5**: p. 8.
251. Jan, Y.J., J.F. Chen, Y. Zhu, Y.T. Lu, S.H. Chen, H. Chung, M. Smalley, Y.W. Huang, J. Dong, L.C. Chen, et al., *NanoVelcro rare-cell assays for detection and characterization of circulating tumor cells.* Adv Drug Deliv Rev, 2018. **125**: p. 78-93.
252. Li, P., Z. Mao, Z. Peng, L. Zhou, Y. Chen, P.H. Huang, C.I. Truica, J.J. Drabick, W.S. El-Deiry, M. Dao, et al., *Acoustic separation of circulating tumor cells.* Proc Natl Acad Sci U S A, 2015. **112**(16): p. 4970-5.
253. Shields Iv, C.W., J.L. Wang, K.A. Ohiri, E.D. Essoyan, B.B. Yellen, A.J. Armstrong, and G.P. Lopez, *Magnetic separation of acoustically focused cancer cells from blood for magnetographic templating and analysis.* Lab Chip, 2016. **16**(19): p. 3833-3844.
254. Mayall, F.G., I. Bodger, J. Pepperell, L. Stevanato, A. Hustler, and K.M. Mumford, *The precious cell block.* J Clin Pathol, 2018. **71**(7): p. 659-660.
255. Hvichia, G.E., Z. Parveen, C. Wagner, M. Janning, J. Quidde, A. Stein, V. Muller, S. Loges, R.P. Neves, N.H. Stoecklein, et al., *A novel microfluidic platform for size and deformability based separation and the subsequent molecular characterization of viable circulating tumor cells.* Int J Cancer, 2016. **138**(12): p. 2894-904.
256. Chudziak, J., D.J. Burt, S. Mohan, D.G. Rothwell, B. Mesquita, J. Antonello, S. Dalby, M. Ayub, L. Priest, L. Carter, et al., *Clinical evaluation of a novel microfluidic device for epitope-independent enrichment of circulating tumour cells in patients with small cell lung cancer.* Analyst, 2016. **141**(2): p. 669-78.
257. Lemaire, C.A., S.Z. Liu, C.L. Wilkerson, V.C. Ramani, N.A. Barzanian, K.W. Huang, J. Che, M.W. Chiu, M. Vuppalapaty, A.M. Dimmick, et al., *Fast and Label-Free Isolation of Circulating Tumor Cells from Blood: From a Research Microfluidic Platform to an Automated Fluidic Instrument, VTX-1 Liquid Biopsy System.* SLAS Technol, 2018. **23**(1): p. 16-29.
258. Dhar, M., J. Wong, J. Che, M. Matsumoto, T. Grogan, D. Elashoff, E.B. Garon, J.W. Goldman, E. Sollier Christen, D. Di Carlo, et al., *Evaluation of PD-L1 expression on vortex-isolated circulating tumor cells in metastatic lung cancer.* Sci Rep, 2018. **8**(1): p. 2592.
259. Khan, I.U., C.A. Serra, N. Anton, and T. Vandamme, *Microfluidics: a focus on*

improved cancer targeted drug delivery systems. J Control Release, 2013. **172**(3): p. 1065-74.
260. Valente, K.P., S. Khetani, A.R. Kolahchi, A. Sanati-Nezhad, A. Suleman, and M. Akbari, *Microfluidic technologies for anticancer drug studies.* Drug Discov Today, 2017. **22**(11): p. 1654-1670.
261. Wlodkowic, D. and J.M. Cooper, *Tumors on chips: oncology meets microfluidics.* Curr Opin Chem Biol, 2010. **14**(5): p. 556-67.
262. Ghaemmaghami, A.M., M.J. Hancock, H. Harrington, H. Kaji, and A. Khademhosseini, *Biomimetic tissues on a chip for drug discovery.* Drug Discov Today, 2012. **17**(3-4): p. 173-81.
263. Polini, A., L. Prodanov, N.S. Bhise, V. Manoharan, M.R. Dokmeci, and A. Khademhosseini, *Organs-on-a-chip: a new tool for drug discovery.* Expert Opin Drug Discov, 2014. **9**(4): p. 335-52.
264. Sackmann, E.K., A.L. Fulton, and D.J. Beebe, *The present and future role of microfluidics in biomedical research.* Nature, 2014. **507**(7491): p. 181-9.
265. Sleeboom, J.J.F., H. Eslami Amirabadi, P. Nair, C.M. Sahlgren, and J.M.J. den Toonder, *Metastasis in context: modeling the tumor microenvironment with cancer-on-a-chip approaches.* Dis Model Mech, 2018. **11**(3).
266. Cui, P. and S. Wang, *Application of microfluidic chip technology in pharmaceutical analysis: A review.* J Pharm Anal, 2019. **9**(4): p. 238-247.
267. Ye, N., J. Qin, W. Shi, X. Liu, and B. Lin, *Cell-based high content screening using an integrated microfluidic device.* Lab Chip, 2007. **7**(12): p. 1696-704.
268. Xu, Z., Y. Gao, Y. Hao, E. Li, Y. Wang, J. Zhang, W. Wang, Z. Gao, and Q. Wang, *Application of a microfluidic chip-based 3D co-culture to test drug sensitivity for individualized treatment of lung cancer.* Biomaterials, 2013. **34**(16): p. 4109-4117.
269. Eduati, F., R. Utharala, D. Madhavan, U.P. Neumann, T. Longerich, T. Cramer, J. Saez-Rodriguez, and C.A. Merten, *A microfluidics platform for combinatorial drug screening on cancer biopsies.* Nat Commun, 2018. **9**(1): p. 2434.
270. Chen, Y.A., A.D. King, H.C. Shih, C.C. Peng, C.Y. Wu, W.H. Liao, and Y.C. Tung, *Generation of oxygen gradients in microfluidic devices for cell culture using spatially confined chemical reactions.* Lab Chip, 2011. **11**(21): p. 3626-33.
271. Ying, L., Z. Zhu, Z. Xu, T. He, E. Li, Z. Guo, F. Liu, C. Jiang, and Q. Wang, *Cancer Associated Fibroblast-Derived Hepatocyte Growth Factor Inhibits the Paclitaxel-Induced Apoptosis of Lung Cancer A549 Cells by Up-Regulating the PI3K/Akt and GRP78 Signaling on a Microfluidic Platform.* PLoS One, 2015. **10**(6): p. e0129593.
272. Faley, S.L., M. Copland, D. Wlodkowic, W. Kolch, K.T. Seale, J.P. Wikswo, and J.M. Cooper, *Microfluidic single cell arrays to interrogate signalling dynamics of individual, patient-derived hematopoietic stem cells.* Lab Chip, 2009. **9**(18): p. 2659-64.
273. Choi, Y., E. Hyun, J. Seo, C. Blundell, H.C. Kim, E. Lee, S.H. Lee, A. Moon, W.K. Moon, and D. Huh, *A microengineered pathophysiological model of early-stage breast cancer.* Lab Chip, 2015. **15**(16): p. 3350-7.
274. Bai, J., T.Y. Tu, C. Kim, J.P. Thiery, and R.D. Kamm, *Identification of drugs as single agents or in combination to prevent carcinoma dissemination in a microfluidic 3D environment.* Oncotarget, 2015. **6**(34): p. 36603-14.

275. Sobrino, A., D.T. Phan, R. Datta, X. Wang, S.J. Hachey, M. Romero-Lopez, E. Gratton, A.P. Lee, S.C. George, and C.C. Hughes, *3D microtumors in vitro supported by perfused vascular networks.* Sci Rep, 2016. **6**: p. 31589.
276. Walsh, C.L., B.M. Babin, R.W. Kasinskas, J.A. Foster, M.J. McGarry, and N.S. Forbes, *A multipurpose microfluidic device designed to mimic microenvironment gradients and develop targeted cancer therapeutics.* Lab Chip, 2009. **9**(4): p. 545-54.
277. Terrell-Hall, T.B., M.I. Nounou, F. El-Amrawy, J.I.G. Griffith, and P.R. Lockman, *Trastuzumab distribution in an in-vivo and in-vitro model of brain metastases of breast cancer.* Oncotarget, 2017. **8**(48): p. 83734-83744.
278. Pavesi, A., A.T. Tan, S. Koh, A. Chia, M. Colombo, E. Antonecchia, C. Miccolis, E. Ceccarello, G. Adriani, M.T. Raimondi, et al., *A 3D microfluidic model for preclinical evaluation of TCR-engineered T cells against solid tumors.* JCI Insight, 2017. **2**(12).
279. Joyce, J.A. and D.T. Fearon, *T cell exclusion, immune privilege, and the tumor microenvironment.* Science, 2015. **348**(6230): p. 74-80.
280. Ruppen, J., F.D. Wildhaber, C. Strub, S.R. Hall, R.A. Schmid, T. Geiser, and O.T. Guenat, *Towards personalized medicine: chemosensitivity assays of patient lung cancer cell spheroids in a perfused microfluidic platform.* Lab Chip, 2015. **15**(14): p. 3076-85.
281. Aref, A.R., M. Campisi, E. Ivanova, A. Portell, D. Larios, B.P. Piel, N. Mathur, C. Zhou, R.V. Coakley, A. Bartels, et al., *3D microfluidic ex vivo culture of organotypic tumor spheroids to model immune checkpoint blockade.* Lab Chip, 2018. **18**(20): p. 3129-3143.
282. Jenkins, R.W., A.R. Aref, P.H. Lizotte, E. Ivanova, S. Stinson, C.W. Zhou, M. Bowden, J. Deng, H. Liu, D. Miao, et al., *Ex Vivo Profiling of PD-1 Blockade Using Organotypic Tumor Spheroids.* Cancer Discov, 2018. **8**(2): p. 196-215.
283. Shirure, V.S., Y. Bi, M.B. Curtis, A. Lezia, M.M. Goedegebuure, S.P. Goedegebuure, R. Aft, R.C. Fields, and S.C. George, *Tumor-on-a-chip platform to investigate progression and drug sensitivity in cell lines and patient-derived organoids.* Lab Chip, 2018. **18**(23): p. 3687-3702.
284. Denkert, C., C. Liedtke, A. Tutt, and G. von Minckwitz, *Molecular alterations in triple-negative breast cancer-the road to new treatment strategies.* Lancet, 2017. **389**(10087): p. 2430-2442.
285. Di Cosimo, S., *Advancing immunotherapy for early-stage triple-negative breast cancer.* Lancet, 2020. **396**(10257): p. 1046-1048.
286. Pastushenko, I. and C. Blanpain, *EMT Transition States during Tumor Progression and Metastasis.* Trends Cell Biol, 2019. **29**(3): p. 212-226.
287. Shibue, T. and R.A. Weinberg, *EMT, CSCs, and drug resistance: the mechanistic link and clinical implications.* Nat Rev Clin Oncol, 2017. **14**(10): p. 611-629.
288. Horn, L.A., K. Fousek, and C. Palena, *Tumor Plasticity and Resistance to Immunotherapy.* Trends Cancer, 2020. **6**(5): p. 432-441.
289. Dongre, A., M. Rashidian, F. Reinhardt, A. Bagnato, Z. Keckesova, H.L. Ploegh, and R.A. Weinberg, *Epithelial-to-Mesenchymal Transition Contributes to Immunosuppression in Breast Carcinomas.* Cancer Res, 2017. **77**(15): p. 3982-3989.
290. Noman, M.Z., B. Janji, A. Abdou, M. Hasmim, S. Terry, T.Z. Tan, F. Mami-Chouaib, J.P. Thiery, and S. Chouaib, *The immune checkpoint ligand PD-L1 is upregulated in*

EMT-activated human breast cancer cells by a mechanism involving ZEB-1 and miR-200. Oncoimmunology, 2017. **6**(1): p. e1263412.
291. Chen, L., D.L. Gibbons, S. Goswami, M.A. Cortez, Y.H. Ahn, L.A. Byers, X. Zhang, X. Yi, D. Dwyer, W. Lin, et al., *Metastasis is regulated via microRNA-200/ZEB1 axis control of tumour cell PD-L1 expression and intratumoral immunosuppression.* Nat Commun, 2014. **5**: p. 5241.
292. Lou, Y., L. Diao, E.R. Cuentas, W.L. Denning, L. Chen, Y.H. Fan, L.A. Byers, J. Wang, V.A. Papadimitrakopoulou, C. Behrens, et al., *Epithelial-Mesenchymal Transition Is Associated with a Distinct Tumor Microenvironment Including Elevation of Inflammatory Signals and Multiple Immune Checkpoints in Lung Adenocarcinoma.* Clin Cancer Res, 2016. **22**(14): p. 3630-42.
293. Yoshihara, K., M. Shahmoradgoli, E. Martinez, R. Vegesna, H. Kim, W. Torres-Garcia, V. Trevino, H. Shen, P.W. Laird, D.A. Levine, et al., *Inferring tumour purity and stromal and immune cell admixture from expression data.* Nat Commun, 2013. **4**: p. 2612.
294. Colaprico, A., T.C. Silva, C. Olsen, L. Garofano, C. Cava, D. Garolini, T.S. Sabedot, T.M. Malta, S.M. Pagnotta, I. Castiglioni, et al., *TCGAbiolinks: an R/Bioconductor package for integrative analysis of TCGA data.* Nucleic Acids Res, 2016. **44**(8): p. e71.
295. Tan, T.Z., Q.H. Miow, Y. Miki, T. Noda, S. Mori, R.Y. Huang, and J.P. Thiery, *Epithelial-mesenchymal transition spectrum quantification and its efficacy in deciphering survival and drug responses of cancer patients.* EMBO Mol Med, 2014. **6**(10): p. 1279-93.
296. Thorsson, V., D.L. Gibbs, S.D. Brown, D. Wolf, D.S. Bortone, T.H. Ou Yang, E. Porta-Pardo, G.F. Gao, C.L. Plaisier, J.A. Eddy, et al., *The Immune Landscape of Cancer.* Immunity, 2018. **48**(4): p. 812-830 e14.
297. Xu, L., C. Deng, B. Pang, X. Zhang, W. Liu, G. Liao, H. Yuan, P. Cheng, F. Li, Z. Long, et al., *TIP: A Web Server for Resolving Tumor Immunophenotype Profiling.* Cancer Res, 2018. **78**(23): p. 6575-6580.
298. Li, B., E. Severson, J.C. Pignon, H. Zhao, T. Li, J. Novak, P. Jiang, H. Shen, J.C. Aster, S. Rodig, et al., *Comprehensive analyses of tumor immunity: implications for cancer immunotherapy.* Genome Biol, 2016. **17**(1): p. 174.
299. Li, T., J. Fan, B. Wang, N. Traugh, Q. Chen, J.S. Liu, B. Li, and X.S. Liu, *TIMER: A Web Server for Comprehensive Analysis of Tumor-Infiltrating Immune Cells.* Cancer Res, 2017. **77**(21): p. e108-e110.
300. Li, T., J. Fu, Z. Zeng, D. Cohen, J. Li, Q. Chen, B. Li, and X.S. Liu, *TIMER2.0 for analysis of tumor-infiltrating immune cells.* Nucleic Acids Res, 2020. **48**(W1): p. W509-W514.
301. Terry, S., P. Savagner, S. Ortiz-Cuaran, L. Mahjoubi, P. Saintigny, J.P. Thiery, and S. Chouaib, *New insights into the role of EMT in tumor immune escape.* Mol Oncol, 2017. **11**(7): p. 824-846.
302. Dongre, A., M. Rashidian, E.N. Eaton, F. Reinhardt, P. Thiru, M. Zagorulya, S. Nepal, T. Banaz, A. Martner, S. Spranger, et al., *Direct and Indirect Regulators of Epithelial-Mesenchymal Transition (EMT)-mediated Immunosuppression in Breast Carcinomas.* Cancer Discov, 2020.

303. Derynck, R. and R.A. Weinberg, *EMT and Cancer: More Than Meets the Eye.* Dev Cell, 2019. **49**(3): p. 313-316.
304. Hsu, H.C., L.C. Liu, H.Y. Wang, C.M. Hung, Y.C. Lin, C.T. Ho, and T.D. Way, *Stromal Fibroblasts from the Interface Zone of Triple Negative Breast Carcinomas Induced Epithelial-Mesenchymal Transition and its Inhibition by Emodin.* PLoS One, 2017. **12**(1): p. e0164661.
305. Poudel, P., G. Nyamundanda, Y. Patil, M.C.U. Cheang, and A. Sadanandam, *Heterocellular gene signatures reveal luminal-A breast cancer heterogeneity and differential therapeutic responses.* NPJ Breast Cancer, 2019. **5**: p. 21.
306. Fan, Q.M., Y.Y. Jing, G.F. Yu, X.R. Kou, F. Ye, L. Gao, R. Li, Q.D. Zhao, Y. Yang, Z.H. Lu, et al., *Tumor-associated macrophages promote cancer stem cell-like properties via transforming growth factor-beta1-induced epithelial-mesenchymal transition in hepatocellular carcinoma.* Cancer Lett, 2014. **352**(2): p. 160-8.
307. Bonde, A.K., V. Tischler, S. Kumar, A. Soltermann, and R.A. Schwendener, *Intratumoral macrophages contribute to epithelial-mesenchymal transition in solid tumors.* BMC Cancer, 2012. **12**: p. 35.
308. Qian, B.Z. and J.W. Pollard, *Macrophage diversity enhances tumor progression and metastasis.* Cell, 2010. **141**(1): p. 39-51.
309. Su, S., Q. Liu, J. Chen, J. Chen, F. Chen, C. He, D. Huang, W. Wu, L. Lin, W. Huang, et al., *A positive feedback loop between mesenchymal-like cancer cells and macrophages is essential to breast cancer metastasis.* Cancer Cell, 2014. **25**(5): p. 605-20.
310. Viel, S., A. Marcais, F.S. Guimaraes, R. Loftus, J. Rabilloud, M. Grau, S. Degouve, S. Djebali, A. Sanlaville, E. Charrier, et al., *TGF-beta inhibits the activation and functions of NK cells by repressing the mTOR pathway.* Sci Signal, 2016. **9**(415): p. ra19.
311. Teicher, B.A., *Transforming growth factor-beta and the immune response to malignant disease.* Clin Cancer Res, 2007. **13**(21): p. 6247-51.
312. Scheel, C., E.N. Eaton, S.H. Li, C.L. Chaffer, F. Reinhardt, K.J. Kah, G. Bell, W. Guo, J. Rubin, A.L. Richardson, et al., *Paracrine and autocrine signals induce and maintain mesenchymal and stem cell states in the breast.* Cell, 2011. **145**(6): p. 926-40.
313. Chae, Y.K., S. Chang, T. Ko, J. Anker, S. Agte, W. Iams, W.M. Choi, K. Lee, and M. Cruz, *Epithelial-mesenchymal transition (EMT) signature is inversely associated with T-cell infiltration in non-small cell lung cancer (NSCLC).* Sci Rep, 2018. **8**(1): p. 2918.
314. Kudo-Saito, C., H. Shirako, T. Takeuchi, and Y. Kawakami, *Cancer metastasis is accelerated through immunosuppression during Snail-induced EMT of cancer cells.* Cancer Cell, 2009. **15**(3): p. 195-206.
315. Bruni, D., H.K. Angell, and J. Galon, *The immune contexture and Immunoscore in cancer prognosis and therapeutic efficacy.* Nat Rev Cancer, 2020. **20**(11): p. 662-680.
316. Duan, Q., H. Zhang, J. Zheng, and L. Zhang, *Turning Cold into Hot: Firing up the Tumor Microenvironment.* Trends Cancer, 2020. **6**(7): p. 605-618.
317. Fridman, W.H., F. Pages, C. Sautes-Fridman, and J. Galon, *The immune contexture in human tumours: impact on clinical outcome.* Nat Rev Cancer, 2012. **12**(4): p. 298-

306.
318. Bindea, G., B. Mlecnik, M. Tosolini, A. Kirilovsky, M. Waldner, A.C. Obenauf, H. Angell, T. Fredriksen, L. Lafontaine, A. Berger, et al., *Spatiotemporal dynamics of intratumoral immune cells reveal the immune landscape in human cancer.* Immunity, 2013. **39**(4): p. 782-95.
319. Gajewski, T.F., *The Next Hurdle in Cancer Immunotherapy: Overcoming the Non-T-Cell-Inflamed Tumor Microenvironment.* Semin Oncol, 2015. **42**(4): p. 663-71.
320. Zemek, R.M., E. De Jong, W.L. Chin, I.S. Schuster, V.S. Fear, T.H. Casey, C. Forbes, S.J. Dart, C. Leslie, A. Zaitouny, et al., *Sensitization to immune checkpoint blockade through activation of a STAT1/NK axis in the tumor microenvironment.* Sci Transl Med, 2019. **11**(501).
321. Liu, Z., C. Han, and Y.X. Fu, *Targeting innate sensing in the tumor microenvironment to improve immunotherapy.* Cell Mol Immunol, 2020. **17**(1): p. 13-26.
322. Garcia-Lora, A., I. Algarra, and F. Garrido, *MHC class I antigens, immune surveillance, and tumor immune escape.* J Cell Physiol, 2003. **195**(3): p. 346-55.
323. Fruci, D., M. Benevolo, L. Cifaldi, S. Lorenzi, E. Lo Monaco, E. Tremante, and P. Giacomini, *Major histocompatibility complex class i and tumour immuno-evasion: how to fool T cells and natural killer cells at one time.* Curr Oncol, 2012. **19**(1): p. 39-41.
324. Schmid, P., J. Cortes, L. Pusztai, H. McArthur, S. Kummel, J. Bergh, C. Denkert, Y.H. Park, R. Hui, N. Harbeck, et al., *Pembrolizumab for Early Triple-Negative Breast Cancer.* N Engl J Med, 2020. **382**(9): p. 810-821.
325. Keenan, T.E. and S.M. Tolaney, *Role of Immunotherapy in Triple-Negative Breast Cancer.* J Natl Compr Canc Netw, 2020. **18**(4): p. 479-489.
326. Esteva, F.J., V.M. Hubbard-Lucey, J. Tang, and L. Pusztai, *Immunotherapy and targeted therapy combinations in metastatic breast cancer.* Lancet Oncol, 2019. **20**(3): p. e175-e186.
327. Roodhart, J.M., L.G. Daenen, E.C. Stigter, H.J. Prins, J. Gerrits, J.M. Houthuijzen, M.G. Gerritsen, H.S. Schipper, M.J. Backer, M. van Amersfoort, et al., *Mesenchymal stem cells induce resistance to chemotherapy through the release of platinum-induced fatty acids.* Cancer Cell, 2011. **20**(3): p. 370-83.
328. Sun, L., Q. Wang, B. Chen, Y. Zhao, B. Shen, H. Wang, J. Xu, M. Zhu, X. Zhao, C. Xu, et al., *Gastric cancer mesenchymal stem cells derived IL-8 induces PD-L1 expression in gastric cancer cells via STAT3/mTOR-c-Myc signal axis.* Cell Death Dis, 2018. **9**(9): p. 928.
329. O'Malley, G., O. Treacy, K. Lynch, S.D. Naicker, N.A. Leonard, P. Lohan, P.D. Dunne, T. Ritter, L.J. Egan, and A.E. Ryan, *Stromal Cell PD-L1 Inhibits CD8(+) T-cell Antitumor Immune Responses and Promotes Colon Cancer.* Cancer Immunol Res, 2018. **6**(11): p. 1426-1441.
330. Davies, L.C., N. Heldring, N. Kadri, and K. Le Blanc, *Mesenchymal Stromal Cell Secretion of Programmed Death-1 Ligands Regulates T Cell Mediated Immunosuppression.* Stem Cells, 2017. **35**(3): p. 766-776.
331. Yang, Y., X. Zhang, F. Lin, M. Xiong, D. Fan, X. Yuan, Y. Lu, Y. Song, Y. Zhang, M. Hao, et al., *Bispecific CD3-HAC carried by E1A-engineered mesenchymal stromal cells against metastatic breast cancer by blocking PD-L1 and activating T cells.* J

Hematol Oncol, 2019. **12**(1): p. 46.
332. Krueger, T.E., D.L.J. Thorek, A.K. Meeker, J.T. Isaacs, and W.N. Brennen, *Tumor-infiltrating mesenchymal stem cells: Drivers of the immunosuppressive tumor microenvironment in prostate cancer?* Prostate, 2019. **79**(3): p. 320-330.
333. Aref, A.R., R.Y. Huang, W. Yu, K.N. Chua, W. Sun, T.Y. Tu, J. Bai, W.J. Sim, I.K. Zervantonakis, J.P. Thiery, et al., *Screening therapeutic EMT blocking agents in a three-dimensional microenvironment.* Integr Biol (Camb), 2013. **5**(2): p. 381-9.
334. Emens, L.A., *Breast Cancer Immunotherapy: Facts and Hopes.* Clin Cancer Res, 2018. **24**(3): p. 511-520.
335. Yu, H., K.P. Lim, S. Xiong, L.P. Tan, and W. Shim, *Functional morphometric analysis in cellular behaviors: shape and size matter.* Adv Healthc Mater, 2013. **2**(9): p. 1188-97.
336. Zou, W., J.D. Wolchok, and L. Chen, *PD-L1 (B7-H1) and PD-1 pathway blockade for cancer therapy: Mechanisms, response biomarkers, and combinations.* Sci Transl Med, 2016. **8**(328): p. 328rv4.
337. Zeng, D., M. Li, R. Zhou, J. Zhang, H. Sun, M. Shi, J. Bin, Y. Liao, J. Rao, and W. Liao, *Tumor Microenvironment Characterization in Gastric Cancer Identifies Prognostic and Immunotherapeutically Relevant Gene Signatures.* Cancer Immunol Res, 2019. **7**(5): p. 737-750.
338. Biswas, S., G. Mandal, S.R. Chowdhury, S. Purohit, K.K. Payne, C.M.A. Galindo, A. Gupta, X. Yu, J.R. Conejo-Garcia, and A. Bhattacharyya, *Mesenchymal stem cells educate breast tumor associated macrophages to acquire increased immunosuppressive features.* The Journal of Immunology, 2019. **202**(1 Supplement): p. 135.25-135.25.
339. Moravej, A., M.H. Karimi, B. Geramizadeh, N. Azarpira, A.H. Zarnani, R. Yaghobi, M. Khosravi, M. Kalani, and B. Gharesi-Fard, *Mesenchymal Stem Cells Upregulate the Expression of PD-L1 But Not VDR in Dendritic Cells.* Immunol Invest, 2017. **46**(1): p. 80-96.
340. Shahar, T., U. Rozovski, K.R. Hess, A. Hossain, J. Gumin, F. Gao, G.N. Fuller, L. Goodman, E.P. Sulman, and F.F. Lang, *Percentage of mesenchymal stem cells in high-grade glioma tumor samples correlates with patient survival.* Neuro Oncol, 2017. **19**(5): p. 660-668.
341. Hossain, A., J. Gumin, F. Gao, J. Figueroa, N. Shinojima, T. Takezaki, W. Priebe, D. Villarreal, S.G. Kang, C. Joyce, et al., *Mesenchymal Stem Cells Isolated From Human Gliomas Increase Proliferation and Maintain Stemness of Glioma Stem Cells Through the IL-6/gp130/STAT3 Pathway.* Stem Cells, 2015. **33**(8): p. 2400-15.
342. Mittendorf, E.A., A.V. Philips, F. Meric-Bernstam, N. Qiao, Y. Wu, S. Harrington, X. Su, Y. Wang, A.M. Gonzalez-Angulo, A. Akcakanat, et al., *PD-L1 expression in triple-negative breast cancer.* Cancer Immunol Res, 2014. **2**(4): p. 361-70.
343. Malta, T.M., A. Sokolov, A.J. Gentles, T. Burzykowski, L. Poisson, J.N. Weinstein, B. Kaminska, J. Huelsken, L. Omberg, O. Gevaert, et al., *Machine Learning Identifies Stemness Features Associated with Oncogenic Dedifferentiation.* Cell, 2018. **173**(2): p. 338-354 e15.
344. Truong, D.D., A. Kratz, J.G. Park, E.S. Barrientos, H. Saini, T. Nguyen, B. Pockaj, G. Mouneimne, J. LaBaer, and M. Nikkhah, *A Human Organotypic Microfluidic*

Tumor Model Permits Investigation of the Interplay between Patient-Derived Fibroblasts and Breast Cancer Cells. Cancer Res, 2019. **79**(12): p. 3139-3151.
345. Zhuang, J., Q. Lu, B. Shen, X. Huang, L. Shen, X. Zheng, R. Huang, J. Yan, and H. Guo, *TGFbeta1 secreted by cancer-associated fibroblasts induces epithelial-mesenchymal transition of bladder cancer cells through lncRNA-ZEB2NAT.* Sci Rep, 2015. **5**: p. 11924.
346. Miyazaki, K., J. Oyanagi, D. Hoshino, S. Togo, H. Kumagai, and Y. Miyagi, *Cancer cell migration on elongate protrusions of fibroblasts in collagen matrix.* Sci Rep, 2019. **9**(1): p. 292.
347. Fernandez-Nogueira, P., M. Mancino, G. Fuster, A. Lopez-Plana, P. Jauregui, V. Almendro, E. Enreig, S. Menendez, F. Rojo, A. Noguera-Castells, et al., *Tumor-Associated Fibroblasts Promote HER2-Targeted Therapy Resistance through FGFR2 Activation.* Clin Cancer Res, 2019.
348. Wang, X., X. Li, X. Wei, H. Jiang, C. Lan, S. Yang, H. Wang, Y. Yang, C. Tian, Z. Xu, et al., *PD-L1 is a direct target of cancer-FOXP3 in pancreatic ductal adenocarcinoma (PDAC), and combined immunotherapy with antibodies against PD-L1 and CCL5 is effective in the treatment of PDAC.* Signal Transduct Target Ther, 2020. **5**(1): p. 38.
349. Zhang, S., M. Zhong, C. Wang, Y. Xu, W.Q. Gao, and Y. Zhang, *CCL5-deficiency enhances intratumoral infiltration of CD8(+) T cells in colorectal cancer.* Cell Death Dis, 2018. **9**(7): p. 766.
350. Prager, B.C., Q. Xie, S. Bao, and J.N. Rich, *Cancer Stem Cells: The Architects of the Tumor Ecosystem.* Cell Stem Cell, 2019. **24**(1): p. 41-53.
351. Ferguson, L.P., E. Diaz, and T. Reya, *The Role of the Microenvironment and Immune System in Regulating Stem Cell Fate in Cancer.* Trends Cancer, 2021. **7**(7): p. 624-634.
352. Wu, S.Z., D.L. Roden, C. Wang, H. Holliday, K. Harvey, A.S. Cazet, K.J. Murphy, B. Pereira, G. Al-Eryani, N. Bartonicek, et al., *Stromal cell diversity associated with immune evasion in human triple-negative breast cancer.* EMBO J, 2020. **39**(19): p. e104063.
353. Fiori, M.E., S. Di Franco, L. Villanova, P. Bianca, G. Stassi, and R. De Maria, *Cancer-associated fibroblasts as abettors of tumor progression at the crossroads of EMT and therapy resistance.* Mol Cancer, 2019. **18**(1): p. 70.
354. Cox, T.R., *The matrix in cancer.* Nat Rev Cancer, 2021. **21**(4): p. 217-238.
355. Zanconato, F., M. Cordenonsi, and S. Piccolo, *YAP and TAZ: a signalling hub of the tumour microenvironment.* Nat Rev Cancer, 2019. **19**(8): p. 454-464.
356. Sahai, E., I. Astsaturov, E. Cukierman, D.G. DeNardo, M. Egeblad, R.M. Evans, D. Fearon, F.R. Greten, S.R. Hingorani, T. Hunter, et al., *A framework for advancing our understanding of cancer-associated fibroblasts.* Nat Rev Cancer, 2020. **20**(3): p. 174-186.
357. Polydorou, C., F. Mpekris, P. Papageorgis, C. Voutouri, and T. Stylianopoulos, *Pirfenidone normalizes the tumor microenvironment to improve chemotherapy.* Oncotarget, 2017. **8**(15): p. 24506-24517.
358. Kozono, S., K. Ohuchida, D. Eguchi, N. Ikenaga, K. Fujiwara, L. Cui, K. Mizumoto, and M. Tanaka, *Pirfenidone inhibits pancreatic cancer desmoplasia by regulating*

stellate cells. Cancer Res, 2013. **73**(7): p. 2345-56.
359. Li, C., V. Rezov, E. Joensuu, V. Vartiainen, M. Ronty, M. Yin, M. Myllarniemi, and K. Koli, *Pirfenidone decreases mesothelioma cell proliferation and migration via inhibition of ERK and AKT and regulates mesothelioma tumor microenvironment in vivo.* Sci Rep, 2018. **8**(1): p. 10070.
360. Aboulkheyr Es, H., S. Zhand, J.P. Thiery, and M.E. Warkiani, *Pirfenidone reduces immune-suppressive capacity of cancer-associated fibroblasts through targeting CCL17 and TNF-beta.* Integr Biol (Camb), 2020. **12**(7): p. 188-197.
361. Gao, J., B.A. Aksoy, U. Dogrusoz, G. Dresdner, B. Gross, S.O. Sumer, Y. Sun, A. Jacobsen, R. Sinha, E. Larsson, et al., *Integrative analysis of complex cancer genomics and clinical profiles using the cBioPortal.* Sci Signal, 2013. **6**(269): p. pl1.
362. Snel, B., G. Lehmann, P. Bork, and M.A. Huynen, *STRING: a web-server to retrieve and display the repeatedly occurring neighbourhood of a gene.* Nucleic Acids Res, 2000. **28**(18): p. 3442-4.
363. Szklarczyk, D., A.L. Gable, K.C. Nastou, D. Lyon, R. Kirsch, S. Pyysalo, N.T. Doncheva, M. Legeay, T. Fang, P. Bork, et al., *The STRING database in 2021: customizable protein-protein networks, and functional characterization of user-uploaded gene/measurement sets.* Nucleic Acids Res, 2021. **49**(D1): p. D605-D612.
364. Aboulkheyr Es, H., B. Bigdeli, S. Zhand, A.R. Aref, J.P. Thiery, and M.E. Warkiani, *Mesenchymal stem cells induce PD-L1 expression through the secretion of CCL5 in breast cancer cells.* J Cell Physiol, 2021. **236**(5): p. 3918-3928.
365. Wang, Z., J. Liu, H. Huang, M. Ye, X. Li, R. Wu, H. Liu, and Y. Song, *Metastasis-associated fibroblasts: an emerging target for metastatic cancer.* Biomark Res, 2021. **9**(1): p. 47.
366. Zanconato, F., M. Cordenonsi, and S. Piccolo, *YAP/TAZ at the Roots of Cancer.* Cancer Cell, 2016. **29**(6): p. 783-803.
367. Wilson, M.M., R.A. Weinberg, J.A. Lees, and V.J. Guen, *Emerging Mechanisms by which EMT Programs Control Stemness.* Trends Cancer, 2020. **6**(9): p. 775-780.
368. Balachander, G.M., P.M. Talukdar, M. Debnath, A. Rangarajan, and K. Chatterjee, *Inflammatory Role of Cancer-Associated Fibroblasts in Invasive Breast Tumors Revealed Using a Fibrous Polymer Scaffold.* ACS Appl Mater Interfaces, 2018. **10**(40): p. 33814-33826.
369. Nallanthighal, S., J.P. Heiserman, and D.J. Cheon, *The Role of the Extracellular Matrix in Cancer Stemness.* Front Cell Dev Biol, 2019. **7**: p. 86.
370. Sharma, M., R.C. Turaga, Y. Yuan, G. Satyanarayana, F. Mishra, Z. Bian, W. Liu, L. Sun, J. Yang, and Z.R. Liu, *Simultaneously targeting cancer-associated fibroblasts and angiogenic vessel as a treatment for TNBC.* J Exp Med, 2021. **218**(4).
371. Chen, X. and E. Song, *Turning foes to friends: targeting cancer-associated fibroblasts.* Nat Rev Drug Discov, 2019. **18**(2): p. 99-115.
372. Fujiwara, A., S. Funaki, E. Fukui, K. Kimura, T. Kanou, N. Ose, M. Minami, and Y. Shintani, *Effects of pirfenidone targeting the tumor microenvironment and tumor-stroma interaction as a novel treatment for non-small cell lung cancer.* Sci Rep, 2020. **10**(1): p. 10900.
373. Kurimoto, R., T. Ebata, S. Iwasawa, T. Ishiwata, Y. Tada, K. Tatsumi, and Y. Takiguchi, *Pirfenidone may revert the epithelial-to-mesenchymal transition in human*

lung adenocarcinoma. Oncol Lett, 2017. **14**(1): p. 944-950.
374. Takai, K., A. Le, V.M. Weaver, and Z. Werb, *Targeting the cancer-associated fibroblasts as a treatment in triple-negative breast cancer.* Oncotarget, 2016. **7**(50): p. 82889-82901.
375. Marwitz, S., K. Turkowski, D. Nitschkowski, A. Weigert, J. Brandenburg, N. Reiling, M. Thomas, M. Reck, D. Dromann, W. Seeger, et al., *The Multi-Modal Effect of the Anti-fibrotic Drug Pirfenidone on NSCLC.* Front Oncol, 2019. **9**: p. 1550.
376. Liu, Y., L. Siles, X. Lu, K.C. Dean, M. Cuatrecasas, A. Postigo, and D.C. Dean, *Mitotic polarization of transcription factors during asymmetric division establishes fate of forming cancer cells.* Nat Commun, 2018. **9**(1): p. 2424.
377. Shao, D.D., W. Xue, E.B. Krall, A. Bhutkar, F. Piccioni, X. Wang, A.C. Schinzel, S. Sood, J. Rosenbluh, J.W. Kim, et al., *KRAS and YAP1 converge to regulate EMT and tumor survival.* Cell, 2014. **158**(1): p. 171-84.
378. Yu, M., Y. Chen, X. Li, R. Yang, L. Zhang, L. Huangfu, N. Zheng, X. Zhao, L. Lv, Y. Hong, et al., *YAP1 contributes to NSCLC invasion and migration by promoting Slug transcription via the transcription co-factor TEAD.* Cell Death Dis, 2018. **9**(5): p. 464.
379. Wang, T., B. Mao, C. Cheng, Z. Zou, J. Gao, Y. Yang, T. Lei, X. Qi, Z. Yuan, W. Xu, et al., *YAP promotes breast cancer metastasis by repressing growth differentiation factor-15.* Biochim Biophys Acta Mol Basis Dis, 2018. **1864**(5 Pt A): p. 1744-1753.
380. Li, S., H. Zhu, H. Chen, J. Xia, F. Zhang, R. Xu, and Q. Lin, *Glucose promotes epithelial-mesenchymal transitions in bladder cancer by regulating the functions of YAP1 and TAZ.* J Cell Mol Med, 2020. **24**(18): p. 10391-10401.
381. Giannoni, E., F. Bianchini, L. Calorini, and P. Chiarugi, *Cancer associated fibroblasts exploit reactive oxygen species through a proinflammatory signature leading to epithelial mesenchymal transition and stemness.* Antioxid Redox Signal, 2011. **14**(12): p. 2361-71.
382. Mukaida, N., D. Zhang, and S.I. Sasaki, *Emergence of Cancer-Associated Fibroblasts as an Indispensable Cellular Player in Bone Metastasis Process.* Cancers (Basel), 2020. **12**(10).
383. Ren, Y., H.H. Jia, Y.Q. Xu, X. Zhou, X.H. Zhao, Y.F. Wang, X. Song, Z.Y. Zhu, T. Sun, Y. Dou, et al., *Paracrine and epigenetic control of CAF-induced metastasis: the role of HOTAIR stimulated by TGF-ss1 secretion.* Mol Cancer, 2018. **17**(1): p. 5.
384. Mosa, M.H., B.E. Michels, C. Menche, A.M. Nicolas, T. Darvishi, F.R. Greten, and H.F. Farin, *A Wnt-Induced Phenotypic Switch in Cancer-Associated Fibroblasts Inhibits EMT in Colorectal Cancer.* Cancer Res, 2020. **80**(24): p. 5569-5582.
385. Lamouille, S., J. Xu, and R. Derynck, *Molecular mechanisms of epithelial-mesenchymal transition.* Nat Rev Mol Cell Biol, 2014. **15**(3): p. 178-96.
386. Yeow, Y.L., V.R. Kotamraju, X. Wang, M. Chopra, N. Azme, J. Wu, T.D. Schoep, D.S. Delaney, K. Feindel, J. Li, et al., *Immune-mediated ECM depletion improves tumour perfusion and payload delivery.* EMBO Mol Med, 2019. **11**(12): p. e10923.
387. Su, S., J. Chen, H. Yao, J. Liu, S. Yu, L. Lao, M. Wang, M. Luo, Y. Xing, F. Chen, et al., *CD10(+)GPR77(+) Cancer-Associated Fibroblasts Promote Cancer Formation and Chemoresistance by Sustaining Cancer Stemness.* Cell, 2018. **172**(4): p. 841-856 e16.

388. Casagrande, N., C. Borghese, L. Visser, M. Mongiat, A. Colombatti, and D. Aldinucci, *CCR5 antagonism by maraviroc inhibits Hodgkin lymphoma microenvironment interactions and xenograft growth.* Haematologica, 2019. **104**(3): p. 564-575.
389. Highfill, S.L., Y. Cui, A.J. Giles, J.P. Smith, H. Zhang, E. Morse, R.N. Kaplan, and C.L. Mackall, *Disruption of CXCR2-mediated MDSC tumor trafficking enhances anti-PD1 efficacy.* Sci Transl Med, 2014. **6**(237): p. 237ra67.
390. Sangaletti, S., C. Tripodo, A. Santangelo, N. Castioni, P. Portararo, A. Gulino, L. Botti, M. Parenza, B. Cappetti, R. Orlandi, et al., *Mesenchymal Transition of High-Grade Breast Carcinomas Depends on Extracellular Matrix Control of Myeloid Suppressor Cell Activity.* Cell Rep, 2016. **17**(1): p. 233-248.
391. Ouzounova, M., E. Lee, R. Piranlioglu, A. El Andaloussi, R. Kolhe, M.F. Demirci, D. Marasco, I. Asm, A. Chadli, K.A. Hassan, et al., *Monocytic and granulocytic myeloid derived suppressor cells differentially regulate spatiotemporal tumour plasticity during metastatic cascade.* Nat Commun, 2017. **8**: p. 14979.
392. Omland, S.H., E.E. Wettergren, S. Mollerup, M. Asplund, T. Mourier, A.J. Hansen, and R. Gniadecki, *Cancer associated fibroblasts (CAFs) are activated in cutaneous basal cell carcinoma and in the peritumoural skin.* BMC Cancer, 2017. **17**(1): p. 675.
393. Yousafzai, M.S., G. Coceano, S. Bonin, J. Niemela, G. Scoles, and D. Cojoc, *Investigating the effect of cell substrate on cancer cell stiffness by optical tweezers.* Journal of biomechanics, 2017. **60**: p. 266-269.
394. Prager-Khoutorsky, M., A. Lichtenstein, R. Krishnan, K. Rajendran, A. Mayo, Z. Kam, B. Geiger, and A.D. Bershadsky, *Fibroblast polarization is a matrix-rigidity-dependent process controlled by focal adhesion mechanosensing.* Nature cell biology, 2011. **13**(12): p. 1457.
395. Rico, F., P. Roca-Cusachs, N. Gavara, R. Farré, M. Rotger, and D. Navajas, *Probing mechanical properties of living cells by atomic force microscopy with blunted pyramidal cantilever tips.* Physical Review E, 2005. **72**(2): p. 021914.
396. Nakai, K., M.-C. Hung, and H. Yamaguchi, *A perspective on anti-EGFR therapies targeting triple-negative breast cancer.* American journal of cancer research, 2016. **6**(8): p. 1609.
397. Cavazzoni, A., R.R. Alfieri, D. Cretella, F. Saccani, L. Ampollini, M. Galetti, F. Quaini, G. Graiani, D. Madeddu, and P. Mozzoni, *Combined use of anti-ErbB monoclonal antibodies and erlotinib enhances antibody-dependent cellular cytotoxicity of wild-type erlotinib-sensitive NSCLC cell lines.* Molecular cancer, 2012. **11**(1): p. 91.
398. Wang, Y., M.H. Kim, S.R. Tabaei, J.H. Park, K. Na, S. Chung, V.P. Zhdanov, and N.-J. Cho, *Spheroid formation of hepatocarcinoma cells in microwells: experiments and Monte Carlo simulations.* PloS one, 2016. **11**(8): p. e0161915.
399. Rueden, C.T., J. Schindelin, M.C. Hiner, B.E. DeZonia, A.E. Walter, E.T. Arena, and K.W. Eliceiri, *ImageJ2: ImageJ for the next generation of scientific image data.* BMC bioinformatics, 2017. **18**(1): p. 529.
400. Rom-Jurek, E.-M., N. Kirchhammer, P. Ugocsai, O. Ortmann, A.K. Wege, and G. Brockhoff, *Regulation of Programmed Death Ligand 1 (PD-L1) Expression in Breast Cancer Cell Lines In Vitro and in Immunodeficient and Humanized Tumor Mice.*

International journal of molecular sciences, 2018. **19**(2): p. 563.
401. Soliman, H., F. Khalil, and S. Antonia, *PD-L1 expression is increased in a subset of basal type breast cancer cells.* PloS one, 2014. **9**(2): p. e88557.
402. Kim, S., J. Koh, D. Kwon, B. Keam, H. Go, Y.A. Kim, Y.K. Jeon, and D.H. Chung, *Comparative analysis of PD-L1 expression between primary and metastatic pulmonary adenocarcinomas.* European Journal of Cancer, 2017. **75**: p. 141-149.
403. Raczkowska, J. and S. Prauzner-Bechcicki, *Discrimination between HCV29 and T24 by controlled proliferation of cells co-cultured on substrates with different elasticity.* Journal of the mechanical behavior of biomedical materials, 2018. **88**: p. 217-222.
404. Prauzner-Bechcicki, S., J. Raczkowska, E. Madej, J. Pabijan, J. Lukes, J. Sepitka, J. Rysz, K. Awsiuk, A. Bernasik, and A. Budkowski, *PDMS substrate stiffness affects the morphology and growth profiles of cancerous prostate and melanoma cells.* Journal of the mechanical behavior of biomedical materials, 2015. **41**: p. 13-22.
405. Miyazawa, A., S. Ito, S. Asano, I. Tanaka, M. Sato, M. Kondo, and Y. Hasegawa, *Regulation of PD-L1 expression by matrix stiffness in lung cancer cells.* Biochemical and biophysical research communications, 2018. **495**(3): p. 2344-2349.
406. Takada, K., G. Toyokawa, T. Tagawa, K. Kohashi, M. Shimokawa, T. Akamine, S. Takamori, F. Hirai, F. Shoji, and T. Okamoto, *PD-L1 expression according to the EGFR status in primary lung adenocarcinoma.* Lung Cancer, 2018. **116**: p. 1-6.
407. Li, X., Z. Lian, S. Wang, L. Xing, and J. Yu, *Interactions between EGFR and PD-1/PD-L1 pathway: implications for treatment of NSCLC.* Cancer letters, 2018.
408. Kumaraswamy, E., K.L. Wendt, L.A. Augustine, S.R. Stecklein, E.C. Sibala, D. Li, S. Gunewardena, and R.A. Jensen, *BRCA1 regulation of epidermal growth factor receptor (EGFR) expression in human breast cancer cells involves microRNA-146a and is critical for its tumor suppressor function.* Oncogene, 2015. **34**(33): p. 4333.
409. Tanei, T., D.S. Choi, A.A. Rodriguez, D.H. Liang, L. Dobrolecki, M. Ghosh, M.D. Landis, and J.C. Chang, *Antitumor activity of Cetuximab in combination with Ixabepilone on triple negative breast cancer stem cells.* Breast Cancer Research, 2016. **18**(1): p. 6.
410. Zhang, N., Y. Zeng, W. Du, J. Zhu, D. Shen, Z. Liu, and J.-A. Huang, *The EGFR pathway is involved in the regulation of PD-L1 expression via the IL-6/JAK/STAT3 signaling pathway in EGFR-mutated non-small cell lung cancer.* International journal of oncology, 2016. **49**(4): p. 1360-1368.
411. Sasada, T., K. Azuma, J. Ohtake, and Y. Fujimoto, *Immune responses to epidermal growth factor receptor (EGFR) and their application for cancer treatment.* Frontiers in pharmacology, 2016. **7**: p. 405.
412. Moya-Horno, I., S. Viteri, N. Karachaliou, and R. Rosell, *Combination of immunotherapy with targeted therapies in advanced non-small cell lung cancer (NSCLC).* Therapeutic advances in medical oncology, 2018. **10**: p. 1758834017745012.
413. Alsuliman, A., D. Colak, O. Al-Harazi, H. Fitwi, A. Tulbah, T. Al-Tweigeri, M. Al-Alwan, and H. Ghebeh, *Bidirectional crosstalk between PD-L1 expression and epithelial to mesenchymal transition: significance in claudin-low breast cancer cells.* Molecular cancer, 2015. **14**(1): p. 149.
414. Malta, T.M., A. Sokolov, A.J. Gentles, T. Burzykowski, L. Poisson, J.N. Weinstein,

B. Kamińska, J. Huelsken, L. Omberg, and O. Gevaert, *Machine learning identifies stemness features associated with oncogenic dedifferentiation.* Cell, 2018. **173**(2): p. 338-354. e15.
415. You, Y., Q. Zheng, Y. Dong, X. Xie, Y. Wang, S. Wu, L. Zhang, Y. Wang, T. Xue, and Z. Wang, *Matrix stiffness-mediated effects on stemness characteristics occurring in HCC cells.* Oncotarget, 2016. **7**(22): p. 32221.
416. Abhold, E.L., A. Kiang, E. Rahimy, S.Z. Kuo, J. Wang-Rodriguez, J.P. Lopez, K.J. Blair, M.A. Yu, M. Haas, and K.T. Brumund, *EGFR kinase promotes acquisition of stem cell-like properties: a potential therapeutic target in head and neck squamous cell carcinoma stem cells.* PloS one, 2012. **7**(2): p. e32459.
417. Chen, C., Y. Wei, M. Hummel, T.K. Hoffmann, M. Gross, A.M. Kaufmann, and A.E. Albers, *Evidence for epithelial-mesenchymal transition in cancer stem cells of head and neck squamous cell carcinoma.* PloS one, 2011. **6**(1): p. e16466.
418. Ventola, C.L., *Cancer immunotherapy, part 3: Challenges and future trends.* Pharmacy and Therapeutics, 2017. **42**(8): p. 514.
419. Rodrigues, J., M.A. Heinrich, L.M. Teixeira, and J. Prakash, *3D In Vitro Model (R)evolution: Unveiling Tumor-Stroma Interactions.* Trends Cancer, 2021. **7**(3): p. 249-264.
420. Carter, E.P., R. Roozitalab, S.V. Gibson, and R.P. Grose, *Tumour microenvironment 3D-modelling: simplicity to complexity and back again.* Trends Cancer, 2021. **7**(11): p. 1033-1046.
421. Haykal, M.M., C. Nahmias, C. Varon, and O.C.B. Martin, *Organotypic Modeling of the Tumor Landscape.* Front Cell Dev Biol, 2020. **8**: p. 606039.
422. Monteiro, M.V., Y.S. Zhang, V.M. Gaspar, and J.F. Mano, *3D-bioprinted cancer-on-a-chip: level-up organotypic in vitro models.* Trends Biotechnol, 2021.
423. Cattaneo, C.M., K.K. Dijkstra, L.F. Fanchi, S. Kelderman, S. Kaing, N. van Rooij, S. van den Brink, T.N. Schumacher, and E.E. Voest, *Tumor organoid-T-cell coculture systems.* Nat Protoc, 2020. **15**(1): p. 15-39.
424. Yuki, K., N. Cheng, M. Nakano, and C.J. Kuo, *Organoid Models of Tumor Immunology.* Trends Immunol, 2020. **41**(8): p. 652-664.
425. Neal, J.T., X. Li, J. Zhu, V. Giangarra, C.L. Grzeskowiak, J. Ju, I.H. Liu, S.H. Chiou, A.A. Salahudeen, A.R. Smith, et al., *Organoid Modeling of the Tumor Immune Microenvironment.* Cell, 2018. **175**(7): p. 1972-1988 e16.
426. Dijkstra, K.K., C.M. Cattaneo, F. Weeber, M. Chalabi, J. van de Haar, L.F. Fanchi, M. Slagter, D.L. van der Velden, S. Kaing, S. Kelderman, et al., *Generation of Tumor-Reactive T Cells by Co-culture of Peripheral Blood Lymphocytes and Tumor Organoids.* Cell, 2018. **174**(6): p. 1586-1598 e12.
427. Zhang, S., Z. Wan, and R.D. Kamm, *Vascularized organoids on a chip: strategies for engineering organoids with functional vasculature.* Lab Chip, 2021. **21**(3): p. 473-488.
428. Sachs, N., J. de Ligt, O. Kopper, E. Gogola, G. Bounova, F. Weeber, A.V. Balgobind, K. Wind, A. Gracanin, H. Begthel, et al., *A Living Biobank of Breast Cancer Organoids Captures Disease Heterogeneity.* Cell, 2018. **172**(1-2): p. 373-386 e10.
429. Campisi, M., S.K. Sundararaman, S.E. Shelton, E.H. Knelson, N.R. Mahadevan, R. Yoshida, T. Tani, E. Ivanova, I. Canadas, T. Osaki, et al., *Tumor-Derived cGAMP*

Regulates Activation of the Vasculature. Front Immunol, 2020. **11**: p. 2090.
430. Hajal, C., L. Ibrahim, J.C. Serrano, G.S. Offeddu, and R.D. Kamm, *The effects of luminal and trans-endothelial fluid flows on the extravasation and tissue invasion of tumor cells in a 3D in vitro microvascular platform.* Biomaterials, 2021. **265**: p. 120470.
431. Xiao, Y., C. Liu, Z. Chen, M.R. Blatchley, D. Kim, J. Zhou, M. Xu, S. Gerecht, and R. Fan, *Senescent Cells with Augmented Cytokine Production for Microvascular Bioengineering and Tissue Repairs.* Adv Biosyst, 2019. **3**(8).
432. Lee, S.W.L., M. Campisi, T. Osaki, L. Possenti, C. Mattu, G. Adriani, R.D. Kamm, and V. Chiono, *Modeling Nanocarrier Transport across a 3D In Vitro Human Blood-Brain-Barrier Microvasculature.* Adv Healthc Mater, 2020. **9**(7): p. e1901486.
433. Xiao, Y., D. Kim, B. Dura, K. Zhang, R. Yan, H. Li, E. Han, J. Ip, P. Zou, J. Liu, et al., *Ex vivo Dynamics of Human Glioblastoma Cells in a Microvasculature-on-a-Chip System Correlates with Tumor Heterogeneity and Subtypes.* Adv Sci (Weinh), 2019. **6**(8): p. 1801531.
434. Bai, J., M. Khajavi, L. Sui, H. Fu, S. Tarakkad Krishnaji, A.E. Birsner, L. Bazinet, R.D. Kamm, and R.J. D'Amato, *Angiogenic responses in a 3D micro-engineered environment of primary endothelial cells and pericytes.* Angiogenesis, 2021. **24**(1): p. 111-127.
435. Haase, K., G.S. Offeddu, M.R. Gillrie, and R.D. Kamm, *Endothelial Regulation of Drug Transport in a 3D Vascularized Tumor Model.* Adv Funct Mater, 2020. **30**(48).
436. Park, Y.K., T.Y. Tu, S.H. Lim, I.J. Clement, S.Y. Yang, and R.D. Kamm, *In Vitro Microvessel Growth and Remodeling within a Three-dimensional Microfluidic Environment.* Cell Mol Bioeng, 2014. **7**(1): p. 15-25.
437. Skardal, A., S.V. Murphy, M. Devarasetty, I. Mead, H.W. Kang, Y.J. Seol, Y. Shrike Zhang, S.R. Shin, L. Zhao, J. Aleman, et al., *Multi-tissue interactions in an integrated three-tissue organ-on-a-chip platform.* Sci Rep, 2017. **7**(1): p. 8837.
438. Mansour, A.A., J.T. Goncalves, C.W. Bloyd, H. Li, S. Fernandes, D. Quang, S. Johnston, S.L. Parylak, X. Jin, and F.H. Gage, *An in vivo model of functional and vascularized human brain organoids.* Nat Biotechnol, 2018. **36**(5): p. 432-441.
439. Nashimoto, Y., R. Okada, S. Hanada, Y. Arima, K. Nishiyama, T. Miura, and R. Yokokawa, *Vascularized cancer on a chip: The effect of perfusion on growth and drug delivery of tumor spheroid.* Biomaterials, 2020. **229**: p. 119547.
440. Nashimoto, Y., T. Hayashi, I. Kunita, A. Nakamasu, Y.S. Torisawa, M. Nakayama, H. Takigawa-Imamura, H. Kotera, K. Nishiyama, T. Miura, et al., *Integrating perfusable vascular networks with a three-dimensional tissue in a microfluidic device.* Integr Biol (Camb), 2017. **9**(6): p. 506-518.
441. Takebe, T., K. Sekine, M. Enomura, H. Koike, M. Kimura, T. Ogaeri, R.R. Zhang, Y. Ueno, Y.W. Zheng, N. Koike, et al., *Vascularized and functional human liver from an iPSC-derived organ bud transplant.* Nature, 2013. **499**(7459): p. 481-4.
442. Cakir, B., Y. Xiang, Y. Tanaka, M.H. Kural, M. Parent, Y.J. Kang, K. Chapeton, B. Patterson, Y. Yuan, C.S. He, et al., *Engineering of human brain organoids with a functional vascular-like system.* Nat Methods, 2019. **16**(11): p. 1169-1175.
443. Pham, M.T., K.M. Pollock, M.D. Rose, W.A. Cary, H.R. Stewart, P. Zhou, J.A. Nolta, and B. Waldau, *Generation of human vascularized brain organoids.* Neuroreport,

2018. **29**(7): p. 588-593.
444. Worsdorfer, P., N. Dalda, A. Kern, S. Kruger, N. Wagner, C.K. Kwok, E. Henke, and S. Ergun, *Generation of complex human organoid models including vascular networks by incorporation of mesodermal progenitor cells.* Sci Rep, 2019. **9**(1): p. 15663.